Analysis of Reelin function in the molecular mechanisms underlying Alzheimer's disease

Daniela Rossi

UNIVERSITAT DE BARCELONA
FACULTAT DE BIOLOGIA
DEPARTAMENT DE BIOLOGIA CEL·LULAR

INSTITUT DE RECERCA BIOMÈDICA, BARCELONA
PARC CIENTÍFIC DE BARCELONA

Analysis of Reelin function in the molecular mechanisms underlying Alzheimer's disease

Daniela Rossi

Barcelona, 2013

UNIVERSITAT DE BARCELONA
FACULTAT DE BIOLOGIA
DEPARTAMENT DE BIOLOGIA CEL·LULAR

INSTITUT DE RECERCA BIOMÈDICA, BARCELONA
PARC CIENTÍFIC DE BARCELONA

Memoria presentada por Daniela Rossi
para optar al grado de Doctora por la Universidad de Barcelona

Analysis of Reelin function in the molecular mechanisms underlying Alzheimer's disease

Análisis de la función de Reelina en los mecanismos moleculares implicados en la enfermedad de Alzheimer

Programa de Doctorado en Biomedicina Bienio 2009-2011

Octubre 2013

Doctorando

Daniela Rossi

Directores de Tesi

Eduardo Soriano García

Lluís Pujadas Puigdomènech

« Considerate la vostra semenza:
fatti non foste a viver come bruti,
ma per seguir virtute e canoscenza »

« Consider the seed that gave you birth:
you were not made to live as brutes,
but to follow virtue and knowledge »

Divina Commedia "Inferno", Canto XXVI, Dante Alighieri

AGRADECIMIENTOS

Un capítulo de mi vida está a punto de cerrarse y quiero dar las gracias a las personas que me han acompañado en esta importante experiencia y en mucho más.

En primer lugar quiero dar las gracias a mis directores de tesis. A Eduardo, por haberme dejado ser parte de su grupo, por las cosas que me enseñó en estos años y por la confianza que puso en mí.

I a tu, Lluís, que des del primer dia has estat molt més que un director! Gràcies pels consells, per les llargues discussions sobre ciència, per ensenyar-me a pensar i per pensar junt amb mi, per ser-hi sempre. I encara diría més, per haver-me regalat, de la manera més natural possible, una llengua i una cultura. Gràcies!!!

També vull donar les gràcies a la doctora Natàlia Carulla, perquè sense ser-ho formalment, realment ha estat la meva mentora, donant-me nous enfocaments i valuosos suggeriments que m'han fet aprendre molt.

En segundo lugar quiero dar las gracias a mis compañeros de laboratorio, a los Soriano's y a los Toni's, por darme la bienvenida a mi nuevo mundo hace 4 años, por ayudarme en todo recién llegada, por haberme hecho también una *poli-idiota*! Per les calçotades, les cerveçetes, els soparets i els cafés. Gracias a los que ya marcharon y a los que siguen aquí... ha sido un muy buen viaje y espero que no se acabe aquí!!!

En tercer lugar quiero dar las gracias a los amigos conocidos en estos años y que poco a poco se han convertido en mi cotidiano, porque sin saberlo contribuyeron a que todo me fuera bien. Gracias a la "familia napolitana" y gracias a mis *Olzinelles*, que *"cogieron a una niña y entregaron una mujer"* (cit.).

Grazie alle mie *Ancorette*, per essere ancor più nel mio quotidiano, pur essendo lontane. Perché ciò che ci lega non conosce distanze. Perché la natura non mi ha dato sorelle, ma la vita tre, grazie a voi io lo so!

Grazie a Paolo, il mio "*piccolo*" uomo, perché tra le multiformi tue passioni altalenanti hai scelto me tra le poche costanti, ed io te! Grazie per ciò che abbiamo costruito insieme e per ciò che insieme faremo. Per la gioia e l'amore di ogni giorno!

Infine il ringraziamento più forte non può essere che per la mia famiglia. Dalla risata di mia nonna alle estati passate con i cugini, tutto ha contribuito a fare di me ciò che sono, e non posso che ritenermi fortunata ad avervi. Grazie ad Alessandro, che mi ha sempre aiutato e motivato, e che da molto lontano continua a farlo! Grazie alla dolcezza di mia madre e alla saggezza di mio padre, perché da molto prima di me sognavano di vedere i miei obiettivi realizzati. Questo piccolo traguardo è dedicato a voi.

TABLE OF CONTENTS

INTRODUCTION

1.1 Alzheimer-type dementia

Alzheimer's disease (AD) is the most common cause of dementia in the elderly, with more than 25 million people affected worldwide (Alzheimer's Association, http://www.alz.org/). First described in 1907 by the German physician Alois Alzheimer (Alzheimer et al., 1995), AD is a neurodegenerative disease characterized by a dramatic progressive loss of synapses and neuronal populations, initially affecting medial temporal lobe structures and finally resulting in diffuse cortical atrophy. The earliest clinical symptoms are episodic memory loss, especially in remembering new items (anterograde amnesia). As the disease progresses, amnesia occurs in conjunction with major executive dysfunctions, such as impairment of language (aphasia), object use (apraxia), recognition of faces or objects (agnosia), abstract reasoning, step-by-step planning, and decision making (McKhann et al., 1984). This gradual erosion of cognition slowly increases in severity until the symptoms eventually become incapacitating, and at the histological level it is reflected by the progressive spread of specific pathological lesions in a non-random manner across various brain regions. On the basis of this extension, it has been possible to distinguish six stages (also known as Braak stages) of disease progression (Braak and Braak, 1991, 1995): the transentorhinal stages I–II, representing clinically silent cases; the limbic stages III–IV of incipient AD; and the neocortical stages V–VI of fully developed AD. In the late stages of disease, cognitive decline is often accompanied by psychiatric features, such as confusion, agitation and behavioral disturbances, and by neurological symptoms, which may include seizures, hypertonia, myoclonus, incontinence, and mutism. AD is a terminal illness with death commonly being caused by external factors such as infections, pneumonia, malnutrition or comorbidities, but not the disorder itself.

1.1.1 Genetics of Alzheimer's disease

Depending on the age of onset, two major types of AD are generally differentiated: early-onset forms beginning before the age of 65, and late-onset forms thereafter. A considerable proportion of the early-onset AD (EOAD) forms occurs in a family history context, and they are caused by rare, autosomal dominant mutations in the genes

encoding *amyloid beta precursor protein* (APP), *presenilin-1* (PSEN1 or PS1) and *presenilin-2* (PSEN2 or PS2) (Bertram et al.; Ballard et al., 2011; Selkoe, 2011). Due to their Mendelian inheritance, these cases are also referred to as Familial Alzheimer's disease (FAD). In contrast, late-onset forms of AD (LOAD) are not directly linked to genetic mutations, and only association genetic risk factors have been proposed for these. The absence of obvious inheritance led to the classification of LOAD as Sporadic Alzheimer's disease (SAD).

To date, at least 24 *APP*, 185 *PSEN1* and 14 *PSEN2* highly penetrant missense mutations have been described to cause EOAD (**Table 1**). Duplications in *APP* are also responsible for EOAD (Rovelet-Lecrux et al., 2006; Tanzi, 2012) and in Down's syndrome (caused by trisomy of the chromosome 21, carrying *APP*) overexpression of *APP* results in early onset dementia with an AD-like phenotype (Hof et al., 1995).

Table 1. Early-omset familial Alzheimer's disease genes and their pathogenic effects

Gene	Protein	Chromosome	Mutations	Molecular phenotype
APP	Amyloid β (A4) protein precursor	21q21	24 (duplication)	Increased $A\beta_{42}/A\beta_{40}$ ratio Increased Aβ production Increased Aβ aggregation
PSEN1	Presenilin 1	14q24	185	Increased $A\beta_{42}/A\beta_{40}$ ratio
PSEN2	Presenilin 2	1q31	14	Increased $A\beta_{42}/A\beta_{40}$ ratio

From: Tanzi R.E., 2012

FAD mutations can be examined in detail on the online Alzheimer Disease and Frontotemporal Dementia Mutation Database website (**http://www.molgen.ua.ac.be/ADmutations/**). Identification of these EOAD genes has encouraged functional and molecular studies of the mutated gene products, which have provided a wealth of information about the pathogenetic mechanisms underlying AD.

In particular amyloid beta (Aβ) peptide, one of the major toxic agents in AD, is a product of the catabolism of APP protein, endoproteolyzed by the subsequent action of β- and γ-secretases (Cole and Vassar, 2008; Steiner, 2008). Interestingly, most of the AD-related APP mutations are located at the secretase cleavage sites, often leading to increased cleavage and greater Aβ production, like the cases of the missense APP "London" and "Swedish" mutations (at the β-secretase cleavage site of APP, improving APP as a substrate for β-secretase) (Goate et al., 1991; Mullan, 1992). Moreover, the catalytic center of γ-secretase is encoded by the EOAD genes *PSEN1* and *PSEN2*, and their mutations often prove to be connected to an abnormal production of the Aβ

peptide or to favor the production of the more amyloidogenic 42-amino acid form of Aβ ($A\beta_{42}$) over the shorter form of 40 amino acids ($A\beta_{40}$) (Bertram et al., 2010; O'Brien and Wong, 2011). Finally, mutations in the middle of the Aβ peptide enhance or alter Aβ aggregation properties. For example, four distinct point mutations in a single residue (E693) were observed to have distinct effects on the biophysical properties of $A\beta_{42}$ and on the clinical phenotype (Nilsberth et al., 2001; Tomiyama et al., 2008). This observation thus strongly supports the pathogenic significance of Aβ peptides. Among these, the arctic mutation (E693G) causes AD by enhanced Aβ protofibril formation, although decreasing $A\beta_{42}$ and $A\beta_{40}$ levels in plasma (Nilsberth et al., 2001).

Taken together, the observation that most mutations causing FAD either increase Aβ production or shift the $A\beta_{42}/A\beta_{40}$ ratio towards $A\beta_{42}$ provides strong evidence of a causal role of Aβ peptides in FAD pathogenesis, although their contribution to SAD remains less clear. This convergence of genetic and molecular evidence has given support to the ‘‘Amyloid hypothesis’, which postulates that the abnormal production of Aβ is the initial step in triggering the pathophysiological cascade that eventually leads to AD (Glenner and Wong, 1984; Hardy and Higgins, 1992; Hardy, 1997; Hardy and Selkoe, 2002; Tanzi and Bertram, 2005) (**Chapter 1.1.2**). In spite of the extensive body of knowledge acquired in the last 30 years about the possible pathogenic mechanisms of FAD, these cases account for only approximately 1-6% of AD cases (Bekris et al., 2010). The remaining ~95% of cases are attributable to SAD, for which no clear pathogenic mechanisms are yet known.

While EOAD is caused by rare and highly penetrant mutations, the genetics of LOAD is more complex. Currently, it is believed that susceptibility for LOAD is conferred by numerous genetic risk factors of relatively high frequency but low penetrance. Thus it is important to emphasize that although LOAD is classified as a sporadic form of AD, up to 60%–80% of this form of the disease is associated with genetic predisposition. In addition to susceptibility genes, environmental and epigenetic factors may make a significant contribution to determining an individual’s risk, thus making AD a complex multifactorial disease that arises from the interaction of several determinants (Gatz et al., 2006).

From 1993 to 2009, the Apoε4 allele for APOE, a major brain apolipoprotein, was the only unequivocally established genetic risk factor for LOAD (Corder et al., 1993; Saunders et al., 1993; Schmechel et al., 1993; Strittmatter et al., 1993a; Strittmatter et

al., 1993b). Compared to patients with no ε4 alleles, the increased risk for AD is two-to four-fold in patients carrying one ε4 allele and about 12-fold in ε4 homozygotes (Farrer et al., 1997; Bertram et al., 2007). Carriers of Apoε4 also show earlier accumulation of amyloid plaques and a younger age of onset of dementia. The neuropathological pathway by which APOE increases the risk of disease is unclear. However, evidence suggests that the Apoε4 isoform is associated with less efficient clearing of Aβ from the brain (Castellano et al., 2011). It was recently reported that Apoε4 increases the formation of soluble oligomeric forms of Aβ, which are crucial for synaptic dysfunction, cognitive impairment and neurodegeneration (Hashimoto et al., 2012).

Recent advances in large-scale sequencing technologies allowed the development of several powerful Genome-Wide Association Studies (GWAS), which have produced a wealth of literature in the last few years, thus greatly improving our understanding of AD genetics. Apart from confirming Apoε4 as the top LOAD gene with extremely high confidence (Bertram et al., 2010), new additional loci associated with AD, such as CLU, PICALM, CR1, BIN1, ABCA7 and EPHA1, emerged from GWAS (Harold et al., 2009; Lambert et al., 2009; Hollingworth et al., 2011; Naj et al., 2011; Tanzi, 2012) (**Table 2**).

Table 2. Results of GWAS of late-onset Alzheimer's disease

Genome-wide association studies	Study design	Population	Major genes identified
Reiman et al. 2007	Case–control	US	*APOE, GAB2*
Bertram 2008	Family-based	US	*APOE, ATXN1, CD33, GWA_14q31*
Lambert et al. 2009	Case–control	US, Europe	*APOE, CLU, CR1*
Harold et al. 2009	Case–control	US, Europe	*APOE, CLU, PICALM*
Seshadri et al. 2010	Case–control	US, Europe	*APOE, BIN1*
Naj et al. 2011	Case–control	US, Europe	*MS4A6A/MS4A4E, EPHA1, CD33, CD2AP*
Hollingworth et al. 2011	Case–control	US, Europe	*ABCA7, MS4A6A/MS4A4E, EPHA1, CD33, CD2AP*

From: Tanzi R.E., 2012

A combination of intensive, systematic efforts in this genetic studies approach, together with replication in large, independent populations and functional analyses, will be needed to determine the true contribution of these new genes to AD. We are now progressing towards building a completely new picture of AD genetics. Finally, in addition to genetic risk factors, an environmental component for AD has been proposed, with factors like age, education, physical activity, diet, eventual presence of

comorbidities (obesity, diabetes, inflammatory diseases) playing a role in its onset (Arendash et al., 2004; Rovio et al., 2005; Halagappa et al., 2007).

In spite of their distinct genetic backgrounds, FAD and SAD are indistinguishable at the histopathological level and show two main hallmarks: amyloid plaques and neurofibrillary tangles (**Fig. 1.1**), occurring in a context of vascular damage, inflammation, oxidative stress, synaptic loss and neurodegeneration (Braak and Braak, 1997; Nussbaum and Ellis, 2003; Goedert and Spillantini, 2006; Serrano-Pozo et al., 2011; Spires-Jones and Knafo, 2012; Orsucci et al., 2013).

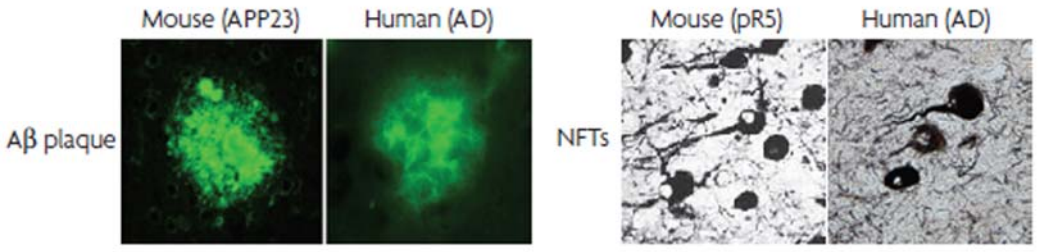

From Götz J. and Ittner L.M., 2008

Figure 1.1 Histopathology of Alzheimer's disease. Representative Aβ plaques from a transgenic mouse model (APP23) and a human AD brain, visualized with the dye thioflavin S, are shown on the left. Neurofibrillary tangles (NFTs) from a a transgenic mouse model (pR5) and a human AD brain, visualized with the Gallyas silver impregnation technique, are shown on the right.

1.1.2 Aβ in the pathogenesis of Alzheimer's disease

APP proteolytic processing and functions: Amyloid plaques are one of the main histopathological lesions of AD. These are extracellular insoluble deposits composed mainly by Aβ peptide, arranged in a fibrillar β-pleated sheet secondary structure. The deposition of amyloid plaques starts in cortical areas and follows a specific sequence during disease progression moving to allocortical regions first, then to diencephalic nuclei, the striatum, and the cholinergic nuclei of the basal forebrain, ending with the involvement of additional brainstem nuclei and cerebellum (Thal et al., 2002). The Aβ peptide derives from the proteolytic cleavage of the single-pass transmembrane protein APP by the action of integral membrane proteases termed secretases. APP is cleaved sequentially: first by either α- or β-secretase, and then by γ-secretase (Sheng et al., 2012). In the amyloidogenic pathway, which gives rise to the Aβ peptide, the proteases involved are β- and γ-secretase, whose sequential action releases the soluble

extracellular domain of APP (sAPPβ), the Aβ peptide, and the intracellular carboxy-terminal domain of APP (AICD). In contrast, cleavage by α-secretase prevents the formation of Aβ, producing sAPPα, p3 peptide and AICD (**Fig. 1.2a**). α- and β-secretase cleave at single sites in the extracellular domain of APP, whereas γ-secretase can cut the products of the α- or β-cleavage at various sites, giving rise to Aβ peptides and intracellular fragments of varying length. Depending on the specific γ-secretase cleavage site, the two most frequent forms of Aβ peptide can vary from 40 ($A\beta_{40}$) to 42 amino acids ($A\beta_{42}$) in length (**Fig. 1.2b**), with $A\beta_{40}$ being the most common species, and $A\beta_{42}$ the less common but the most fibrillogenic and neurotoxic species (O'Brien and Wong, 2011).

Many studies have addressed the physiological functions of APP and Aβ peptide; however, little is yet known. In mammals, APP is a member of a gene family that includes APLP1 and APLP2 (APP-like protein 1 and 2), which are also cleaved by α-, β-, and γ-secretases. Like for APP, the action of these proteases on APLPs also produces a large number of protein fragments and peptides, although these peptides are not capable of aggregating *in vivo* and they show no pathogenic effects. A possible clue to the physiological function of APP is the activity-dependent regulation of Aβ production and/or secretion. Aβ secretion is enhanced by neural activity *in vitro* and *in vivo* (Kamenetz et al., 2003; Cirrito et al., 2005; Wei et al., 2010); however, it is unclear whether the regulation occurs at the level of α-, β- or γ-secretase. In turn, Aβ itself can regulate neuronal and synaptic activities, with accumulation of Aβ in the brain, causing a vicious cycle of Aβ production with an intriguing combination of aberrant network activity and synaptic depression (Palop and Mucke, 2010). In the human brain, functional MRI imaging reveals that regions with high resting "default mode" activity (the mode that is active when we do not think about anything in particular) show a higher Aβ plaque load (Buckner et al., 2005). Moreover, Holtzman and colleagues (Kang et al., 2009) measured the amount of Aβ *in vivo* in the extracellular interstitial fluid of the hippocampus and found that extracellular Aβ varied with a diurnal rhythm, correlating with wakefulness in both wild-type and mutant APP transgenic mice. Sleep deprivation acutely elevated extracellular Aβ. Remarkably, in AD transgenic mice, chronic sleep restriction significantly increased amyloid plaque load while inhibition of wakefulness decreased this parameter. Given that wakefulness is associated with a net increase in brain synaptic activity, the control of Aβ by the sleep–wake cycle is consistent with the notion that neuronal activity is a key regulator of APP processing.

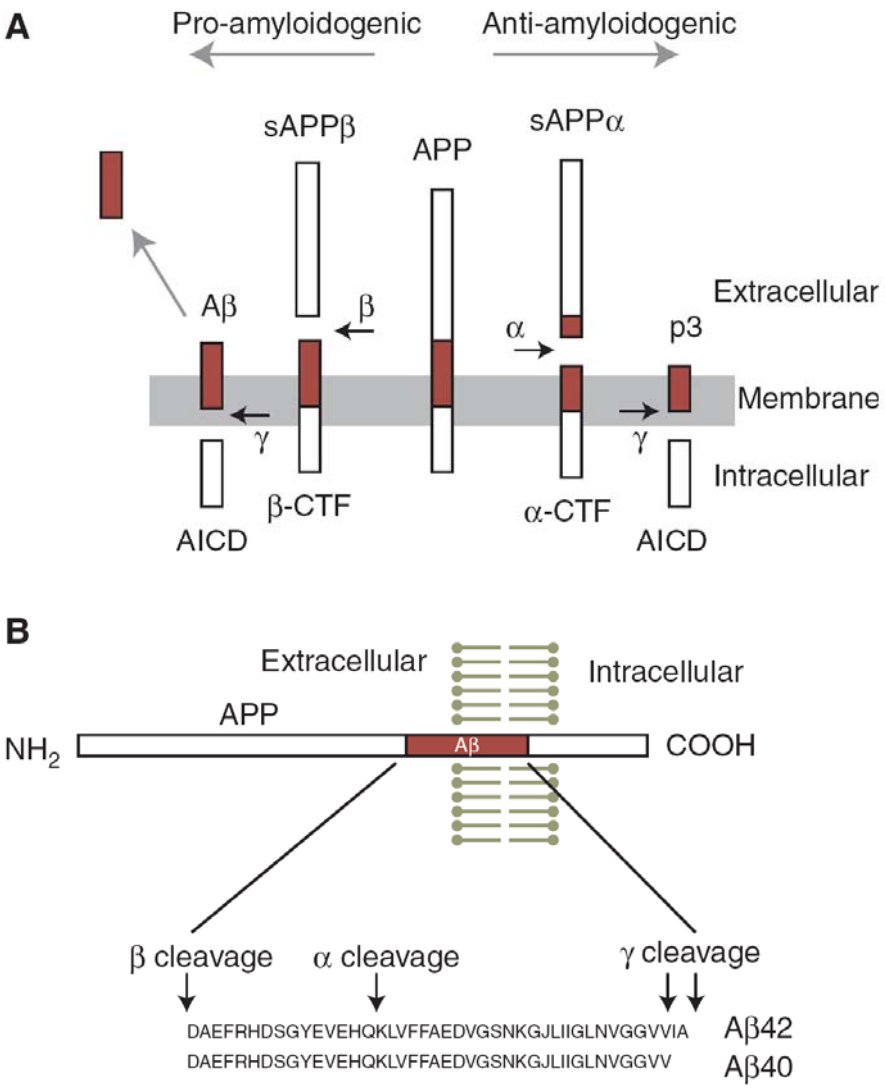

From: Sheng et al., 2012

Figure 1.2 APP processing and the formation of Aβ peptides. **a)** The full-length human amyloid precursor protein (APP) (middle) is a single transmembrane protein with an intracellular carboxyl terminus. Horizontal arrows indicate specific protease cleavage sites. In the amyloidogenic pathway (to the left), sequential cleavage of APP by β-secretase and γ-secretase releases the soluble extracellular domain of APP (sAPPβ), Aβ peptide, and the intracellular carboxy-terminal domain of APP (AICD). Cleavage by α-secretase instead (to the right) prevents formation of Aβ, producing sAPPα and p3 peptide. **b**) Diagram of the APP polypeptide and sequence of $A\beta_{40}$ and $A\beta_{42}$ peptides, with secretase cleavage sites indicated. CTF, Carboxy-terminal fragment of APP, before cleavage by γ-secretase.

Finally, the cytoplasmic AICD, which is released by γ-secretase cleavage (**Fig. 1.2a**), can translocate to the nucleus, regulate gene transcription, and affect calcium signaling, synaptic plasticity, and memory (Cao and Sudhof, 2001; Gao and Pimplikar, 2001; Ma et al., 2007). As a transcriptional regulator, AICD was proposed to affect chromatin

remodeling via binding to the histone acetyltransferase Tip60 (Cao and Sudhof, 2001). Interestingly, transgenic mice overexpressing the AICD alone exhibit AD-like features, including hyperphosphorylation and aggregation of Tau, neurodegeneration, and memory deficits (Ghosal et al., 2009). These studies underscore the importance of considering the involvement of non-Aβ products of APP in the pathogenesis of AD. Among the biological functions proposed for full-length APP, two are related to development. It has been proposed that APP is required to prune excess axon growth, through Caspase-6-mediated axonal degeneration upon growth factor withdrawal (Nikolaev et al., 2009) (Nikolaev et al. 2009). Also, full-length APP is required for proper migration of neuronal precursor into the cortical plate during neurodevelopment (Young-Pearse et al., 2007). Finally, during commissural axon navigation, APP, expressed at the growth cone, regulates Netrin-1-mediated commissural axon outgrowth (Rama et al., 2012).

Amyloid hypothesis and Aβ oligomers: As mentioned in **Chapter 1.1.1**, so far the only mutations classified as causative of EOAD are in *APP* or *presenilin 1* and *2* (encoding the catalytic subunits of γ-secretase), and almost all of them are responsible for an increased production of Aβ peptide or an increased $A\beta_{42}$/ $A\beta_{40}$ ratio (Tanzi and Bertram, 2005) (Blennow et al., 2006; Bettens et al., 2010). For many years, these findings strengthened the "Amyloid cascade hypothesis", postulated in 1992 by Hardy and Higgins (Hardy and Higgins, 1992). According to this hypothesis, the abnormal production of Aβ is the initial step in triggering the pathophysiological cascade that eventually leads to AD (Glenner and Wong, 1984; Hardy, 1997; Tanzi and Bertram, 2005). Aβ deposition and amyloid plaque formation are described as the main processes responsible for neuronal death and the other neuropathological hallmarks of AD (hyperphosphorylated Tau-protein and neurofibrillary tangles, vascular damage, and neuroinflammation) are consequences rather than causes of the disease. The proposed mechanism for Aβ causing neuronal loss and tangles formation goes through alterations in calcium homeostasis. SAD, in which there is no APP mutation causing high levels of Aβ deposition, is explained as due to other possible external causes that finally unchain the same cascade of events that triggers FAD. As an example, association between head trauma and Alzheimer's is proposed. Dementia pugilistica, exhibited by boxers, is thought of as a variant of Alzheimer's disease because these individuals exhibit both amyloid deposits and neurofibrillary tangles. Furthermore, amyloid deposition occurs as

an acute response to neuronal injury in both man and animals. This deposition could be caused by an induction of the APP gene through an interleukin-mediated stress response, because APP increases in response to a number of neuronal stresses. In this way no mechanistic difference is made between sporadic and familial cases of AD since in both cases the event initiating the pathology is amyloid deposition. Later studies revealed that the "Amyloid cascade hypothesis" failed to reconcile clinical and pathological observations, because of poor correlation between amyloid plaque burden and the severity of cognitive impairments in AD patients (Terry et al., 1991; Hibbard and McKeel, 1997; McLean et al., 1999; Giannakopoulos et al., 2003). Moreover, AD mouse models overexpressing mutated forms of human APP (hAPP) exhibited behavioral deficits long before the appearance of amyloid plaque pathology (Hsia et al., 1999; Mucke et al., 2000; Lesne et al., 2006). This observation suggested that synaptic damage rather than amyloid plaque-induced neuronal death better fitted the cognitive impairments observed. The most recent version of the "Amyloid cascade hypothesis" proposes that AD arises not from Aβ plaque-induced cytotoxicity but rather from synaptic toxicity mediated by soluble globular aggregates of Aβ. These non-fibrillar forms of Aβ have been shown to be the true toxic agent (Haass and Selkoe, 2007). In contrast to monomeric or fibrillar Aβ, non-fibrillar oligomeric forms induce synaptic dysfunction and synapse loss ("synapse failure") (Lambert et al., 1998; Walsh et al., 2002a; Cleary et al., 2005; Lesne et al., 2006; Haass and Selkoe, 2007; Lacor et al., 2007; Shankar et al., 2007). To gain greater insight into the mechanisms of action of Aβ oligomers, many laboratory protocols have been set up to experimentally reproduce them. One such protocol, published in 1998, allows the *in vitro* formation of an heterogeneous solution mainly composed by trimer, tetramer, pentamer and higher molecular weights up to 24-mer of Aβ peptide (Lambert et al., 1998; Lambert et al., 2001; Chromy et al., 2003; Krafft and Klein, 2010). The oligomers obtained by this protocol have been named Amyloid β-derived diffusible ligands (ADDLs), to emphasize the ligand-like nature of these assemblies and to distinguish them from generic soluble oligomers, which also include inactive assemblies. Indeed, it has been proposed that ADDLs exert their toxicity by directly binding to a membrane receptor in dendritic spines of excitatory pyramidal neurons (Lacor et al., 2007). The binding of ADDLs to the synapse membrane interferes with synaptic functions by disrupting signal transduction, which may be one of the neurotoxic mechanisms of action exerted by Aβ oligomers (Rauk, 2008). Moreover, ADDLs have been found to be responsible for

aberrations in dendritic spine morphology, abnormal synaptic receptor composition and reduced spine density (Lacor et al., 2007); formation of reactive oxygen species (De Felice et al., 2007); Tau hyperphosphorylation (De Felice et al., 2008); prolonged long-term depression (Wang et al., 2002); and inhibition of long-term potentiation (Lambert et al., 1998; Walsh et al., 2002b; Wang et al., 2002). Also, ADDLs trigger cell death and show cell selectivity (limited to neurons) and regional specificity (hippocampal but not cerebellar neurons die, in parallel to AD pathology) (Klein, 2002). These findings have been corroborated with other types of synthetic oligomeric preparations and finally also in the human AD brain. Using a different kind of oligomer preparation, researchers demonstrated that electrical or chemical stimulation increased the synaptic targeting of Aβ oligomers, with colocalization with NR2B N-methyl-$_D$-aspartate (NMDA) receptor subunits (Deshpande et al., 2009). In AD brains, oligomers of different sizes colocalized with synaptic markers in the hippocampus and cortex, where oligomer synaptic accumulation correlated with synaptic loss Different conformations of amyloid beta induce neurotoxicity by distinct mechanisms in human cortical neurons. Finally, of note is that, in addition to binding to plasma membranes, Aβ oligomers also bind to intracellular membranes, altering their permeability through a loss of calcium homeostasis and activating mitochondrial death pathways (Deshpande et al., 2006).

The "Aβ oligomer hypothesis" has resolved the paradox of the classical "Amyloid cascade hypothesis", by recognizing that the immediate relevant AD consequence of elevated Aβ peptide production is increased oligomer formation, not increased plaque deposition. Indeed, the brain levels of soluble Aβ species appear to correlate better with the severity of cognitive impairment than the density of plaque deposition (Lue et al., 1999; Naslund et al., 2000). From this view emerged the notion that insoluble amyloid deposits function as reservoirs of bioactive oligomers, which are continuously formed by detachment and re-association of recycling molecules within the fibril population (Carulla et al., 2005; Haass and Selkoe, 2007; Sanchez et al., 2011). Consistent with the idea that soluble Aβ is the main culprit for the spine shrinkage, a number of reports show synaptic loss in brain regions devoid of amyloid plaques (Mucke et al., 2000; Moolman et al., 2004; Rutten et al., 2005; Alpar et al., 2006). Moreover, since oligomers form at low concentrations, possibly before plaque formation, they provide

an explanation for the fluctuations in memory performance of AD patients at very early stages of the disease, as possible transient changes in oligomer levels.

However amyloid plaques are not totally rid of toxicity: several studies demonstrated a spatial correlation between amyloid plaques and dendritic abnormalities (e.g.changes in spine density), which tended to be more severe in the vicinity of amyloid plaques (Moolman et al., 2004; Tsai et al., 2004; Spires et al., 2005; Dong et al., 2007; Grutzendler et al., 2007; Spires-Jones et al., 2007), suggesting a link between amyloid plaques and spine loss. Also it has been reported a strong reduction of GABAergic innervation on cortical piramidal cells in the proximity of amyloid plaques, further implying that amyloid plaques continue to exert synaptotoxicity (Garcia-Marin et al., 2009; Leon-Espinosa et al., 2012). Moreover, as recently described *in vitro*, amyloid fibrils can catalyze the nucleation of new aggregates starting from Aβ monomers on their surface in a process of secondary nucleation (Cohen et al., 2013). This process begins once a critical concentration of amyloid fibrils has accumulated and, in the presence of new monomers, it overtakes the classical mechanism of primary nucleation and becomes the dominant mechanism by which toxic oligomeric species of Aβ are formed.

Finally, which oligomeric Aβ assemblies are the most pathogenic and how their accumulation in brain causes synaptic and neuronal dysfunction are still hot topics of intense study and debate (Benilova et al., 2012; Huang and Mucke, 2012).

1.1.3 Tau pathology

AD is a polyproteinopathy in which, apart from Aβ peptide, multiple proteins take on potentially pathogenic conformations and accumulate separately or together in the brain. In addition to amyloid plaques, the other main kind of AD histopathological lesion is neurofibrillary tangles (NFTs), which, like amyloid plaques, comprise misfolded or aggregating proteins. NFTs form intracellularly and are made up primarily of the aggregated protein Tau with abnormal posttranslational modifications, including increased phosphorylation and acetylation (Grundke-Iqbal et al., 1986; Iqbal et al., 2010; Cohen et al., 2011). Tau, together with MAP1 and MAP2, is one of the major microtubule-associated protein (MAP) in the mature neuron. An established function of MAPs is their interaction with tubulin and the promotion of its assembly into microtubules, and stabilization of the microtubule network. The microtubule assembly-

promoting activity of Tau is regulated by its degree of phosphorylation, with hyperphosphorylation of this protein depressing its biological activity (Iqbal et al., 2010). In the AD brain, hyperphosphorylated Tau levels are from three-to four-fold higher than in the healthy adult brain, and in this hyperphosphorylated state Tau detaches from microtubules and starts to polymerize into paired helical filaments (PHFs), which can in turn associate into bundles of pairs, finally resulting in the formation of NFTs (**Fig. 1.3**). Like for Aβ-pathology, there is increasing evidence that at early stages of the disease, toxicity is exerted by soluble and lower order tau species rather than by NFTs (Kopeikina et al., 2012; Ward et al., 2012).

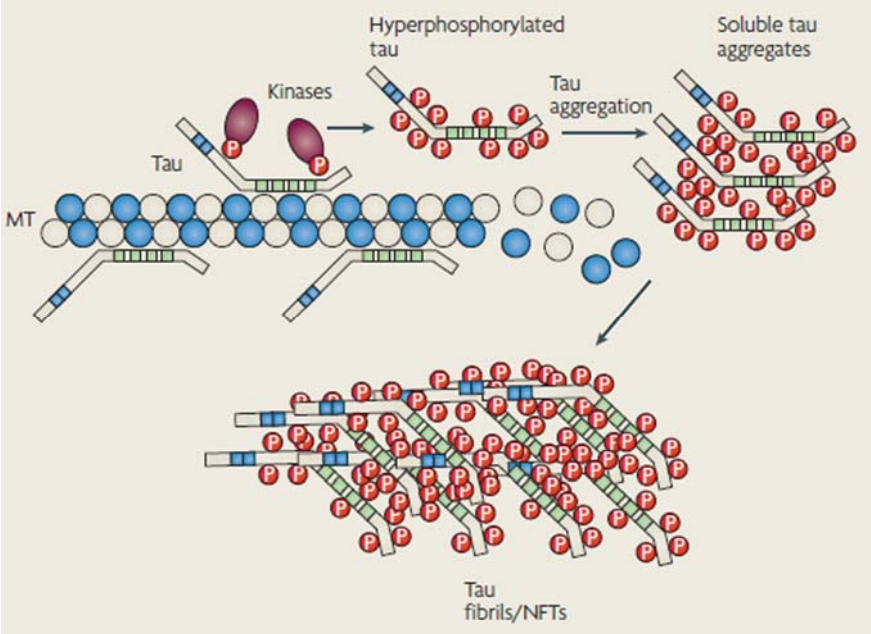

Adapted from Gotz and Ittner, 2008

Figure 1.3 Tau hyperphosphorylation and NFTs formation. The neurofibrillary lesions contain aggregates of the microtubule (MT)-associated protein Tau. Tau is a phosphoprotein owing to its high numbers of serine and threonine residues, and is therefore a substrate of many kinases. Under physiological conditions Tau is mainly localized to the axon for stabilization of MTs. Under pathological conditions, Tau is hyperphosphorylated, which means that it is phosphorylated to a higher degree at physiological sites, and also at additional "pathological" sites. Hypophosphorylated Tau dissociates from MTs, causing them to depolymerize, while Tau is deposited in aggregates such as NFTs. Like for Aβ-pathology, there is increasing evidence that at early stages of the disease, toxicity is exerted by soluble and lower order Tau species rather than by NFTs.

Tau can be phosphorylated at tyrosine, threonine or serine residues by various protein kinases, glycogen synthase kinase 3 (GSK-3) being the kinase that phosphorylates most of the AD-related sites on the Tau molecule (Hanger et al., 2009; Avila et al., 2012). Originally identified to participate in glycogen metabolism regulation, GSK-3 is

abundant in the central nervous system in its β isoform (GSK-3β), and it is precisely this form that modifies several neuronal proteins like Tau (Frame and Cohen, 2001). The phosphorylation of Tau by GSK-3β at specific sites can be analyzed by the use of antibodies such as PHF-1, AT8 or AT180, respectively detecting phosphorylation of Tau at serines 396–404; serines 199-202/threonine 205; and threonine 231/Serine 235 (Bertrand et al., 2010). Tau phosphorylation by GSK-3β in the hippocampus results in a toxic gain of function, since a transgenic mouse model which overexpresses GSK-3β shows degeneration of the dentate gyrus, which increases with age. This result may indicate that phospho-Tau is toxic inside neurons of the dentate gyrus (Avila et al., 2010).

In AD, the abnormally hyperphosphorylated Tau, apart from detaching from microtubules and causing their instability, is also capable of sequestering normal Tau, MAP1 and MAP2, further contributing to microtubule disruption and finally leading to neuronal cytoskeletal collapse (Delacourte and Buee, 1997) and ultimately neuronal failure (Garcia and Cleveland, 2001). Another crucial aspect of the toxicity of Tau is its effects on vesicle trafficking. Neurons are elongated cells that require efficient delivery of cellular organelles (such as mitochondria, endoplasmic reticulum, lysosomes), proteins, and lipids from soma to axons, dendrites and synapses to maintain their functionality. The delivery of organelles is performed jointly by microtubules, motor proteins and adaptors, such as MAPs, including Tau. Overexpressed normal Tau and/or hyperphosphorylated Tau have been found to impair the axonal transport of organelles, such as mitochondria (Stamer et al., 2002; Mandelkow et al., 2003; Dubey et al., 2008). Finally, although Tau is predominantly found in axons, where it is involved in microtubule stabilization and vesicle trafficking, newly discovered dendritic functions for this protein are emerging. Studies in cell cultures and genetically modified mouse models indicate that Tau can facilitate or enhance excitatory neurotransmission by regulating the distribution of synaptic activity-related signaling molecules (Huang and Mucke, 2012). However, when abnormally modified and showing pathogenic conformations, Tau becomes enriched in dendritic spines, where it interferes with neurotransmission (Hoover et al., 2010). Aβ oligomers promote this postsynaptic enrichment of Tau through a process that involves members of the microtubule affinity-regulating kinase (MARK) family (Zempel et al., 2010).

Tau pathology has been found to correlate with cognitive decline (Giannakopoulos et al., 2003) and with staging of AD (Arriagada et al., 1992) better than amyloid plaque

pathology, and the most used scale to state disease progression is based on NFT abundance and spread across the brain (Braak and Braak, 1995). However, mutations in the gene encoding for Tau (*Microtubule-associated protein Tau* - MAPT) have not been found in AD patients. In contrast, specific MAPT mutations have been described to be causative of Fronto Temporal Dementia (FTD), a neurodegenerative disease that in its familial form, associated with Tau mutations, is also known as FTD with parkinsonism linked to chromosome 17 or FTDP-17 (Cairns et al., 2007). FTD is a specific subtype of Fronto Temporal Lobar Degeneration (FTLD), a wide group of distinct diseases, such as Pick disease, corticobasal degeneration, progressive supranuclear palsy and tangle-only dementia; all characterized by predominant destruction of the frontal and temporal lobes. After AD and dementia with Lewy bodies (DLB), FTLD is the third most common neurodegenerative cause of dementia in industrialized countries. Most commonly, patients with FTD present a change in personal and social conduct, often associated with disinhibition, with gradual and progressive changes in language (McKhann et al., 2001). However, typically, at least in the early course of the disease, they do not have amnestic syndrome, which distinguishes them clinically from AD cases (Liscic et al., 2007). Histopathologically, they present Tau-positive inclusions (with associated neuron loss and gliosis) and amounts of insoluble Tau.

Tau mutations causing FTD generate Tau forms that are more readily phosphorylated and/or less prone to dephosphorylation (Alonso Adel et al., 2004). These forms are more predisposed to assembly into filaments and therefore amenable to rapid fibrilization into PHFs and NFTs (Nacharaju et al., 1999; von Bergen et al., 2001; Goedert and Jakes, 2005), or show impaired microtubule binding properties (Hong et al., 1998; Dayanandan et al., 1999).

Among the Tau mutations that promote its aggregation, some of the most well-known, due to their wide use in many transgenic models of Tau pathology, are P301L, P301S, V337M and R406W, as discussed in **Chapter 1.1.4**.

As in the case of Aβ, Tau aggregation into PHFs and next into NFTs is a multistage process with intermediate stages characterized by the presence of soluble oligomeric forms of the protein (Maeda et al., 2007). The first small non-fibrillary Tau deposits to appear are referred to as 'pretangles' and, unlike NFTs, they cannot be detected by β-sheet-specific dyes. Next, a structural rearrangement involving the formation of the characteristic pleated β-sheet occurs during the transition from pretangles to PHFs. Finally, PHFs further self-assemble to form NFTs (Ballatore et al., 2007). Recently, Tau

oligomers have emerged as the pathogenic species in Tauopathies and a possible mediator of Aβ toxicity in AD (Berger et al., 2007; Sahara et al., 2008). In the "Amyloid hypothesis" of AD, the Taupathology and the associated deficits are classified as consequences of the pathogenic mechanisms of Aβ. The accumulation of Aβ is thought to be one of the earliest molecular events in AD, activating intracellular signaling cascades that finally result in Tau hyperphosphorylation as a downstream event (Oddo et al., 2006).

Many findings support this hypothesis. In a human tissue culture system, Aβ induces Tau filament formation (Busciglio et al., 1995; Ferrari et al., 2003) and stereotaxic injections of $A\beta_{42}$ fibrils into the somatosensory cortex and the hippocampus of P301L human Tau transgenic mice leads to a five-fold increase in NFTs (Gotz et al., 2004). Also, Aβ-producing Tg2576 mice crossed with P301L Tau mutant mice show a more than seven-fold increase in NFT numbers in the olfactory bulb, the entorhinal cortex and amygdala compared to P301L single transgenic mice, whereas plaque formation is unaffected by the presence of the Tau lesions (Lewis et al., 2001). Moreover, a reduction of soluble Aβ oligomers significantly correlates with reduced Tau phosphorylation by GSK-3β, thereby suggesting a mechanism by which Aβ leads to increased NFT formation (Ma et al., 2006).

On the other hand, it was found that the presence of Tau is required for Aβ to induce neuronal and synaptic damage. In a first study, cultured hippocampal neurons obtained from wild-type, Tau knockout, and human Tau transgenic mice were treated with fibrillar Aβ. Neurons expressing either mouse or human Tau proteins degenerated in the presence of Aβ. In contrast, Tau-depleted neurons showed no signs of degeneration in the presence of Aβ (Rapoport et al., 2002). These results reveal a key role of Tau in the mechanisms leading to Aβ-induced neurodegeneration in the central nervous system. Recently, it has been demonstrated that Aβ-associated entorhinal cortex degeneration occurs only in the presence of phospho-Tau (Desikan et al., 2011). Tau-mediated Aβ toxicity has been proposed to involve the dendritic functions of Tau (Ittner et al., 2010). Indeed, Tau interacts with the tyrosine protein kinase Fyn, targeting it to the postsynaptic department, where it phosphorylates the NMDAR subunit 2B (NR2B). This phosphorylation mediates the interaction of NMDAR with the postsynaptic density protein 95 (PSD95), required for the Aβ excitotoxic downstream signaling (Salter and Kalia, 2004; Ittner et al., 2010). Consistently, it has been shown that Tau reduction protects both transgenic and non-transgenic mice against excitotoxicity and prevents

behavioral deficits in transgenic mice expressing human amyloid precursor protein (assessed by Morris water maze test), without altering their high Aβ levels (Roberson et al., 2007) (**Fig. 1.4**).

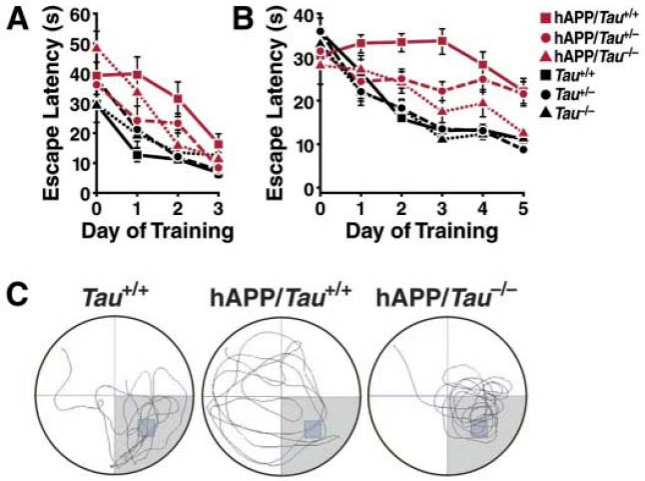

Figure 1.4 Tau reduction prevents cognitive deficits in hAPP mice. Morris water maze tesi in hAPP/*Tau*$^{+/+}$, hAPP/*Tau*$^{+/-}$ and hAPP/*Tau*$^{-/-}$ mice. **a)** Cued platform learning curves. **b)** Hidden platform learning curve. **c)** Representative path tracings on probe trial. hAPP/*Tau*$^{+/-}$ mice are less impaired in spatial learning than hAPP/*Tau*$^{+/+}$ mice, and hAPP/*Tau*$^{-/-}$ mice do not differ from controls without hAPP. Probe trial confirmed the beneficial effects of Tau reduction. hAPP mice are from J20 strain. Tau$^{-/-}$ are knockout mice for Tau protein. Tau$^{+/-}$ and Tau$^{+/+}$ mice express human Tau, respectively in homozygosis or in eterozygosis.

From: Roberson et al., 2007

Tau reduction also prevents the compensatory remodeling of inhibitory hippocampal circuits documented in AD mice as a consequence of the aberrant excitatory neuronal activity. In particular, Tau removal prevents the Aβ-induced increase in neuropeptide Y in the dentate gyrus and mossy fibers of the hippocampus and the calbindin depletion in granule cells of the dentate gyrus (Palop et al., 2007). Finally, in causing downstream toxicity, Aβ and Tau have been shown to target several components of the same system, thereby amplifying each other's toxic effects. A good example of this mode of interplay is the mitochondrial dysfunction that occurs in mouse models of AD, a pathogenic mechanism that is increasingly recognized to participate in neurodegeneration. In triple transgenic mice, which display Aβ and Tau pathologies (3xTg-AD mouse model, **Chapter 1.1.4**), both Aβ and Tau impair mitochondrial respiration, thus emphasizing a synergistic toxic effect of the two species (Ittner and Gotz, 2011).

Thus, while Aβ acts upstream of Tau, its adverse effects depend to a large extent on Tau, and the presence of both species exacerbates each other's toxicity. These conclusions are consistent with genetic studies: mutations in APP or presenilins that cause Aβ accumulation in the brain cause AD with amyloid plaques and NFTs, whereas

Tau mutations cause NFTs but not amyloid plaques or AD. The latter mutations cause FTD instead.

1.1.4 Mouse models of Alzheimer's disease

The identification of FAD-linked mutations led to the development of several mouse models that reproduce the main pathological hallmarks of this disorder. The generation of transgenic mice carrying mutations in AD-related genes (such as APP, APOE, BACE (encoding for β-secretase), PSEN1, PSEN2), combined with the use of different promoters, results in the reproduction of a broad variety of AD phenotypes, ranging from amyloid plaques to NFTs, neuritic dystrophy, gliosis, synaptic deficits and cognitive impairments. While none of the singly available transgenic models recapitulates the full spectrum of the human disease, they are a useful tool to dissect the complexity of AD and to assess the relative pathogenic impact of individual factors *in vivo*. A list of the currently available transgenic models of AD can be found at the Alzheimer research forum webpage: http://alzforum.org/res/com/tra/ and are here summarized in **Tables 3**, **4** and **5**.

APP models: The first APP transgenic mouse model showing significant amyloid pathology was published in 1995 (Games et al., 1995). In this mouse, known as the PDAPP mouse, neuronal expression of human APP (hAPP) bearing the Indiana mutation (V717F) is driven by the platelet-derived growth factor-β (PDGF-β) promoter. Mutant APP expression in this model is approximately 10-fold higher than the endogenous APP levels. The first plaques are observed in the hippocampus and cerebral cortex at 6 to 9 months of age, and both the number and the density of plaques increase with age. Astrocytosis and microgliosis have been reported (Games et al., 1995; Chen et al., 1998). Phosphorylated Tau-immunoreactive dystrophic neurites were observed after 14 months of age; however no paired helical filaments were detected (Masliah et al., 2001). Although PDAPP mice show significant amyloid deposition, with decreased synaptic and dendritic densities, no neuronal loss has been described in this model (Irizarry et al., 1997). Cognitive deficits in spatial learning discrimination have been reported in the Novel Object Recognition (NOR) test from the age of 6 months and in

the Morris water maze test from 13 months of age onwards (Dodart et al., 1999; Chen et al., 2000).

One year later, Hsiao et al. (Hsiao et al., 1996) generated the Tg2576 mouse. This strain expresses the most abundant APP isoform, APP695, with the Swedish double mutation, defined as amino acid substitutions at codons 670 and 671, first reported in a Swedish family (Axelman et al., 1994; Haass et al., 1995). Expression of the hAPP K670N/M671L transgene is driven by the hamster Prp promoter, reaching a five-fold overexpression of mutant APP on the endogenous mouse APP. Detergent-insoluble Congo Red-positive Aβ plaques were visible in frontal, temporal and entorhinal cortices, hippocampus, presubiculum and subiculum of APP695SWE mice as early as 7 months, increasing with age (Kawarabayashi et al., 2001; Westerman et al., 2002). Aβ plaques also surround vessel walls, causing microhemorrhages (Frackowiak et al., 2001; Fryer et al., 2003; Domnitz et al., 2005). Phosphorylated Tau was detected in dystrophic neurites, but no Tau filaments or NFTs were observed (Tomidokoro et al., 2001a; Tomidokoro et al., 2001b). Although these mice do not show significant neuronal loss, pronounced synaptic loss was observed near senile plaques (Spires et al., 2005). Nine- to ten-month-old Tg2576 mice develop memory deficits (Hsiao et al., 1996). These behavioral alterations correlate with the development of amyloid plaques and with impaired long-term potentiation.

A variety of other AD models combined the Swedish and the Indiana mutations. Several independent lines of transgenic mice were established with the same $hAPP^{Sw/Ind}$ construct, driven by the platelet-derived growth factor-β (PDGF-β) promoter, among these the J9 and J20 lines (Mucke et al., 2000). These two models show similar characteristics, with an exacerbation of phenotype in J20 compared to J9, which correlates with levels of hAPP present in the two models. Cerebral transgene expression, hAPP protein and Aβ peptide concentration were determined for both strains, with J20 showing higher transgene and protein levels than J9 (Mucke et al., 2000). The onset of amyloid plaque deposition was also different, with mice expressing higher levels of Aβ showing earlier and more extensive amyloid deposition. Many behavioural AD abnormalities were reported for J20 mice, such as cognitive impairments in the NOR task and in the Morris water maze test, starting from the age of 2-3 months (Palop et al., 2003; Harris et al., 2010). J20 Aβ-dependent deficits in hippocampal learning and memory have been described to correlate well with alterations in calcium- and synaptic activity-related proteins in granule cells of the

dentate gyrus, such as depletion of calbindin-D28K and of the immediate-early gene products Arc and Fos (Chin et al., 2005; Palop et al., 2005). In addition, J20 and J9 mice were observed to show spontaneous non-convulsive seizure activity in cortical and hippocampal networks, accompanied by compensatory GABAergic sprouting and enhanced synaptic inhibition (Palop and Mucke, 2010). Region-specific electrophysiological alterations described include LTP depression and lower Paired-Pulse ratio in the medial perforant pathway and lower synaptic transmission along the Schaffer collaterals. As already reported in other hAPP transgenic mouse models, no NFTs or Taupathology have been found for J20 and J9; however, for both models Tau reduction rescues the synaptic, network and cognitive impairments described above (Roberson et al., 2011), thus indicating the copathogenic relationship between APP and Tau. Neither of these models is representative of the massive degeneration of neural cell population found in AD patients.

It is important to mention that although APP is highly conserved evolutionarily, the sequence of Aβ is not, and Aβ derived from non-primates does not appear to aggregate or cause neurotoxicity. This observation explains why all the APP mouse models here reported have been engineered using hAPP.

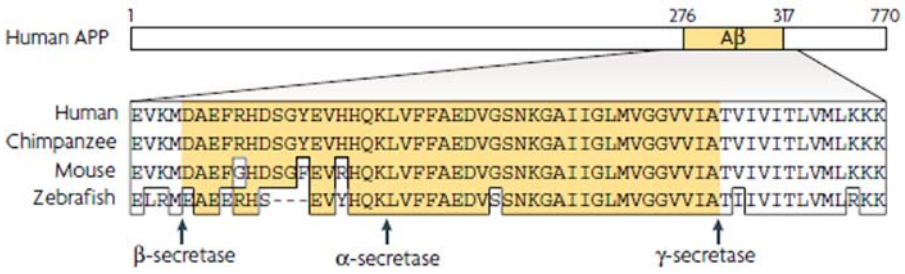

From Gotz and Ittner, 2008

Figure 1.5 Sequence of Aβ peptide. Sequence alignment of Aβ and flanking sequences from the human, chimpanzee, mouse and zebrafish.

Table 3. hAPP, BACE, PS-1 and PS-2 transgenic mouse models of AD

NAME/ SYMBOL	STRAIN NAME	TRANSGENE/ PROMOTER AND REGULATORY ELEMENTS	BEHAVIORAL PHENOTYPE	NEUROLOGICAL CHARACTERISTICS	PRIMARY CITATION
PDAPP (Line109) Symbol:APP		Minigene encoding codon 717 Valine to Phenylalanine mutation. Modified hAPP introns 6,7,8 in construct resulted in expression of 770, 751 and 695 isoforms of human APP/PDGF-β promoter.	Significant impairment on a variety of different learning and memory tests	Aβ deposits, neuritic plaques, synaptic loss, astrocytosis and microgliosis	Games et al., 1995; Rockenstein et al., 1995
APPSWE (2576) Symbol: APP	B6;SJL-Tg(APPSWE)2576Kha	Human AP695 cDNA with KM670/671NL/ hamster prion protein gene promoter	Memory deficits seen in 9-10 month old tg mice.	Numerous Aβ plaques, oxidative lipid and glycoxidative damages	Hsiao et al., 1996
APP751 Swedish (APP23) Symbol: APP		APP751Swedish/ murine Thy-1.2	Learning impairment in Morris water maze and a passive avoidance paradigm.	7x over expression of APP mRNA. Aβ deposits at 6 months, by 24 months in neocortex and hippocampus. Inflammation, neuritic and synaptic degeneration and Tau hyperphosphorylation. Evidence for Cerebral amyloid angiopathy (CAA)	Sturchler-Pierrat et al., 1997
PDGF-APP^{SwInd} line J9		The Swedish mutation was introduced into the PDGF-APP^{Ind} transgene. PDGF-APP$^{Sw, Ind}$ transgene injected into (C57BL/6 × DBA/2) F2 one-cell embryos.	N/A	2-4 month old tg mice had almost twice as much Aβ in their hippocampi, but much lower human APP levels than APP^{Ind} (line H6) tg mice. No amyloid plaques were detected until 8-10 months, yet electrophysiological recordings in hippocampal slice preparations detected synaptic transmission deficits.	Hsia et al., 1999
PDAPP^{SwInd} J20 Symbol:App	B6.Cg-Tg(PDGFB-APPSwInd)20Lms/2J	Tg construct: hAPPSwInd Promotor: PDGFB Injected: C57BL/6 x DBA/2F2 embryos	Spatial memory retention until acquisition of deficits at 6-7 months (Palop et al., 2003)	Total Aβ, and $Aβ_{42}$ in neocortical and hippocampus. High levels of $Aβ_{(1-42)}$ resulted in age-dependent formation of Aβ plaques in mutant hAPP mice but not wild-type hAPP mice	Mucke et al., 2000
Bace1 $^{-/-}$ Symbol: BACE	B6.129-Bace^{tm1Pcw}/J	Disrupted 2-kb of BACE 1 containing exon 1 (residues 1-87)/replaced with a neomycin-resistance gene/transfected into R1 ES cells/C57BL/6J blastocysts	Viable, fertile, normal in size and do not display any gross physical or behavioral abnormalities	No gene product detected in brain tissue. Primary cultures of cortical neurons do not secrete amyloid-β peptides (Aβ1-40/42 or Aβ11-40/42) or beta C-terminal fragments (CTFs)	Cai et al., 2001
hBACE Symbol: APP		hBACE / MoPrP.Xho /a 15.9-kb NotI linear fragment	N/A	BACE L, M and H express 7, 10 and 20-fold BACE over endogenous levels, respectively. No evidence of Aß deposition. Increased BACE expression in neuronal cell bodies, axons and synaptic elements of the hippocampus, puncta within the granule cell layer of the cerebellum, and neuropil within the spinal cord.	Lee et al., 2005
PS1 Null or **Presenilin 1** Symbol: Psen1	B6;129S-Psen1^{tm1Shn}/J	A targeting construct designed to disrupt exons 2 and 3 containing a neomycin cassette was electroporated into J1 and D3 ES cells.	Homozygous mutants die shortly after natural birth. Heterozygous mutants are viable and fertile.	Gross skeletal malformation, impairment in neurogenesis, massive neuronal loss, hemorrhages in the CNS.	Shen et al., 1997
TgAPParc Symbol: APP		HuAPP695 cDNA/ Arctic mutation (E693G)/ mouse Thy 1.2.	Spatial learning and memory deficit at 15 months in Barnes maze.	APParc levels ~threefold higher than endogenous; amyloid deposition in subiculum at seven months, spreading to thalamus at 18 months.	Ronnback et al., 2011
PS2 N141I		Human PS2 cDNA with N141I/ chicken b-actin promoter	N/A	Age-dependent increase in $Aβ_{42}$, higher level of insoluble Aβ	Oyama et al., 1998
PS2 null	B6.129P-*Psen2*^{tm1Bdes}/J	Exon 5 was replaced by a hygromycin cassette under the control of the PGK promoter	Viable and fertile no behavioral abnormalities.	No abnormal pathology, develop only mild pulmonary fibrosis and hemorrhage with age.	Herreman et al., 1999.

Adapted from http://alzforum.org/res/com/tra/

Tau models: In contrast to APP, no Tau mutations have been found in AD to date, thus accounting for an early lack of mouse models reproducing NFT and Tauopathy. In 1998, exonic and intronic mutations of Tau were identified in FTDP-17 (Hutton et al., 1998; Poorkaj et al., 1998; Spillantini et al., 1998). These findings established that Tau dysfunction causes neurodegeneration and dementia and opened the way for several research groups to reproduce NFT formation in mouse models.

The first published NFT-forming model expressed human P301L Tau under the control of the murine PrP promoter (Lewis et al., 2000). These mice developed NFTs (both in brain and spinal cord), abnormal Tau filaments in astrocytes, and oligodendrocytes, and displayed progressive motor disturbances by 10 months of age with a 50% reduction in the number of motor neurons in the spinal cord. Since then, of the 42 known mutations in Tau, several more have been expressed in transgenic mice. These include the missense mutations G272V, P301L, P301S, V337M and R406W, all of which make Tau more prone to abnormal hyperphosphorylation (Gotz et al., 2001a; Tanemura et al., 2001; Allen et al., 2002; Tatebayashi et al., 2002). One example is a model of Taupathology called VLW (Lim et al., 2001). VLW mice express human Tau bearing three FTDP-17 mutations (G272V, P301L and R406W), resulting in increased Tau phosphorylation and aggregation into neurofilaments with a pretangle appearance. Tau modification leads to lysosomal aberrations, the latter possibly causing neurodegeneration in Tauopathies.

The abnormalities caused by Tau hyperphosphorylation have also been studied using transgenic expression of GSK-3β, the main kinase for Tau. One approach used a tetracycline transactivation system that drives the overexpression of GSK-3β under the control of the CamK II α promoter in cortex, hippocampus and striatum (Tet/GSK-3β mouse, (Lucas et al., 2001). Transgenic GSK-3β is co-expressed with a β-galactosidase reporter, and is fusioned with a c-myc epitope, so that it is distinguishable from the endogenous one. By this model it was found that the overexpression of GSK-3β alone accounted for hyperphosphorylation of Tau in hippocampal neurons, resulting in pretangle-like somatodendritic localization of Tau. Reactive astrocytosis and microgliosis were also found in this model, accompanied by a neurodegeneration of dentate gyrus hippocampal cells and impairments in learning and memory.

Further, Tet/GSK-3β mice were crossed with VLW mice, and the progeny developed thioflavin S-positive Tau aggregates and filaments, and a faster and stronger development of the atrophy of the dentate gyrus of the hippocampus, indicating a

synergistic contribution of both genotypes to the exacerbation of the Tau phenotype described (Engel et al., 2006b).

Table 4. Tau models

NAME/ SYMBOL	STRAIN NAME	TRANSGENE/ PROMOTER AND REGULATORY ELEMENTS	BEHAVIORAL PHENOTYPE	NEUROLOGICAL CHARACTERISTICS	PRIMARY CITATION
***Tau* P301L-JNPL3** Symbol:Tau P301L	STOCK Tg(Prnp-MAPT*P301L) JNPL3Hlmc	Longest human Tau isoform with 4 repeats containing exon 10 and lacking exons 2 and 3 with P301L/ mouse prion promoter (MoPrP)	Severe motor and behavioral disturbances observed early	hTau level equal to endogenous Tau in hemizygous mice, but 2x the level in homozygous mice. NFT and neuronal loss in brain and spinal cord	Lewis et al., 2000
Tau G272V		Human Tau40 with G272V mutation/ murine prion protein promoter	No neurological deficits readily noticeable	Filaments in murine oligodendrocytes, associated with Tau phosphorylation at AT8 epitope 202/205 in vivo. In the spinal cord, fibrillary inclusions identified by thioflavin-S in oligodendrocytes and motor neurons	Gotz et al., 2001b
Tau P301L Line: pR5-182		Human Tau40 isoform with 4 repeats, exons 2 and 3 with P301L/ neuron-specific mouse Thy1.2 promoter.	Signs of Wallerian degeneration, neurogenic muscle atrophy, muscle weakness.	Numerous abnormal, Tau-reactive nerve cell bodies and dendrites; large numbers of pathologically enlarged axons containing neurofilament and Tau-reactive spheroids. Neuronal lesions similar to FTDP-17.	Gotz et al., 2001a
Tau R406W		Human longest Tau cDNA with R406W mutation containing myc and FLAG tags at N- and C- terminal ends, respectively/αCaMk-II promoter	Impaired associative memory in contextual and cued fear conditioning test. Abnormality in prepulse inhibition and forced swim test. No overt sensorimotor deficit.	Accumulation of insoluble Tau in aged mice. Congophilic hyperphosphorylated Tau inclusions only in forebrain neurons of aged mice.	Tatebayashi et al., 2002
Tau V337M		Human longest Tau cDNA with V337M mutation/PDGF-β promoter, neuron-specific mouse Thy1.2 promoter	Higher overall spontaneous locomotion. No significant difference in a Morris water maze test. Significant difference in elevated plus maze test and conditional fear test.	Neurons of irregular shape in hippocampus were immunoreactive for paired helical filament-associated Tau, and showed signs of atrophic cell death disappeared microtubules.	Tanemura et al., 2002
Tau^{vlw} Symbol: Tau		Linked mutations G272V, P301L, and R406W/site directed mutagenesis hCNS Tau cDNA/Mouse Thy-1 promoter with deleted lymphoid enhancer.		Mice overexpress human mutant Tau in cortex and hippocampus, minimally in spinal cord. Pretangle appearance in neurons expressing mutant Tau with filaments of Tau and lysosomes having aberrant morphology.	Lim et al., 2001
Tet/GSK3β Symbol: GSK-3β		Tet/GSK-3ß mice were generated by crossing mice expressing tTA under control of the CamKIIa promoter (tTA) with mice that have incorporated the BitetO construct in their genome (TetO). The double transgenic progeny (Tet/GSK-3ß) express transgenic GSK-3β in the brain.	Mice are viable and fertile	Overexpression of GSK-3β results in neurodegeneration such as β-catenin destabilization and pretangle-like somatodendritic localization of hyperphosphorylated Tau. Highest level of transgenic GSK-3β expression is in the hippocampus, then cortex.	Lucas et al., 2001

Adapted from http://alzforum.org/res/com/tra/

Crossbreedings of Aβ and Tau models: Since neither hAPP nor Tau transgenic mice recapitulate the full spectrum of AD-like pathology, double and triple transgenic mice have been developed, with the aim to generate a mouse model that simultaneously simulates more aspects of the human condition. For instance, some of the hAPP transgenic mice were crossed with mice expressing mutated forms of Tau. One example is the APP^{sw}-Tau^{vlw} transgenic mouse, obtained by crossing Tg2576 and VLW Tau lines (Ribe et al., 2005). This model shows enhanced amyloid deposition accompanied by neurofibrillary degeneration and overt neuronal loss in selectively vulnerable limbic brain areas.

In 2003, Oddo et al. reported a transgenic mouse model for AD that develops both amyloid plaques and Taupathology in AD-related brain regions (Oddo et al., 2003b). This was a triple transgenic mouse (3xTg-AD) bearing the mutated form of Tau_{P301L}, the mutated form of Presenilin-1 ($PS1_{M146V}$) and the mutated form of APP_{Swe}. This mouse model shows diffuse and fibrillar Aβ-aggregates initially in neocortical areas and later also in limbic areas. In contrast, Tau aggregates occur first in the hippocampus and then expand into further cortical regions. Both Aβ-deposition and Tau-aggregates follow a very similar expansion pattern to that described in AD patients. In 3xTg-AD mice, intracellular Aβ is the first manifestation of pathology, and extracellular Aβ-deposits occur prior to the aggregates of abnormal Tau. Synaptic dysfunction, including Long Term Potentiation (LTP) deficits, occurs in an age-related manner, prior to the onset of Aβ-pathology. Therefore, 3xTg-AD mice best reproduced the neuropathology of AD and became a most useful model for analyzing the relation between the proteins involved in AD. However, the simultaneous alteration of three mutant proteins does not allow the study of the pathological effects of one of these proteins alone.

Clearly the suitability of the AD models currently available largely depends on the purpose of the study in question. Even the most reductionist model can be informative when looking for a general proof of principle linking one specific aspect of AD pathology to a cause or an effect, in the absence of other copathogens. On the other hand, more complex models, simulating a broader spectrum of pathology aspects, may be appropriate in drug screening, for the identification of disease modifiers, or when looking at the interaction between more components of pathological cascades.

Finally, the extensive availability of AD models allows researchers to critically confirm findings across models, with the main purpose to ultimately translate them to the human condition.

Table 5. Double or triple-crossed models of AD

NAME/ SYMBOL	STRAIN NAME	TRANSGENE/ PROMOTER AND REGULATORY ELEMENTS	BEHAVIORAL PHENOTYPE	NEUROLOGICAL CHARACTERISTICS	PRIMARY CITATION
APPswe/PS1 (A246E) Symbol: APP695; Psen1 (See JAX datasheet)	B6C3-Tg(APP695)3Dbo Tg(PSEN1)5Dbo/J	Psen-1 tg: hPsen-1 (A246E substitution) (line N-5)/Prnp/B6C3H pronuclei. APP tg: StrainC3B6-Tg(APP695)3Dbo (founder line C3-3). Psen-1(A246E) crossed with APPSwe = double trangenic		Elevated levels of the $A\beta_{1-42(43)}$ peptide detected in mouse brain homogenates. By 9 months of age, numerous amyloid deposits detected and they increase dramatically between the ages of 10 and 12 months	Borchelt et al., 1997
APP sw/Tau (P301L)/PS1 (M146V) 3x tgSymbol: APP/Tau/PS1	B6;129-*Psen1*^{tm1Mpm}Tg(APPSwe,TauP301L)1Lfa/J	$APP_{Sw(KM670/671NL)}Tau_{(P301L)}$/Thy-1.2 promoter/ co-microinjected into pronuclei of embryos of $PS1_{M14V}$KI mice	Cognitive impairments by 4 months as retention/retrieval deficits occur prior to any plaques or tangle pathology. Early cognitive deficits can be reversed by immunotherapy.	Age related and progressive plaques and tangles. Deficits in LTP correlate with accumulation of intraneuronal Aβ. Tau and APP expression doubled in homozygous mice in hippocampus and cerebral cortex.	Oddo et al., 2003
BACE x APP(V717I) Symbol: BACE/APP		Crossed BACE-1 (Line 16) (Willem) withAPP(V717I)/mutation hBACE and APP London/mouse Thy 1		Amyloidogenic processing is increased at Asp1 and Glu11 resulting in more Aβ peptides in bigenic brains. In older bigenic mice BACE1 increased the number of diffuse and senile amyloid plaques. Vascular amyloid deposition was reduced compared single APPV717I mice.	Willem et al., 2004
APP^{swe}/Tau^{vlw} Symbol: APP/Tau		Crossed APPSwe (Tg2576) and Tau^{vlw}	At 16 months single APPSwe and double tg mice have increased spatial memory impairment compared to single Tau^{vlw}	Double tg mice showed enhanced amyloid deposition accompanied by neurofibrillary degeneration and overt neuronal loss in selectively vulnerable brain areas.	Perez et al., 2005
Tet/GSK-3β/ Tau^{vlw} Symbol: GSK-3β/Tau		Crossed Tet/GSK-3β with Tau^{vlw}/CamKIIa and Thy1.2	Mice are viable and fertile	Mice show Tau hyperphosphorylation in hippocampal neurons, with thioflavin-S staining and formation of >10nm filaments. Atrophy seen in Tet/GSK-3β mice develops faster in these Tet/GSK-3β/Tau^{vlw} mice.	Engel et al., 2005

Adapted from http://alzforum.org/res/com/tra/

1.1.5 Alternative hypotheses of AD

Although widely accepted for the explanation of FAD, the "amyloid hypothesis" is today under profound discussion as far as the understanding of sporadic forms of the disease is concerned. In fact, twenty years after the postulation of the hypothesis, efficient clinical trials for the therapy of AD are still lacking, possibly due to the fact that, in contrast to assumptions made, the molecular mechanisms underlying the genetic and sporadic forms differ. In this case, many of the transgenic animal models of AD mirroring the genetic form of the disease would still be of great use to unravel Aβ pathology, but would be incomplete in the representation of SAD mechanisms (Schwab

et al., 2004). As SAD is the most common form of the disease, intense research effort is being channeled into its complex biology beyond Aβ, and new hypotheses are emerging that take into account the most common risk factor for this late-onset form of the disease, namely age (Bekris et al., 2010).

***Age-based hypothesis*:** The so-called "Age-based hypothesis" of AD (Herrup, 2010) proposes a new cascade of events: first an initiating injury, followed by a chronic neuroinflammatory response that would finally lead to a cellular change of state for almost all cell types of the brain, resulting in degeneration and dementia. In this sequence of events, the amyloid cascade of plaque deposition is included as tightly linked with neuroinflammation in a feed-forward cycle in which each one exacerbates the other; however, the two processes are mechanistically distinct. Starting from aging, the first thing taken into account by the new hypothesis is the fact that an elderly brain is physiologically characterized by a progressive slowing of brain functions in every domain (cognition, motor functions etc); a progressive loss of the structural complexity of brain cells; a progressive loss of responsiveness of the immune system, and a progressive failure of neuroprotective features such as mechanisms of clearance of misfolded proteins. These conditions, although not pathological, make the elderly brain weaker against the insults of diseases. Therefore any kind of injury could unchain an uncontrolled response that could mark the difference between physiological cognitive decline and the start of conditions that may lead to Alzheimer's dementia. Examples of such injuries include a physical head trauma, an infection, a vascular event or metabolic stress associated with concomitant pathologies such as adult-onset diabetes. The hypothesis of vascular injuries (e.g. a microstroke) as the initiating event of the conditions leading to AD would fit with the observed protective effect of improved cardiovascular health against AD onset and with APOε4 as a genetic risk factor, since ApoE is recognized to affect the cardiovascular system. Whatever the initial injury, while in a young brain it would lead to a limited inflammatory response, the failure of homeostatic mechanisms in the aged brain triggers an exacerbated immune response that could eventually transform into chronic inflammation. Although we do not know whether chronic inflammation is the cause or consequence of the disease, it has been shown to be tightly correlated with AD pathology. Indeed, it has been reported that non-steroidal anti-inflammatory drugs (NSAIDs) lower the risk for AD (McGeer et al., 1996; Stewart et al., 1997; Vlad et al., 2008); elevated levels of cytokines Il-1, Il-6 and

TNFα have been found in human AD brains (Griffin et al., 1998; Akiyama et al., 2000); microgliosis and astrogliosis are also prevalent (Heneka and O'Banion, 2007). Moreover, inflammation cytokines increase Aβ peptide production, and Aβ aggregates can in turn stimulate the immune response generating a feed-forward loop of amyloid deposition (Griffin, 2006). In this way, the inflammation step of the "Aging hypothesis" is connected to the classical "Amyloid hypothesis", as it involves two independent cycles, each one strengthening the other. This would explain why FAD arises before SAD, since in the former cases no injury is required to develop sustained amyloid deposition and chronic inflammation. It would also explain why cases of SAD are characterized, exactly like the familial phenotype, by the presence of amyloid plaques. Finally this hypothesis would suggest that patients with high levels of amyloid deposition but cognitively normal possibly result from the absence of the establishment of the sustained inflammatory environment required for the progression of disease, even after amyloid deposition has started. The last step of disease progression, according to "Aging hypothesis", would involve changes in cellular state, attributable to the setting up of a new brain chemistry in the chronic inflammation environment. Indeed, stressed neurons show a transition from a normal postmitotic state to the re-activation of cell cycle events, with complete DNA replication but without undergoing cell division (Yang et al., 2001; Arendt, 2012). In this new state, from which neurons cannot further reverse, cells are at risk of death, thus increasing the global risk of neurodegeneration and dementia. The new model incorporates Taupathology in the final stages of the disease as a part of the cell death program, after the establishment of the cellular change of state.

***Inflammation hypothesis*:** Another alternative postulation to the "Amyloid hypothesis" stresses neuroinflammation as the primary cause of illness, rather than a consequence of amyloid pathology. This alternative notion is based on the above-mentioned observation of the concomitance of AD and chronic inflammation, and on new findings such as those provided by GWAS, which implicate inflammatory mediators of the innate immune system (e.g. CLU, PICALM, CR 1) in the aetiology of the disease. Moreover, recent paradigms of immune challenge in embryonic mouse brain during late gestation predisposed adult animals to the development of an AD-like phenotype in later life (Krstic et al., 2012b). The "Inflammation hypothesis" of AD (reviewed in Krstic and Knuesel, 2013) first proposes a new mechanism of protein extrusion, originating from

spheroid-like varicosities along axons (Doehner et al., 2010). In the elderly brain, this mechanism compensates for aging-dependent failure in protein clearance. Chronic inflammation and cellular stress during aging, caused by infections or diseases, could lead to hyperphosphorylation of Tau (Krstic et al., 2012b), which in turn is missorted to somatodendritic compartments, thus impairing axonal transport and the protein extrusion mechanism. Blockade of axonal transport leads to synaptic destabilization or loss and is accompanied by PHF formation in neurites. A further increase in Tau phosphorylation can destabilize microtubules and the actin cytoskeleton along axons, with the induction of axonal swellings and membrane leakage at the site of extrusion varicosities. Cellular proteins on their way to be extrused along axons become exposed to lysosomal proteinases, thereby promoting the formation of neurotoxic peptides. Glia, which normally remove the extrused proteins by phagocytosis, becomes hyperreactive and cannot properly remove the forming dystrophic neurites, thus leading to a toxic pro-inflammatory environment that affects surrounding neurons. Supported by electron microscopy analysis, senile A plaques in this model are proposed to be formed from axonal swellings and leakage, where APP starts to be accumulated, while PHFs at the somatodendritic compartment continue along their way to NFTs. Finally, imbalances in excitatory–inhibitory neurotransmission and the neurotoxic pro-inflammatory environment initiate pathology in interconnected brain areas (Krstic and Knuesel, 2013).

In both alternative models proposed, chronic inflammation is the main trigger for the onset of AD. More evidence is required to ascertain the new models of SAD emerging from revisiting the classical “Amyloid cascade hypothesis”. Shedding light on the new biology of late-onset AD, accounting for the majority of patients, is the highest priority, in order to find new therapeutic targets and strategies.

1.2 Extracellular matrix protein Reelin and Alzheimer's disease

1.2.1 Extracellular matrix in health and disease

Around 20% of the human brain is occupied by Extracellular space (ECS), with volume and composition varying in the different brain regions (Dansie and Ethell, 2011). The ECS is filled with Extracellular Matrix (ECM), an intricate network of macromolecules (mainly proteins and polysaccharides) that surround neuronal cell bodies and proximal dendrites, controlling the three-dimensional organization, growth, movement, and shape of neurons and maintaining their structural integrity (Celio et al., 1998). The ECM also extends into the synaptic cleft, maintaining synapse integrity as well as mediating trans-synaptic communications between neurons (Dansie and Ethell, 2011). ECM composition ranges from scaffolding proteins such as laminin, fibronectin and tenascin, which link various ECM components into a net, to heavily glycosylated proteins such as proteoglycans, to proteolytic enzymes that cleave ECM components or receptors, like matrix metalloproteases (MMPs). Laminin, fibronectin and tenascins, which provide a structural scaffold for the ECM, are involved in cell migration and axon guidance during brain development (Powell and Kleinman, 1997; Dansie and Ethell, 2011). In the adult brain, the ECM regulates various aspects of synaptic plasticity, a term that refers to all the structural, morphological and functional changes occurring at synaptic level as a consequence of neuronal activity (e.g. the formation of dendritic filopodia, the remodeling of dendritic spines on excitatory neurons). The ECM controls synaptic plasticity induction (which is associated mainly with Ca^{2+} influx in postsynaptic excitatory neurons and Ca^{2+} homeostasis) and consolidation (which is related mainly to changes in the actin cytoskeleton, local protein synthesis and synaptic adhesion, which are thought to support the stabilization of the new synaptic configurations) (Dityatev et al., 2010). Activity-dependent modification of the ECM regulates dendritic spine growth by inducing ECM interaction with specific postsynaptic receptors, such as integrins, apolipoprotein E2 receptor (ApoER2), low density lipoprotein receptor (LRP), and very low density lipoprotein receptors (VLDLR). Alternatively, the ECM can control dendritic spine growth by influencing the functions of other synaptic proteins, e.g. ECM modifiers, like MMPs9, that cleave cell adhesion molecules (CAMs), such as dystroglycan, activating integrin receptors and finally provoking the

actin cytoskeleton modifications responsible for the growth of spines (Wlodarczyk et al., 2011).

Since synaptic plasticity is the key process underlying the maintenance of cognitive functions in the adult brain (such as learning and memory), the control of ECM functions is fundamental to maintain brain health and for implications in neurodegenerative diseases. For instance, recent studies implicate MMP-9 in aberrant synaptic plasticity, which is postulated to underlie neuropsychiatric disorders (Kaczmarek, 2013). It is noteworthy in this regard that the AD brain is characterized by abnormal dendritic spine morphology and density (Spires-Jones and Knafo, 2012), that may be influenced by alterations in ECM components. Since Aβ-containing senile plaques form within the ECS, they most likely affect ECM organization and composition. Several proteoglycans, such as agrin, syndecans and glypicans are associated with senile plaques (Bonneh-Barkay and Wiley, 2009). It appears that the ECM helps to protect against the neurodegenerative decline while age-related changes in the ECM composition may contribute to the AD pathology (Dansie and Ethell, 2011).

1.2.2 Reelin protein in the developing and adult brain

Reelin gene and protein: Among the ECM proteins that control synaptic functions and synaptic plasticity in the adult brain is the glycoprotein Reelin. This ECM protein is encoded by *RELN* gene in humans, located on chromosome 7q22, while the orthologous mouse *Reln* gene maps on chromosome 5 (DeSilva et al., 1997; Royaux et al., 1997). The genomic structures of the mouse and human Reelin genes are highly conserved and both encode an mRNA of approximately 12 kb, which is translated in a large secretable protein of ~450 kDa (Lacor et al., 2000; Derer et al., 2001). Mouse full-length Reelin is a protein of 3461 aminoacids. Its N-terminus is highly glycosylated and contains a 27 aminoacids signal peptide that drives Reelin extracellular secretion (D'Arcangelo et al., 1995). This is followed by a homology domain to the ECM protein F-spondin. Next comes a Reelin unique domain, a region with no homology with other known proteins that hosts the CR-50 epitope. Reelin-specific antibodies against this epitope have been realized, showing neutralizing activity both *in vitro* and *in vivo* (Ogawa et al., 1995; Del Rio et al., 1997; Miyata et al., 1997; Nakajima et al., 1997). The central sequence consists of eight ‘‘Reelin repeats’’, each of which is composed by two domain of 350–390 amino acids called A and B, separated by an Epidermal growth factor (EGF)-like

motif in the center. This is followed by a highly positively charged C-terminus, indispensable for protein extracellular secretion (D'Arcangelo et al., 1995) (**Fig. 1.6**). In a study made in cerebellar neurons it was found that Reelin secretion takes place through the constitutive secretory pathway (Lacor et al., 2000). One year after in Cajal-Retzius (CR) cells, the neurons expressing Reelin in developing cortex and hippocampus, it was discovered a novel secretory pathway for Reelin that is transported by a specialized rough endoplasmic reticulum (RER) to axon terminals, where it is released in the Marginal Zone of developing cortex (Derer et al., 2001).

Reelin is processed proteolytically at two sites to produce a total of five distinct fragments named after the position and number of repeats and ranging from 80 to 370 kDa in size (Lambert de Rouvroit et al., 1999; Tissir and Goffinet, 2003) (**Fig. 1.6**). The proteases involved in Reelin cleavage are still unclear; however, two recent studies identified the serine protease tissue plasminogen activator (tPA) and two matrix metalloproteinases, ADAMTS-4 and ADAMTS-5, as Reelin- cleaving enzymes (Hisanaga et al., 2012; Krstic et al., 2012a). Neither are the physiological relevance of Reelin processing and the specific functions for individual Reelin fragments fully undestrood. While, as mentioned above, blocking Reelin N-terminus neutralizes its activity, the central fragment is required and sufficient for normal cortical development in cultured embryonic brain slices (Jossin et al., 2007). Cell adhesion assays have shown that the CR-50 epitope in the N-terminal domain Reelin form large homomeric protein complexes, while full-length Reelin forms disulfide-linked dimers (Utsunomiya-Tate et al., 2000; Kubo et al., 2002).

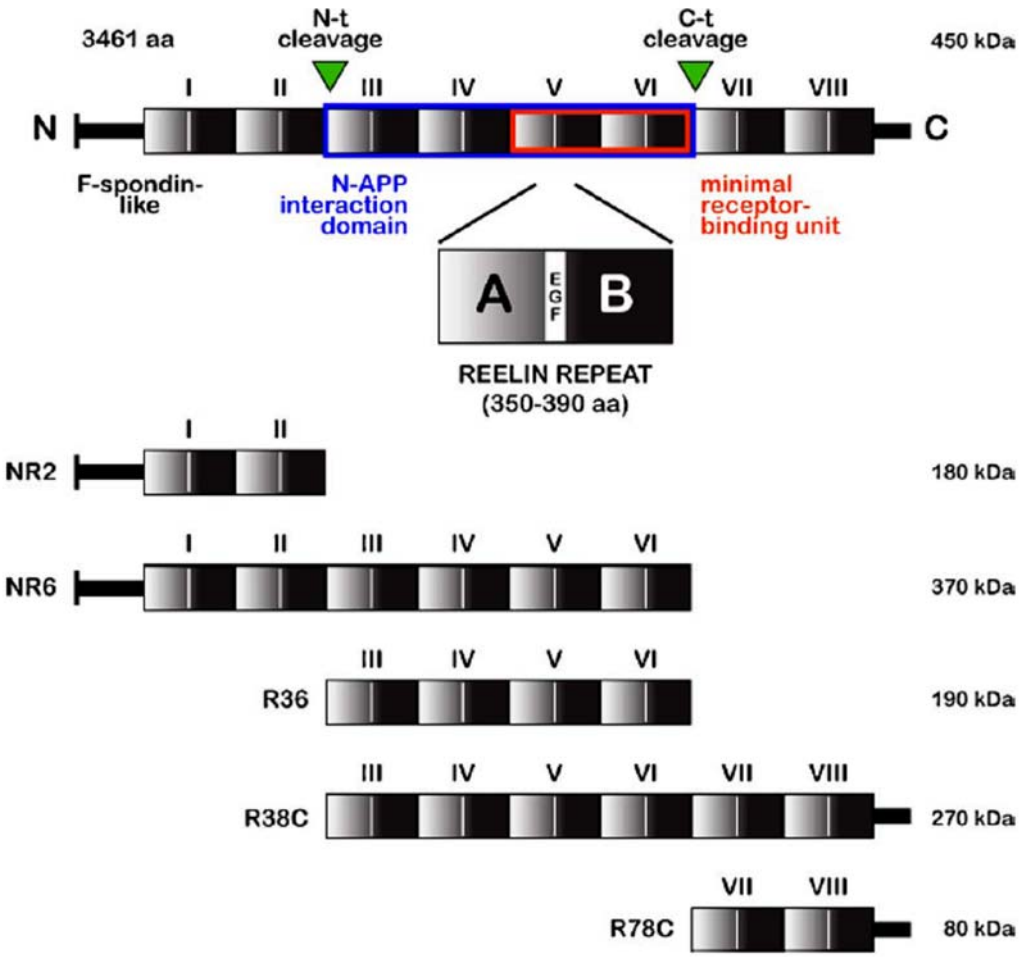

From: Knuesel, 2010

Figure 1.6 Reelin protein and proteolytic processing. Schematic representation of Reelin protein showing the N-terminal domain, F-spondin homology domain, Reelin unique domain, eight ‘‘Reelin repeat’’ domains, and the C-terminal domain. Each Reelin repeat is composed by two homologous subrepetitions (A and B), separated by an EGF-like motif in the center. Reelin is processed proteolytically at two sites (arrowheads) to produce a total of five distinct fragments ranging from 80 to 370 kDa in size, whereas full-length Reelin molecular weight is of 450 kDa.

Reelin signaling pathway: Reelin acts through the receptors apolipoprotein E receptor 2 (ApoER2) and very-low density lipoprotein receptor (VLDLR) (D'Arcangelo et al., 1999; Hiesberger et al., 1999; Utsunomiya-Tate et al., 2000; Strasser et al., 2004). Binding of Reelin to VLDLR and ApoER2 induces their clustering and the phosphorylation of disabled 1 (Dab1) (Howell et al., 1999), an intracellular adaptor protein that interacts with NpxY motifs in the cytoplasmic tails of both receptors. The phosphorylation of Dab1 requires the Src family of tyrosine kinases (SFKs) Fyn and Src (Bock and Herz, 2003; Jossin et al., 2003; Kuo et al., 2005) and triggers the activation of a complex signaling cascade, involving many cytosolic kinases, among these

phosphatidylinositol-3-kinase (PI3K), Akt/PKB, Erk1/2 and mTor, ending with the inhibition of GSK-3β, one of the main kinases that phosphorylates the microtubule-stabilizing protein Tau (Howell et al., 1997; D'Arcangelo et al., 1999; Hiesberger et al., 1999; Howell et al., 1999; Beffert et al., 2002; Arnaud et al., 2003b; Bock and Herz, 2003; Ballif et al., 2004; Gonzalez-Billault et al., 2005; Simo et al., 2007) (**Fig 1.7**).

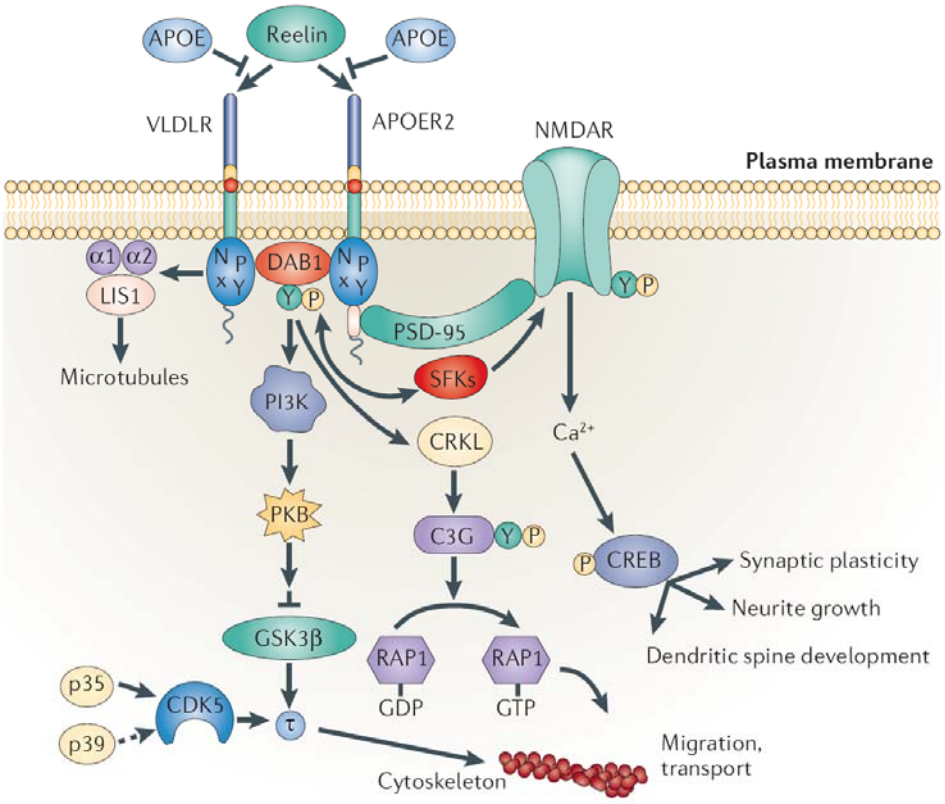

Adapted from: Herz and Chen, 2006

Figure 1.7 Reelin signalling events in neurons. Scematich representation of Reelin signaling cascade. Reelin binds to lipoprotein receptors, the VLDLR and the APOER2, with high affinity at the cell surface. Binding of Reelin to the receptors induces feed-forward activation of DAB1, an adaptor protein that interacts with NPxY motifs in both receptor tails. The clustering of DAB1 activates SRC family tyrosine kinases (SFKs), which potentiates tyrosine phosphorylation of DAB1. Phosphorylated DAB1 further activates, among other cytosolic kinases, phosphatidylinositol-3-kinase (PI3K) and subsequently protein kinase B (PKB). PKB activation inhibits the activity of glycogen synthase kinase 3β (GSK3β). As a result, phosphorylation of Tau is reduced, promoting microtubule stability.

Tyrosine phosphorylation of Dab1 in response to Reelin leads to Dab1 polyubiquitination and degradation via the proteasome pathway (Arnaud et al., 2003a). These events may mediate the phosphorylation-dependent endocytosis of the entire Reelin signaling complex. With Reelin being targeted to the lysosome and Dab1 being

degraded by the proteasome, the signal is terminated and the receptors recycle back to the membrane (Bock et al., 2004; Morimura et al., 2005). It is important to remark that *reeler*, *Dab1*$^{(-/-)}$ and *Apoer2*$^{(-/-)}$/*Vldlr* $^{(-/-)}$ mice are phenotypically almost identical, which highlights the essential role of Dab1 and Reelin receptors in the Reelin pathway.

***Reelin expression pattern and functions*:** In the embryonic brain, Reelin is expressed by Cajal-Retzius (CR) cells at the surface of the developing neocortex (Marginal Zone) (Tissir and Goffinet, 2003) and in the Outern Marginal Zone of Hippocampus starting from E10. From these sites Reelin directs corticogenesis and lamination of hippocampus (Alcantara et al., 1998; Rice and Curran, 2001; Soriano and Del Rio, 2005) (**Fig. 1.8**). Reelin is also expressed in granule cells of the developing cerebellar cortex, where it is necessary for the migration and positioning of Purkinje cells (Mariani et al., 1977).

reeler mice (bearing a homozygous mutation of *Reln* gene that impairs protein function) (Falconer, 1951) show inversion of neocortical layers and the loss of the classical inside-outside pattern of lamination (Caviness, 1976), a severe perturbation of the lamination of the hippocampus and a very small and non-foliated cerebellum (Hambrugh, 1963). For a schematic representation see **Fig. 1.8**. Phenotypically, *reeler* mice exhibit uncoordinated and unsteady gait, tremors, severe ataxia, and usually early death around the time of weaning (Falconer, 1951), a condition that resembles lissencephaly in humans.

Apart from guiding neuronal migration, there is increasing evidence that Reelin controls synaptogenesis and synaptic maturation during development (D'Arcangelo et al., 1995; Alcantara et al., 1998; Rice and Curran, 2001; Soriano and Del Rio, 2005; Cooper, 2008).

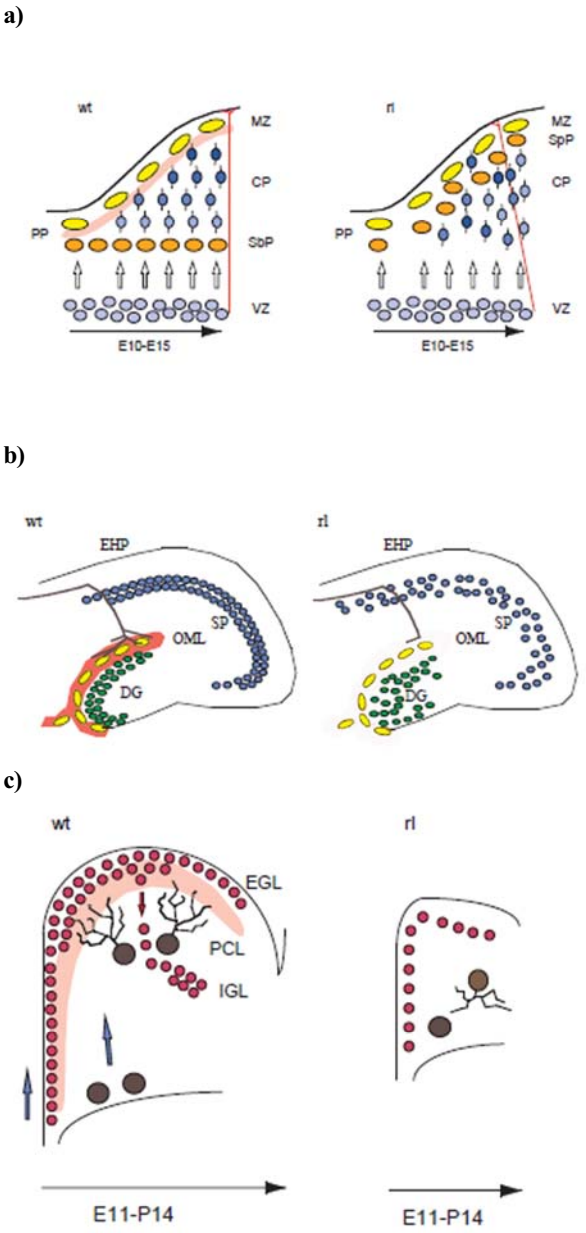

Figure 1.8 Reelin and the development of the neocortical layers, hippocampus and cerebellum.

a) During embryonic days (E) 10–16, cortical neurons are born near the ventricular zone (VZ) and migrate radially toward the pial surface along radial fibers (red line). The first migrating neurons form the preplate (PP), composed of CR (yellow) and subplate neurons (orange). CR cells produce Reelin (shaded red) and secrete it into the extracellular environment of normal mice (wt). The first cortical neurons (light blue) bypass the subplate neurons in the normal but not in the reeler cortex, where Reelin is absent. Later-generated cortical neurons (darker shades of blue) bypass cohorts of earlier neurons and form distinct layers within the cortical plate (CP) that develops between the marginal zone (MZ) and subplate (SbP) in normal mice. In reeler mice, cortical neurons do not form layers, and they are found deep to subplate neurons, which form a superplate (SpP) near the marginal zone.

b) In hippocampus of normal mice (wt), Reelin (shaded red) is expressed by CR-like cells (yellow) in the outer molecular layer (OML) separating the dentate gyrus (DG) from the hippocampus proper. Hippocampal pyramidal cells (blue) in normal mice form a compact layer, the stratum pyramidale (SP), which remains scattered in reeler mice. Also, the granule cells of the DG (green) do not form a compact layer in reeler mice. In addition to cell migration defects, the absence of Reelin in the OML causes a reduction of the branching of entorhinohippocampal (EHP) fibers (brown) in reeler mice.

c) Cerebellum development begins around E11. Granule cells (red) originate from the rhombic lip and migrate tangentially over the surface of the developing cerebellum to form the external granular layer (EGL). These cells produce Reelin (shaded red) in normal animals (wt). Purkinje cells (brown) migrate radially from the ventricular zone to a location near the Reelin producing granule cells. In reeler mice, granule cells do not produce Reelin, Purkinje cells remain in a deep subcortical location, and granule cells are reduced in number. As a result, the reeler cerebellum is very small. During postnatal days 0–14, granule cells in the normal cerebellum migrate inwardly across the Purkinje cell layer (PCL) to form the inner granular layer (IGL).

From: D'Arcangelo and Curran, 1998

In the adult cerebral cortex most CR cells disappear starting from P5, leading to decreased Reelin expression. Concomitantly it is reported a switch of Reelin expression from CR cells to a subset of Calretinin negative GABAergic interneurons throughout the neocortex (mainly in layers I and V) and hippocampus (strata oriens and radiatum of CA1 and CA3; stratum lacunosum moleculare and hilus of dendate gyrus). Starting from P21, CR cells are no longer found in cortex, while some few remnant CR cells survive in hippocampus maintaining Reelin expression (Alcantara et al., 1998).

In adult brain Reelin is also expressed in hypothalamus, caudate-putamen, medial septum and olfactory bulb (Alcantara et al., 1998). In the olfactory bulb Reelin is expressed by mitral cells from E12 until adult life, although expression levels decrease starting from the first postnatal week. In addition, Reelin in adults is expressed in peripheral tissues: in serum and platelet-poor plasma of rats, mice, and humans; and in chromaffin cells within the rat adrenal medulla and in liver (Smalheiser et al., 2000).

The shift in Reelin expression between the embryonic and postnatal brain is indicative of a different, non-developmental function for the Reelin signaling pathway in the adult. In contrast to the developing brain, where Reelin functions have been widely unraveled, less is known about its function in the adult brain yet. In adults, this protein is expressed in synaptic contacts, where it regulates the induction of synaptic plasticity, by controlling Ca^{2+} influx in postsynaptic excitatory neurons through NMDA receptors (Herz and Chen, 2006). Indeed Reelin-induced phosphorylation of Dab1 triggers phosphorylation of NR2 subunits of NMDA receptors, through activation of SFKs, resulting in the potentiation of NMDA receptor-mediated Ca^{2+} influx and transmission (Durakoglugil et al., 2009). Neurons deficient in ApoER2 or VLDLR receptors have impaired LTP in the hippocampus (Weeber et al., 2002). The coupling of the Reelin signaling complex to NMDA receptors requires ApoER2 association with postsynaptic density protein 95 (PSD95), an abundant scaffolding protein in the postsynaptic density, through a domain encoded by exon 19, and mice lacking this exon in ApoER2 do not show increased NMDA receptor-mediated currents and LTP after the application of Reelin and perform poorly in contextual fear conditioning and water maze tasks (Beffert et al., 2005). It has recently been demonstrated that Reelin also participates in the composition, recruitment and trafficking of NMDA receptor subunits (Sinagra et al., 2005; Groc et al., 2007). Phosphorylated Dab1 further activates PI3K, resulting in increased cell surface expression of α-amino-3-hydroxy-5-methyl-4-isoxazole propionic acid (AMPA) receptors after application of exogenous Reelin in hippocampal slices and cultures (Qiu et al., 2006). Consistent with these findings, *in vivo* enhancement of Reelin signaling through stereotaxical injection of purified Reelin in wild-type mice increased dendritic spine density, augmented hippocampal CA1 LTP, and enhanced performance in memory tasks (Rogers et al., 2011). Moreover, Reelin has been implicated in the generation of dendrites in the postnatal hippocampus (Matsuki et al., 2008); and in the formation of dendritic spines (Niu et al., 2008). Finally, Reelin has a stabilizing effect on mature neuronal circuitry, thus being involved in the consolidation

of synaptic plasticity. Indeed, Reelin was recently found to stabilize the actin cytoskeleton by inducing the phosphorylation of cofilin, which in an unphosphorylated state acts as an actin-depolymerizing protein that promotes the disassembly of F-actin (Frotscher, 2010).

All together, these observations support the notion that, in the adult brain, Reelin is involved in the control of synaptic transmission and in the proper formation and maintenance of synapses, thus controlling memory and learning. Moreover deficits, in Reelin levels and genetic variants have been associated with several psychiatric disorders, such as schizophrenia, autism, and psychotic bipolar disorder, possibly as a result of a decrease in hippocampal spine density and molecular alterations in synapse composition (Fatemi et al., 2001; Fatemi, 2002, 2005; Fatemi et al., 2005; Goes et al., 2009; Ventruti et al., 2011).

***Conditional Reelin-expressing mouse model*:** Most studies on Reelin functions in adult brain have involved the analyses of *reeler* mice (or $Dab1^{(-/-)}$ or $Apoer2^{(-/-)}/Vldlr^{(-/-)}$ mice) and heterozygous *reeler* mice, as models of Reelin haploinsufficiency. However, studies in *reeler* mice (or $Dab1^{(-/-)}$ or $Apoer2^{(-/-)}/Vldlr^{(-/-)}$ mice) are hampered by the dramatic defects in brain lamination and organization shown by these animals. These observations raise the question as to whether defects in adult *reeler* mouse are secondary to neuronal mispositioning, rather than to a specific fail in adult Reelin functionality. To gain greater insight into the function of Reelin in the adult brain, previously in our laboratory it was generated a gain-of-function transgenic mouse model (TgRln) that conditionally overexpresses Reelin, specifically in the postnatal and adult forebrain, under the control of the calcium-calmodulin-dependent kinase II promoter (CaMKIIα) (Pujadas et al., 2010) (Fig. **1.9a**). CaMKII-dependent Reelin expression is driven by a tetracycline-controlled transactivator (tTA), which is inactive when bound to doxycycline (Mayford et al., 1996), so that Reelin overexpression can be switched off by doxycycline administration.

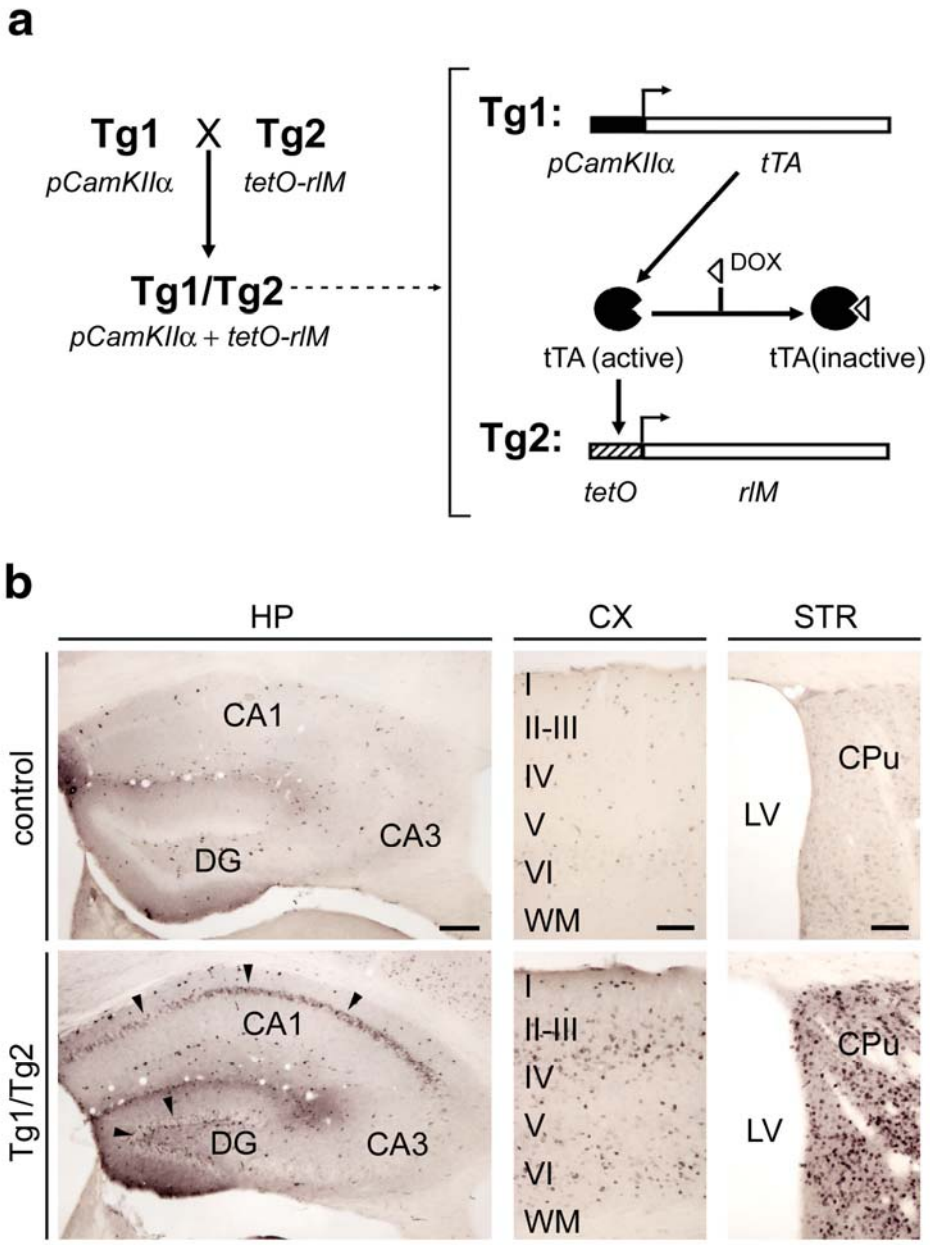

From: Pujadas et al., 2010

Figure 1.9 Generation and characterization of conditional Tg1/Tg2 transgenic mice (TgRln). a) Transgenic mice that overexpress Reelin were based on the Tet-off regulated binary system: the Tg1 transgene contains the *tTA* transactivator set under the control of *pCaMKIIα*, while the Tg2 transgene contains *rlM* controlled by the *tetO* promoter. Double transgenic mice (Tg1/Tg2 or TgRln) express Reelin in neurons expressing CaMKII; transgene expression can be switched off by doxycycline administration, which inactivates tTAtransactivator. **b)** Immunohistochemical detection of Reelin shows that expression of this protein in control adult mice is restricted to a subset of interneurons distributed throughout the cortex and hippocampal layers, while the striatum shows a diffuse staining (top). In Tg1/Tg2 mice, overexpression of Reelin is observed in hippocampal pyramidal cells and in granule cells of the dentate gyrus (arrows in bottom left panel); Reelin is also expressed in neocortical pyramidal cells (bottom middle) and in striatal neurons (bottom right). I–VI, Cortical layers; CA1–CA3, hippocampal regions; CPu, caudate–putamen nucleus; DOX, doxycycline; H, hilus; LV, lateral ventricle; ML, molecular layer; SP, stratum pyramidale; WM, white matter. Scale bars: ***b*** (left): 200 μm; ***b*** (middle and right): 100 μm.

In this model, referred to as TgRln, Reelin overexpression is driven in hippocampal pyramidal cells and in granule cells of the dendate gyrus. Reelin is also expressed in striatal neurons and in neocortical pyramidal cells (**Fig. 1.9b**). Given that this protein is essential for brain development, TgRln mice have been used to mainly address the impact of Reelin protein levels on developmental-like processes that remain active in the adult brain, namely adult neurogenesis, neural migration, and synaptic plasticity. This model provided evidence that Reelin overexpression increases adult hippocampal neurogenesis and modulates the migration and positioning of adult-generated hippocampal neurons. Furthermore, hippocampal overexpression of Reelin caused an increase in synaptic contacts in all hippocampal layers, without enhancing dendritic spine density. Although the number of dendritic spines in Reelin transgenic mice was unvaried, they appeared hypertrophic and more complex (**Fig. 1.10**). Indeed, most of these spines display mushroom-like shapes with two or more synaptic active zones.

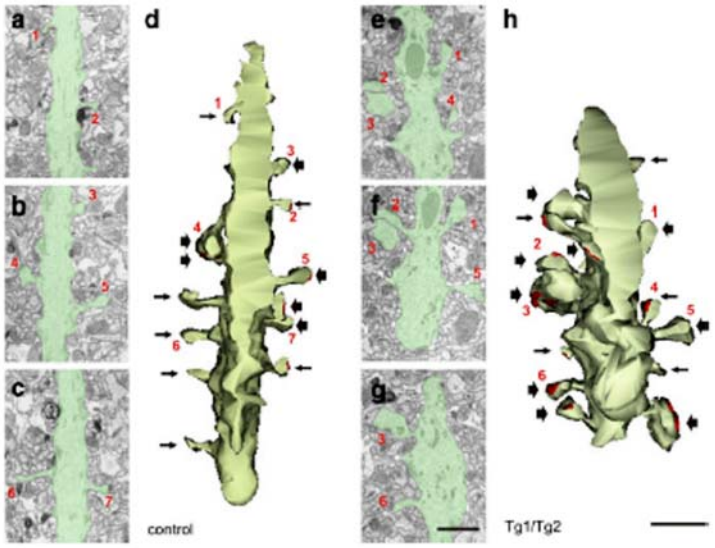

From: Pujadas et al., 2010

Figure 1.10 TgRln show hypertrophy of dendritic spines. Three-dimensional serial electron microscopic reconstructions of dendrites in the SR of CA1 region in control (**a-d**) and TgRln (Tg1/Tg2) (**e-h)** mice. Dendritic spine heads with sizes below and above 0.4 μm in diameter are represented by small and large arrows respectively, illustrating hypertrophy of dendritic spines in Tg1/Tg2 mice. Scale bars**:** 1 μm.

Doxycycline treatment of *TgRln* mice strongly reverses the synaptic phenotype in adult mice, thereby indicating that this phenotype depends on acute overexpression of Reelin (Pujadas et al., 2010). Persistent dendritic spine enlargement is commonly associated with increased physiological efficacy and stable LTP, and the latter is thought to underlie long-lasting memory and learning (Yuste and Bonhoeffer, 2001; Yang et al., 2008). In

fact, the induction of LTP in the CA3-CA1 synapse in alert behaving mice showed that Reelin overexpression evokes a dramatic increase in LTP responses (Pujadas et al., 2010). These data are consistent with those reported in previous studies showing that ApoER2/VLDLR-deficient mice display reduced LTP in slices *in vitro,* which indicates that the effects described in *TgRln* mice are mediated by these receptors (Weeber et al., 2002; Beffert et al., 2005). Interestingly, Reelin has been found to control NMDA and AMPA subunit receptor composition and trafficking during development (Jones et al., 2001; Ju et al., 2004; Chen et al., 2005; Qiu et al., 2006; Groc et al., 2007), and both types of ionotropic glutamate receptors are essential for LTP induction (Jones et al., 2001; Ju et al., 2004). Furthermore, GSK-3ß, a downstream effector of the Reelin signaling cascade, has been found to be involved in LTP (Peineau et al., 2007). Taken together, these data suggest that extracellular Reelin acts through the ApoER2/VLDLR receptors to trigger a signaling cascade that is sufficient to induce marked LTP physiological alterations *in vivo*. Moreover, Reelin overexpression also leads to increased LTP responses over several days. This finding thus suggests that this extracellular protein controls gene expression and protein synthesis required for late phases of LTP (Jones et al., 2001; Ju et al., 2004). All together, TgRln mouse model provides further evidence that in the adult brain Reelin levels are crucial for the modulation of neurogenesis and migration, particularly in the hippocampus, as well as for the modulation of the structural and functional plastic properties of adult synapses, including the induction and maintenance of LTP. Thus, Reelin, a protein with pivotal roles in normal development, also controls plasticity processes in the adult brain that are reminiscent of developmental processes.

1.2.3 At the crossway between the Reelin pathway and Alzheimer's disease

In recent years, research in the field of Reelin has produced increasing evidence of a relationship between the Reelin pathway and AD. The first link comes from ApoER2, one of the main signal transducers for the Reelin pathway and at the same time a receptor for the ε4 isoform of ApoE, the major genetic risk factor for SAD (Tsai et al., 1994). On the basis of these observations, it is conceivable that there is a potential mechanism of competition between Reelin and Apoε4 for ApoER2, possibly interfering with Reelin-mediated potentiation of NMDA neurotransmission. Second, Reelin signaling through

VLDLR and APOE receptors downregulates the activity of GSK-3β, the major kinase for Tau protein (Gonzalez-Billault, C. 2005; Beffert, U. 2002), and mutant mice that have deficits in Reelin, in its transducer Dab1 or in ApoER2 and/or VLDLR show increased levels of Tau phosphorylation (Hiesberger et al., 1999). Third, both Dab1 and Reelin physically interact with APP and regulate its trafficking and proteolytic processing, thereby promoting non-amyloidogenic αAPP cleavage (Hoe et al., 2006; Hoe et al., 2008; Hoe et al., 2009). Fourth, Reelin counteracts Aβ-induced downregulation of glutamatergic synaptic transmission (**Fig. 1.11**; Durakoglugil et al., 2009).

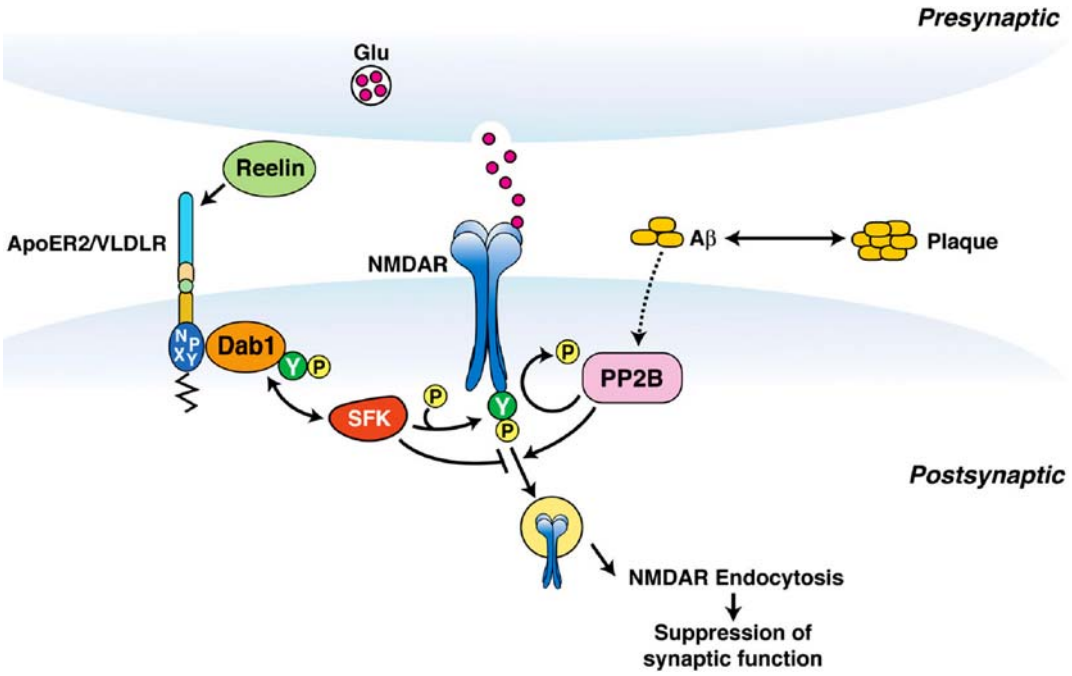

From: Durakoglugil et al., 2009

Figure 1.11 Model of the regulation of synaptic functions by Reelin. Aβ activates PP2B leading to dephosphorylation of tyrosine residues on NMDA receptors. Dephosphorylation of the NR2B subunit correlates with increased NMDA receptor endocytosis and suppression of its synaptic function. Reelin instead, by activating Src family tyrosine kinases (*SFK*), enhances tyrosine phosphorylation of NR2A and NR2B subunits,counteracting the suppressive effect of Aβ at the synapse and maintening normal synaptic function.

Indeed, incubation of hippocampal slices with Aβ oligomers at concentrations that are found in AD patients impairs endocytosis and trafficking of AMPA and NMDA receptors, thus decreasing LTP (Kamenetz et al., 2003; Hsieh et al., 2006); conversely addition of recombinant Reelin to acute hippocampal slices results in enhanced LTP

(Weeber et al., 2002) as a result of Reelin-dependent tyrosine phosphorylation of the NR2 subunit of NMDAR through SFKs activation. These data have been corroborated in conditional transgenic mice overexpressing Reelin, which show enhanced LTP in the hippocampus (Pujadas et al., 2010).

Finally, *RELN* gene bears polymorphic variants associated with normal cognitive function in AD pathology (Kramer et al.; Seripa et al., 2008). All the aforementioned findings point to a possible protective role of the Reelin pathway in the pathogenesis of AD. In contrast other aspects of the Reelin-AD relationship are not so easily interpreted. First of all, Reelin accumulates in extracellular aggregates in adult wild-type mice and primates and co-localizes with Aβ in extracellular plaques in AD mouse models (Doehner et al.; Knuesel et al., 2009). Several proteoglycans, such as agrin, syndecans and glypicans, have been shown to be associated with senile plaques (Bonneh-Barkay and Wiley, 2009). For many of them, as for Reelin, it remains to be clarified whether they play a role in plaque formation or not and whether ECM molecules sequestering into amyloid fibrils could impair ECM functionality, thus being detrimental for neurons. As a possible indication, accelerated Aβ plaque formation and Tau pathology in Reelin-deficient AD mice has been reported (Kocherhans et al., 2010). Second, AD patients show an increase of about 40% in the levels of Reelin in frontal cortex and cerebrospinal fluid (CSF) and an altered pattern of glycosylation (Botella-Lopez et al., 2006). In contrast, Reelin depletion has been found in the Enthorinal cortex of AD mouse models and of human AD patients (Chin et al., 2007).

All together, these findings point to a contribution of Reelin, its receptors, and downstream signaling proteins to the aetiology of AD. The analysis of the molecular mechanisms by which Reelin is involved in AD and its possible neuroprotective or neurodegenerative role are object of this work.

AIMS OF THE STUDY

The main aim of this study is to investigate the involvement of Reelin in AD aetiology, addressing the question of whether Reelin could act as a protective factor, or rather if it might favour the onset of the pathology, with eventual therapeutic implications.
To this end we established the following objectives:

1. *In vitro* investigation of Reelin-Aβ_{42} peptide interplays

Reelin protein purification

Analysis of Reelin influence on Aβ_{42} aggregation

Analysis of Reelin-Aβ_{42} interaction

Analysis of Reelin influence on the toxicity of Aβ_{42} species

2. Generation of AD mouse models overexpressing Reelin

Generation of $hAPP_{Swe/Ind}$ (J20) mice overexpressing Reelin (TgRln/J20)

Generation of Tet/GSK-3β mice overexpressing Reelin (TgRln/GSK-3β)

3. Histological, biochemical and behavioural characterization of AD mouse models overexpressing Reelin

Analysis of transgene expression in the mouse models generated

Analysis of the impact of Reelin overexpression on amyloid plaque deposition

Analysis of the impact of Reelin overexpression on AD synaptopathology and neurodegeneration

Analysis of the impact of Reelin overexpression on the phosphorylation of Tau protein

Analysis of the impact of Reelin overexpression on AD cognitive impairments

MATERIAL AND METHODS

3.1 Material

3.1.1 Animals

Line TgRln (Tg1/Tg2) is a conditional regulated double transgenic line that gets overexpression of Reelin under the control of calcium-calmodulin dependent kinase II α promoter (pCaMKIIα) (Pujadas et al., 2010). Line J20 produces hAPP with the Swedish (KM670/671NL) and Indiana (V717F) mutations ($hAPP_{Swe/Ind}$) under the control of plateled derived growth factor (PDGF) promoter (Mucke et al., 2000). It was purchased from Jackson. Tet/GSK-3β (BitetO β-Gal/GSK-3β; Lucas JJ et al., 2001) and VLW (Tau^{vlw}; Lim et al., 2001) mice were kindly provided by Dr. J. Avila. All the transgenic animals used in this study are kept in hemizygosis for each transgene. Mice were bred in the animal research facilities at the Barcelona Science Park and the Faculty of Biology of the University of Barcelona. NOR test was performed at the animal research facility of the Barcelona Biomedical Research Park. Animals were provided with food and water *ad libitum* and maintained in a temperature-controlled environment in a 12/12 h light-dark cycle. For doxycycline treatment, adult mice were fed *ad libitum* with doxycycline containing feed (Bio-Serv, 200 mg/kg). All the experiments using animals were performed in accordance with the European Community Council directive and the National Institute of Health guidelines for the care and use of laboratory animals. Experiments were also approved by the local ethical committees.

3.1.2 Chemicals

Thioflavin-T (ThT), ammonium persulfate (APS), tris(bipyridine)ruthenium(II) chloride ($Ru(bpy)_3^{2+}$), Diaminobenzidine reagent (DAB), Hydrogen Peroxide (H2O2), 4'-6'-Diamino-2-Phenylindole (DAPI), Triton X-114, Dimethyl Sulfoxide, Nissl (Cresyl violet acetate and Thionine acetate salt), Hoechst 33342, acetic acid and propidium iodide (PI) were from Sigma. Coomassie G-250 and Sypro Ruby were from Invitrogen. MTT Cell Proliferation Kit I was from Roche. Paraformaldehyde, Eukitt mounting medium, Glycerol, Ethylene Glycol, and gelatine were from Panreac. Mowiol 4-88 was from VWR.

3.1.3 Antibodies

Mouse monoclonal anti-Aβ amino acids 1-5 (clone 3D6) was provided by Elan Pharmaceuticals. Mouse anti-phopsho-Tau (ser 396/404) PHF-1 was a kind gift from Dr. Peter Davies, Albert Einstein College of Medicine, New York, NY (Greenberg et al., 1992). The commercial primary antibodies used were: anti-Reelin (clone G10) (Chemicon), anti-Dab1 (Chemicon) for WB, anti-Dab1 (ExAlpha) for immunoprecipitation, anti-Aβ (clone 6E10,Covance), rabbit anti-$A\beta_{40/42}$ (Chemicon AB5076), anti-phospho-tyrosines (clone 4G10, Millipore), anti-Aβ-oligomers (A11, Invitrogen), anti-phospho-Tau (ser202/thr205, clone AT8, Innogenetics), anti-phospho-Tau (T231, clone AT180, Innogenetics), anti total Tau (clone Tau-5, Millipore), anti-Doublecortin (AB5910, Millipore), anti-β-Tubulin (clone AA2, Millipore), anti-actin (Chemicon, MAB1501) and anti-β Galactosidase (AB986, Millipore). The HRP-labeled secondary antibodies used for Western blot were from DAKO. Biotinylated-secondary antibodies and Streptavidin-biotinylated/HRP complex, and Protein A and Protein G Sepharose 4 Fast Flow were from GE Healthcare. F(ab')2 fragment anti-mouse IgG was from Jackson Immuno Research. Fluorescent secondary antibodies used for immunofluorescence were from Invitrogen (Alexafluor). Colloidal gold-coated secondary antibodies were from BBI.

3.1.4 Softwares

GelPro; Image J; GraphPad Prism; NetNGlyc 1.0 Server; Proteome Discoverer (v. 1.3.0.339); Sequest; Thermo Xcalibur (v.2.1.0.1140); and Percolator

3.2 Methods

3.2.1 $A\beta_{42}$ purification

$A\beta_{42}$ was synthesized and purified by Dr. James I. Elliott at Yale University (New Haven, CT, USA). The lowest aggregation state in which $A\beta_{42}$ can be prepared corresponds to Low Molecular Weight (LMW) $A\beta_{42}$, which contains monomer in rapid equilibrium with low-n Aβ oligomer forms, where n is the order of the oligomer. A LMW $A\beta_{42}$ preparation was obtained using Size Exclusion Chromatography. Aβ peptide was dissolved in 6 M Gdn·HCl at 5 mg/mL, sonicated for 5 min, centrifuged at 10,000 *g* for 6 min, and passed through a 0.45-μm Millex filter. The resulting solution was injected into a Superdex 75 HR 10/300 column (GE Healthcare) previously equilibrated using 10 mM phosphate pH 7.4, and eluted at a flow rate of 0.5 mL/min. The peak attributed to LMW Aβ42, eluted between 13 and 15 mL, was collected, and its protein concentration was determined by the Bradford assay. The peptide solution was then diluted to the desired concentration (24 μM) to initiate aggregation studies.

3.2.2 Preparation of Aβ-derived diffusible ligands (ADDLs)

$A\beta_{42}$ was dissolved in hexafluoro-2-propanol (HFIP) (1mg/mL), aliquoted in low binding Eppendorf tubes, and then HFIP was removed by freeze-drying. An aliquot of $A\beta_{42}$ was dissolved in anhydrous dimethyl sulfoxide (DMSO) to 5 mM, and then further diluted with ice-cold F12 medium without phenol red to 100 μm. This solution was incubated at 4 ºC for 24 h and then centrifuged at 14,000 g for 10 min. Centrifugation typically produced a small clear or white pellet. The $A\beta_{42}$ concentration in the supernatant was determined using the Bradford assay.

3.2.3 Reelin production and purification

Reelin supernatants were prepared from 293 cells stably transfected with full-length Reelin clone pCrl (Forster et al., 2002) and cultured with OPTI-MEM medium (GIBCO). The collected Reelin supernatants were washed with double the initial volume of 10mM Phosphate Buffer/30 mM NaCl (pH 7.4) and then subjected to 10X

concentration using ultrafiltration Vivaflow 50 filters (Sartorius; 100 kDa MWCO), previously blocked with 1% BSA. Concentrated supernatants from Reelin were subjected to anion exchange chromatography performed with HiTrap IEX ANX column (GE Healthcare), mobile phase NaCl 30 mM/Phosphate buffer 10mM (pH 7.6), at a flow rate of 2 ml/min. Sample fractionation was performed by a five-steps gradient elution, increasing NaCl concentration from 30 mM up to 150, 250, 350, 650, and 1000 mM. Reelin containing fractions eluting at 350mM, were collected and subjected to 10X concentration using Vivaspin filters (Sartorius; 100 kDa MWCO), previously blocked with 1% BSA. These concentrated samples were loaded onto a 25 mL pre-packed Superose 6 10/300 size exclusion column (GE Healthcare), previously equilibrated with 10mM Phosphate Buffer/ 30 mM NaCl (pH 7.4), and eluted at a flow rate of 0.4 ml/min in a FPLC system. Fractions eluted between 9 and 11 ml were collected and Reelin concentration was estimated measuring absorbance at 595 nm in a typical Bradford assay (Bio-Rad) in 96 well plates; BSA was used as a protein standard. In parallel to Reelin, Mock supernatants were produced from 293 cells stably transfected with GFP (Forster et al., 2002) and subjected to same protocol of purification.

3.2.4 Aggregation studies

$A\beta_{42}$ was left to aggregate at 24 μM in 10mM Phosphate Buffer/5 mM NaCl (pH 7.4) at 20ºC, alone or in the presence of purified Reelin in a w/w ratio of 4:1; 6:1 or 12:1 ($A\beta_{42}$/Reelin). As for Reelin, equivalent Mock volumes were left to aggregate with $A\beta_{42}$. Finally, Reelin and Mock preparations without $A\beta_{42}$ were used as controls. Thus, aggregation was monitored in parallel for the following aggregating solutions: $A\beta_{42}$, $A\beta_{42}$/Mock, $A\beta_{42}$/Rln, Rln, Mock. Aliquots were taken from each solution every 24 hours for the assays described below.

3.2.5 Thioflavin T assay

The ThT binding assay was performed by mixing 15 μM of a peptide solution with 15 μM ThT dye (Aβ/ThT ratio = 1:1) and 50 mM glycine–NaOH, pH 8.5 (final concentrations) in Hard Shell® Thin Wall 96-well fluorescence plates (Bio-Rad) (100 μl/well assay volume). The ThT fluorescence of each sample was measured in a

FluoDiaTM T70 fluorometer (Photon Technology International) at excitation and emission wavelengths of 450 and 485 nm, respectively. The samples were analyzed in triplicate and average fluorescence values and standard deviation were plotted. To determine the effect of Reelin on fibril formation, raw data obtained for the different aggregating solutions were fitted by a sigmoidal curve described by equation 1 using GraphPad Prism software, as described previously (Nielsen et al., 2001; Ghosh et al., 2010):

$$(1) \qquad Y = \text{bottom} + \frac{(top - bottom)}{1 + \exp(\frac{t - t_{0.5}}{b})}$$

Y is the fluorescence intensity, *t* is time, $t_{0.5}$ is the time to 50% of maximal fluorescence, *b* is the slope, and *top* and *bottom* values correspond to the maximum and minimum fluorescence intensities. Stimated lag-time is $t_{0.5}$-2*b* in each condition.

3.2.6 Transmission Electron Microscopy and Immunogold labelling

For Transmission Electron Microscopy a 10 uL aliquot of the samples subjected to aggregation studies was applied to a 200-mesh carbon-coated formvar grid, previously glow discharged for 5 minutes. After 1 minute the grid was washed with water and negatively stained by treatment with 2% uranyl acetate for one minute. Samples were observed in a JEOL JEM 1010 transmission electron microscope operating at 80 kV.

For Immunogold labelling a 10 µL aliquot of the samples subjected to aggregation studies was applied for 3 minutes to a carbon-coated nickel formvar grid, previously glow discharged for 5 minutes. Grids were then blocked three times for 5 minutes with FBS 10% in PBS 0.1M. Primary antibodies were dissolved in a FBS 5% solution in PBS 0.1M and applied to the grid for 30 minutes (Mouse anti-Reelin (G10) 1:25; rabbit anti-$A\beta_{40/42}$ 1:25) Grids were then rinsed with 1% FBS in PBS 0.1M and secondary antibodies conjugated to Monomaleimido Nanogold particles were applied, to a dilution of 1:30 in a 5% FBS solution in PBS 0.1M for 30 minutes. Nano-gold particles with a diameter of 12 nm or 18 nm were conjugated to antirabbit IgG and anti-mouse IgG, respectively. Grids were washed 5 times with PBS 0.1M and then fixed for 5 minutes with 2% glutaraldehyde. Finally grids were rinsed three times with water and negatively

stained by treatment with 2% uranyl acetate for one minute. Samples were observed in a JEOL JEM 1010 transmission electron microscope operating at 80 kV.

3.2.7 Dot blot

To analyze the oligomer content during the time-course of $A\beta_{42}$ aggregation, aliquots of $A\beta_{42}$/Mock and $A\beta_{42}$/Rln samples (3 µl drops) were applied to a nitrocellulose membrane and let dry. Then membranes were processed as for western blot, using anti-oligomer antibody A11 (1:1000) as primary antibody.

3.2.8 Neuronal primary culture treatment

Hippocampal neurons were obtained from E16 OF1 mouse embryos (Charles River Laboratories). Brains were dissected in PBS containing 0.6% glucose and hippocampi were excised. After trypsin (Gibco) and DNAse (Roche Diagnostics) treatments, tissue pieces were dissociated by gentle sweeping. Cells were then counted and seeded onto poly-D-lysine-coated dishes in Neurobasal medium containing B27 supplement (GIBCO). In all the cases, treatments were performed 72-96 hours after cell seeding.

3.2.9 Testing the biological activity of Reelin

Primary hippocampal neurons seeded at 10^6 cells/well in 6-well plates were treated with Reelin at a working concentration of 2-5 ng/ml (Mock samples were used in equivalent volumes). After 15 min of Reelin treatment, lysates were collected in Lysis Buffer (Hepes 50mM pH 7.5, 150mM sodium chloride, 1.5mM magnesium chloride, 1mM EGTA, 10% glycerol and 1% Triton X-100) containing Complete Mini protease inhibitor cocktail (Roche) and phosphatase inhibitors (10 mM tetra-sodium pyrophosphate, 200 µM sodium orthovanadate and 10 mM sodium fluoride); insoluble debris were removed by centrifugation (30 min, 16000 *g*). To detect phosphorylation of Dab1, lysates were incubated with the primary antibody for immunoprecipitation overnight (o/n) at 4ºC (3 µg/sample). Protein G-Sepharose beads were added for 90 min at 4ºC, recovered by centrifugation and washed 3 times with Lysis Buffer. Immunoprecipitated samples or their supernatants (used as loading controls) were diluted 1:6 with 6X Loading Buffer

(0.5M Tris-HCl pH 6.8, 2.15M β-mercaptoethanol, 10% SDS, 30% glycerol and 0.012% bromophenol blue), boiled for 5 min at 95ºC and processed for Western blot.

3.2.10 Western blot

Samples were resolved by SDS-polyacrylamide gels and transferred onto nitrocellulose membranes. Membranes were then blocked for 1 hour at room temperature (RT) in TBST (Tris 10mM pH 7.4, sodium chloride 140mM (TBS) with 0.1% Tween 20) containing 5% non-fat milk or 3% BSA. Primary antibodies were incubated for 90 min in TBST-0.02% azide (anti-APP (1:2000); anti-phospho-tyrosine (clone 4G10) (1:1000); anti-Reelin (1:1000); anti-Dab1 (1:1000); anti-actin 1:100,000; PHF-1 (1:500); AT8 (1.500); AT180 (1:1000)). After incubation with anti-mouse secondary HRP-labeled antibodies for 1 hour at RT (diluted 1:2000 in TBST-5% non-fat milk), membranes were developed with the ECL system (GE Healthcare). Densitometric analysis of protein bands was realized using GelPro software.

3.2.11 PICUP assay

The set up and optimization of the PICUP reaction was based on detailed descriptions given in the literature (Fancy and Kodadek, 1999; Bitan and Teplow, 2004). As reported, the set up consisted of a camera body and a 150-W slide projector. A PCR tube containing the reaction mixture to be cross-linked, holded by a glass vial, was placed inside the camera body for irradiation. The sample was irradiated by means of the 150-W slide projector for 4 seconds, precisely controlled by the camera shutter. PICUP reactions were carried out using an $A\beta_{42}$:$Ru(bpy)_3^{2+}$:APS ratio of 1:2:40. To this end, 0.8 µL of 1 mM $Ru(bpy)_3^{2+}$ and 0.8 µL of 20 mM APS were added to 18 µL of 24 µM $A\beta_{42}$, $A\beta_{42}$/Mock and $A\beta_{42}$/Rln in 10 mM Phosphate Buffer/30 mM NaCl (pH 7.4). The mixture was irradiated for 4 seconds at a distance of 25 cm and immediately quenched by adding 5 µL of 0.3 M DTT to the sample. 10 µL of 3X loading buffer was added to 20 µL of the sample to be analyzed by SDS-PAGE. Samples were boiled at 95ºC for 5 min and kept at -20ºC until analysis by Western blot using 6E10 as primary antibody.

3.2.12 Reelin interaction with soluble $A\beta_{42}$ species

Co-immunoprecipitation assays for $A\beta_{42}$ and Reelin during the pre-fibrillar phase of aggregation were performed in two independent experimental conditions: (1) using $A\beta_{42}$/Rln sample (40-80 µl) from a very early stage of the *in vitro* aggregation experiment (days 2-4); and (2) from 100 µl of ADDLs preparation (10 µM) mixed with Reelin (10 ng/µl) in Neurobasal medium and incubated for 1h at 37 ºC. In both conditions, lysis Buffer (Hepes 50mM pH 7.5, 150mM sodium chloride, 1.5mM magnesium chloride, 1mM EGTA, 10% glycerol and 1% Triton X-100) was added to the samples up to 500uL, and the mixtures were incubated with 2 µg of the required immunoprecipitation antibody (i.e: anti-Reelin (G10) and anti-Aβ (6E10)) for 1 hour at 4ºC. Insoluble debris was removed by centrifugation (10 min, 16000 *g*) and supernantants incubated with Protein A and Protein G Sepharose 4 Fast Flowbeads for 90 minutes at 4ºC, recovered by centrifugation and washed 3 times with Lysis Buffer. Immunoprecipitated samples or their supernatants (used as loading controls) were diluted 1:6 with 6X Loading Buffer, boiled for 5 min at 95ºC, and processed for Western blot to detect cross-reaction of Reelin and $A\beta_{42}$ in the immunoprecipitates. A diversity of control samples were processed in parallel including either Reelin or $A\beta_{42}$ alone (condition 1) or ADDLs (condition 2). Negative controls without addition of antibody were also carried out in each experimental condition.

3.2.13 Deglycosylation and trypsin digestion for Mass Spectrometry

Purified Reelin, together with same volumes of Mock control, underwent deglycosylation in native conditions using Enzymatic Protein Deglycosylation Kit (EDEGLY) from SIGMA. 3 µg of purified protein were digested for 1–5 days at 37 °C with PNGase F, O-Glycosidase, α-(2→3,6,8,9)-Neuraminidase, β-N-Acetylglucosaminidase and β-(1→4)-Galactosidase, according to manufacturer's directions. Digested samples were run on a 6% SDS-PAGE for further analysis.

Bands of interest from SDS-PAGE were sequentially washed with 25 mM ammonium bicarbonate (NH_4HCO_3) and acetonitrile (MeCN). Next, samples were reduced with 10 mM DTT for 30 minutes at 56 °C and alkylated with iodoacetamide 55 mM at room temperature for 15 minutes. Finally, samples were digested overnight at 37 °C with Pig Trypsin (80 ng, Promega) in a Progest robot (Genomic Solutions). Peptides coming

from tryptic digestion were extracted from gel matrix with 10% formic acid and acetonitrile, and dried using a speed vac.

3.2.14 Coomassie and Sypro Ruby staining

After electroforesis, polyacrilamide gels were stained with Coomassie G-250 from Invitrogen according to manifacturer's directions. Sensibility of the technique is from 7 ng minimum.

Alternatively, for high sensibility protein detection (from 0,25 ng), electrophoresis gels underwent staining with Sypro Ruby from Invitrogen. Staining was performed according to manifacturer's directions.

Scanned images from stained gels were analyzed using GelPro software.

3.2.15 Mass Spectometry

Samples were analyzed using a liquid chromatograph nanoACQUITY (Waters) coupled to a mass spectrometer Orbitrap-Velos (Thermo Scientific). The samples were resuspended in 1% formic acid, an aliquot was injected for chromatographic separation with a C18 reverse phase column (75 µm Øi, 25 cm, nanoACQUITY, 1.7µm BEH column, Waters); the gradient used for the separation was 1 to 40% B in 30 minutes, followed by a gradient of 40 to 60% B in 5 minutes with a flow of 250 nl/min (A: 0.1% formic acid, B: 0.1% formic acid in acetonitrile). The eluted peptides were ionized using a metallic silica needle (PicoTip^{TM}, New Objective). The voltage applied to the needle was about 2000V. The masses of peptides (*m/z* 300-1700) were measured in Full Scan MS in the Orbitrap with a resolution of 60,000 FWHM at 400 m/z. Up to 10 of the most abundant peptides (minimum intensity of 500 counts) are selected for each MS analysis to be fragmented in the Ionic trap (CID) with helium as the collision gas with a normalized collision energy of 38%. Data were acquired with Thermo Xcalibur software (v.2.1.0.1140) in raw data format. The raw data files were analyzed with Proteome Discoverer software (v. 1.3.0.339) and the search engine Sequest. Search was made within UniprotSwissport (version May 2011) without species restriction, using Percolator to estimate the confidence of peptides. Search parameters were:

- Database / Taxonomy: UniprotSwissprot all.
- Enzyme: trypsin; Missed cleavages: 2.

- Fixed modifications: carbamidomethyl of cystein.
- Variable modifications: oxidation of methionine, pyro-Glu (N-term Glutamine), deamidation of N.
- Peptide tolerance: 10 ppm and 0.6 Da (respectively for MS and MS / MS spectra)

3.2.16 X-ray diffraction

Aligned fibrils of $A\beta_{42}$/Rln and $A\beta_{42}$/Mock samples were prepared by suspending a 5 µl drop of aged fibril solution between two glass rods with beeswax tips approximately 1.5 mm apart; before complete drying of the first drop, sequential addition of extra drops of 5 µl was performed twice. Finally, fibrils were allowed to dry completely. Fibril diffraction data were collected at on a crystallography beamline at the Department of Biochemistry of the University of Cambridge. Azimutal plots from diffractions were represented using Image J software.

3.2.17 MTT

Primary hippocampal neurons were seeded at 3.10^4 cells/well in 96-well plates and maintained for 72-96 hours before treatment. ADDLs, or corresponding volumes of vehicle (0.1% DMSO in F12 medium), were added to the concentrations of 10 µM, with or without addition of Reelin at 5 ng/mL (or equivalent volumes of Mock). After 24 hours at 37ºC, the MTT assay was run according to manufacturer's directions (Cell Proliferation Kit I (MTT), Roche). The assay was quantified at 595-690 nm on an absorbance plate reader.

3.2.18 Propidium Iodide staining

Primary hippocampal neurons seeded at 10^5 cells/well in 4-well plates containing coverslips were treated with ADDLs (5 and 10 µM) or corresponding volumes of vehicle (0.1% DMSO in F12 medium), with or without addition of Reelin at 5 ng/ml (or equivalent volumes of Mock). After 24h, cells were incubated for 30 minutes with PI (1,5 µg/ml) and Hoechst 33342 (1 µg/ml) for counterstaining. Cells were then washed for 3 times with PBS and fixed for 20 min with 0.1M PB containing 4% of paraformaldehyde (PF). Next, cells were washed with PBS and coverslips were

mounted on slide glass with Mowiol. Fluorescent micrographs were randomly taken from coverslips for each condition. Number of dying neurons (PI and Hoechst double-labeled picnotic nuclei) versus total amount of cells (Hoechst-labeled) per field were counted for statistics.

3.2.19 Bradford assay

Bradford assay was performed in 96-well microplates, using Bradford dye from Bio-Rad and a BSA (Fluka) and a calibration curve ranging from 0 to 20 μg/mL. Measurements were done at 595 nm on an absorbance plate reader.

3.2.20 Histology

Animals were anesthetized and perfused for 20 min with 0.1M phosphate buffer (PB) containing 4% of paraformaldehyde (PF). Brains were removed, postfixed overnight with PB-4% PF, cryoprotected with PB-30% sucrose and frozen. Brains were sectioned coronally at 30μm, distributed in 10 series and maintained at -20ºC in PB-30% glycerol-30% ethylene glycol. For immunodetection of antigens, sections were blocked for 2 h at RT with PB saline (PBS) containing 10% of either normal goat serum (NGS) or normal horse serum (NHS), 0.2% of gelatine, and F(ab')2 fragment anti-mouse IgG (1:300) when needed. Primary antibodies (PHF-1 1:150; anti-$A\beta_{40/42}$ (AB5076) 1:100; anti-Aβ (clone 6E10) 1:500; anti-Doublecortin 1:500; anti-β Galactosidase 1:200; anti-Reelin 1: 200) were incubated overnight at 4ºC with PBS-5% NGS or -5% NHS. For immunohistochemistry, sequential incubation with biotinylated secondary antibodiy (1:200; 2h at RT) and streptavidin-HRP (1:400; 2h at RT) was performed in PBS-5% NGS or -5% NHS. Bound antibodies were visualized by reaction using DAB and H_2O_2 as peroxidase substrates. Sections were eventually stained with Nissl, dehydrated, and mounted (Eukitt). For immunohistofluorescence, incubation with fluorescent secondary antibody (1:200; 2h at RT) and DAPI was performed in PBS-5% NGS or -5% NHS. Sections were mounted in Mowiol.

3.2.21 Novel Object Recognition test

The NOR task was performed in groups of 9-12 males per genotype (control; TgRln; J20; TgRln/J20). Mice were individually placed in an L-shaped maze (equal arms of 15 x 5 cm) with grey, non reflective base plate for 15 min (Day 0, habituation phase). The next day, animals were exposed to two identical elements (located at the edge of each arm) for 15 min (Day 1, acquisition phase). The following day, mice were returned to the maze that now contained one familial and one novel object (Day 2, recognition phase). The type and positions of the familialand novel objects in the chamber were changed semi-randomly between mice but kept constant for any given animal. The time that mice spent exploring each of the two objects in the acquisition and recognition phases was measured. The discrimination index for the novel object was calculated as the time exploring the novel object minus time exploring the familial object, relative to total time exploring (exploration of familial and novel object).

3.2.22 Golgi staining

For Golgi-Colonnier staining, adult mice (n=3 per group) were deeply anesthetized and transcardially perfused with 2% paraformaldehyde-2% glutaraldehyde in 0.12 M phosphate buffer. Brains were removed from the skull and postfixed in the same fixative solution overnight. Pieces containing the whole hippocampal formation were dissected and incubated in a dichromate-Colonnier solution (3% K2Cr2O7, 5% glutaraldehyde in H2O) for 5 days at 15ºC. Pieces were then transferred to a 0.75% AgNO3 solution for 3 days. After embedding the pieces in paraffin, 200-µm thick sections were obtained and subsequently dehydrated. The sections were then mounted onto slides and coverslipped with an Araldite solution.

3.2.23 Statistical analysis

To determine plaque load in the hippocampus (from 1.35 mm to 2.30 mm posterior to Bregma), an area immunostained with anti-Aβ amino acids 1-5 (clone 3D6) was determined using ImageJ software and normalized to the total hippocampal area in 30-µm thick sections containing one hemisphere. Significance between groups (J20;

TgRln/J20) was analyzed using the unpaired Student's t test (n=3-5 animals per group; 6-8 sections per animal).

To quantify toxicity from the PI stained cell cultures, fluorescent micrographs were randomly taken from coverslips for each condition. The number of dying neurons (PI/Hoechst double-labeled picnotic nuclei) versus total amount of cells (Hoechst-labeled) per field were counted for statistics from 4 independent experiments. Percentage of survival (%survival) per field was calculated following equation 2:

$$(2) \qquad \%survival = 100 - \frac{(\%field - \bar{x}\ vehicle)}{(\bar{x}\ triton - \bar{x}\ vehicle)}$$

%field is the percentage of died cells in a specific field; $\dot{x}$ *vehicle* is the average percentage of died cells per field in vehicle-treatment conditions in a specific experiment; $\dot{x}$ *triton* is the average percentage of died cells in 0.01% triton X-100-treatment conditions in a specific experiment. Significance between treatment conditions was analyzed by ANOVA or unpaired Student's t test (n=15-40 fields counted per condition).

To quantify toxicity from the MTT assay, measures from 3-4 replicates from 4 independent experiments were used. Percentage of survival was calculated considering vehicle treatments as 100% survival for each experiment.

Spine density from golgi-stained preparation was counted at hippocampal area over 10 µm in secondary dendrites from the *stratum radiatum* (SR) and the *stratum lacunosum moleculare* (SLM) of CA1 piramidal neurons starting at 5-10 µm from the ramification point (n=3 animals per group; 20-35 neurons per animal). Significance between groups was analyzed by ANOVA or unpaired Student's t test.

To determine differences in NOR task between groups, discrimination indexes were analyzed by ANOVA or unparied Student's t test (n=8-12 animals per group).

RESULTS

4.1 In vitro purification of Reelin

4.1.1 Setting up a protocol of Reelin purification from cell supernatants

With the aim of analysing *in vitro* possible interplays between Reelin and Aβ peptide, we first needed to set up conditions for the purification of Reelin from supernatants of a cell line stably transfected with full-length Reelin (clone pCrl, Forster et al., 2002). Many of the existing protocols using Reelin in biological assays are simply based on the collection of supernatants from Reelin-expressing cells (Simo et al., 2007). The main disadvantage of using enriched supernatants, whatever the protein in question, lays in the low purity of the enriched protein, due to the presence of many contaminating proteins in the cell medium. To avoid any kind of interference from proteins in the preparation that may affect the specificity of the results observed, we decided to subject Reelin supernatants to a two-step strategy of chromatography purification: an ion-exchange chromatography followed by a size exclusion chromatography (SEC) in a Fast Protein Liquid Chromatography (FPLC) system. In parallel to Reelin, as a negative control, Mock supernatants were produced from 293 cells stably transfected with GFP (Forster et al., 2002) and subjected to same protocol of purification.

The theoretical isoelectric point of Reelin protein is around pH 5.2 (estimated by ProtParam software (Gasteiger et al., 2005)), meaning that for pH values around 7.5 Reelin is negatively charged and thus suitable for an anion exchange (ANX) chromatography. Reelin and Mock supernatants are thus passed through a positively-charged column in a mobile phase of NaCl 30 mM/Phosphate buffer 10mM at pH 7.6. Elution is made by increasing the ionic strength of the mobile phase in five steps. This allowed us to separate a Reelin-enriched peak (between 250 and 350 mM NaCl) (delimitated by violet dashed lines in **Fig. 4.1a**), corroborated by western blot analysis of the eluted fractions. A correspondent peak in Mock sample, of lower intensity, is eluted in the same fractions (Fig. **4.1a**). This indicates that the Reelin-containing peak coming from the ANX chromatography still contains proteins coming from the cell culture medium.

Next, Reelin and Mock ANX-collected sample were concentrated and passed through a SEC column, in order to further separate, by gel filtration, Reelin from the impurities

coming from the previous step. Samples were released for isocratic elution in 10 mM Phosphate Buffer/30 mM NaCl (pH 7.4). As we can see in the chromatogram, around the mL 11 a Reelin-containing peak is eluted (**Fig 4.1b**, peak on the red continuous curve among the violet dashed lines), corroborated by western blot of the collected fractions. The peak appearing in correspondence with the column void volume (mL 7.5), where high molecular weight aggregates of proteins appear, also contains Reelin. Differently from the ANX elution profile, in the SEC chromatogram, Reelin peak gets rid of any correspondent peak in the Mock sample (**Fig. 4.1b**).

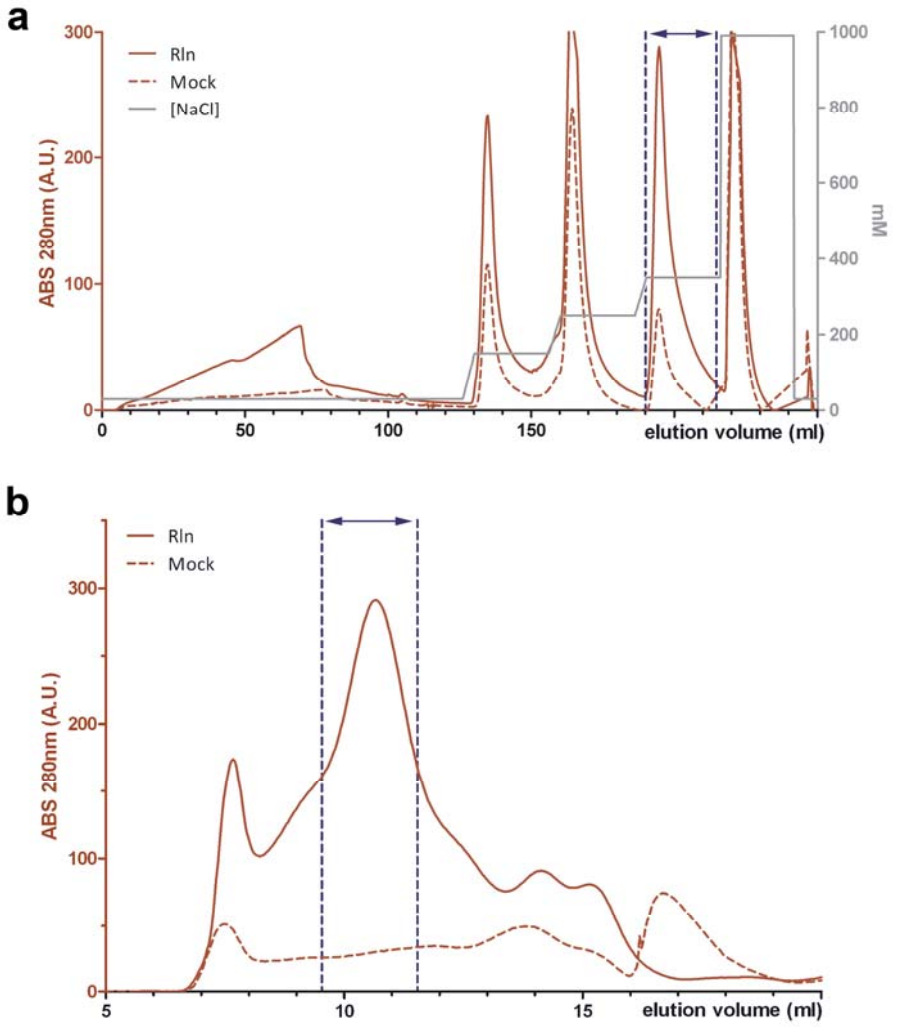

Figure 4.1. Reelin purification. a) Anion exchange (ANX) chromatogram of supernatants from 293T cells stably transfected with Reelin or GFP (Mock). Reelin and Mock elution profiles are represented by a red continuous and a red dashed curve respectively. The gray line represents mobile phase elution gradient. Reelin peak, and the correspondent Mock fractions, are delimitated by violet dashed lines. **b)** Size exclusion chromatogram of ANX-collected peaks. Reelin and Mock elution profiles are represented by a red continuous and a red dashed curve respectively. Reelin peak, and the correspondent Mock fractions, delimitated by violet dashed lines, are used as purified samples for *in vitro* studies.

4.1.2 Analysis of purified Reelin sample

In order to test the purity of the Reelin obtained, Reelin and Mock samples were analysed by sodium dodecyl sulphate-polyacrylamide gel electrophoresis (SDS-PAGE), followed by either Coomassie or Sypro Ruby staining. Throughout the process of purification, we observed a decrease in the intensity of unspecific bands and a concomitant increase in the percentage of the bands of a molecular weight corresponding to full-length Reelin, or to its fragments (**Fig. 4.2**). The purity level of the Reelin obtained was estimated to be around 85%.

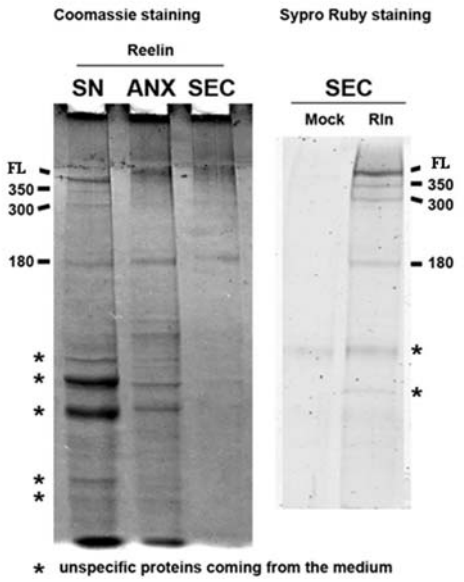

Figure 4.2. Reelin purity. Reelin samples were subjected to an SDS-PAGE, followed by Coomassie staining (left). Full length (FL) Reelin and its 350, 300 and 180 kDa fragments are indicated. Asterisks indicate non-specific proteins coming from the cell supernatant. Throughout the different purification steps, the intensity of unspecific bands decreases while Reelin bands are maintained. Quantification by Sypro Ruby staining (right) of Reelin and Mock purified samples allows estimating the purity level for Reelin bands to be around 85% of the total protein. The remaining 15% corresponds to unspecific bands in the sample. SN, supernatant; ANX, Anion-exchange chromatography; SEC, Size Exclusion chromatography.

The concentration of Reelin obtained was quantified by Bradford assay or by comparison with known amounts of BSA on Coomassie staining, and ranged from 100 to 200 ng/µl. The process described above allowed us to obtain, in a reproducible manner, suitable amounts of purified Reelin for its use in further biological and/or biophysical assays.

To confirm the presence of Reelin in purified samples a bottom up proteomic approach was chosen. After running pure Reelin samples on SDS-PAGE, Reelin bands were digested with trypsin, followed by analysis of the digested peptides through liquid chromatography (LC), coupled to tandem mass spectometry (MS/MS). This strategy allows sequencing each of the peptides. Each peptide fragmentation mass spectrum is used to identify the protein from which it derives by searching against a protein

sequence database or annotated peptide spectra in a peptide spectral library. In this way, peptides can be identified and multiple peptide identifications are assembled into a protein identification. After the database search, each peptide-spectrum match (PSM) needs to be evaluated by bioiformatic analysis.

One of the limitations of this strategy lays in the analysis of proteins subjected to glycosylation, mainly N-glycosylation (the most common type of glycosylation in eukaryotic proteins, that consists in the attachment of glycans to a nitrogen of asparagine or arginine side-chains (Aebi, 2013) or O-glycosylation (where glycans are attached to the hydroxyl oxygen of serine, threonine, tyrosine, hydroxylysine or hydroxyproline side-chains) (Hounsell et al., 1996). These types of post-translational modifications can considerably change the mass of a peptide from its non-glycosylated form, depending on the kind and length of glycans attached, and on the percentage of glycosylation coverage for any residue. Thus highly glycosylated proteins would result in glycosylated peptides that are not going to be detected through analysis of their Mass Spectra.

Reelin is highly glycosylated in its N-terminal, mainly through N-glycosylations, and, to a lesser extent, through O-glycosylation (D'Arcangelo et al., 1997). Since this could possibly impair the proteomic analysis of our sample, purified Reelin, together with Mock control, was previously subjected to deglycosylation with PNGase F (Peptide-*N*-Glycosidase F), an amidase that releases asparagine-linked oligosaccharides from glycoproteins and glycopeptides by hydrolyzing the amide group of the asparagine (Asn) side chain. This enzymatic reaction removes with high efficiency N-linked oligosaccharides from glycoproteins (Tarentino and Plummer, 1994), leaving the oligosaccharide intact, while the Asn residue from which the sugar is removed is deaminated to aspartic acid. Together with PNGase F, a cocktail of other four deglycosylation enzymes (namely α-Neuraminidase, O-Glycosidase, β-Galactosidase and β -N-Acetylglucosaminidase) was applied to the samples, to remove O-linked glycans.

Next, deglycosylated samples, together with non-deglycosylated controls, were run on a 6% SDS-PAGE and stained with Sypro Ruby. We observed an increased electromobility for Reelin bands in the deglycosylated samples, confirming the presence of abundant glycosylations (**Fig 4.3a**).

Sypro Ruby-stained bands containing either full length Reelin or Reelin fragments coming from deglycosylated or not-deglycosylated samples, underwent protein

extraction. Protein extracts, constituting the real object of our proteomic analysis, underwent trypsin digestion, followed by peptide analysis by LC coupled to MS/MS (LC-MS/MS) (**Fig. 4.3b**).

A difference of 1 Dalton between the mass of a deglycosylated peptide and the expected mass for the same peptide in its not-glycosylated state was registered in the Mass Spectra of peptides that actually underwent deglycosylation. This is due to the enzymatic deamidation of an Asn residue, then converted to an aspartic one. Mass Spectra were analysed with the software Proteome Discoverer and the search engine Sequest, and matched to the UniprotSwissport Data Base. This analysis revealed that 123 distinct peptides with medium to high reliability (Percolator software) were consistent with the Reelin sequence, confirming that actually the purification protocol we set up leads to Reelin (**Fig. 4.3c**).

Though it is known that Reelin protein is highly glycosylated, its exact sites of glycosylation and the type of glycans involved, have not been described yet. To determine which Reelin-residues are N-glycosilated, an i*n silico* analysis on Reelin protein sequence was performed with NetNGlyc 1.0 Server (Blom et al., 2004). This software searches for the N-glycosylation consensus sequence Asn-Xaa-Ser/Thr, where Xaa is any aminoacid except Proline, and Ser/Thr is either Serine or Threonine. Since the consensus tripeptide Xaa-Ser/Thr is a prerequisite, but is not sufficient alone, for N-glycosylation, other parameters are taken into account in the prediction, such as the protein fold. This analysis indicated 25 possible sites of N-glycosylation for Reelin along its full-length sequence, with different prediction scores, ranging from 0 to 1. Scores under 0.5 indicate potential N-glycosylation sites, while scores above 0.5 indicate predicted N-glycosylation sites (**Fig. 4.3d**).

To eventually confirm some of the N-glycosylation sites predicted by our bioinformatic analysis, Asn deamidation was analyzed in the Mass Spectra of peptides from deglycosylated versus non-deglycosylated samples. In particular, non-glycosylated peptides are expected to be found in a non-deamidated state, both before and after deglycosylation reaction. Glycosylated peptides instead are expected to be masked before deglycosylation reaction and to be found in a deamidated state after deglycosylation. By this criterion we found 3 deamidated-asparagine-containing peptides specifically in the deglycosylated sample, which were not detected in the non-deglycosylated sample (**Fig. 4.3e**). This indicates a possible 100% N-glycosylation of these peptides that made them undetectable in the not deglycosylated sample. The three

glycosylated fragments detected are located in the N-terminal domain and extend respectively from the aminoacids 290-300, 303-321 and 1267-1282. This search established that three of the Reelin Asn residues indicated in the bioinformatic analysis as potential (Asn 291 and 1267; arrowheads in **Fig. 4.3d**) or predicted (Asn 306; arrow in **Fig. 4.3d**) sites for N-glycosylation, actually undergo this type of modification.

In conclusion our proteomic analysis confirmed that we purified Reelin protein. Moreover, although it is known that N-glycosylation of Reelin occurs mainly in the N-terminal domain (D'Arcangelo et al., 1997), our work reveals the position of three glycosylation sites. Further studies will be needed to find out more Reelin glycosylation sites and to uncover the type of glycans involved in these glycosylations. A workflow of the whole proteomic approach is represented in **Fig. 4.3**.

Figure 4.3 Proteomic workflow. Bottom up proteomic approach. **a)** Reelin-expressing cell supernatant and Mock control underwent purification as described in **Chapter 4.1.1** and were subjected to deglycosylation with PNGase F and α-Neuraminidase, O-Glycosidase, β-Galactosidase and β -N-Acetylglucosaminidase to remove N-and O-glycosylations. Reelin bands show increased electromobility as a consequence of deglycosylation. Asterisks indicate residual impurities coming from the cell culture medium, both in Reelin and in Mock samples. Arrowheads indicate deglycosylation enzymes, in Mock and Reelin deglycosylated samples. **b)** Deglycosylated and not deglycosylated samples underwent trypsin digestion followed by LC peptide separation coupled to Tandem Mass Spectometry (LC-MS/MS). **c)** Bioinformatic analysis of Mass Spectra revealed 123 peptides overlapping to Reelin sequence, with medium (yellow fragments, 45-75%) to high (green fragments, 76-99%) confidence. **d)** A bioinformatic analysis of Reelin protein sequence reveals 25 possible sites of N-glycosylation for Reelin protein. Among these, Asn 291 and Asn 1267 are indicated as potential N-glycosylation sites (arrowheads), and Asn 306 is indicated as a predicted N-glycosylation site (arrow). **e)** Comparison between Mass Spectra from glycosylated and deglycosylated Reelin sample revealed three peptides only detected in the deglycosylated sample in a deamidated state, thus indicating that they are N-glycosylated. The three peptides contain the asparagines 291, 306 and 1267. FL, full length; DB, data base; n, deamidated asparagine.

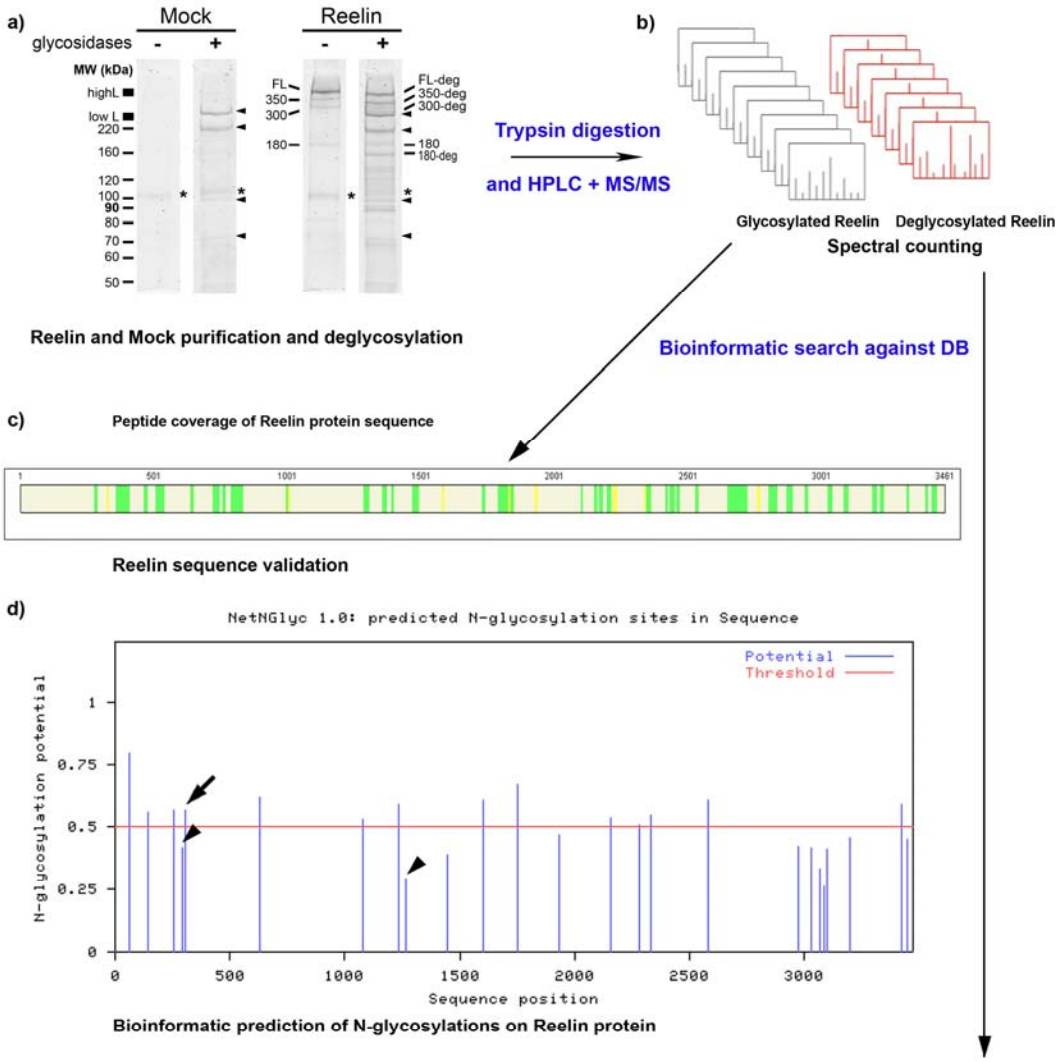

4.1.3 Analysis of Reelin functionality

To assess the biological functionality of the purified Reelin, primary neuronal cultures from E16 mouse forebrain were cultured for 3-5 days and treated with either Reelin or Mock samples. Treatment with Reelin supernatant led to a significant increase in the phosphorylation of its transducer Dab1, detected by Dab1 immunoprecipitation followed by WB anti-phosphotyrosines. In particular a 8,6 fold increase in the levels of

phosphorylated Dab1 is produced by treatment with Reelin supernatant compared to Mock supernatant (**Fig. 4.4**, lanes 4 and 3). The process of Reelin purification did not affect its functionality (**Fig. 4.4**, lane 5). Storage of purified Reelin samples by nitrogen freezing or nitrogen freezing followed by lyophilisation did not affect its biological properties (**Fig. 4.4**, lane 6 and 7). Indeed no significant difference in the levels of phosphorylated Dab1 is observed between treatments with Reelin supernatants, fresh purified Reelin or purified Reelin that was thawed after either nitrogen freezing or nitrogen freezing and lyophilisation (**Fig. 4.4**, lanes 4, 5, 6 and 7).

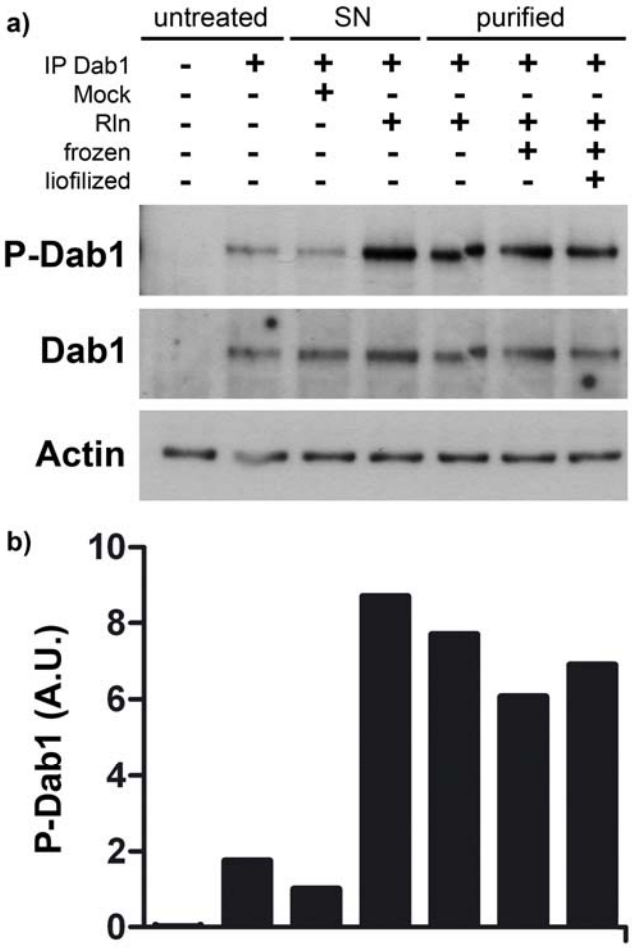

Figure 4.4. Analysis of purified Reelin functionality. Reelin functionality is assessed as the ability to induce phosphorylation of Dab1 after 15 minutes treatment of mouse neuronal primary cultures. Phosphorylation of Dab1 is detected by immunoprecipitation (IP) of total Dab1, followed by western blot (WB) anti-phosphotyrosines. **a)** Negative control of IP and basal levels of Dab1 phosphorylation are shown respectively in lane 1 and 2. Mock supernatant does not induce changes in the basal levels of Dab1 phosphorylation (Lane 3), while Reelin supernatant induce a high increase in the phosphorylation of Dab1 (Lane 4). Freshly purified Reelin is also functional (Lane 5) and maintains its biological activity after nitrogen freezing (Lane 6) or nitrogen freezing followed by lyophilisation (Lane 7). **b)** Densitometric analysis of phosphorylated Dab1 WB image shows a 6-8 fold increase upon Reelin treatment.

4.2 In vitro analysis of Reelin influence on the dynamics of Aβ aggregation and the toxicity of Aβ oligomers

4.2.1 Reelin delays the formation of $A\beta_{42}$ fibrils

To analyze whether Reelin affects the kinetics of $A\beta_{42}$ aggregation into amyloid fibrils, a freshly isolated $A\beta_{42}$ preparation (24 μM), which contained monomeric $A\beta_{42}$ in rapid equilibrium with low molecular weight (LMW) oligomers, was allowed to aggregate in the presence or in the absence of either purified Reelin or equivalent volumes of purified Mock (**Chapter 4.1.1**). Aggregation was carried out in 10 mM Phosphate Buffer, at low-salinity conditions (5 mM NaCl). The following mixtures were run in parallel: $A\beta_{42}$; $A\beta_{42}$:Reelin ($A\beta_{42}$/Rln) in a ratio 6:1 w/w (18 ng/μL of Reelin); and $A\beta_{42}$:Mock control ($A\beta_{42}$/Mock) (same volumes as for Reelin). Additionally, Reelin (Rln) and Mock preparations without addition of $A\beta_{42}$ were tested. $A\beta_{42}$ aggregation process was performed at 20ºC and monitored every 24 hours by thioflavin T (ThT) fluorescence assay and transmission electron microscopy (TEM).

ThT is an organic compound able to bind to amyloid fibrils containing β-sheet structures. When bound to fibrils, ThT exhibits fluorescence emission at 485 nm upon stimulation at 450 nm, so that measuring ThT fluorescence intensity is an assay for monitoring amyloid aggregation.

In the absence of Reelin (i.e. $A\beta_{42}$ and $A\beta_{42}$/Mock samples) a time dependent increase in ThT fluorescence emission was observed from day seven onwards (**Fig. 4.5a**, gray and black curves). Lag-phase of aggregation, considered as the nucleation phase previous to fibril growth, was calculated by adjusting a sigmoidal curve to the experimental data (i.e. 8,3 days for $A\beta_{42}$ and 7,9 days for $A\beta_{42}$/Mock). ThT binding assay of $A\beta_{42}$/Rln sample shows a slowdown in the kinetics of the process with a 2,5-day delay in the appearance of amyloid fibrils (**Fig. 4.5a**, red curve) and an estimated Lag-phase duration of 10,9 days. In agreement with ThT data, TEM images obtained during the Lag-phases showed merely amorphous deposits without fibrils (**Fig. 4.5b**). At day 9, for $A\beta_{42}$/Mock sample, isolated fibril-like structures start to appear, while presence of mature fibrils can be observed from day 11 onwards coinciding with maximum ThT emission fluorescence (**Fig. 4.5b**, upper panels). As expected from the ThT data, electron micrographs from $A\beta_{42}$/Rln sample confirm a 2,5-day delay in the

process of aggregation with appearance of isolated fibrils on day 11 and mature fibrils from day 13 onwards (**Fig. 4.5b**, bottom panels).

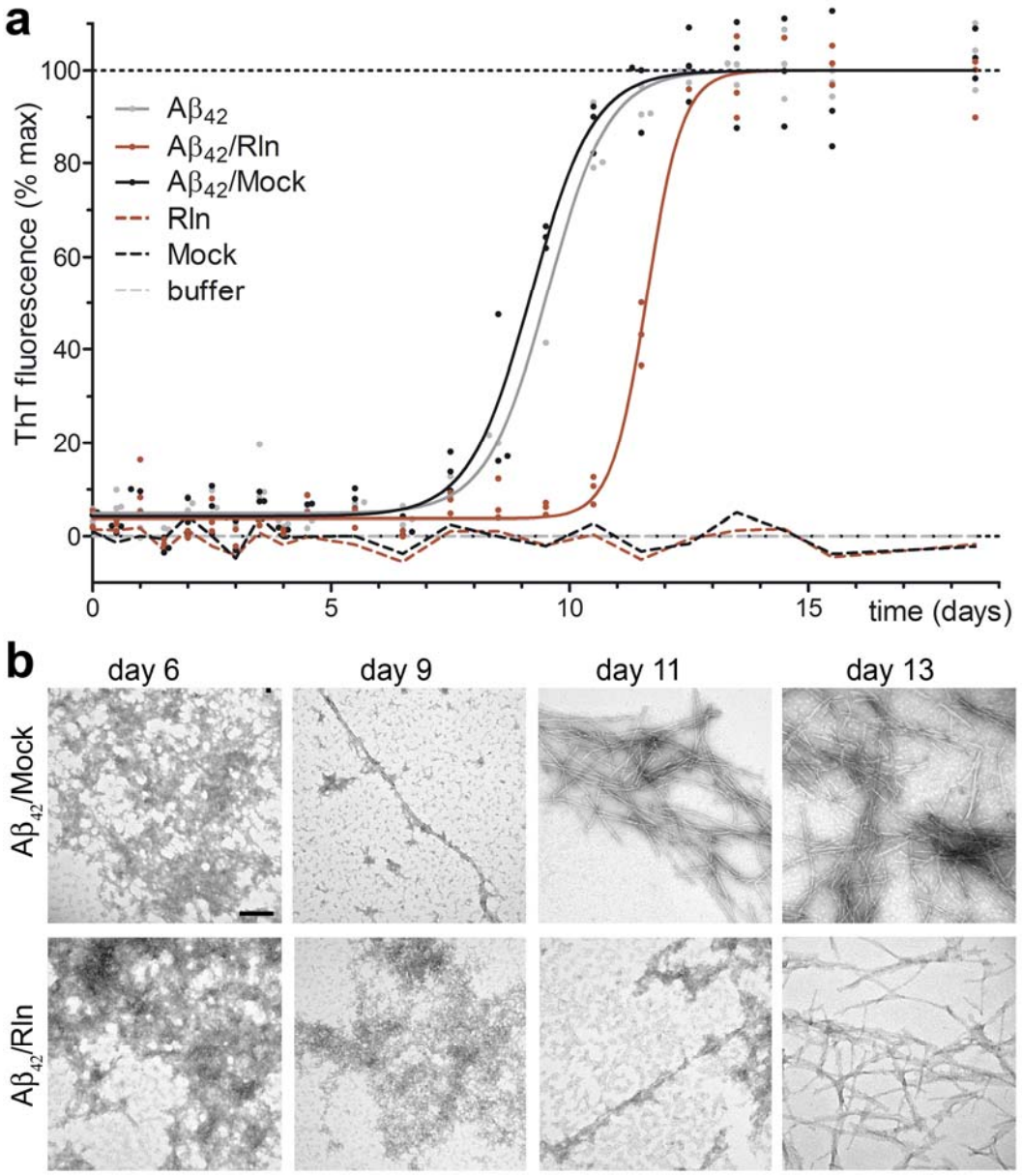

Figure 4.5. Reelin modulates the kinetics of Aβ$_{42}$ aggregation. a) Time-course quantification of amyloid fibril content detected by Thioflavin-T binding assay in Aβ$_{42}$, Aβ$_{42}$/Rln, Aβ$_{42}$/Mock, Rln and Mock preparations. Reelin induces a 2,5-day delay in the appearance of fibrils when present in the preparation of Aβ$_{42}$/Rln sample at a rate of 6:1 (w/w) . **b)** Transmission electron micrographs obtained during the time-course of aggregation showing that fibrillar structures appear with a 2-day delay when Reelin is present (lower pannels). Scale bar: **b**, 100 nm.

To study whether the delay induced by Reelin in amyloid aggregation kinetics was dependent on Reelin concentration we prepared Aβ$_{42}$/Rln mixtures with 24 μM Aβ$_{42}$

and two additional concentrations of Reelin: 9 ng/µL ($A\beta_{42}/Rln^{9}$) and 27 ng/µL ($A\beta_{42}/Rln^{27}$), maintaining $A\beta_{42}$ at the concentration of 24 µM. Aggregation was carried out in 10 mM Phosphate Buffer/17 mM NaCl, a higher salinity condition compared with the previous experiment. The increased salinity of the experiment was necessary to get a higher concentration of Reelin and caused a faster start of the aggregation for all samples in comparison with the previous aggregation experiment (**Fig. 4.6**).

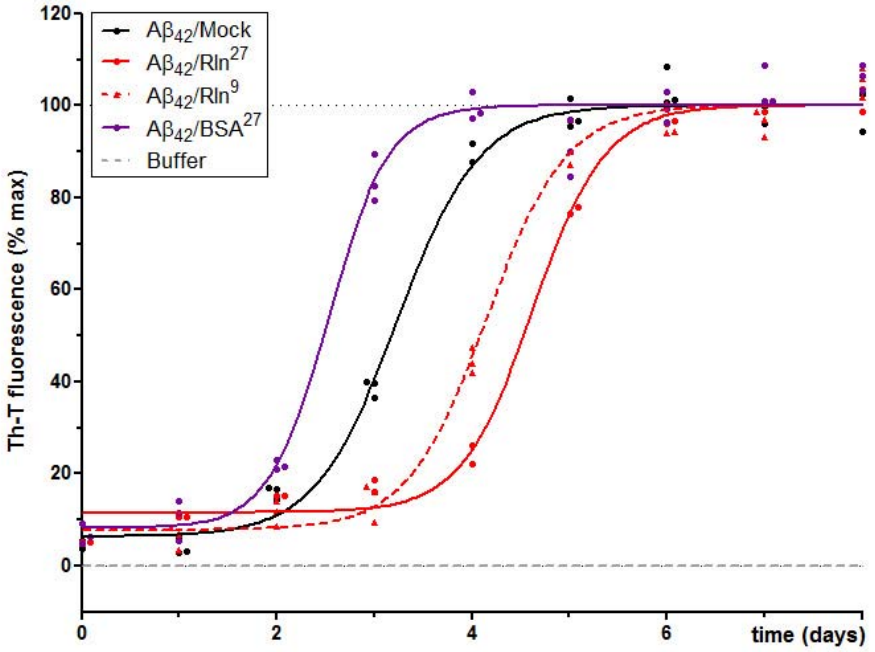

Figure 4.6. Reelin delays $A\beta_{42}$ aggregation kinetics in a specific and concentration-dependent fashion. Time-course of amyloid fibrillization detected by Thioflavin-T binding assay in $A\beta_{42}$ (24 µM) preparations, 17 mM NaCl. Using two different Reelin concentrations (9 and 27 ng/µL) a delay proportional to Reelin concentration is produced (black curve represents $A\beta_{42}$/Mock aggregation, red dashed curve represents $A\beta_{42}/Rln^{9}$; red continuous curve represents $A\beta_{42}/Rln^{27}$). Violet curve represents the aggregation of $A\beta_{42}/BSA^{27}$ samples, ensuring that Reelin induced delay in a specific manner.

Even in the new conditions the Reelin-induced delay was conserved, indeed both $A\beta_{42}/Rln^{27}$ and $A\beta_{42}/Rln^{9}$ started the aggregation later than the control $A\beta_{42}$/Mock, and Reelin-induced slowdown in the aggregation kinetics was found to be dependent on the concentration of Reelin in solution, being $A\beta_{42}/Rln^{27}$ sample more delayed than $A\beta_{42}/Rln^{9}$ sample ($A\beta_{42}$/Mock lag phase duration: 1,23 days; $A\beta_{42}/Rln^{9}$ lag phase duration: 2,15 days; $A\beta_{42}/Rln^{27}$ lag phase duration: 2,63 days; **Fig. 4.6** black curve, red dashed curve and red continuous curve respectively). A mixture of $A\beta_{42}$ with Bovine Serum Albumin (BSA) at the concentration of 27 ng/µL ($A\beta_{42}/BSA^{27}$) was used as a

further control, to ensure that the observed slow-down was specifically dependent on Reelin. $A\beta_{42}$/BSA[27] sample aggregated faster than the $A\beta_{42}$/Mock sample, with a lag phase duration of 0,53 days (**Fig. 4.6**, violet curve).
Altogether these data show that Reelin delayed the appearance of amyloid fibrils in a specific and dose-dependent fashion.

4.2.2 Reelin elongates life span of $A\beta_{42}$ oligomers

To get insights into the molecular mechanisms of Reelin-induced delay in fibril formation, we studied the nature of $A\beta_{42}$ oligomeric species present during the initial steps of amyloidogenesis, before fibril formation. Oligomers of amyloidogenic proteins exist as metastable mixtures, in which the oligomers dissociate into monomers and associate into larger assemblies simultaneously. One of the techniques most frequently used to stabilize oligomer populations is the Photo-Induced Crosslinking of Unmodified Proteins (PICUP) (Bitan and Teplow, 2004). This technique is based on covalent cross-linking of the oligomeric species in solution and when combined with fractionation methods, such as SDS-PAGE or SEC, PICUP provides snapshots of the oligomer size distributions that existed before cross-linking (Rahimi et al., 2009). Thus, to test whether Reelin affected the distribution of specific oligomeric population, we analysed by PICUP, followed by western blotting against Aβ, the distribution of low-molecular weight (LMW) $A\beta_{42}$ oligomers (going from dimers to heptamers) in the conditions used for the experiment in **Fig. 4.5**: 10 mM Phosphate Buffer, low-salinity (5 mM NaCl), $A\beta_{42}$ 24 μM, ratio $A\beta_{42}$:Reelin 6:1 w/w. Before the appearance of fibrils, we found unvaried distribution of LMW oligomeric species between $A\beta_{42}$/Mock and $A\beta_{42}$/Rln samples (day 6 in **Fig. 4.7a**, lanes 1 and 2). Contrariwise, during the 2,5-day delay induced by Reelin, LMW oligomers disappeared from $A\beta_{42}$/Mock sample while maintained in $A\beta_{42}$/Rln sample (day 9 in **Fig. 4.7a**, lanes 3 and 4). LMW oligomers were no longer visible when fibrils are present in both $A\beta_{42}$/Mock and $A\beta_{42}$/Rln samples (**Fig. 4.7a**, lanes 5 and 6). The effect of Reelin on the formation of high molecular weight (HMW) soluble oligomers, containing species up to 40-mer, was also studied by dot blot analysis with A11 antibody, a conformation-specific antibody that binds to oligomeric forms of Aβ, but not to monomeric nor fibrillar ones (Kayed et al., 2003). Our results again showed a 2-day prolonged A11 specific signal during the delay

phase of the aggregation in the $A\beta_{42}$/Rln sample as compared with $A\beta_{42}$/Mock (**Fig. 4.7b**). Altogether these results indicate that Reelin is delaying *in vitro* the formation of $A\beta_{42}$ fibrils, by extending the life-time of LMW and HMW oligomeric species.

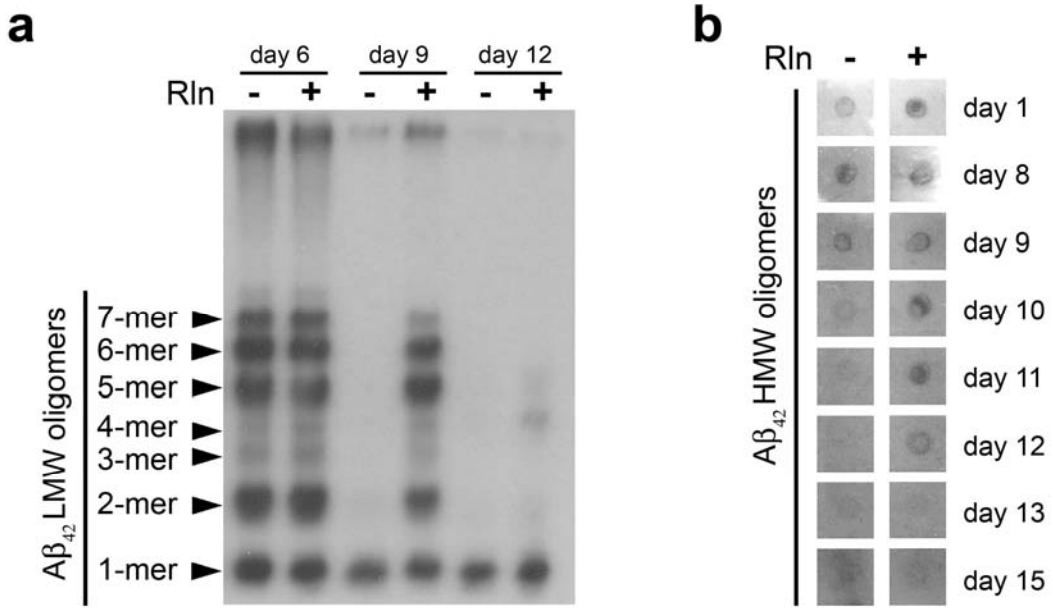

Figure 4.7. Reelin prolonges life span of $A\beta_{42}$ LMW and HMW oligomers. a) Western Blot detection of $A\beta_{42}$ peptides after Photo-Induced Crosslinking of Unmodified Proteins (PICUP) at different time-points during the process of aggregation of $A\beta_{42}$ in the presence or in the absence of Reelin. Reelin expands the time-window in which LMW oligomeric species of 2 to 7-mer are present. **b)** Dot-blot detection of HMW oligomeric species of $A\beta_{42}$ by A11 oligomer-specific immunoreactivity in the presence and in the absence of Reelin. Reelin expands the time-window in which HMW oligomeric species of >40-mer are present. LMW, low-molecular weight; HMW, high-molecular weight.

4.2.3 Reelin interacts with soluble $A\beta_{42}$, is sequestered by amyloid fibrils and loses its biological functionality

Once observed that Reelin modulates $A\beta_{42}$ fibril formation, we examined possible interactions between Reelin and amyloid species. To this aim, we performed immunoprecipitation assays of $A\beta_{42}$/Rln samples obtained at pre-fibrillar stages of aggregation (days 2-4), in the conditions used for the experiment in **Fig. 4.5**: 10 mM Phosphate Buffer, low-salinity (5 mM NaCl), $A\beta_{42}$ 24 μM, ratio $A\beta_{42}$:Reelin 6:1 w/w. Western blot analysis of anti-Aβ and anti-Reelin immunoprecipitated samples revealed a specific interaction between Reelin and soluble $A\beta_{42}$ species (**Fig. 4.8a**).

We next analyzed the distribution of Reelin in $A\beta_{42}$/Rln samples taken at the fibrillar stage of aggregation, when insoluble $A\beta_{42}$ fibrils are formed. Western blot analysis of

$A\beta_{42}$/Rln aliquots taken during aggregation revealed that concomitantly with the start of fibril formation, Reelin bands disappear from their expected MW and appear at the well-bottom of the SDS-PAGE gel (day 12, **Fig. 4.8b**). This finding suggests that Reelin is sequestered into the assembling amyloid fibrils. As a further indication of the Reelin-$A\beta_{42}$-fibril interaction, $A\beta_{42}$/Rln fibrils assembled *in vitro* were subjected to double immunogold labelling for Reelin and $A\beta_{42}$, using 18 and 12 nm diameter Nanogold particles respectively. Electron micrographs revealed the colocalization of Reelin and $A\beta_{42}$ into the *in vitro* aggregated fibrils (indicated by arrowheads and arrows in **Fig. 4.8c**). Taken together, our experiments with purified Reelin and $A\beta_{42}$ show a direct interaction between Reelin and $A\beta_{42}$ at early pre-fibrillar stages of amyloid aggregation. Moreover, in the fibrillar stage of amyloid aggregation, our data support the interaction of Reelin and $A\beta_{42}$ fibrils, which occurs independently of additional partners that may be present in the senile plaques *in vivo*.

To analyse whether the presence of Reelin into $A\beta_{42}$ fibrils could have any effect on their structural properties, we examined dryed fibrils by X-ray diffraction. $A\beta_{42}$/Mock fibrils showed the two characteristic perpendicular reflection arcs at equatorial (4.73 Å, corresponding to the hydrogen bonds in beta sheets) and meridional (10.5 Å, corresponding to the sidechains distances in beta sheets) axes, as expected for fibrillar cross-beta structure of aligned fibrils (with β strands arranged perpendicular to fribril axis (Petkova et al., 2002)) (**Fig. 4.8d**). $A\beta_{42}$/Rln also showed the same reflexions, evidencing that fibrils have been properly aligned and maintain cross-beta structure (**Fig. 4.8d**). This observation indicates that Reelin does not promote any systematic alteration in the fibrillar pattern, but rather could interact with Aβ along the surface of the fibril.

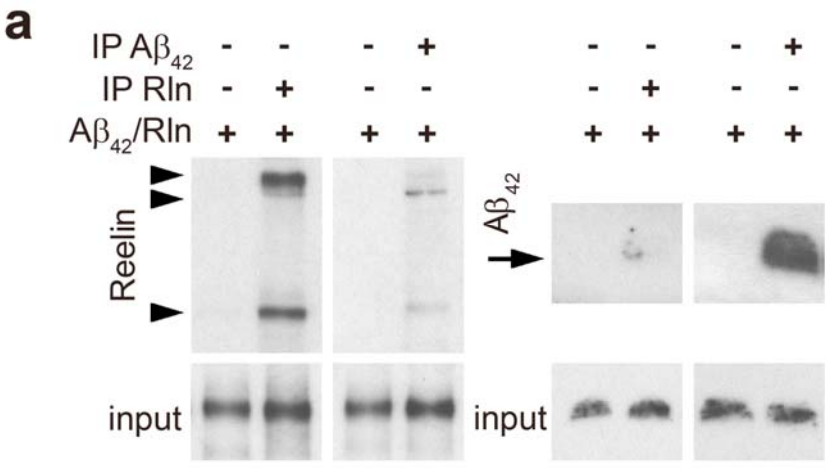
a
IP Aβ42
IP Rln
Aβ42/Rln
Reelin
Aβ42
input
input

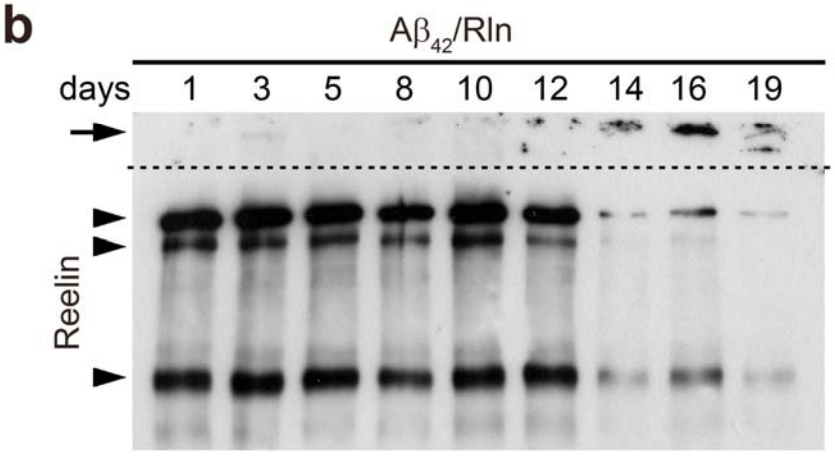
b
Aβ42/Rln
days 1 3 5 8 10 12 14 16 19
Reelin

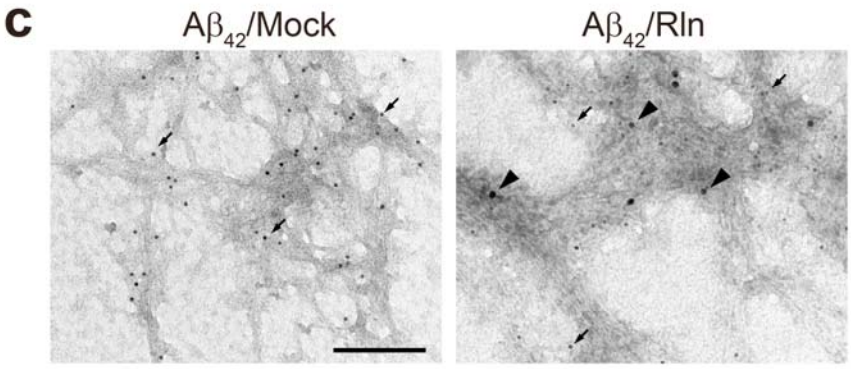
c
Aβ42/Mock
Aβ42/Rln

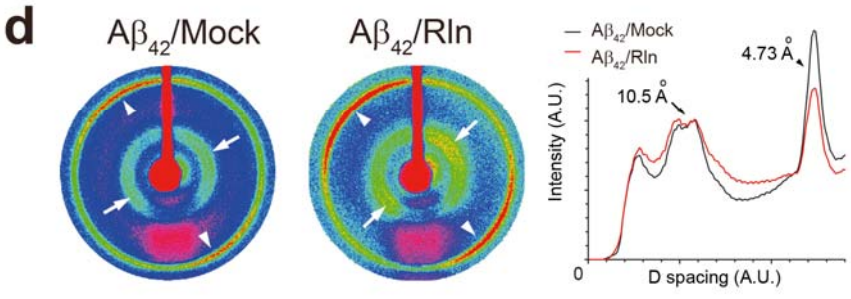
d
Aβ42/Mock
Aβ42/Rln
Aβ42/Mock
Aβ42/Rln
10.5 Å
4.73 Å
Intensity (A.U.)
0
D spacing (A.U.)

Figure 4.8. Reelin interacts with aggregating Aβ$_{42}$ and gets trapped into fibrils. a) Aβ$_{42}$ and Reelin immunoprecipitation on pre-fibrillar Aβ$_{42}$/Rln, followed by western blot against either Reelin (arrowheads; left panels) or Aβ (arrow; right panels). Negative controls of not-immunoprecipitated samples are shown in lanes 1, 3, 5 and 7 (upper panels). Lanes 2 and 8 show the positive controls of immunoprecipitated Reelin and Aβ$_{42}$ respectively (upper panels). Reelin and Aβ co-immunoprecipitate, as shown in lanes 4 and 6, indicating a specific interaction. Lower panels show input samples for Reelin (180 kDa band; left panels) and Aβ$_{42}$ (right panels) before immunoprecipitation. **b)** Western blot of Reelin during the time-course of Aβ$_{42}$/Rln aggregation showing a decrease in soluble Reelin (arrowheads), coinciding with the time-point when Aβ$_{42}$ fibrils start appearing. A Reelin-specific signal appears at the well-bottom, indicating the presence of this protein in insoluble debris (arrow). **c)** Transmission electron micrographs of double immuno-gold labelling of Aβ (12-nm particles; arrows) and Reelin (18-nm particles; arrowheads). Reelin-specific signal is detected colocalizing with fibrils. **d)** X-ray fibril diffraction pattern for aligned fibrils showing the two characteristic reflection arcs on the equatorial (parallel with the fibril axis at 4.73 Å (arrowheads)) and meridional (at 10.5 Å (arrows)) axes. Diffraction signal intensity is pseudocolored in ImageJ software using spectrum LUT. One-dimensional azimuthal plots showing intensity of diffractions as a function of D-spacing indicates that, in the presence of Reelin, the structure of the fibrils is conserved. Scale bar: **c**, 200 nm

Parallel to Reelin immunodetection into amyloid fibrils, we analysed its biological functionality before and after the aggregation process. In detail, we looked at phosphorylation levels of Reelin transducer Dab1 in primary embryonic mouse forebrain cultures treated with Aβ$_{42}$/Mock, Aβ$_{42}$/Rln or purified Reelin samples taken before the appearance of fibrils (pre-fibrillar phase) or at the end point of aggregation (fibrillar phase). Samples not treated with Reelin show low basal levels of Dab1 phosphorylation (**Fig. 4.9**, lanes 1 and 4). Aβ$_{42}$/Rln sample is able to induce phosphorylation of Dab1 in the prefibrillar phase, but not in the fibrillar phase (**Fig. 4.9**, lanes 2 and 5). A control of purified Reelin subjected to same experimental conditions but without Aβ$_{42}$ retains its biological activity throughout the experiment, indicating that experimental conditions do not cause loss of Reelin functionality (**Fig. 4.9**, lanes 3 and 6).

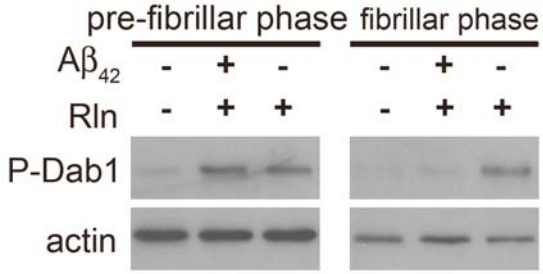

Figure 4.9. Reelin loses its biological activity once trapped into amyloid fibrils. Reelin-activity is assessed as the ability to induce phosphorylation on Dab1 protein after 15 min treatment of neuronal primary cultures. Reelin induces phosphorylation of Dab1 even in the presence of Aβ$_{42}$ before fibril formation (pre-fibrillar phase) but not after formation of fibrils (fibrillar phase). Reelin without Aβ$_{42}$ under the same conditions retains its activity throughout the time-scale of the experiment.

Altogether these data indicate that, during the process of *in vitro* amyloidogenesis, Reelin interacts with aggregating $A\beta_{42}$ and ends up making part of amyloid fibrils. During this process we observe a loss of Reelin biological activity specifically due to its sequestration into $A\beta_{42}$ fibrils, although Reelin do not alter their fibrillar structure in any repetitive manner.

4.2.4 Reelin rescues ADDLs-induced toxicity

Soluble $A\beta_{42}$ oligomers are now considered the real pathogenic forms of Aβ in AD (Haass and Selkoe, 2007). To test how Reelin affects Aβ oligomer-induced cytotoxicity, we used a standard preparation of soluble Aβ oligomers: Aβ-derived diffusible ligands (ADDLs) (**Chapter 1.1.2**; Lambert et al., 2001; Lambert et al., 1998). We first corroborated the interaction of Reelin and $A\beta_{42}$ ADDLs. To this aim purified Reelin was incubated for 1 hour with ADDLs, and the mixture was then subjected to immunoprecipitation assay. Western blot analysis of anti-Aβ and anti-Reelin immunoprecipitated samples revealed a specific interaction between Reelin and soluble $A\beta_{42}$ in the form of ADDLs (**Fig. 4.10a**).

Next we treated primary hippocampal neuronal cultures for 24h with soluble ADDLs, plus either Reelin or Mock purified supernatants. ADDLs are known for being toxic in neuronal cell lines at the concentrations of 3, 5 and 10 μM (**Chapter 1.1.2**; Lambert et al., 2001). Neuronal damage was assessed by analysis of propidium iodide (PI) nuclear staining. Exposure of cultures to ADDLs (5 or 10 μM) plus Mock caused an increase in PI nuclear staining, as compared with vehicle treatment (**Fig. 4.10b,c**). Cell survival after 5 or 10 μM ADDLs treatment was reduced to 70.4 and 62.6% respectively as compared to vehicle treated neurons (100% survival) (**Fig. 4.10c**). Reelin was able to increase neuronal survival up to 94.4 and 81.5% for 5 and 10 μM ADDLs treatment respectively (**Fig. 4.10c**).

To corroborate Reelin protection against ADDLs-induced neuronal death we also performed MTT assay, again in primary mouse hippocampal cultures treated with 10 μM ADDLs, plus either Reelin or Mock purified supernatants. Upon 24h treatment with 10 μM ADDLs we found a cell survival below 50%, as compared with vehicle (**Fig. 4.10d**). Treatment with Reelin rescued ADDLs–induced toxicity, bringing vitality to 68.7%, while treatment with Mock did not (**Fig. 4.10d**).

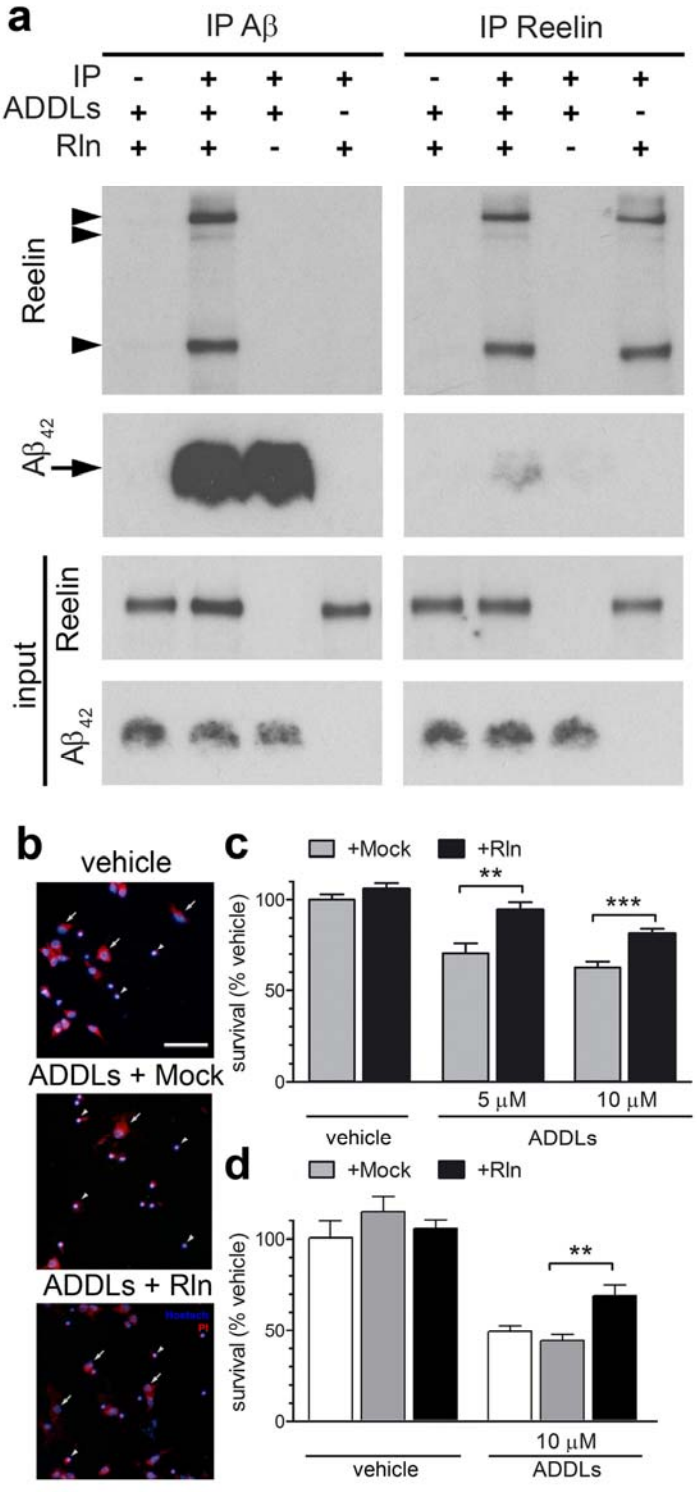

Figure 4.10. Reelin interacts with $A\beta_{42}$ in the form of ADDLs and reduces their toxicity. a) $A\beta_{42}$ and Reelin immunoprecipitation (IP) after 1 hour incubation of purified Reelin with ADDLs. IP was followed by western blot (WB) against either Reelin or Aβ, as indicated. Negative controls of not-immunoprecipitated samples are shown in lanes 1 and 5 (upper panels). Reelin and Aβ co-immunoprecipitated, as shown in lanes 2 and 6, indicating a specific interaction. Lower panels show input samples before immunoprecipitation, as indicated. **b)** Representative images from 24 hours treated neuronal primary cultures labelled with propidium iodide (PI) and Hoechst 33342. Dying neurons show double-labeled picnotic nuclei (arrowheads). Healthy cells are indicated by arrows. Treatments were performed with 5μM of ADDLs, with Reelin (Rln) added at a concentration of 6 ng/μL, or equivalent volumes of Mock. **c)** Quantification of cell survival after a 24 hours treatment followed by PI staining. The toxicity of ADDLs at 5-10 μM is significantly reduced by Rln. Results are shown as averages of measures from four independent experiments. **d)** Quantification of cell viability assessed by MTT test after 24 hours ADDLs treatment as compared to vehicle (considered as 100% viability). ADDLs have toxicity at 10 μM that is reduced by Reelin. Results are shown as averages of measures from four independent experiments. Scale bar: **b**, 200 μm. Data are represented as mean±SEM; $^{**}p<0.01$; $^{***}p<0.001$; Student's *t* test.

Altogether these results show that addition of Reelin to toxic Aβ oligomers reduces their impact on neuronal death, possibly being this reduction the result of the interaction between Reelin and $A\beta_{42}$ oligomers.

4.3 In vivo analysis of the impact of Reelin overexpression in mouse models of Alzheimer's disease

4.3.1 Generation and characterization of AD mouse models overexpressing Reelin

In order to get more insight *in vivo* into the involvement of Reelin in AD pathology, we bred the conditional transgenic mouse model of Reelin overexpression from our lab (TgRln) (**Chapter 1.2.2** and Pujadas et al., 2010) with three different models of AD. The first Alzheimer's disease mouse model used overexpresses a mutated form of the human APP gene bearing both the Swedish and the Indiana mutation (J20 strain from The Jackson Laboratory) (**Chapter 1.1.4** and Mucke et al., 2000). In this transgenic model human APP (hAPP) expression is under the control of the platelet-derived growth factor-β (PDGF-β) promoter to address its neuronal expression. Triple transgenic animals from the breeding of TgRln with J20 mice are referred to as TgRln/J20 and were identified by PCR. A schematic representation of the transgenic model generated is given in **Fig. 4.11**.

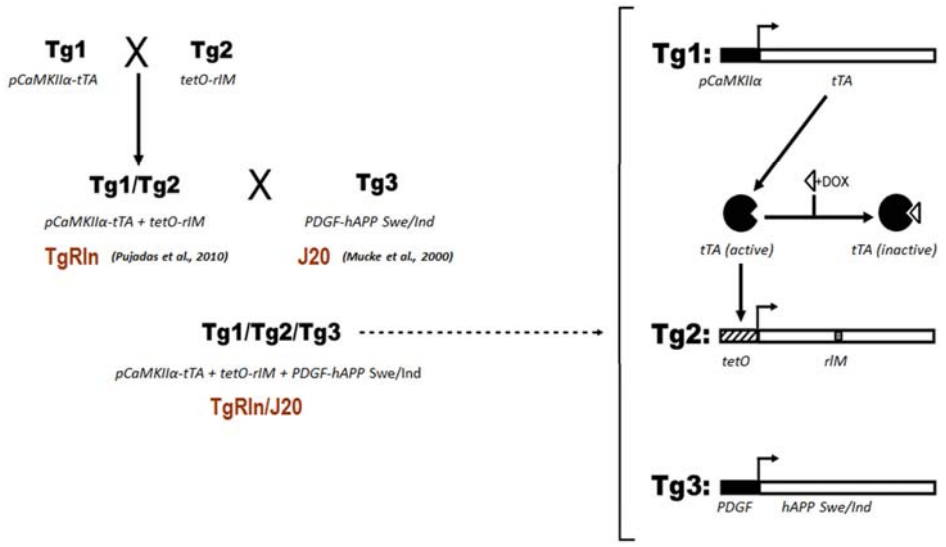

Fig 4.11. TgRln/J20 mouse design. Transgenic mice overexpressing Reelin were generated with a Tet-off regulated binary system: the Tg1 transgene encodes a tetracycline-dependent (tTA) transactivator set under the control of the CaMKIIα promoter (pCaMKIIα), while the Tg2 transgene encodes a myc-tagged reelin (rlM) controlled by the tetO promoter, responsive to tTA. Neuronal expression of transgenic Reelin is driven by CaMKIIα promoter in double transgenic mice (Tg1/Tg2 or TgRln); transgene expression can be switched off by doxycycline administration, which inactivates tTA transactivator. Double transgenic mice were further cross-bred with J20 mice, constitutively expressing the Tg3 transgene, encoding a mutated form of hAPP (bearing the Swedish and Indiana FAD mutation). Neuronal expression of the mutated hAPP is driven by PDGF-β promoter. The resulting triple transgenic mice (Tg1/Tg2/Tg3 or TgRln/J20) conditionally express Reelin and constitutively express the mutated hAPP. CaMKIIα, calcium-calmodulin-dependent kinase II alpha.

Expression of transgenic hAPP in TgRln/J20 mice was found in neocortex and in CA1, CA2, CA3 and granular cell layers of hippocampus, matching with the expression of hAPP in J20 mice (**Fig. 4.12**). Overexpression of Reelin in TgRln/J20 mice was detected in striatum, cortex and in hippocampus (mainly in CA1 and in granular cell layer of dentate gyrus), matching with the overexpression of Reelin in TgRln mice (**Fig. 4.12**).
This model allowed us to study *in vivo* the effect of Reelin on Aβ pathology, focusing on plaques deposition, synaptic failure and cognitive impairments (**Chapters 4.3.3 and 4.3.4**). However J20 animals do not show high levels of phosphorylated Tau and do not reproduce AD Tau pathology, nor for western blot analysis nor for immunohistochemistry.

With the aim of analysing whether Reelin overexpression in AD mice could lead to changes in GSK-3β activity and Tau phosphorylation, we decided to move to a model of conditional overexpression of GSK-3β in forebrain neurons: Tet/GSK-3β mice (**Chapter 1.1.4** and Hernandez et al.; Lucas et al., 2001), that recapitulates aspects of AD neuropathology such as Tau hyperphosphorylation, hippocampal dentate gyrus neurodegeneration, reactive astrocytosis and microgliosis, as well as spatial learning deficits. Again we bred it with our TgRln model generating the TgRln/GSK-3β mouse. Triple transgenic animals were identified by PCR and confirmed for immunohistochemistry. A schematic representation of the transgenic model generated is given in **Fig. 4.13**.

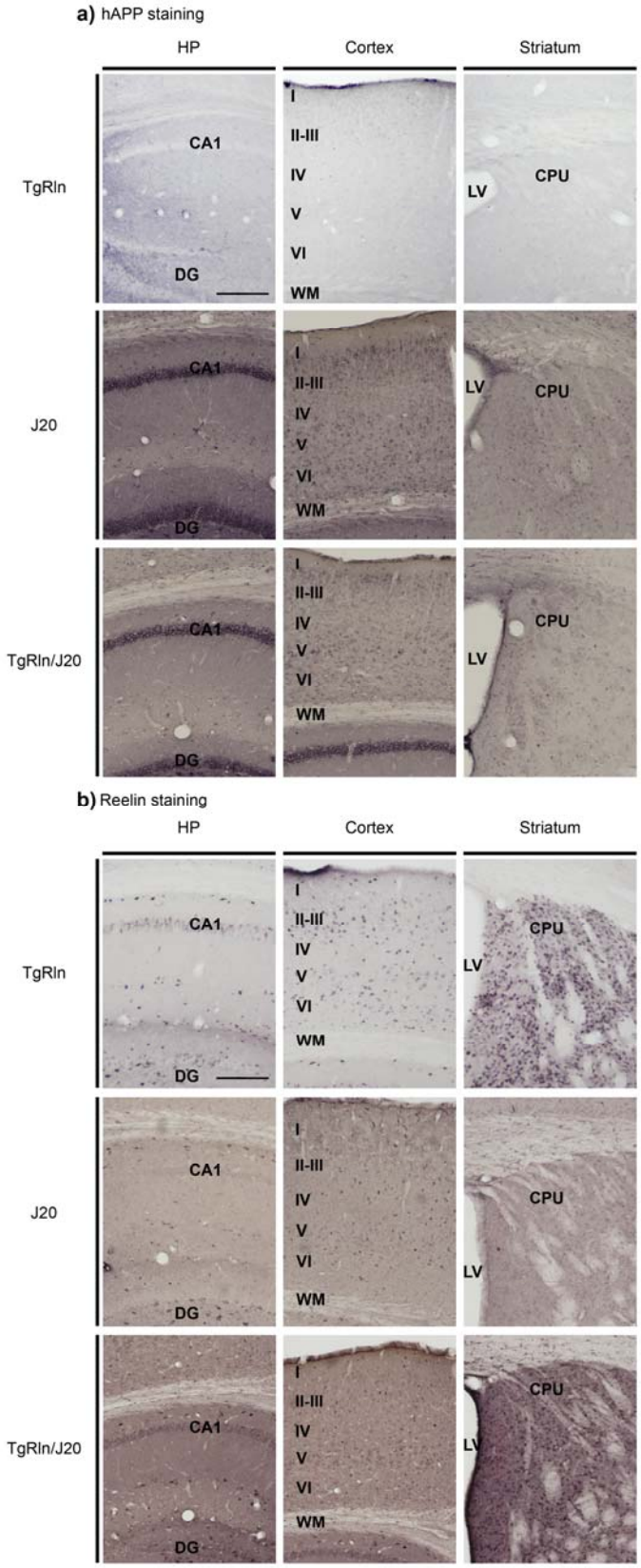

Figure 4.12. Characterization of *TgRln/J20* mice. a) Immunohistochemical detection of hAPP shows that TgRln animals do not express the transgene (upper panels). J20 mice express hAPP in CA1, CA2, CA3 and granular cell layers of hippocampus and in neocortex (middle panels). TgRln/J20 show the same patter of hAPP expression as the J20 mice (lower panels). **b)** Immunohistochemical detection shows that TgRln mice express endogenous Reelin in a subset of interneurons distributed throughout the cortex and hippocampal layers (upper panel, left and middle). Moreover TgRln mice overexpress transgenic Reelin in hippocampal pyramidal cells and in granule cells of the dentate gyrus (upper panel, left); in neocortical pyramidal cells (upper panel, middle) and in striatal neurons (upper panel, right). In J20 mice only endogenous Reelin expression is detected (middle panel). TgRln/J20 mice show the same pattern of Reelin expression as the TgRln mice (lower panel). HP: hippocampus; CA1–CA3, hippocampal regions; I–VI, Cortical layers; CPu, caudate–putamen nucleus; LV, lateral ventricle; WM, white matter. Scale bars: 200 μm.

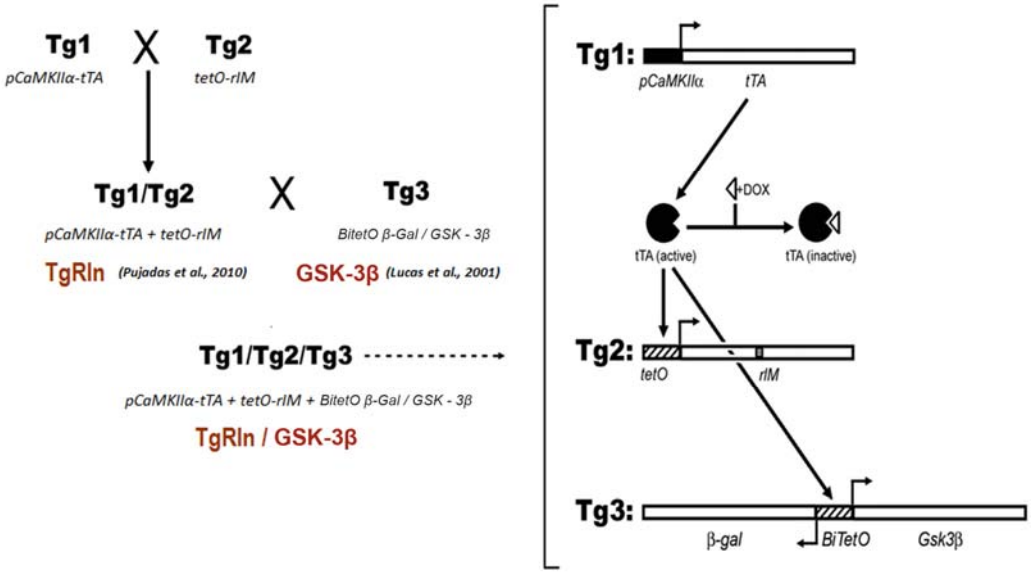

Fig. 4.13. TgRln/GSK-3β mouse design. Transgenic mice overexpressing Reelin (Tg1/Tg2 or TgRln) were generated as illustrated in **Fig. 4.12**. Double transgenic mice were further cross-bred with BitetO β-Gal/GSK-3β mice, expressing the Tg3 transgene, encoding BitetO construct. This consists of seven copies of the palindromic tet operator sequence flanked by two CMV promoter sequences in divergent orientations. This bi-directional promoter is followed by a GSK-3β cDNA sequence (encoding a myc epitope at its 5'-end) in one direction and a β-galactosidase (β-gal) reporter sequence including a nuclear localization signal (NLS) in the other. The resulting triple transgenic mice (Tg1/Tg2/Tg3 or TgRln/GSK-3β) conditionally overexpresses both Reelin and GSK-3β under control of CamKIIα promoter, with doxycycline preventing transactivation by tTA of both Tg2 and Tg3. CaMKIIα, calcium-calmodulin-dependent kinase II alpha.

Being both Reelin and GSK-3β transgenes under the control of CamKIIα promoter, their expression in TgRln/GSK-3β mice takes place in the same tissues, namely striatum, frontal cortex and different zones of hippocampus including CA1, CA2, CA3 and granular cell layer of dentate gyrus, as shown by himmunohistochemical detection of the reporter β-Galactosidase gene in **Fig. 4.14**.

In TgRln/GSK-3β mouse model we addressed the question of Reelin effect on GSK-3β activity and Tau phosphorylation (**Chapter 4.3.5**).

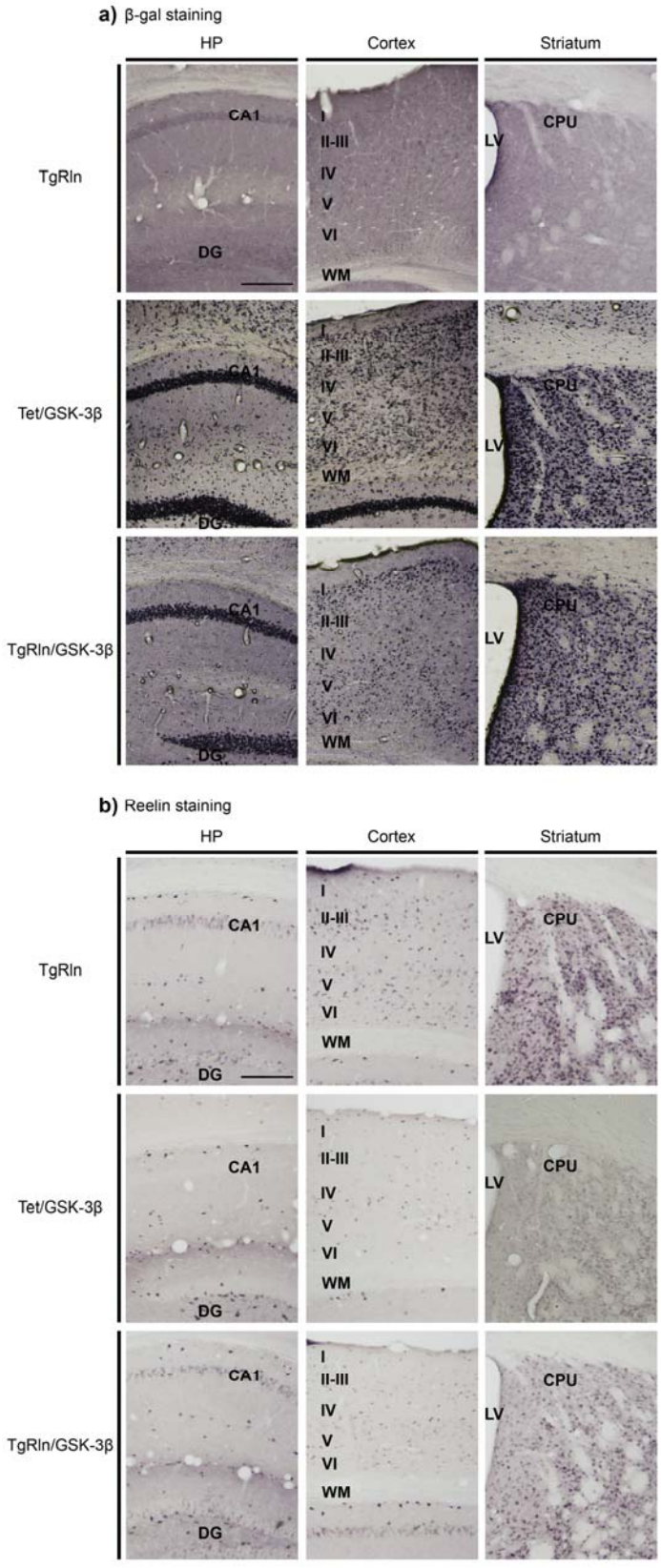

Figure 4.14. Characterization of *TgRln/GSK-3β* mice. a) Immunohistochemical detection of β-gal shows that TgRln animals do not express β-galactosidase reporter gene (upper panels). β-galactosidase reporter gene expression is detected in hippocampus (CA1, CA2,CA3 and granular cell layer of dentate gyrus), frontal cortex and striatum of Tet/GSK-3β mice (middle panels). TgRln/GSK-3β mice show the same pattern of β-galactosidase expression as the Tet/GSK-3β mice (lower panels). **b)** Immunohistochemical detection shows that TgRln mice express endogenous Reelin in a subset of interneurons distributed throughout the cortex and hippocampal layers (upper panel, left and middle). Moreover TgRln mice overexpress transgenic Reelin in hippocampal pyramidal cells and in the granular cell layer of the dentate gyrus (upper panel, left); in neocortical pyramidal cells (upper panel, middle) and in striatal neurons (upper panel, right). In Tet/GSK-3β mice only endogenous Reelin expression is detected (middle panel). TgRln/GSK-3β mice show the same pattern of Reelin expression as the TgRln mice (lower panel). HP: hippocampus; CA1–CA3, hippocampal regions; I–VI, Cortical layers; CPu, caudate–putamen nucleus; LV, lateral ventricle; WM, white matter. Scale bars: 200 μm.

Finally we also bred TgRln mice with a model of Taupathology called VLW (Lim et al., 2001). VLW mice express human Tau bearing three Fronto temporal dementia linked with parkinsonism-17 mutations (G272V, P301L and R406W). Neuron-specific expression is directed by insertion of the cDNA into a murine *thy*1 gene expression cassette, resulting in increased Tau phosphorylation and aggregation into neurofilaments. We bred VLW mice with our TgRln model generating a colony of triple transgenic animals referred to as TgRln/VLW and identified by PCR. This model will allow us to further assess the influence of Reelin pathway on Taupathology.

4.3.2 Reelin overexpression exacerbates dentate gyrus atrophy in J20 mice

The observation of TgRln/J20 hippocampal histological preparations let us notice a strong phenotype of dentate gyrus atrophy. For this reason we performed quantification of dentate gyrus area on Nissl staining of coronal sections on TgRln/J20 and littermates of the other genotypes (wt, TgRln, J20). Dentate gyrus size, expressed in percentage of the total hippocampal area, indicates that overexpression of Reelin alone is able to slightly but significantly reduce the dentate gyrus area in comparison with wild-type animals (reduction from 29% of wt to 24,5% of TgRln, **Fig. 4.15**). J20 mice show a significant and stronger reduction in dentate gyrus area, reaching values for dentate gyrus of around 17% of total hippocampal area (**Fig. 4.15)**. Finally TgRln/J20 mice display the most severe atrophy, with dentate gyrus accounting only for an 8,6 % of total hippocampal area (**Fig. 4.15**). Analysis of the dentate gyrus layers affected by atrophy revealed that TgRln animals are not suffering from reduction in granular cell layer (GCL) thickness but in molecular layer (ML) instead (**Fig. 4.15**). J20 animals display a strong reduction in both GCL and ML. Finally TgRln/J20 mice show a further reduction again in both GCL and ML (**Fig. 4.15**).

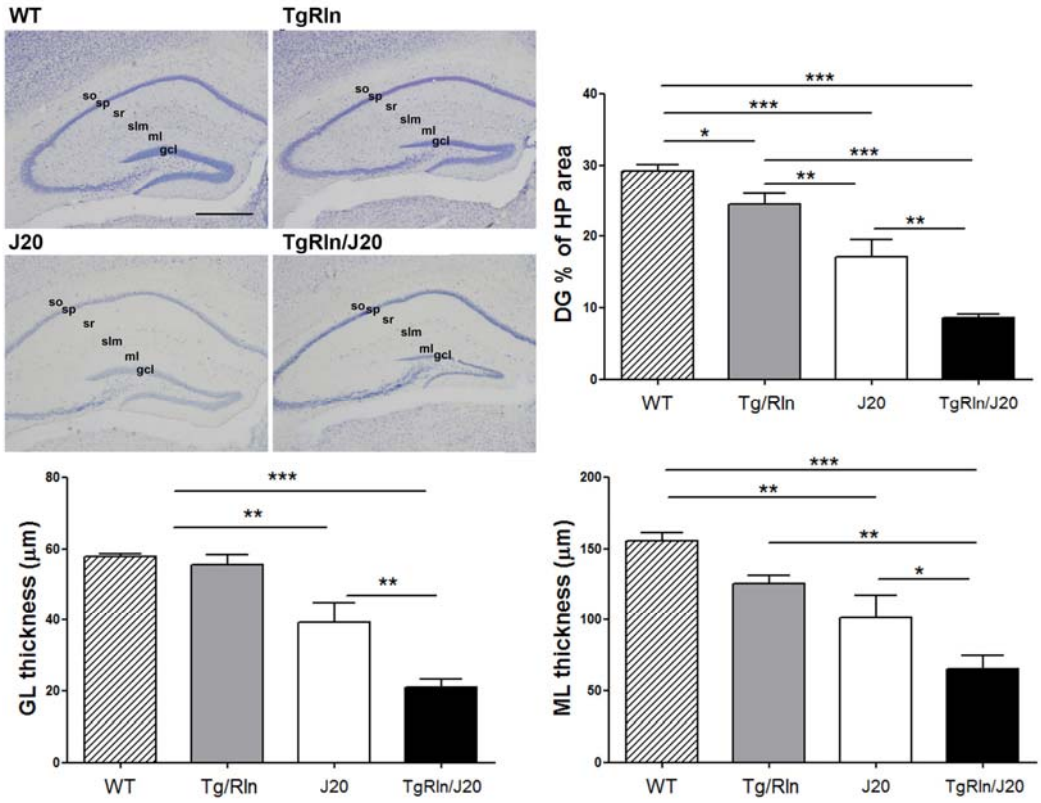

Figure 4.15. Dentate gyrus shrinking in TgRln, J20 and TgRln/J20 mice. Nissl staining for wt, TgRln, J20 and TgRln/J20 4 months mice reveals a dentate gyrus shrinking over the transgenic genotypes. Quantification of dentate gyrus area in percentage over total hippocampal area is reported for the four genotypes (upper panel, right). Quantification of GCL and ML average thickness is reported for the four genotypes (lower panel). GCL reported values are of 57,8 µm for wt, 55,5 µm for TgRln, 39,3 µm for J20 and 21,1 µm for TgRln/J20. ML reported values are of 155,8 µm for wt, 125,6 µm for TgRln, 101,2 µm for J20 and 65 µm for TgRln/J20. so, stratum oriens; sp, stratum piramidale; sr, stratum radiatum; slm, stratum lacunosum molecolare; ml, molecular layer; gcl, granular cell layer. Scale bar: 500 µm. Data are represented as mean±SEM; *p<0.05; **p<0.01; *** p<0.001; Student's t test.

To evaluate whether the GCL volume loss observed in J20 and TgRln/J20 could be linked to altered neurogenesis in the subgranular zone (SGZ), we performed IHC with doublecortin (DCX), a marker of newly born neurons which stains cells generated in the adult dentate gyrus over a 12-day period (Rao and Shetty, 2004). At the age of 4 months, J20 and TgRln/J20 mice display a reduction, more pronounced in TgRln/J20, in the rate of neurogenesis compared to wild types, calculated as number of DCX-positve cells per length of GCL (**Fig. 4.16a and b**). These results suggest that the observed shrinking of dentate gyrus in J20, is possibly associated to impaired neurogenesis. Reelin overexpression in TgRln/J20 exacerbates this phenotype.

Apart from decreased neurogenesis, DCX-positive cells displayed some morphological alterations in J20 and TgRln/J20 mice. First, in both genotypes we did not find a homogenous distribution of proliferating cells along the SGZ and, concomitantly, GCL thinning seemed to be more severe in correspondence of the zones with lower rates of proliferation. Second, we observed mispositioning of DCX-positive cells, with bodies at different depths of the GCL, sometimes even localized in the hilus. Third, dendritic trees were observed to be less developed and in some cases extending improperly towards the hilus instead of the ML. Finally, dystrophic neurites were also observed (**Fig. 4.16a** and **c**).

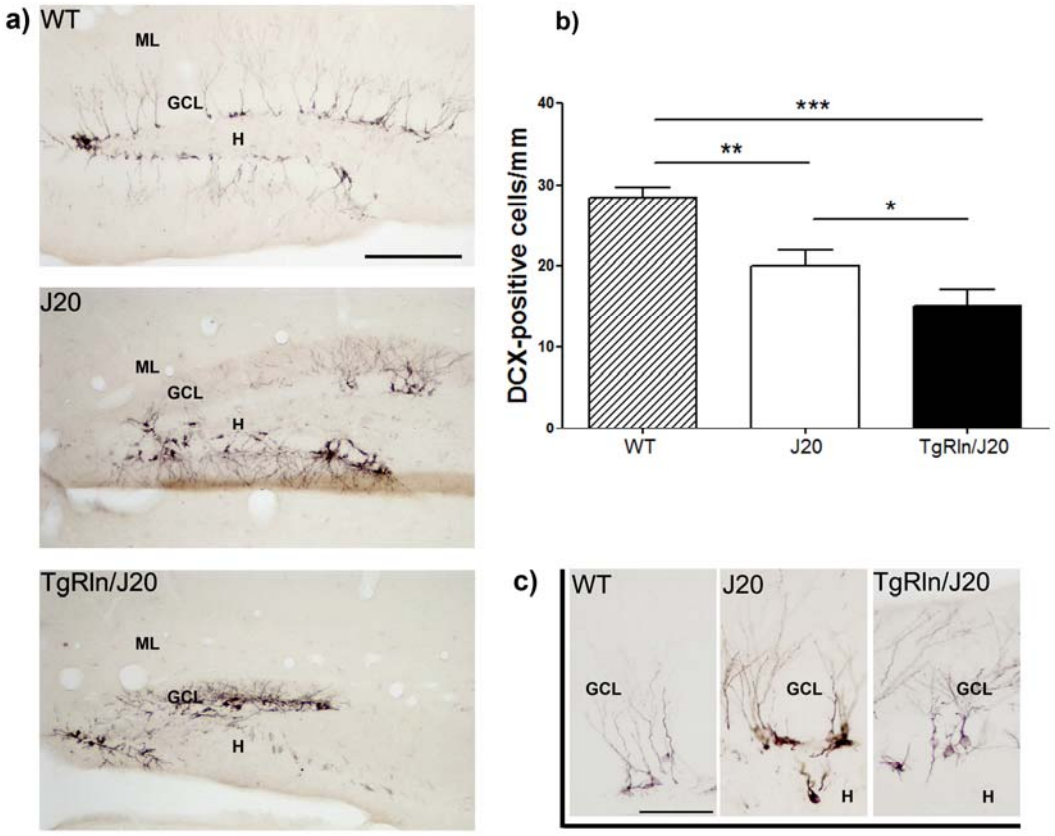

Figure 4.16. Adult hippocampal neurogenesis in TgRln, J20 and TgRln/J20 mice. a) DCX IHC on hippocampal slices from 4 months wt, J20 and TgRln mice. **b)** Quantification of DCX-positive cells/mm of GCL extension revealed an average of 27,8 cells for wt, 19,1 for J20 and 15,6 for TgRln/J20. **c)** Sporadic DCX-positive cells located in the Hilus are detected mainly in J20 mouse, whereas alterations of dendritic trees and dystrophic neurites are visible in both J20 and TgRln/J20 mouse. H, hilus; GCL, granular cell layer; ML, molecular layer. Scale bars: **a)** 200 µm; **c)** 100 µm. Data are represented as mean±SEM; *p<0.05; **p<0.01; *** p<0.001; Student's t test.

4.3.3 Reelin overexpression decreases cortical and hippocampal amyloid plaques deposition in J20 AD mice

In the TgRln/J20 model that we generated we wanted to ensure, as seen in our *in vitro* assembled $A\beta_{42}$ amyloid fibrils and as described for other AD mouse models (Doehner et al.; Knuesel et al., 2009), the presence of Reelin into amyloid plaques. To this aim we performed a double immunofluorescence staining for Reelin and APP/Aβ (**Fig. 4.17**). In hippocampal tissue we detected the presence of Reelin into Aβ amyloid plaque area, even if without perfect co-localization between the two signals, confirming results from previous works (Doehner et al.; Knuesel et al., 2009).

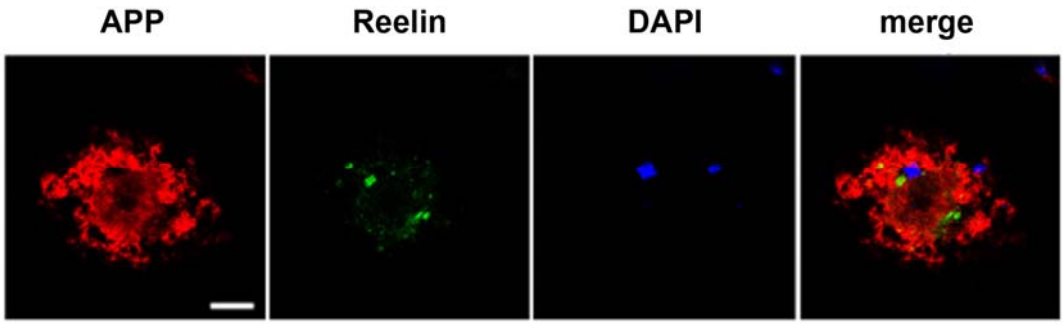

Fig 4.17 ***In vivo*** **association between Aβ plaques and Reelin.** Confocal images of double immunofluorescence against APP and Aβ (red), and Reelin (green) from TgRln/J20 hippocampal tissue. DAPI counterstaining is shown (blue). Reelin staining was detected in tight linkage with Aβ plaques throughout the hippocampus. However there is lack of perfect co-localization between the two markers. Scale bar 1μm.

To analyze whether the changes observed in the *in vitro* aggregation of $A\beta_{42}$ correlate *in vivo* with variations in amyloid plaque load in TgRln/J20, we quantified the area occupied by plaques in different areas of the brain and compared with that of J20 animals. Hippocampus was analysed at 4, 8 and 12 months-old. At the onset of plaque deposition (4 months) a very few amount of plaques are present in both genotypes (occupying a 0.04% of the total area) with no significant differences observed. At a later stage of 8 months, plaque load in TgRln/J20 is slightly increased in percentage of plaque load as compared with J20 with values of 1.2% and 0.5% respectively (**Fig. 4.18a**). In elder animals of 12 months-old, the percentage of area occupied by plaques is significantly lower in TgRln/J20 than in J20 with values of 9% and 13% respectively (**Fig. 4.18a**). Cortical areas, behave similarly as the hippocampus: in Retrosplenial Cortex by the age of 12 months we observed a tendency to lower the levels of plaque deposition in TgRln/J20 than in J20 (**Fig. 4.18c,** upper panels). The same plaque

reduction held true in Entorhinal Cortex, here reaching significance (**Fig. 4.18c,** lower panels).

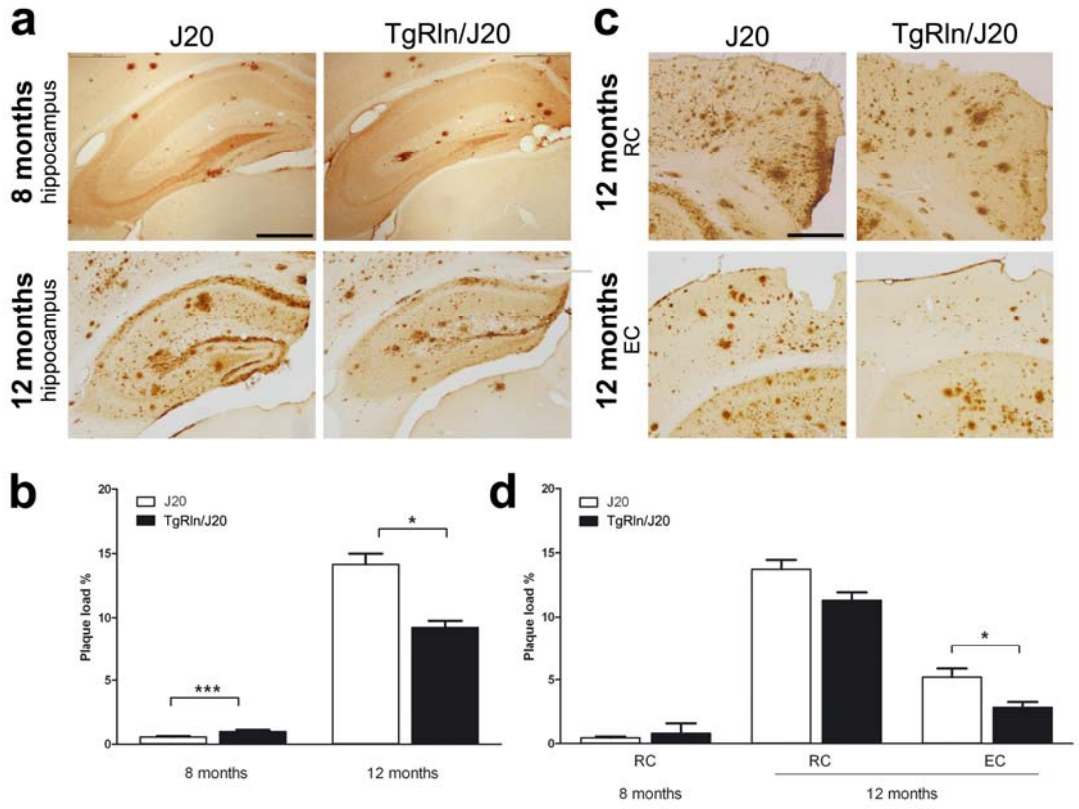

Figure 4.18. Reelin overexpression reduces plaque content in 12-months-old J20 AD mice. a) Immunohistochemical detection of amyloid plaques (3D6 antibody) in 8 and 12-months-old hippocampal sections. **b)** Plaque load was quantified as the percentage of the total hippocampal area stained with 3D6. At 8-months old TgRln/J20 mice show higher occupation than J20s, while at 12 months old area occupied by plaques is markedly reduced in TgRln/J20. **c)** 3D6 immunohistochemical detection of amyloid plaques in cortical sections from retinosplenial cortex (RC; upper panels) and enthorhinal cortex (EC; lower panels) in 12-months-old mice. **d)** Plaque load in RC and EC from J20 and TgRln/J20 at 12 months old animals is reduced in both areas, reaching significance in EC. Scale bars: **a** and **c,** 500 μm. Data are represented as mean±SEM; **p*<0.05; *** *p*<0.001; Student's *t* test.

Other brain areas affected by AD were also analysed. At 12 months Subiculum is highly affected by plaque accumulation in both genotypes reaching rates of around 40% of the area with no differences seen due to Reelin overexpression (not shown).

Altogether our results indicate a similar onset of plaque appearance in both genotypes, with TgRln/J20 mice showing a reduced number of deposits at 12 months of age. These results are consistent with our previous *in vitro* observations of a Reelin-dependent delay in the formation of $A\beta_{42}$ fibrils.

4.3.4 Reelin prevents dendritic spine loss and cognitive impairment in J20 mouse model of Alzheimer's disease

Decreased synaptic contacts and dendritic spine density have been previously described in AD mice (Spires-Jones et al., 2007; Spires-Jones and Knafo, 2012) and humans (DeKosky and Scheff, 1990). Since Reelin is able to reduce *in vitro* some of the toxic effects of amyloid species, we evaluated whether Reelin overexpression could correlate *in vivo* with reduced synaptotoxicity. To this aim, J20 and TgRln/J20 animals, plus littermates wt and TgRln controls, were processed for Golgi staining at 8 months of age and dendritic spines were counted in primary pyramidal dendrites at stratum radiatum (SR) and stratum lacunosum moleculare (SLM) of hippocampus (**Fig. 4.19**). In both areas, J20 animals show reduced number of dendritic spines if compared with wt and TgRln animals. In TgRln/J20 animals, Reelin overexpression significantly rescued dendritic spines density (**Fig. 4.19b**).

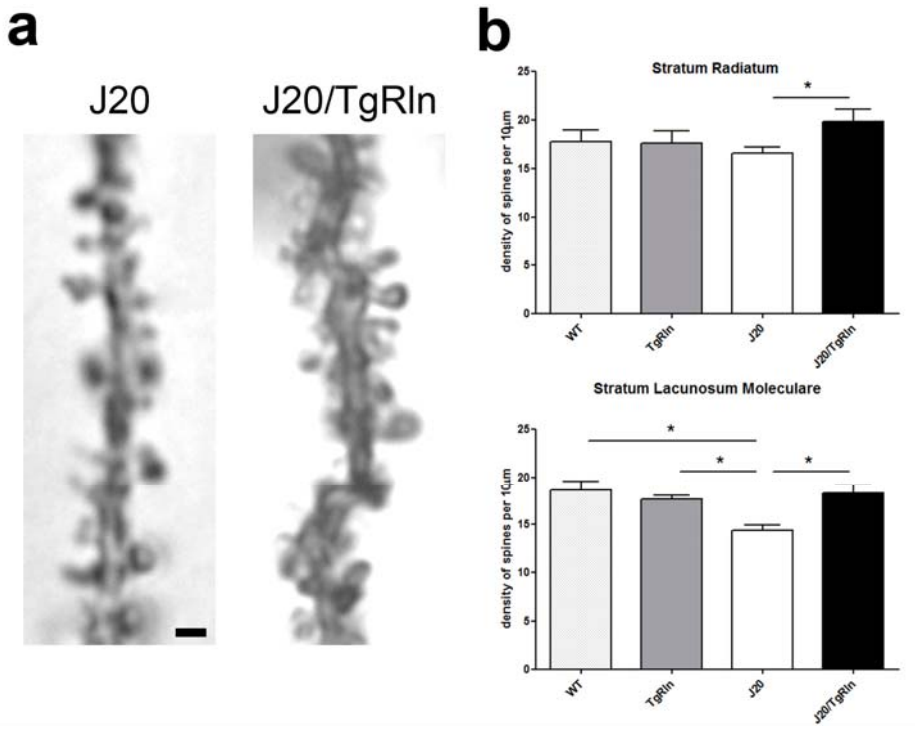

Figure 4.19 Reelin overexpression reverses J20 AD mice dendritic spine loss. a) Micrographies illustrating SLM dendrite sections from 8 months old J20 and TgRln/J20 animals after Golgi staining. **b)** Quantification of the density of dendritic spines in 10 µm length sections from SR and SLM shows that J20 reduced spine content is prevented in TgRln/J20. Data are represented as mean±SEM; **p*<0.05; Student's *t* test. Scale bar: 1µm.

Reduced number of synaptic contacts in AD mice has been shown to correlate with cognitive deficits (Terry et al., 1991) and J20 animals show a wide range of cognitive impairments even before the appearance of amyloid deposits. For instance starting from the age of 2-3 months it has been observed that J20 fail in Novel Object Recognition (NOR) test (Harris et al., 2010), a recognition task used to test short and long term memory (Moore et al., 2013). Briefly, in this test animals are introduced in a chamber equipped with two identical objects that they can freely explore. On the day of the test one of the two familiar objects is replaced by a novel one and the time spent exploring the objects is measured. Normal mice remember the familiar object and thus spend more time exploring the novel one. Since we found that Reelin is able to prevent the loss of dendritic spines in J20 mice, we wanted to to analyse whether this could lead to an improvement in congnitive performances. To this aim littermate mice from the different genotypes (control; TgRln; J20; and TgRln/J20) were subjected to NOR test at different ages: 4-5 and 8-10 months old. The cognitive performance of each mouse was expressed by the discrimination index (DI) for the novel object, calculated as the time spent exploring the novel object minus the time spent exploring the familial object, relative to the total time spent exploring. DI of 0.3 indicates that the time spent exploring the novel object doubles the time spent exploring the familial one, so that animals successfully behave in this task for DI ranging from 0.3 to 0.5. Wt and TgRln animals, from both age groups, spent a significantly higher proportion of time exploring the new object versus a familiar one than J20 animals, reflected in a higher discrimination index (DI >0.3) (**Fig. 4.20,** upper panel). This result indicates cognitive deficits in the J20 animals (DI <0.2) as already documented (Harris et al., 2010) (**Fig. 4.20,** upper and lower panel). Significant differences were found between J20 and TgRln/J20 groups at 4-5 and 8-10 months, with TgRln/J20 animals acting as wt controls (**Fig. 4.20,** upper panel). These data indicate that Reelin provokes a significant reversion of the recognition memory deficits observed in J20 up to 8-10 months. In older animals of 11-12 months the control wt group did not differ from J20, demonstrating an age-dependent decline in the recognition memory (**Fig. 4.20,** lower panel, left). Nevertheless, at the same age, TgRln strain partially maintained recognition capacity (DI between 0.2 and 0.3) significantly higher than control group. Interestingly, 12 months old TgRln/J20 animals retained the same level of discrimination capabilities as TgRln despite abnormal Aβ production (**Fig. 4.20,** lower panel, left). TgRln and TgRln/J20 groups were re-evaluated after one month of doxycicline treatment to stop

Reelin over-expression. DI in both groups diminishes to reach value zero, indicating a complete loss of long-lasting Reelin-dependent protection in one month of depletion (**Fig. 4.20,** lower panel, right).

Altogether, our data suggest that Reelin overexpression recovers the cognitive impairment caused by Aβ production in J20 strain, probably through a rescue in dendritic spine density. Moreover Reelin overexpression also decreases the physiological age-dependent cognitive decline in control animals. The beneficial effect of Reelin overexpression is lost in one month of Reelin depletion, showing that it was specifically dependent on Reelin. In conclusion Reelin seems to be a neuroprotective factor, able to prevent Aβ toxicity.

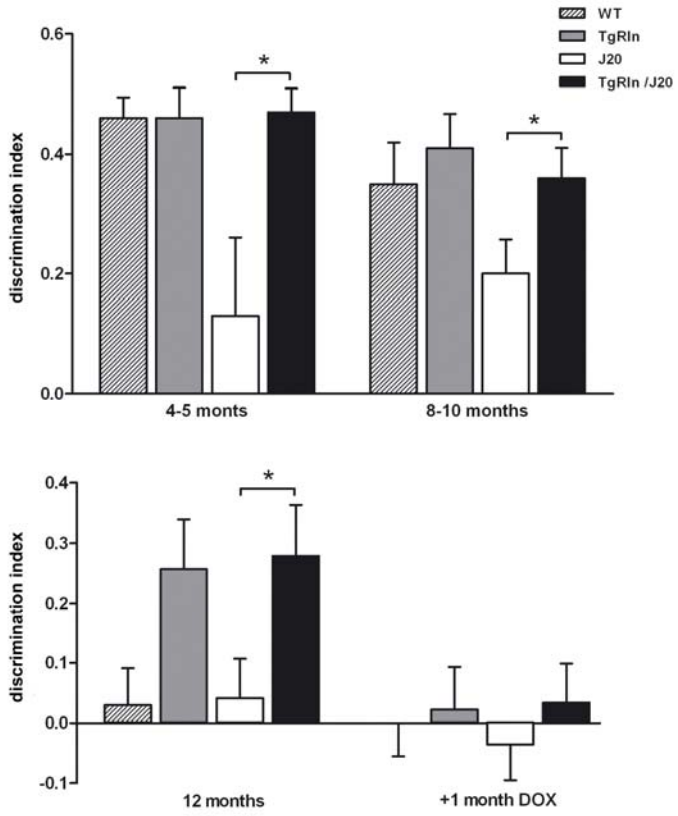

Figure 4.20. Reelin prevents J20 mice from cognitive impairments in the NOR task. Novel object recognition (NOR) behavioural task was performed on littermates from the different genotypes (WT, TgRln, J20 and TgRln/J20) at the ages of interest (4-5, 8-10 and 12 months-old). Overexpression of Reelin prevents behavioural alterations observed in J20s throughout all ages tested and also the physiological decline of WT 12-months-old mice (upper panel and lower panel, left). Immediately after the 12-month-old NOR testing, the same groups of animals were treated with DOX-diet (200 mg/kg) for 1 month and tested again for NOR. Reelin protection is lost after one month of depletion, with all the groups failing the test (lower panel, right). Data are represented as mean±SEM; *$p<0.05$; Student's *t* test.

Finally, since Reelin acts as a neuroprotective factor in AD, we wanted to test its potential role as a therapeutic factor as well, in case of overt AD. To this aim J20 and TgRln/J20 animals, plus littermates wt and TgRln controls, were subjected to Doxocycline diet from birth until the age of 4 months, thus avoiding transgenic Reelin

overexpression until the onset of disease is appreciated. Onset of the disease was checked by NOR test, in which both J20 and TgRln/J20 mice reached a DI <0.1 at this age (**Fig. 4.21,** left). Next, normal diet substituted the Doxocycline one, and mouse groups were re-evaluated for NOR after 1 month of Reelin overexpression in order to address possible Reelin dependent improvements in cognition. We did not see any rescue in NOR test performance after 1 month of Reelin overexpression (5 months mice, **Fig. 4.21,** middle), and not even after 3 more months (8 months mice, **Fig. 4.21,** right), with DI ranging around value zero for both J20 and J20/TgRln. This indicates that, while Reelin continuous overexpression from birth is able to prevent the appearance of AD deficits in cognition, its conditional overexpression in adult subjects is not able to overcome these impairments once the pathology developed.

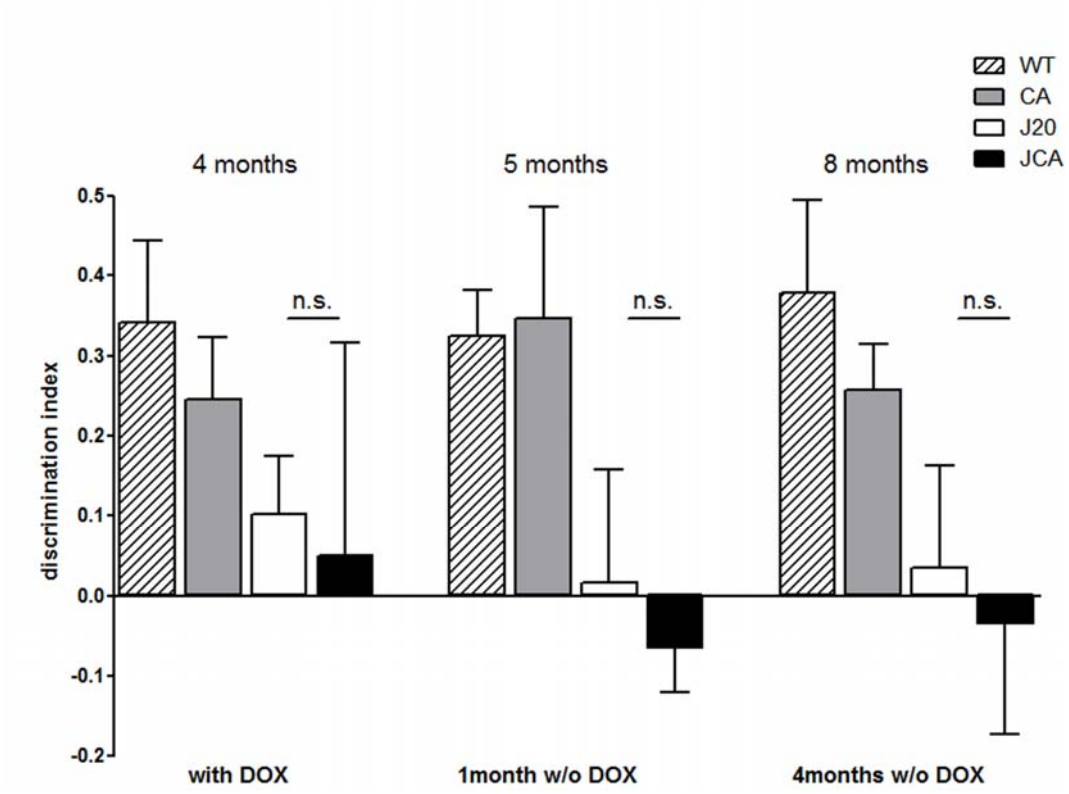

Figure 4.21. Reelin fails to rescue J20 mice from cognitive impairments in NOR task once AD pathology began. Novel object recognition (NOR) test was performed on 4 months-old littermates from the different genotypes (WT, TgRln, J20 and TgRln/J20) subjected from birth to Doxocycline (DOX) diet (200 mg/kg) in order to switch off the expression of transgenic Reelin. Wt and TgRln mice performed better than J20 and TgRln/J20, who reached a DI<0.1 (left). Immediately after the 4-month-old NOR testing, the same groups of animals were left with normal diet and tested again for NOR at the age of 5 and 8 months (respectively 1 and 4 months after Reelin transgene activation). Overexpression of Reelin is not able to rescue the behavioural alterations observed in J20s throughout all ages tested, with both J20 and TgRln/J20 mice being unable to discriminate between familial versus novel object (middle and right). Data are represented as mean±SEM; n.s., not significant; Student's *t* test.

4.3.5 Reelin reduces Tau phosphorylation in GSK-3β overexpressing mice

To investigate the effect of Reelin overexpression on GSK-3β activity and Tau phosphorylation, we performed western blot analysis on hippocampal extracts from the TgRln/GSK-3β mice plus wt, TgRln and Tet/GSK-3β littermate controls. At the age of five months we found that GSK-3β overexpression, caused a 2.5 folds increase in the levels of Tau phosphorylation, similarly to what was reported for younger animals (Lucas et al., 2001; Engel et al., 2006b). This increase was assessed by western blot analysis using the PHF-1 antibody, which detects the GSK-3β-dependent phosphorylation of Tau on serines 396-404, a phosphorylation that is related to the formation of Tau aggregates in a tangle stage (Lucas et al., 2001). Overexpression of Reelin in this background (TgRln/GSK-3β) reduces Tau phosphorylation, restoring the phosphorylation levels of wt animals (**Fig 4.22**). Hyperphosphorylation on other Tau epitopes was also tested, using antibodies AT8 and AT180. Both AT8 and AT180 have been associated to the early phase of Tau pathology in neurodegenerative diseases such as AD (Bertrand et al., 2010), and they bind respectively to phosphorylated Tau on serines 199-202/threonine 205 and threonine 231/Serine 235. We found that Tau phosphorylation at AT8 and AT 180 epitopes was increased by GSK-3β overexpression and restored to wt level by Reelin overexpression (**Fig 4.22).** The reduction in GSK-3β-dependent Tau phosphorylation produced by Reelin is not due to altered levels of total Tau, since unvaried levels of total Tau are found by using the the phosphorylation-independent antibody Tau5 (**Fig 4.22**).

Phosphorylation of Tau at the epitopes recognized by PHF-1, AT8 and AT180 antibodies is believed to start in the axon, and to result in the detachment of Tau from microtubules and in its redistribution to the somato-dendritic compartment (Bertrand et al., 2010). To analyze hippocampal distribution and intracellular localization of phosphorylated Tau, we performed immunohistochemistry with PHF-1 antibody in hippocampal slices from the TgRln/GSK-3β mice plus wt, TgRln and Tet/GSK-3β littermate controls, at the same age as for western blot (5 months). All genotypes displayed appreciable staining of interneurons throughout hippocampal layers, although Reelin overexpression, both in TgRln and in TgRln/GSK-3β, apparently reduce the number of stained cells (**Fig. 4.23a,** arrowheads). PHF-1 staining also revealed that wt and TgRln animals display a predominant axonic signal in the mossy fibers, both in the proximal (Hilus) and in the distal fragment projecting to CA3 (**Fig. 4.23a**, distal fragment indicated by arrows).

Somato-dendritic immunoreactivity is also present in some granule cell of dentate gyrus and sporadically detected in hilar mossy cells (**Fig. 4.23b**). Tet/GSK-3β animals, as already described, show a shift to higher somato-dendritic immunostaining in granule cells (**Fig. 4.23b**, arrow), consistent with the detachment of Tau from microtubules and its localization to somato-dendritic compartment, where they assemble in a pretangle stage (Lucas et al., 2001). Staining of Mossy cells is also detected (**Fig. 4.23b**, arroeheads). Moreover we found that the axonic mark in the distal fragment of mossy fibers to CA3 mostly disappeared (**Fig. 4.23a**). TgRln/GSK-3β animals, similarly to wt and TgRln animals, revert to a predominant axonic signal in mossy fibers, both at the proximal and at the distal segment, possibly indicating that the decrease in Tau phosphorylation induced by Reelin overexpression prevents the detachment of Tau from microtubules and its somatodentritic localization.

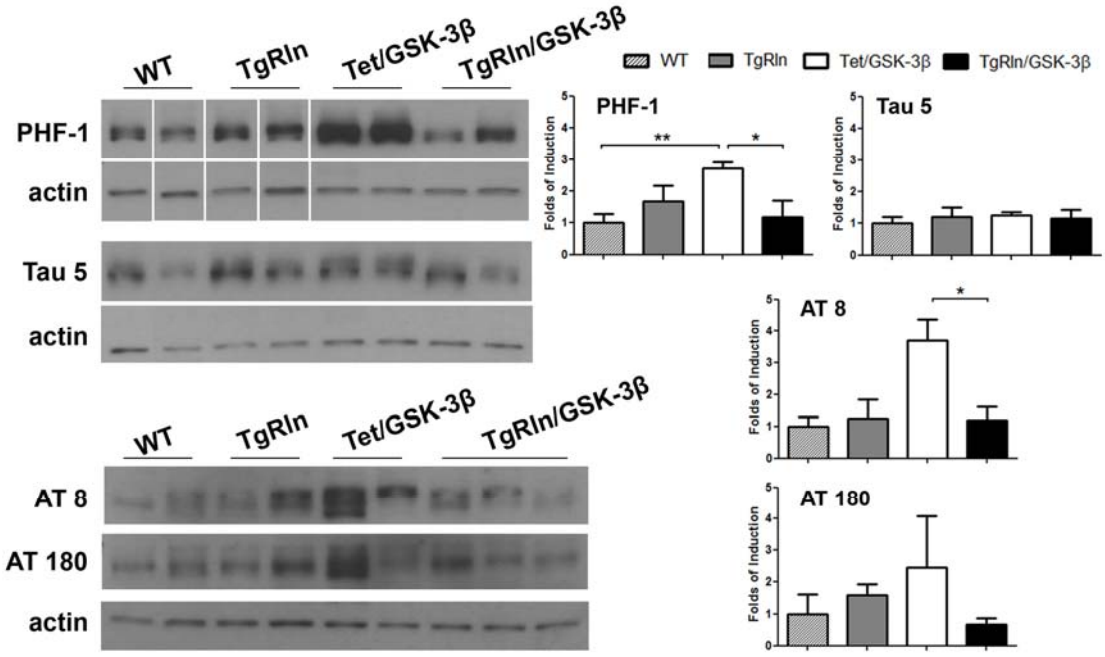

Figure 4.22 Reelin reduces Tau phosphorylation in a model of GSK-3β overexpression. Hippocampal protein extracts from 5 months-old TgRln/GSK-3β mice, plus littermate wt, TgRln and Tet/GSK-3β, were subjected to WB analysis of GSK-3β-dependent Tau phosphorylation through antibodies PHF-1, AT8 and AT180. Reelin overexpression in TgRln/GSK-3β mice counteracts the increase in Tau phosphorylation found in Tet/GSK-3β mice, restoring the basal levels of phosphorylation. Changes in phosphorylation levels are not due to total Tau protein level varations, as shown by phosphorylation-independent WB analysis of Tau. WB, western blot. Data are represented as mean±SEM; *$p<0.05$; **$p<0.01$; Student's *t* test.

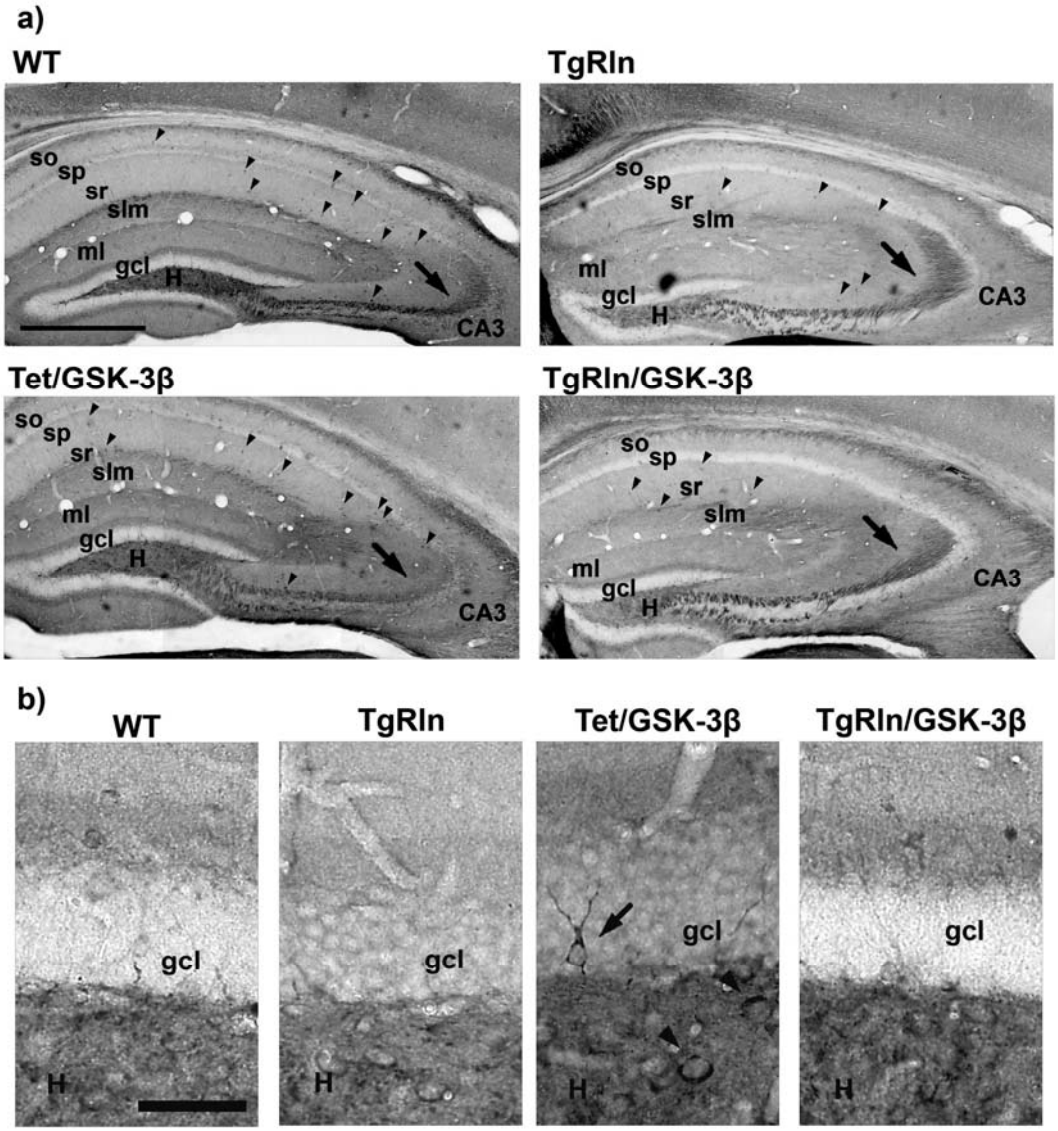

Figure 4.23. Reelin reverts the somato-dendritic localization of phosphorylated Tau in Tet/GSK-3β mice. Immunohistochemistry analysis of phosphorylated Tau (PHF-1 antibody) on hippocampal slices from 5-month old wt, TgRln, Tet/GSK-3β and TgRln/GSK-3β mice. **a**) Some interneurons from hippocampal layers are stained in all genotypes (arrowheads), although to a lesser extent in Reelin-overexpressing genotypes (TgRln and TgRln/GSK-3β). TgRln/GSK-3β mice, similarly to wt and TgRln, display a predominant axonic staining in mossy fibers, both in the hilus and in CA3 (arrows). **b**) In dentate gyrus, Tet/GSK-3β mice display a shift to somato-dendritic staining of granule cells (arrow) and mossy cells (arrowheads). so, stratum oriens; sp, stratum piramidale; sr, stratum radiatum; slm, stratum lacunosum molecolare; ml, molecular layer; gcl, granular cell layer; H, hilus. Scale bar **a**, 500 μm; **b**. 50 μm.

DISCUSSION

5.1 Reelin involvement in AD: initial hypotheses

A huge body of literature indicates that the Reelin signalling pathway interferes in the molecular pathways leading to AD and vice versa.

Starting from the transduction of Reelin signalling, we find the membrane receptor apolipoprotein E receptor 2 (ApoER2), which is at the same time a receptor for the ε4 isoform of apoE, the major genetic risk factor for SAD (Tsai et al., 1994). Reelin signaling unchained through ApoER2 and VLDLR receptors downregulates the activity of GSK-3β, the major kinase for Tau protein (Gonzalez-Billault et al., 2005; Beffert et al., 2002), and mutant mice that have deficits in Reelin, in its transducer Dab1 or in ApoER2 and/or VLDLR show increased levels of Tau phosphorylation (Hiesberger et al., 1999). At the synaptic level, Reelin counteracts Aβ-induced downregulation of glutamatergic synaptic transmission (Durakoglugil et al., 2009). Indeed, the incubation of hippocampal slices with Aβ oligomers at concentrations that are found in AD patients impairs endocytosis and trafficking of AMPA and NMDA receptors, thus decreasing LTP (Kamenetz et al., 2003; Hsieh et al., 2006); conversely, the addition of recombinant Reelin to acute hippocampal slices results in enhanced LTP (Weeber et al., 2002) as a result of Reelin-dependent tyrosine phosphorylation of the NR2 subunit of NMDAR through SFKs activation. These data fit those found in studies in transgenic mice. Indeed, it has been shown that FAD mice (J20 strain) show impairments in LTP and paired-pulse ratio at the perforant path to granule cell synapse in the dentate gyrus (DG) (Palop and Mucke, 2010), whereas TgRln mice overexpressing Reelin show enhanced LTP at the Schaffer collaterals to CA1 pyramidal cells (Pujadas et al., 2010), again confirming a functional antagonism between Reelin and Aβ-related pathways. The mechanisms behind Reelin counteraction of Aβ-induced toxicity are still unclear, although in an *in vitro* approach both Dab1 and Reelin have been found to physically interact with APP and regulate its trafficking and proteolytic processing, thereby promoting non-amyloidogenic αAPP cleavage (Hoe et al., 2006; Hoe et al., 2008; Hoe et al., 2009). Conversely overexpression of Aβ in Down's syndrome has been associated with altered processing and levels of Reelin protein (Botella-Lopez et al., 2010), thereby suggesting a mutual control of Reelin and APP/Aβ, whose fine tuning could be altered in AD.

At the time we started our research into the involvement of Reelin in AD pathology, new findings were emerging in this scenario. Normal aging in wild-type rodents and primates was found to be accompanied by extracellular accumulation of Reelin-positive deposits and a reduction of Reelin-expressing neurons in the hippocampal formation (Knuesel et al., 2009). These deposits, referred to as Reelin plaques, are Reelin extracellular accumulations of amyloid-like nature, since they bind to Thioflavin-S (Doehner et al.; Knuesel et al., 2009). They are found in areas normally expressing Reelin (mainly the hippocampus and cortex) and they co-localize with endogenous Aβ (Knuesel et al., 2009). Moreover, these plaques are invaded by activated microglia and astrocytes (Knuesel et al., 2009). The phenomenon of Reelin plaque deposition is highly increased in AD mice, and in 3xTg-AD mice Reelin plaques co-localize with non-fibrillary species of human Aβ (colocalization of Reelin with Aβ oligomers stained with A11 antibody). However, no direct co-localization of Reelin plaques with the fibrillar forms of Aβ is detected (**Fig. 5.1**) (Doehner et al., 2010). Indeed, Reelin deposits are in a tight association with Aβ plaques in transgenic AD mice, above all at the edges of extracellular deposits, but without perfect co-localization.

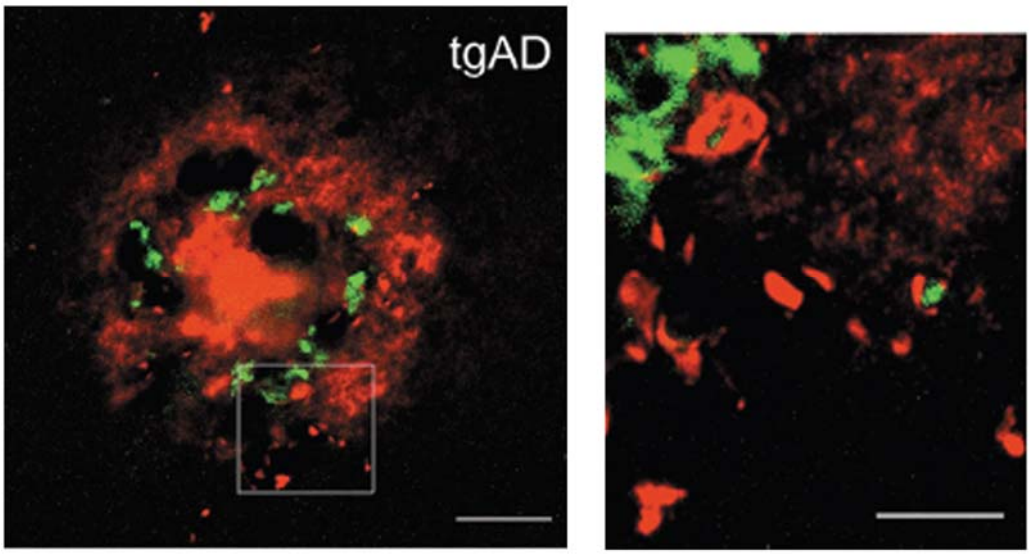

Adapted from Doehner et al., 2010

Fig. 5.1. Reelin-positive plaques associate with Aβ in AD mice. Immunofluorescence staining of brain tissue obtained from 15-month-old transgenic ArcA*β* AD mice using mouse anti-Reelin and rabbit anti-$A\beta_{40/42}$ antibodies. Granular Reelin-positive deposits (green) were detected at high densities and close association with Aβ plaques (red) throughout the hippocampus. Right panel shows a higher magnification of the boxed area outlined in the left panel. Note the lack of co-localization between the two markers. Scale bars: **left**, 30 μm; **right** panel, 5 μm

Finally, the reduction in Reelin-expressing neurons with the concomitant deposition of Reelin plaques is associated with episodic-like memory impairments (Knuesel et al., 2009).

A fascinating hypothesis emerging from these new findings was that part of physiological aging possibly involves the loss of Reelin-expressing interneurons and the accumulation in extracellular plaques of the Reelin from dying neurons that is not properly degraded by clearance mechanisms. The loss of active Reelin by this mechanism could be responsible for the start of cognitive decline. Since in AD this phenotype is exacerbated with earlier and higher Reelin aggregate deposition (Knuesel et al., 2009), and since Reelin plaques have also been found to co-localize with soluble pre-fibrillar forms of human Aβ, the combination of all these observations prompted us to speculate that the accumulation of Reelin in non-fibrillary plaques promotes the aggregation of Aβ species, potentially acting as a nucleation factor for fibrillary amyloid Aβ plaques. The involvement of Reelin plaques in the formation of amyloid Aβ plaques would add a further layer of complexity to the interference of Reelin with AD-related pathways, shifting the focus from the analysis of a putative neuroprotective or neurodegenerative role for Reelin in AD to a possible separation of Reelin protein functions along different stages of life. Indeed, if on the one one hand functional Reelin antagonizes AD-related pathways, favoring alpha-cleavage of APP and counteracting Aβ-induced depression of glutamatergic transmission and Tau phosphorylation, on the other hand a Reelin that is no longer functional and is extruded by dying neurons could act in the opposite way, thus promoting Aβ deposition.

To test the new hypothesis, we designed an *in vivo* approach consisting of the generation of a transgenic mouse model of conditional ablation of Reelin-expressing neurons. In detail, in this model the diphtheria *toxin* A (DTA) is conditionally expressed in Reelin-expressing GABAergic interneurons, causing their death (**Fig. 5.2**). In contrast to a conditional Reelin knock-out, this approach is designed to mimic the death of adult Reelin-expressing neurons as a result of aging. Thus it was considered as an experimental tool by which to follow the fate of Reelin protein after its extrusion from dying interneurons. Moreover, the crossbreeding of this model with a model of AD (e.g. J20 FAD) (**Fig. 5.2**) would allow us to evaluate whether the expected increase in extracellular accumulation of Reelin plaques affects the deposition of Aβ amyloid plaques.

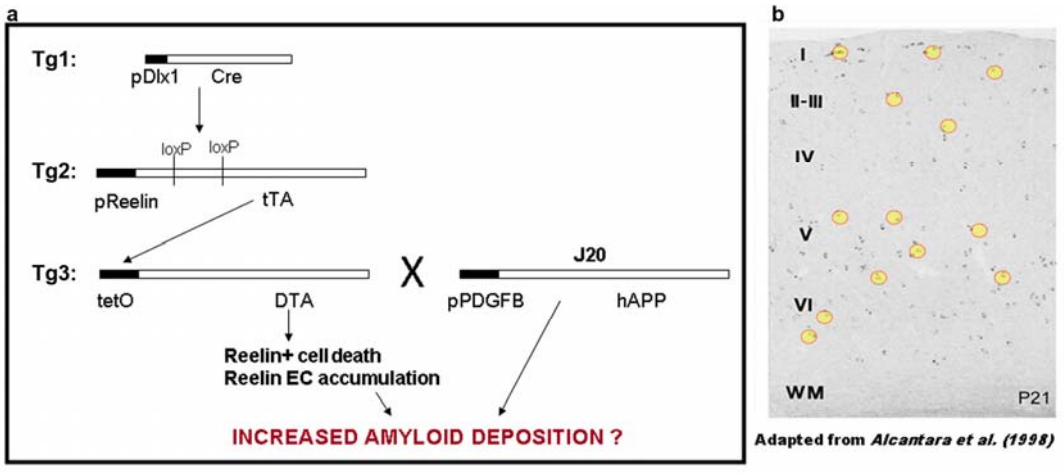

Fig. 5.2. Generation of a transgenic mouse model of conditional ablation of Reelin-expressing interneurons. a) Conditional ablation of Reelin-expressing interneurons is obtained in a triple transgenic model Tg1/Tg2/Tg3. In Tg1 transgene the Cre recombinase is put under the control of the distal-less homeobox 1 (Dlx1) promoter to drive its expression in adult GABAergic interneurons. Here the Tg2 transgene is recombined at two *Lox P* sites, activating the expression of a tTA tetracycline transactivator under the control of Reelin promoter. Finally, in Reelin-expressing GABAergic interneurons, the tTA conditionally activates the expression of the Tg3 transgene, encoding for DTA and causing cellular death. Crossbreeding of this mouse model with J20 FAD would add neuronal expression of hAPP, allowing the analysis of the influence of Reelin plaque deposition on Aβ plaque deposition. **b)** Reelin expression in adult mouse GABAergic interneurons in the neocortex. Yellow and red dots represent eventual sites of Reelin and Aβ amyloid plaque deposition. DTA, diphtheria *toxin* A. EC, extracellular.

As explained in **Fig. 5.2**, the implementation of the aforementioned conditional ablation model requires the crossbreeding of three independent mouse lines (Tg1, Tg2 and Tg3), two of which (Tg1 and Tg3) are commercially available, while the Tg2 line requires the cloning of the cDNA Tg2 vector. With this aim, we designed a three-step cloning strategy for the vector production that is underway. In parallel we developed some faster alternative approximations with the same objective.

An alternative strategy for ablating Reelin-expressing neurons can be obtained through kainic acid (KA) injections in TgRln or TgRln/J20 mice. KA is a specific agonist of kainate receptor, so it mimics the effects of glutamate and acts as an epileptogenic and neuroexcitotoxic drug. Intraperitoneal injections in mice cause convulsive seizures accompanied by the death of CA1, CA2 and CA3 hippocampal neurons (Wang et al., 2005). Since TgRln and TgRln/J20 mice are characterized by overexpression of transgenic Reelin in CA1, intraperitoneal injections of KA were administered to 4-month-old TgRln/J20 mice, with the aim to induce convulsive non-lethal seizures and the death of Reelin-expressing CA1 pyramidal neurons. Animals were sacrificed one

month after injections and tested for the death of Reelin-expressing cells and for plaque formation. The unexpected hypersensitivity of TgRln mice to KA required the previous administration of Diazepam to reduce mouse death. Although all animals had convulsive seizures, they did not show high levels of neuronal death, as assessed by Fluorojade and Nissl staining (not shown). This finding could be attributable to the administration of Diazepam. Immunohistochemistry against Reelin and Aβ did not show considerable increase in Aβ or in Reelin plaque deposition after KA injections in TgRln/J20 animals compared with non-injected controls. Neither did we observe appreciable changes in Aβ or in Reelin plaque deposition, after KA injections in TgRln/J20 compared with J20 animals, attributable to the overexpression of Reelin. Nevertheless, KA-injected TgRln/J20 mice showed an accumulation of intracellular Aβ deposits in Reelin-overexpressing CA1 and CA2 pyramidal neurons, the most sensitive areas to KA-induced death (**Fig. 5.3**, right panels). Instead J20 KA-injected mice, which do not express Reelin in CA1 pyramidal neurons, did not display the same intracellular deposits (**Fig. 5.3**, left panels). These data might support the starting hypothesis that Reelin is present and participates in the nucleation of amyloid plaques. Indeed, intracellular Aβ deposits have been described as precursors to plaques both in humans (Gyure et al., 2001) and mice (Oddo et al., 2003a; Oddo et al., 2006). However, no clear evidence of a Reelin-promoted Aβ plaque formation was obtained from this attempt, possibly due also to the low levels of neural death detected and the young age of mice, or to the short time to animal sacrifice after KA injection.

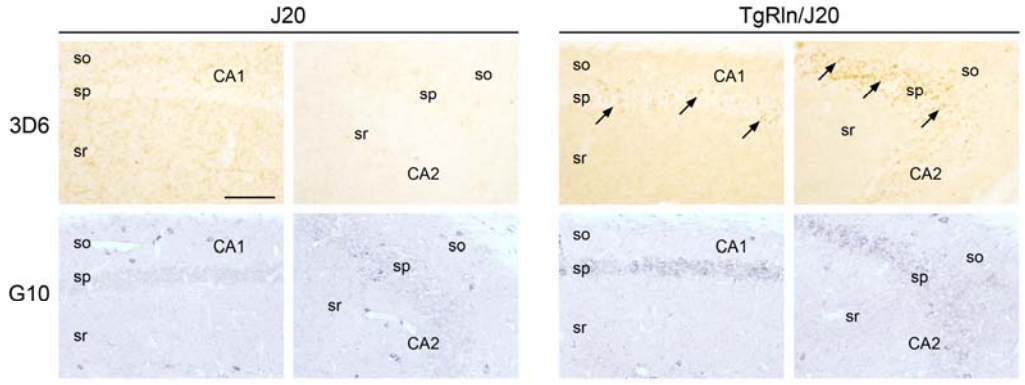

Fig. 5.3. Accumulation of intracellular Aβ deposits in KA-injected TgRln/J20 mice. Immunohistochemistry of J20 and TgRln/J20 mouse brains one month after KA injections. 3D6 antibody stains Aβ deposits, G10 antibody stains Reelin. TgRln/J20, but not J20 mice, show intracellular accumulation of Aβ in CA1 and CA2 Reelin-expressing neurons (arrows). Scale bar, 100 μm. so, stratum oriens; sp, stratum piramidale; sr, stratum radiatum; slm, stratum lacunosum molecolare.

Another way by which we addressed whether Reelin contributes to the nucleation of amyloid Aβ plaques was by stereotaxically injecting purified Reelin (**Chapter 4.1.1**) in the anterior hippocampus of 4-month-old J20 animals. Mice were killed 1 month after surgery and were processed for IHC against Reelin and Aβ plaques. Neither did this approach allow us to conclude that Reelin favours Aβ plaque deposition, since no nucleation was found in the sites of Reelin injection nor was a general increase in hippocampal Aβ plaques observed.

Despite some indication gained with KA injections in TgRln/J20 animals, neither of the three experimental approaches gave us strong evidence to support our initial hypothesis. Moreover, subsequent IF analysis of hippocampal Aβ amyloid plaques in TgRln/J20 animals revealed, as explained in **Chapter 4.3.2** and corroborating the previous finding of Irene Knuesel's group (Doehner et al., 2010), no perfect co-localization of Reelin and Aβ plaques, although Reelin tightly surrounded these structures. Moreover, as we found later (**Chapter 4.3.2)**, Reelin overexpression in J20 mice did not modify the onset of Aβ amyloid plaques appearance, slightly increased the number of Aβ plaques at the age of 8 months, and in more aged mice (12 months) strongly reduced plaque deposition. The overall vision of these data did not prompt us to proceed in the investigation of Reelin as a nucleator for Aβ plaques, although its co-localization with non-fibrillar oligomeric forms of Aβ (Doehner et al., 2010) and its tight association with Aβ amyloid plaques was a key finding to keep in mind, since it fitted further observations discussed below in **Section 5.2**.

We then reformulated the problem, channeling our efforts into studying the possible molecular interaction of Reelin with any Aβ form, i.e. monomers, oligomers, fibrils or plaques. To this end, we started from an *in vitro* approach, where the only possible focus was on two purified species, Reelin and $A\beta_{42}$ peptide, without any external interference, and on their dynamics of interaction during Aβ aggregation.

5.2 Neuroprotective role for Reelin in AD: interpretation of in vitro results

Our *in vitro* approach (**Sections 4.1 and 4.2**) contributed to shedding some light on the molecular relationship between Reelin an $A\beta_{42}$ in the process of amyloid aggregation. First, we detected a direct influence of Reelin protein on the kinetics of $A\beta_{42}$ amyloid aggregation. Contrarily to what was expected, in our system Reelin delayed the appearance of amyloid fibrils in a specific and dose-dependent fashion, as assessed by ThT and TEM. Second, we found that Reelin-induced delay in fibril formation was accompanied by a prolonged life span of both LMW and HMW $A\beta_{42}$ oligomers, as assessed respectively by PICUP and dot blot. Third, Reelin interacts with soluble $A\beta_{42}$ species in the pre-fibrillar stage of amyloid aggregation. As the process of $A\beta_{42}$ aggregation goes on, Reelin progressively disappears from the soluble fraction, as assessed by Western blot, and gets trapped in the $A\beta_{42}$ amyloid fibrils that finally form, as visualized by electron microscopy. Concomitantly, Reelin loses its biological functionality, being unable to induce the phosphorylation of its transducer Dab1 after sequestration into the $A\beta_{42}$ fibrils. Fourth, although we found that Reelin forms part of amyloid fibrils, neither their classical cross β-fibrillar structure nor the distances between lateral chains, as shown by X-ray diffraction of fibrils formed with or without Reelin, are altered. This finding implies that Reelin possibly interacts with structures at the surface of $A\beta_{42}$ amyloid fibrils in a non-regular manner. Finally short-term treatment of neuronal cultures with toxic $A\beta_{42}$ oligomers (ADDLs) in the presence of Reelin demonstrate that Reelin is protective, reducing cytotoxicity in two survival assays: PI staining and MTT.

The body of data we collected with our *in vitro* approach provides new and interesting insights into the field of Reelin and AD. The emerging perspective for Reelin in this context is that of a neuroprotective player that slows down amyloid fibril formation, interacts with toxic $A\beta_{42}$ oligomeric species, and, although prolonging their life span, impairs them from exerting toxicity. Ongoing experiments are underway to evaluate the effect of Reelin on the synaptotoxicity of $A\beta_{42}$ oligomers, looking at the density of dentritic spines in low-density hippocampal primary cultures treated with $A\beta_{42}$ in the presence or in the absence of Reelin. This approach would let us work in more physiologic conditions, using lower concentrations of $A\beta_{42}$ that would better reproduce

the conditions found *in vivo* in brain, and could let us appreciate a finer tuning of $A\beta_{42}$ toxicity by Reelin pathway.

Elucidation of the molecular mechanisms underlying Reelin neuroprotection will require further investigation, although some speculations can be made on the basis of these findings. The interaction of Reelin and $A\beta_{42}$ oligomers, although not affecting their size or their distribution, as shown by PICUP for LMW oligomers, could still induce some conformational modification of the oligomeric species that may affect their biological properties. For instance, a conformational change induced by Reelin on $A\beta_{42}$ oligomers may impair the interaction of the latter with their membrane receptors at the synaptic level, possibly explaining the relevant phenomenon of the reduction in their toxicity that we observed. Alternatively, the mere interaction of both LMW and HMW oligomers with Reelin could remove the former from interaction with synapses, thus having extracellular oligomers for longer periods but without being toxic. Also, it is conceivable that Reelin, although not changing amyloid fibril structure, actually stabilizes it, thus hampering oligomer recycling; if this were the case, there would be a lower rate of circulating oligomers detaching from fibrils but this process would last longer.

Another conceivable hypothesis is that Reelin, already interacting with amyloid fibrils, simultaneously interacts with oligomeric $A\beta_{42}$ species that form in a process of secondary nucleation at the surface of pre-formed amyloid fibrils. By "process of secondary nucleation" we refer to amyloid fibril nucleation catalyzed by pre-existing fibrils that host the nucleation reaction of new aggregates starting from Aβ monomers on their surface (**Chapter 1.1.2** and Cohen et al., 2013). This process begins once a critical concentration of amyloid fibrils has accumulated and, in the presence of new monomers, it overtakes the classical mechanism of primary nucleation and becomes the dominant mechanism by which toxic oligomeric species of Aβ are formed. Reelin has been shown to interact with Aβ fibrils in a manner that does not affect their structure, as demonstrated by X-ray diffraction. This observation could indicate that Reelin interacts with amyloid fibrils at their surface, precisely the site where the events of secondary nucleation occur. Thus we could speculate that in a system in which the critical concentration of Aβ fibrils for secondary events of nucleation has been reached and the formation of toxic oligomers goes on mainly in a positive feedback loop at the surface of existing fibrils, the presence of Reelin at the same site impairs the nucleation reactions of oligomeric species, thereby reducing their toxicity (**Fig. 5.4**).

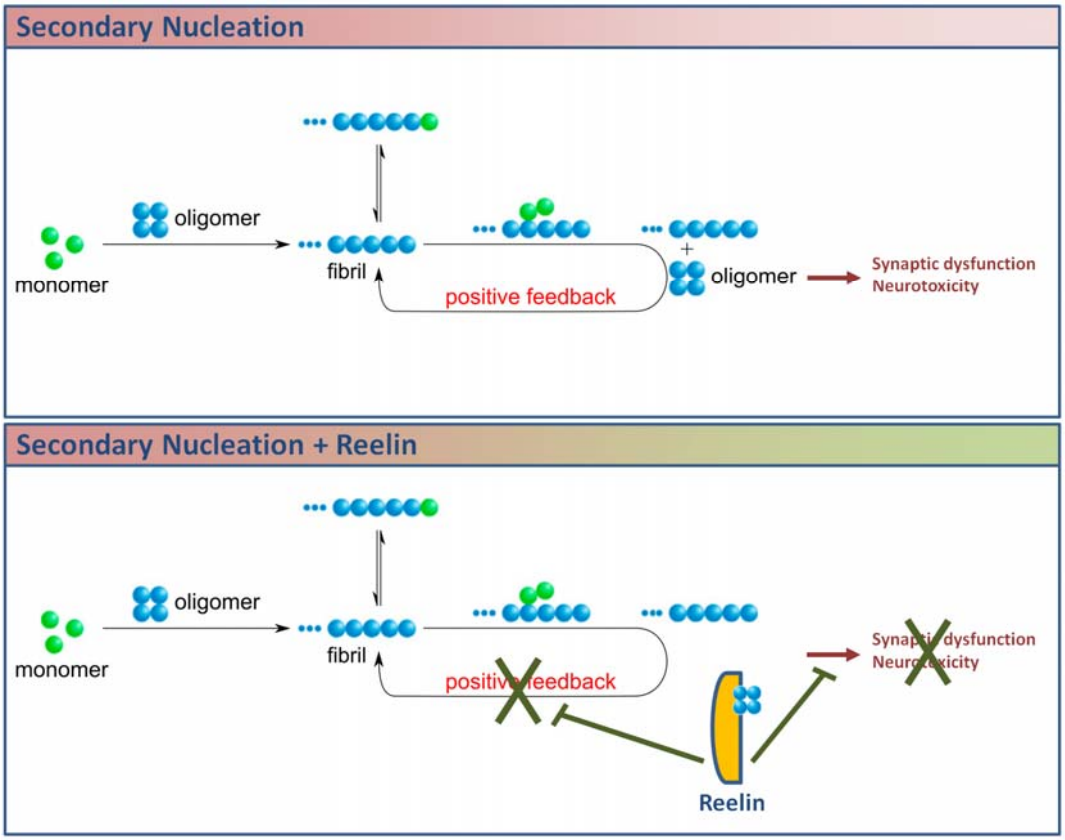

Adapted from Cohen et al., 2013

Fig. 5.4. Hypothesis of the impairment of secondary nucleation events by Reelin. The secondary nucleation is a process of amyloid fibril nucleation catalyzed by pre-existing fibrils. Once a critical concentration of amyloid fibrils has accumulated through a classical mechanism of homogeneous primary nucleation, amyloid fibrils themselves can host the nucleation reaction of new aggregates starting from Aβ monomers on their surface (upper panel). Reelin interaction with Aβ species may subtract them from the interaction with fibrillar forms of Aβ, by which more oligomers and fibrils are formed for secondary nucleation in a positive feedback loop (lower panel). Moreover the presence of Reelin on fibril surface may sterically hamper the secondary nucleation process. The proposed mechanism of competition and/or of steric effect could explain the reduction of toxicity observed in the presence of Reelin.

Last, it is important to remark that the setting up of a strategy for the purification of Reelin protein, together with the following proteomic bottom up analysis (described in **Section 4.1**), led us to the description of three N-glycosylation sites for Reelin protein in asparagines 291, 306 and 1267. This novel finding could have relevant implications for the understanding of Reelin biology, since glycosylations are known to control protein properties such as folding, secretion, cell-cell adhesion or cell-extracellular matrix attachment (Helenius and Aebi, 2004), and thus, in the case of Reelin, glycosylation could be involved in the control of developing and adult brain physiopathological processes. In particular it has been described a change in Reelin glycosylation patterns in AD (Botella-Lopez et al., 2006), therefore it could be useful to

verify whether the sites detected in our approach could be involved in the modifications associated to AD. Further analysis, using similar approaches, can also be applied to the discovery of other glycosylation sites for Reelin protein or finally the study of glycans released by *in vitro* deglycosylation could be tackled.

5.3 Neuroprotective role for Reelin in AD: interpretation of in vivo results

Our *in vivo* approach (**Section 4.3**) revealed the impact of continuous Reelin overexpression in two models of AD, one characterized by the overexpression of a mutated form of human APP (J20) and the other by Tau pathology caused by the overexpression of its kinase GSK-3β (Tet/GSK-3β).

Reelin overexpression in the adult brain of J20 mice provided *in vivo* evidence of the influence of Reelin on amyloid fibril accumulation. In TgRln/J20 mice, the accumulation of amyloid deposits was not blocked, neither was the time of onset of the first deposits delayed; nevertheless, aged animals showed a significantly reduced accumulation of amyloid plaques compared with J20 mice. This observation is compatible with the *in vitro* evidence that Reelin delays the formation of amyloid fibrils. *In vivo* data also indicate a key role for Reelin in neuroprotection at the synaptic level. Consistent with Reelin enhancement of structural and functional properties at the synapses (Pujadas et al., 2010), in TgRln/J20 animals, dendritic spine levels were restored to those of wild-type animals, in contrast with J20 mice, which show synapse loss as a consequence of the disease (Spires-Jones et al., 2007). Thus Reelin counteracts *in vivo* Aβ-induced synaptotoxicity. Consistently, TgRln/J20 animals showed a recovery of cognitive skills, as seen by NOR test, with Reelin preventing memory impairments of J20 mice throughout life: before plaque formation (up to 4-6 months) and during amyloid deposition (8-12 months). This recovery was lost after one-month of depleting Reelin overexpression. This observation implies that the recovery is dependent on the continuous generation of new Reelin and indicates that Reelin itself acts as a "real-time" protector. All together, our data indicate that Reelin induces an *in vivo* recovery at the synaptic structural level that underlies the functional recovery of cognitive skills in a model of AD, in a way that is dependent on the continuous overexpression of Reelin.

We did not analyse *in vivo* the eventual loss of Reelin functionality caused by Reelin sequestration into amyloid fibrils, as we did *in vitro*. In this regard, a relevant difference between *in vivo* and *in vitro* approaches should be taken into account, namely the dose of Reelin and amyloid peptides in the two systems analysed. While *in vitro* we study a "closed system" in which an initial amount of Reelin and monomeric $A\beta_{42}$ are added, *in vivo* there is a continuous production of both new Reelin and Aβ peptides. This new

production increases the complexity of the *in vivo* situation, and, although Reelin was sequestered into amyloid $A\beta_{42}$ fibrils, as shown by IF stainings, the loss of functionality associated with this process could be masked by the continuous generation of new Reelin, thus overcoming the phenotype.

The most interesting observation emerging from this scenario is probably the finding *in vivo* that the reduction of Aβ amyloid plaques is accompanied by decreased toxicity at synapses, where dendritic spine number is recovered, and by a rescue of cognitive skills. Since the focus of amyloid species toxicity has moved from plaques to oligomers, with the formulation of the "Aβ oligomer hypothesis" (**Chapter 1.1.2**), amyloid fibrils were proposed to be inert aggregates possibly with no toxicity *per se* (Haass and Selkoe, 2007). However, this view is not consistent with the observation that, in the proximity of plaques, dendritic spines are disrupted in a manner that depends on their distance from the plaques (Spires-Jones et al., 2007). Also it has been reported a strong reduction of GABAergic innervation on cortical piramidal cells in the proximity of amyloid plaques, further implying that amyloid plaques are still a source of synaptotoxicity (Garcia-Marin et al., 2009; Leon-Espinosa et al., 2012). Additionally amyloid structures undergo continuous mechanisms of dissociation and re-association by which Aβ molecules are recycled within the fibril population and can be released to generate new toxic species (Carulla et al., 2005). A possible reconciliation of these findings comes from the description of the above mentioned secondary nucleation (Cohen et al., 2013) (**Fig. 5.4**), a process in which both monomeric peptide and fibrils are involved in the formation of toxic oligomers. This hypothesis restores the possibility that a reduction in the concentration of amyloid fibrils would be protective against AD pathology, since it would prevent the positive feedback loop by which toxic oligomers start to be formed in an exponential manner at the surface of fibrils. Moreover, this hypothesis still fits with all the previous discoveries regarding oligomer toxicity and fibril recycling events, adding the fibril surface as the place where these reactions are catalyzed. In our case, this would explain why Reelin-induced reduction of amyloid plaque burden *in vivo* overlaps with decreased toxicity at the synaptic level, apart from conciliating, as speculated above, the localization of Reelin at fibrils with a reduced *in vitro* cytotoxicity of Aβ oligomers. The analysis of Aβ soluble levels in TgRln/J20 animals is most definitely a future issue of great relevance in order to deepen our understanding of the molecular mechanisms by which Reelin reduces the number of amyloid plaques and the toxicity of Aβ species. Remarkably, in an *in vitro* approach, it was reported that Reelin

regulates the trafficking and proteolytic processing of APP, promoting non-amyloidogenic αAPP cleavage (Hoe et al., 2006; Hoe et al., 2008; Hoe et al., 2009). It would be of great relevance to corroborate these data in our *in vivo* system.

Furthermore, the overexpression of Reelin in a model of GSK-3β overexpression (Tet/GSK-3β) allowed us to evaluate the influence of the Reelin signalling pathway in the context of Tau pathology, a point that we were not able to address in the TgRln/J20 mouse model, where no hyperphosphorylation of Tau has been detected. Since Reelin acts upstream of GSK-3β, inhibiting its activity (Herz and Chen, 2006), we analysed by western blot disctinct epitopes of GSK-3β-dependent phosphorylation of Tau, a phosphorylation event that is related to the formation of Tau aggregates in a tangle stage (Bertrand et al., 2010). We found that Reelin overexpression in TgRln/GSK-3β mice significantly reduces the amount of phosphorylated Tau in the hippocampus, restoring wild-type levels at 5 months of age, without changing total rates of Tau production (**Fig. 4.22**). Moreover, while Tet/GSK-3β mice display somato-dentritic localization of phospho-Tau (Lucas et al., 2001), associated with pretangle-like stuctures, Reelin overexpression reverts this phenotype, restoring a predominant axonic localization of phospho-Tau. In parallel we tested TgRln/GSK-3β cognitive functions in the NOR and in the Morris water maze test, two spatial memory tasks in which Tet/GSK-3β mice are impaired (Hernandez et al., 2002; Engel et al., 2006a). Preliminary results point in both tasks at a Reelin-mediated reversion of the recognition memory deficits associated with hyperphosphorylated Tau in Tet/GSK-3β. However increasing population per genotype will be needed to evaluate stastical significance and finally assess that the phenotypes mediated by Reelin overexpression in Tet/GSK-3β actually lead to a cognitive rescue. Also it remains to be addressed whether Reelin overexpression reverts other aspects of AD pathology in Tet/GSK-3β mice, such as microgliosis, astrocytosis and neurodegerative processes in the DG of the hippocampus.

Altogether the observations made in TgRln/GSK-3β mice strengthen the results found in the J20 model of FAD and further support Reelin as a protective factor in the context of AD pathology. Indeed, since GSK-3β has been described has a major mediator linking Aβ to Tau phosphorylation (Takashima et al., 1993; Busciglio et al., 1995; Takashima et al., 1996), by antagonizing GSK-3β activity Reelin would position itself at the crossway of the two main AD-related pathways, reducing their toxicity.

5.4 New insights into hippocampal atrophy and neurogenesis in AD mice and the involvement of Reelin

Hippocampal atrophy is one of the early manifestations of AD observed in biopsies (Braak and Braak, 1997; Kerchner et al., 2012), and in many cases it even precedes the state of mild cognitive impairment (MCI) (Smith et al., 2012). In particular, it has been described CA1 atrophy with pyramidal neuron loss (Davies et al., 1992); and the thinning of the CA1-stratum radiatum and stratum lacunosum moleculare (CA1-SRLM) has been described to correlate with episodic memory loss and earliest cognitive symptoms in AD patients (Kerchner et al., 2012). Contrarily, the size of the DG and CA3 do not seem to correlate with any aspect of memory performance (Kerchner et al., 2012).

In contrast to humans, transgenic mouse models of AD bearing hAPP are not characterized by overt neuronal loss, although they display signs of neurodegeneration, such as neuritic dystrophy and synapse loss. One possible explanation for this observation is that the typical lifetime of the mouse is too short for Aβ toxicity to kill neurons, or that the neurodegenerative phenotype is attributable to other aspects of the pathology, such as Tau toxicity or neuroinflammation, more than to Aβ toxicity. However, the lack of the cell death phenotype is indeed a weakness of hAPP AD models.

Our data revealed, for the first time, clear DG atrophy for J20 mice at the age of 4 months, prior to the onset of plaque burden. In these mice we detected a significant reduction in total DG volume, calculated as percentage of DG area compared to total hippocampal area. Such a reduction may point to neurodegeneration. Both the molecular layer (ML) and granule cell layer (GCL) are affected by the thinning through a mechanism that is still unclear (**Fig. 4.15**).

In a first attempt to ascertain the reasons for the observed reduction of DG volume, we analysed whether it was caused by an increased rate of neuronal death. To this end, we performed activated-caspase-3 staining of apoptotic neurons. We did not find enhanced rates of apoptosis by this approach, although we cannot rule out that other kinds of neuronal death, such as necrosis, take place.

Another possible cause of the thinning of the GCL could be a reduced rate of neurogenesis. In several transgenic models, adult neurogenesis is compromised in AD

and, in non-hAPP AD models this precedes neuronal loss. Dysfunctional neurogenesis, both decreased and increased, has been reported for AD transgenic models and for AD patients (Jin et al., 2004b; Lazarov and Marr, 2010; Marlatt and Lucassen, 2010; Winner et al., 2011; Perry et al., 2012). In our case, decreased levels of DCX-labelled cells were found in J20 compared to wild-type animals at the age of four month (**Fig. 4.16**). Instead in J9 mice, another model of hAPP overexpression under the same promoter of J20 (PDGF-β promoter), increased hippocampal and subventricular neurogenesis was found, both at 3 and at 12 months, as shown by BrdU staining (Jin et al., 2004a). Also in J20 mice an increase in hippocampal neurogenesis, assessed by BrdU staining, was detected at the age of 3 months (Lopez-Toledano and Shelanski, 2007). However this increase reverted with aging of the animals, since it was no more detected at the ages of 5, 9 and 11 months. Moreover the increase in neurogenesis was found to be correlated with detectable levels of oligomeric Aβ, measured by ELISA and western blot. An increased rate of adult neurogenesis can be considered as a compensatory mechanism in neurodegenerative processes; it therefore makes mechanistic sense to find this process increased in models of AD, above all as a response to Aβ oligomer or Tau toxicity. On the other hand sustained stimulation of neurogenesis, in the attempt to overcome the continous toxicity of newly generated Aβ toxic species in hAPP models, could even lead to a possible exhaustion of stem cell niches, with a consequent impairment in the replacement of dividing cells at later stages in the life. This could be one conceivaible hypothesis to explain the described increase in adult neurogenesis of J20 mice at an early stage of adulthood (3 months), followed by a reversion at later stages. Moreover the incongruence with the increased neurogenesis reported for J9 hAPP mice until the age of 12 months (Jin et al., 2004a) could be explained taking into account the intrinsic differences between the two models. Indeed, J9 and J20 mice express different levels of $hAPP_{swe/Ind}$ transgene and different levels of Aβ peptide (**Chapter 1.1.4**). This could be translated in a weaker stimulation of neurogenesis in J9, that therefore could be maintained increased over longer time if compared with J20.

Altogether these observation could reconciliate the data of increased neurogenesis in J9 and in J20 at the age of 3 months with our finding of reduced neurogenesis in J20 at 4 months. Actually this could be the result of a possible exhaustion of stem cell niches after sustained over-stimulation of neurogenesis in previous stages. Analysis of

neurogenesis rate at additional time points (e.g. 1-3 months), and correlation with circulating Aβ peptide levels, should be carried out to verify the proposed hypothesis.

Moreover the use of different techniques should be taken into account for the interpretation of these results. BrdU stains all kind of proliferating cells (including for instance glia in our case), whereas DCX specifically stains immature neuronal precursor. Thus BrdU can supply mistaken results due to inespecificity, while with DCX staining a faster neuronal precursors maturation can be interpreted as a decrease in neurogenesis.

Moreover, we found morphological alterations in DCX-positive cells. This finding raises the question as to whether newly born cells can properly integrate into the GCL. If this were not the case, the generation of non-functional neurons or their fail in being integrated into the GCL, could stimulate further waves of neurogenesis, providing another possible cause for the hypothesized exhaustion of stem cell niches. Regarding the morphological alterations observed, first we did not find a homogenous distribution of proliferating cells along the SGZ and concomitantly GCL thinning seemed to be more severe in correspondence of the zones with lower rates of proliferation, thereby supporting the hypothesis that GCL thinning is attributable to a decrease in the ratio of neuronal replacement. Second, we observed mispositioning of DCX-positive cells, with bodies at different depths of the GCL, sometimes even localized in the hilus. Third, dendritic trees were observed to be less developed and in some cases extending going improperly towards the hilus instead of the ML. Finally, dystrophic neurites were also observed (**Fig. 4.16 a** and **c**).

We also detected an involvement of Reelin in both DG atrophy and adult neurogenesis alterations. Our data indicate that Reelin overexpression alone is responsible for a significant thinning of ML in TgRln mice at the age of 4 months, while the GCL is not affected, meaning that while the number of cells is not decreased, their dendritic trees do occupy less space (**Fig. 4.15**). Analysis of neurogenesis rates assessed by DCX staining in TgRln mice revealed an increased number of newly-generated cells with more developed dendritic trees (Pujadas et al., 2010). In contrast to *reeler* mice, which are affected by impaired DG neurogenesis, Reelin overexpression restored neurogenesis at an even higher rate than wild-type animals, thereby implying that Reelin is required for and enhances adult hippocampal neurogenesis. Moreover, Reelin overexpression is found to be responsible for alterations in migration, with an increased number of mispositioned DCX-labelled cells found more than 10 μm away from the SGZ (Pujadas

et al., 2010). This finding is possibly due to the ectopic expression of Reelin in pyramidal GCL neurons in these mice. Indeed, Reelin is normally expressed in interneurons of the ML and hilus of the adult DG, and from there it seems to control the correct formation of the radial glial scaffold required for granule cell migration (Zhao et al., 2007). Overexpression of Reelin in the GCL in TgRln mice may send wrong signals to the dividing cells that could be repelling each other and then departing from the SGZ. Finally, in TgRln/J20 mice, the combined effects of Reelin and hAPP overexpression caused a reduction in ML and GCL volumes (**Fig. 4.15**), again without changes in the rate of apoptosis, as assessed by activated-caspase 3 IHC. Analysis of neurogenesis rates by DCX staining in TgRln/J20 mice revealed, as in J20, a decreased number of newly-generated cells (**Fig. 4.16**). Morphological observation shows a combination of the J20 and TgRln phenotypes. Again, a non-homogenous distribution of proliferating cells along the GCL was found, with concomitant more severe GCL thinning corresponding to the zones with lower rates of proliferation. As in TgRln animals, we also observed the mispositioning of cells, with bodies at different depths of the GCL, quite distant from the SGZ. DCX-labelled cells were only occasionally found in the hilus, probably acquiring this phenotype from J20, although displaying it in a less pronounced way. Dendritic trees also displayed alterations, with lower development. We can speculate that the thinning of the GCL observed in TgRln/J20 animals derives, as suspected in the J20 phenotype, from a previous exhaustion of the stem cells niche, in the case in which (object of ongoing experiments) in previous stages a strong increase in neurogenesis took place as a possible repair mechanism. This phenotype would be exacerbated in TgRln/J20 compared to J20 by the fact that the overexpression of Reelin alone is able to induce significant increase in hippocampal neurogenesis (Pujadas et al., 2010). Thus in the context of synaptic and cellular damage induced by high levels of circulating Aβ peptide, together with the lack on proper integration of newly born neurons in the GCL, TgRln/J20 would be facilitated compared to J20 to establish a sustained stimulation of neurogenesis, with an earlier and accelerated exhaustion of the stem cells niche, resulting in a stronger thinning of GCL at the age tested.

Neither for J20 nor for TgRln/J20 clear atrophy of the CA1-SRLM, the most evident phenotype in humans, has been reported so far. Moreover, it is worth noting that, as mentioned above, the size of the DG in humans has not been found to correlate with any aspect of memory performance. It has been proposed that the excitable population of granule cells in DG is formed by a very small number of cells upon the total, whereas

90-95% of the population could be effectively "retired" (Alme et al., 2010). Therefore a very small number of mossy fibers connecting granule cells to CA 3 is though to be sufficient to maintain network functionality (Rolls, 2013). This theory fits with our data since TgRln/J20 mice displayed strong DG atrophy but their cognitive skills were not affected in the NOR memory task, actually TgRln/J20 mice were even protected by Reelin overexpression until the age of 12 months.

We also attempted a first approach to characterize TgRln/GSK-3β mice in the context of atrophy and neurogenesis. Tet/GSK-3β have been described to show neurodegeneration of DG hippocampal cells through apoptosis, as assessed by TUNEL staining and activated-caspase 3 IHC, although they do not develop a severe atrophy until the age of 18 months (Engel et al., 2006b). In contrast to TgRln/J20, 4-month-old TgRln/GSK-3β animals did not develop severe atrophy of the DG, as assessed by Nissl staining (**Fig. 5.5**), although neurodegenerative events cannot be excluded. This result corroborates that the degenerative process observed in TgRln/J20 mice is the result of the combined action of Aβ and Reelin, since Reelin alone does not produce the same result when overexpressed in another AD-like background. However, DCX staining revealed that the newly-generated neurons in the DG of both Tet/GSK-3β and TgRln/GSK-3β mice showed some of the morphologic alterations described above for J20 and TgRln/J20. Both in Tet/GSK-3β and in TgRln/GSK-3β animals, a non-homogenous distribution of proliferating cells along the SGZ was observed, with wide areas without neurogenesis. Overexpression of Reelin alone again increased neurogenesis and was responsible for the mispositioning of cell bodies along the depth of the GCL. In combination with GSK-3β, the overexpression of Reelin also led to alterations in the development and direction of dendritic trees of newly born neurons in the TgRln/GSK-3β model. More conclusive data will be produced from the quantification of DG volume and from DCX-labelled cell counts.

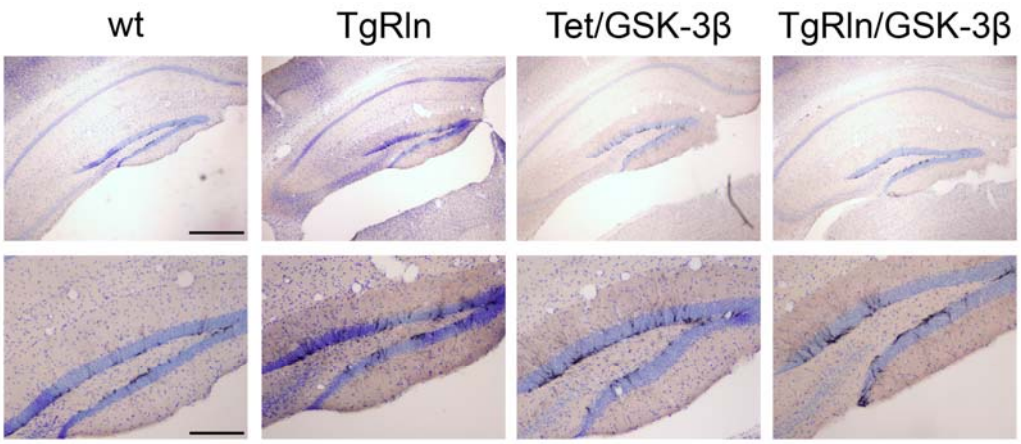

Fig. 5.5. Adult neurogenesis in TgRln/GSK-3β. Nissl and DCX staining of hippocampus of 4-month-old TgRln/GSK-3β plus littermates wt, TgRln and Tet/GSK-3β controls. DG is shown at higher magnification in the lower panels. No evident DG atrophy is observed for any genotype. TgRln mice show an increased rate of neurogenesis and mispositioning of cell bodies along the depth of the granular cell layer (GCL). Both in Tet/GSK-3β and in TgRln/GSK-3β a non-homogenous distribution of proliferating cells along the subgranular zone (SGZ) is observed. Moreover, TgRln/GSK-3β mice display alterations in the development and direction of dendritic trees of newly born neurons. Scale bars: upper panel, 500 μm; lower panel, 200 μm.

Further studies will be needed to elucidate the mechanisms underlying Reelin-dependent ML volume reduction and the combined action of Reelin and Aβ in the atrophy of the GCL in the TgRln/J20 model. Finally, we consider it highly pertinent to address the possible functional consequences of Reelin effects on adult neurogenesis in the context of AD.

5.5 Reelin as a potential therapeutic target for AD

We considered the Reelin-induced retention of the cognitive abilities of J20 mice of great interest for a putative role of Reelin pathway as a pharmacological target for AD. Indeed, Reelin has been shown not only to delay AD progress, but also to be required to prevent the appearance of the cognitive impairments of the disease, and only when Reelin is depleted in TgRln/J20 are the effects of cognitive skill loss evidenced. Our findings are in line with the hypothesis (suggested in Herring et al., 2012) that Reelin signalling depletion is one of the first events in the appearance of AD, and match the observation that Reelin haploinsufficiency in transgenic AD mice results in accelerated AD-like pathology (Kocherhans et al., 2010).

On this basis, a possible therapeutic effect of the Reelin pathway in AD has been envisaged, possibly reverting key indicators of the illness after their appearance. The strategy pursued to test this hypothesis has been to allow TgRln/J20 and J20 mice to develop AD pathology, suppressing Reelin overexpression in the former by continuous doxycycline administration during their first 4 months of life. Once the onset of disease is appreciated, as checked by the NOR test, doxycycline administration was stopped and mouse groups were re-evaluated for the NOR test after 1 and 3 months of Reelin overexpression in order to address possible Reelin-dependent improvements in cognition. Conditional overexpression of Reelin in adult mice did not overcome AD impairments in the NOR test once the pathology developed. This finding indicates that continuous Reelin overexpression overcomes Aβ-induced toxicity and prevents the appearance of cognitive deficits in J20 mice, although the conditional induction of Reelin overexpression in cases of overt AD is not sufficient to revert the cognitive impairments developed. However, we cannot rule out the reversion of other hallmarks of the disease. For instance, we are now analysing whether the conditional induction of Reelin overexpression in adult J20 mice partially reverts amyloid plaque deposition or dendritic spine loss, although these molecular changes would not convey a global functional recovery. Another interesting issue to address is whether Reelin conditional overexpression in adult mice displaying Tau hyperphosphorylation reduces this phenotype.

Altogether, our findings, in line with literature, indicate that Reelin depletion is necessary for the development of cognitive impairments in J20 AD mice, while its

conditional overexpression in cases of overt AD is not sufficient for the reversion of the latter. This observation implies that the Reelin signalling pathway is not of great therapeutic potential alone in the conditions tested, although molecular reversion of some histopathological hallmarks of the disease cannot be ruled out yet. Given that Reelin depletion seems to be a very early phenomenon in AD, another therapeutically relevant possibility could be the administration of this protein immediately before the onset of AD, in an attempt to complement the very early depletion in the Reelin signalling pathway. For instance, in the paradigm we applied, we may have missed this time point since J20 animals possibly experience a decrease in Reelin levels even before the emergence of cognitive impairments. Therefore administration of Reelin at the age of 4 months could be too late for a therapeutic potential to be appreciated, whereas anticipation of the point at which Reelin starts to be depleted could be beneficial. This approach would require setting up a very careful analysis to establish first whether in J20, as in other models, Reelin depletion is an early phenomenon of AD (Chin et al., 2007) and second to determine the time course and areas of the brain in which this depletion takes place. With this information, a more adequate approach could be set up to test the therapeutic potential of Reelin. Finally, in an effort to convey these observations to the human condition, the most relevant issue to emerge is the compelling need to improve the early detection of AD, which is indispensable for the functionality of many therapeutic approaches.

5.6 Unifying hypothesis

Taken together, the results coming from our *in vitro* and *in vivo* approaches highlight the potential of Reelin as a neuroprotective tool and a cognitive enhancer during normal aging and AD pathogenesis, as it has the capacity to overcome the deficits associated with Aβ deposition. This study also shows that Reelin overexpression in J20 mice is sufficient to achieve a functional recovery of behavioral deficits, as shown by the NOR task. In addition, here we show that the trapping of Reelin into $A\beta_{42}$ fibrils causes the loss of Reelin signaling itself. In the adult brain, the Reelin pathway has been shown to favor α-processing of APP; decrease GSK-3β activity and Tau phosphorylation; potentiate glutamatergic neurotransmission, LTP and structural synaptic plasticity; and to positively regulate adult neurogenesis in the hippocampus (Ohkubo et al., 2003; Hoe et al., 2006; Qiu et al., 2006; Pujadas et al., 2010; Teixeira et al., 2012). These processes are necessary for correct neuronal physiology and cognitive adult functions that are impaired in AD. We thus propose that the Reelin cascade is a key "homeostatic" pathway that regulates numerous aspects of normal adult brain function and whose dysfunction may contribute to the pathological and cognitive traits typical of AD. This vision is in agreement with the view that Reelin depletion in the temporal lobe is one of the early events in AD pathogenesis (Herring et al., 2012) and with studies reporting that Reelin haploinsufficiency in AD mice results in accelerated AD-like pathology (Knuesel, 2010; Kocherhans et al., 2010).

In summary, our data support a model (**Fig. 5.6**) in which the Reelin pathway exerts beneficial effects on both AD pathology and cognition by at least two complementary mechanisms. In addition to extracellular Reelin delaying amyloid fibril formation and reducing neurotoxicity by interacting with $A\beta_{42}$ soluble species and fibrils, the activation of the Reelin cascade itself would potentiate adult plasticity events, including synaptic plasticity and adult neurogenesis, and lead to decreased GSK-3β activity and Tau phosphorylation. On the basis of our findings in transgenic mice, we propose that the acute activation of the Reelin pathway represents a new therapeutic strategy for ameliorating the cognitive decline associated with normal aging and the deficits characteristic of AD pathology.

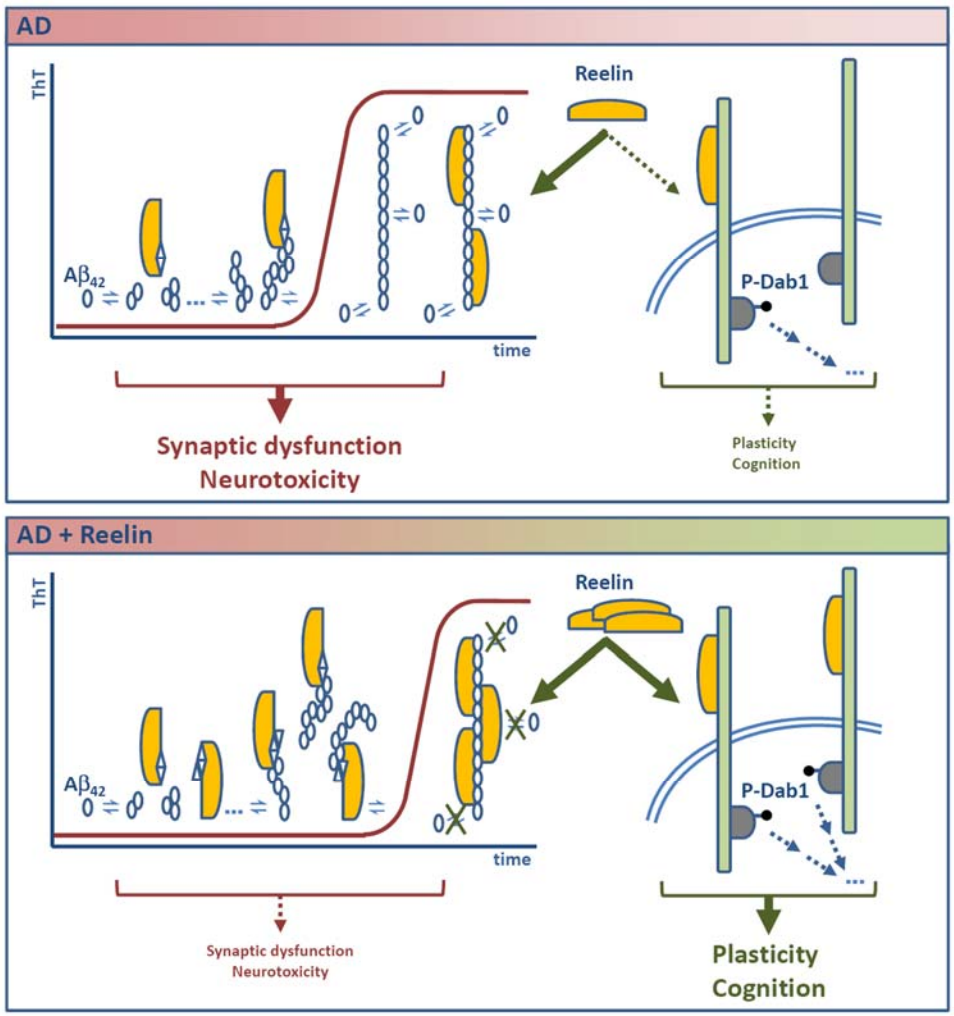

Fig. 5.6. Summary scheme illustrating the involvement of Reelin in Alzheimer Disease. In AD (upper panel), high levels of neurotoxic soluble Aβ oligomers induce a wide range of alterations, including synaptic dysfunction. Reelin interacts with soluble Aβ species, and gets trapped into amyloid fibrils, where it loses its functionality, resulting in a downregulation of the Reelin signalling pathway. Incresed Reelin levels in the context of AD (lower panel), possibly through enhanced Aβ-Reelin interaction, lead to delayed fibril formation, reduced plaque load and decreased Aβ toxicity, with a recovery of synaptic loss and cognitive functions. Additionally, increased levels of functional Reelin might restore its downstream signaling pathway, further exerting neuroprotection. By these two complementary mechanisms, increased Reelin levels in AD overcome Aβ-mediated toxicity and cognitive deficits, pointing at the Reelin pathway as a new therapeutic target for the treatment of AD.

5.7 Future perspectives

The wealth of data presented in this work suggests that Reelin overcomes Aβ toxicity at multiple levels, from synapses, to cells, up to neural networks. Although apparently participating with Aβ in the thinning of hippocampal dentate gyrus, Reelin overexpression in J20 mice (TgRln/J20) is sufficient to lead to functional recovery of AD behavioural deficits, consistent with dendritic spine density rescue and reduction of neuronal death. A great effort remains to be channelled into deciphering the molecular mechanisms underlying Reelin neuroprotection in AD and to fit the observed phenotype of dentate gyrus atrophy.

In this regard it would be of great relevance to analyse the levels of soluble Aβ in TgRln/J20 animals, to deepen our understanding of the molecular mechanisms by which Reelin reduces the number of amyloid plaques and the toxicity of Aβ species. Remarkably, in an *in vitro* approach, it was reported that Reelin regulates the trafficking and proteolytic processing of APP, promoting non-amyloidogenic αAPP cleavage (Hoe et al., 2006; Hoe et al., 2008; Hoe et al., 2009). It would be of great relevance to corroborate these data in our *in vivo* system. Further, gaining insight into the mechanisms of interaction between Reelin and Aβ species, both oligomers and fibrils, is most definitely a future issue of great relevance to address.

Further studies will be also needed to elucidate the mechanisms underlying Reelin-dependent ML volume reduction and the combined action of Reelin and Aβ in the atrophy of the GCL in the TgRln/J20 model. We consider it highly pertinent to address the possible functional consequences of Reelin overexpression on adult neurogenesis in the context of AD. Additionally, it remains to be addressed whether Reelin overexpression reverts other aspects of AD pathology such as neuroinflammation.

Finally, the key mechanism to elucidate *in vivo* is the trapping of Reelin into $A\beta_{42}$ fibrils, with the consequent loss of Reelin signalling. Indeed we propose the Reelin pathway as an important "homeostatic" pathway that regulates numerous aspects of normal adult brain function (glutamatergic transmission, synaptic plasticity, adult neurogenesis, APP processing, Tau phosphorylation) and whose dysfunction, eventually due to Reelin sequestering into amyloid plaques, may contribute to the pathological cognitive traits typical of AD.

CONCLUSIONS

1. **Reelin protein can be purified through sequential anion exchange and size exclusion chromatography**
2. **Reelin protein bears N-glycosylation on asparagines 291, 306 and 1267**
3. **Reelin delays *in vitro* the kinetics of $A\beta_{42}$ fibril formation and extends the life-time of $A\beta_{42}$ oligomeric species**
4. **Reelin interacts with soluble $A\beta_{42}$ species and reduces their citotoxicity**
5. **Reelin gets sequestered into $A\beta_{42}$ fibrils, losing its biological functionality**
6. **Reelin does not alter the cross-β-sheet structure of $A\beta_{42}$ fibrils**
7. **Reelin exacerbates the phenotype of dentate gyrus atrophy and adult neurogenesis reduction in a mouse model of hAPP overexpression**
8. **Reelin reduces hippocampal and cortical amyloid plaque load in a mouse model of hAPP overexpression**
9. **Reelin prevents dendritic spine loss in a mouse model of hAPP overexpression**
10. **Reelin decreases Tau phosphorylation in a mouse model of GSK-3β overexpression**
11. **Reelin prevents cognitive impairments during normal aging and in a mouse model of hAPP overexpression**
12. **Reelin depletion is required for cognitive deficits to manifest in a model of hAPP**
13. **Conditional induction of Reelin overexpression in cases of overt AD is not sufficient to revert the cognitive impairments**

RESUMEN

INTRODUCCIÓN

Demencia tipo Alzheimer

La enfermedad de Alzheimer (*Alzheimer's disease*, AD) es la causa más común de demencia en las personas mayores, con más de 25 millones de personas afectadas en todo el mundo (Asociación de Alzheimer, http://www.alz.org/). Descrito por primera vez en 1907 por el médico alemán Alois Alzheimer (Alzheimer et al., 1995), AD es un trastorno neurodegenerativo caracterizado por una dramática pérdida progresiva de sinapsis y poblaciones neuronales, que afecta inicialmente a las estructuras del lóbulo temporal medial y que finalmente resulta en atrofia cortical difusa. Los síntomas clínicos más comunes son deterioro cognitivo con amnesia, agnosia, incapacidad en la planificación y en el razonamiento abstracto, en conjunto con disfunciones ejecutivas, como afasia y apraxia (McKhann et al., 1984). Esta erosión gradual de la cognición aumenta lentamente en la severidad de los síntomas hasta que finalmente se convierten en incapacitante. A nivel histológico la enfermedad se caracteriza por la difusión de lesiones patológicas en diversas regiones del cerebro, distinguiendose seis estadíos (conocidos cómo estadíos de Braak) de progresión de la enfermedad (Braak and Braak, 1991, 1995): las etapas transentorhinales I-II, que representan casos clínicamente silentes; las etapas límbicas III-IV de AD incipiente y las etapas neocorticales V-VI de AD completamente desarrollada. En las últimas etapas de la enfermedad, el deterioro cognitivo es acompañado a menudo por características psiquiátricas, tales como confusión, agitación y alteraciones del comportamiento, y síntomas neurológicos, que pueden incluir convulsiones, hipertonía, mioclonías, incontinencia y mutismo. AD es una enfermedad terminal con la muerte comúnmente causada por factores externos tales como infecciones, neumonía, desnutrición o comorbilidades, pero no por el trastorno en sí.

Genética de la enfermedad de Alzheimer

Dependiendo de la edad de inicio se distinguen dos tipos principales de AD: las formas de inicio temprano, con comienzo antes de los 65 años, y las formas de aparición tardía. Una proporción considerable de las formas de AD de inicio temprano (EOAD) se produce en un contexto de historia familiar, y se debe a mutaciones raras, autosómicas dominantes de los genes *proteína precursora de la β amiloide* (APP), *presenilina-1* (PSEN1) y *presenilina-2* (PSEN2) (Bertram et al.; Ballard et al., 2011; Selkoe, 2011). Debido a su herencia mendeliana, estos casos se denominan también como AD familiar (FAD). En cambio, las formas de aparición tardía de AD (LOAD) no están directamente vinculadas a mutaciones genéticas, y para ellas sólo se han

propuesto factores de riesgo genéticos. Debido a la ausencia de herencia directa, las formas de aparición tardía de AD también se clasifican como enfermedad de Alzheimer esporádica (SAD). Numerosas mutaciones con error de sentido altamente penetrantes se han descrito en los genes APP, PSEN1 y PSEN2, como indicado en la Tabla 1. Las duplicaciones de APP también son responsables de AD de inicio temprano (Rovelet-Lecrux et al., 2006; Tanzi, 2012), y en el síndrome de Down (causado por la trisomía del cromosoma 21, que contiene el gen APP) la sobreexpresión de APP resulta en demencia de inicio temprano con un fenotipo similar al de la AD (Hof et al., 1995). Las mutaciones responsables de AD familiar se pueden examinar en detalle en la página web del Frontotemporal Dementia Mutation Database (**http://www.molgen.ua.ac.be/ADmutations/**).

La proteína beta amiloide (Aβ), uno de los principales agentes tóxicos en la AD, es un producto del catabolismo de la proteína APP, procesada proteolíticamente por la acción consecutiva de las β- y γ-secretasas (Cole and Vassar, 2008; Steiner, 2008). La mayoría de las mutaciones de APP relacionadas con AD familiar se encuentran en los sitios de corte de las secretasas, y a menudo conducen a un mayor corte proteolítico y a una mayor producción de Aβ, como es el caso de la mutación "Swedish" (Goate et al., 1991; Mullan, 1992). Por otra parte, los genes relacionados con AD familiar PSEN1 y PSEN2 codifican por el centro catalítico de la γ-secretasa, y sus mutaciones también conducen a una producción anómala del péptido Aβ (Bertram et al.). Por último, mutaciones en el centro del péptido Aβ capaces alterar las propiedades de agregación de Aβ, también están relacionadas con AD familiar (Nilsberth et al., 2001; Tomiyama et al., 2008). La observación de que la mayoría de las mutaciones que causan ADF aumentan la producción de Aβ, es una fuerte evidencia de un papel causal del péptido Aβ en la patogénesis de AD. Esta convergencia de las evidencias genéticas y moleculares ha dado soporte a la "hipótesis amiloide", que postula que la producción anormal de Aβ es el paso inicial en el desencadenamiento de la cascada fisiopatológica que con el tiempo conduce a AD (Glenner and Wong, 1984; Hardy and Higgins, 1992; Hardy, 1997; Hardy and Selkoe, 2002; Tanzi and Bertram, 2005) (**capítulo 1.1.2**). Sin embargo, los casos familiares de AD representan sólo aproximadamente un 1-6% del total (Bekris et al., 2010). El restante ~ 95% de los casos son atribuibles a la forma esporádica de AD, por la que no están claros aún los mecanismos patogénicos.

Aunque las formas de aparición tardía de AD se clasifiquen como esporádicas, cabe destacar que hasta un 60%-80% de estos casos tienen predisposición genética. De hecho la susceptibilidad para LOAD está conferida por numerosos factores de riesgo genéticos de frecuencia relativamente alta, pero baja penetrabilidad. Además de los genes de susceptibilidad, los factores ambientales y epigenéticos pueden contribuir significativamente a determinar el riesgo de un individuo, por lo que la forma esporádica de AD es una enfermedad multifactorial compleja que surge de la interacción de varios factores determinantes (Gatz et al., 2006).

El alelo Apoε4 de APOE, una de las principales apolipoproteínas del cerebro, es el mayor factor de riesgo genético conocido para AD esporádica (Corder et al., 1993; Saunders et al., 1993; Schmechel et al., 1993; Strittmatter et al., 1993a; Strittmatter et al., 1993b). En comparación con los pacientes no portadores de ε4, el riesgo de AD se incrementa de dos a cuatro veces en los pacientes portadores de un alelo ε4 y de aproximadamente 12 veces en pacientes ε4 homocigotos (Farrer et al., 1997; Bertram et al., 2007). Los portadores de Apoε4 también muestran la acumulación temprana de placas amiloides y una edad más temprana de inicio de la demencia. La vía neuropatológica por la que APOE aumenta el riesgo de enfermedad no está clara. Sin embargo, la isoforma Apoε4 se asocia con una disminución de la eficiencia de eliminación de Aβ en cerebro (Castellano et al., 2011). Además, Apoε4 parece incrementar la formación de formas oligoméricas solubles de Aβ, que son cruciales para la disminución de la disfunción sináptica, el deterioro cognitivo y la neurodegeneración (Hashimoto et al., 2012).

Estudios de asociación del genoma completo (GWAS) recientes, además de confirmar Apoε4 como el mayor gen asociado a AD esporádica (Bertram et al., 2010), han revelado nuevos locus asociados con AD, cómo CLU, PICALM, CR1, BIN1, ABCA7 y EphA1(Lambert et al., 2009; Hollingworth et al., 2011; Naj et al., 2011; Tanzi, 2012).

Finalmente, además de los factores de riesgo genéticos, se ha propuesto una componente ambiental para AD, con factores como la edad, la educación, la actividad física, la dieta y la eventual presencia de comorbilidades (obesidad, diabetes, enfermedades inflamatorias) que juegan un papel en su aparición (Arendash et al., 2004; Rovio et al., 2005).

A pesar de sus antecedentes genéticos distintos, las formas familiares y esporádicas de AD son indistinguibles a nivel histopatológico y muestran dos características principales: las placas amiloides y los ovillos neurofibrilares (Braak and Braak, 1997; Nussbaum and Ellis, 2003; Goedert and Spillantini, 2006), que aparecen en un contexto de daño vascular, inflamación, estrés oxidativo, pérdida sináptica y neurodegeneración (**Fig 1.1**).

Aβ en la patogénesis de la enfermedad de Alzheimer

El procesamiento proteolítico de APP: Las placas de β-amiloide son una de las principales lesiones histopatológicas de la AD. Se trata de depósitos insolubles extracelulares compuestos principalmente por péptidos Aβ, dispuestos en fibrars con una estructura secundaria de lámina β plegada. La deposición de placas β-amiloides comienza en la corteza Enthorinal y se extiende durante la progresión de la enfermedad a las regiones alocorticales primero, a continuación a los núcleos del diencefálo, al estriado y a los núcleos colinérgicos del cerebro anterior basal, y finalmente al cerebelo (Thal et al., 2002). El péptido Aβ se genera por el corte proteolítico de la proteína transmembrana APP por la acción de unas proteasas de membrana denominadas secretasas. APP se procesa secuencialmente: primero por cualquiera la acción de α- o β-secretasas, y luego por γ-secretasa (Sheng et al., 2012). En la vía amiloidogénica, que da lugar

al péptido Aβ, las proteasas implicadas son β- y γ-secretasa, cuya acción secuencial libera el dominio extracelular soluble de APP (sAPPβ), el péptido Aβ, y el dominio carboxi-terminal intracelular de APP (AICD). En contraste, la escisión por la α- y γ-secretasas previene la formación de Aβ, produciendo sAPP, péptido p3 y AICD (**Fig. 1.2a**). α- y β-secretasas cortan en sitios únicos del dominio extracelular de APP, mientras que γ-secretasa puede cortar los productos de la α- o la β- escisión en varias posiciones, dando lugar a péptidos Aβ y fragmentos intracelulares de longitud variable. Dependiendo del sitio de escisión específica de la γ-secretasa la longidud del péptido Aβ puede variar, siendo las formas de 40 ($A\beta_{40}$) y 42 aminoácidos ($A\beta_{42}$) las más frecuentes (**Fig. 1.2b**), de las cuales $A\beta_{42}$ es la menos común, pero más fibrilogénica y neurotóxica (O'Brien and Wong, 2011).

Hipótesis amiloide y oligómeros de Aβ: Como se ha mencionado en el **capítulo 1.1.1**, hasta ahora las únicas mutaciones clasificadas como causantes de AD familiar son a cargo de los genes APP, PSEN 1 y PSEN 2 y casi todas son responsables de un aumento de la producción de péptido Aβ o bién de un aumento de la proporción $A\beta_{42}/A\beta_{40}$ (Tanzi and Bertram, 2005; Blennow et al., 2006; Bettens et al., 2010). Durante muchos años, estos hallazgos fortalecieron la "hipótesis de la cascada amiloide", postulada en 1992 por Hardy y Higgins (Hardy and Higgins, 1992). De acuerdo con esta hipótesis, la producción anómala de Aβ es el paso inicial en el desencadenamiento de la cascada fisiopatológica que con el tiempo conduce a AD (Glenner and Wong, 1984; Hardy, 1997; Tanzi and Bertram, 2005). La deposición de Aβ y la formación de placas amiloides se describen como los principales procesos responsables de la muerte neuronal y las otras lesiones neuropatológicas distintivas de AD (ovillos neurofibrilares, daño vascular, neuroinflamación) son consecuencias y no causas de la enfermedad. Tampoco se hace ninguna diferencia mecanística entre los casos esporádicos y familiares de AD, ya que en ambos casos el suceso iniciador de la patología es la deposición de amiloide que, en los casos esporádicos con ausencia de mutaciones, se atribuye a otras causas externas que desencadenan la misma cascada de eventos que en AD familiar. Estudios posteriores revelaron que la "hipótesis de la cascada amiloide" no podía conciliar las observaciones clínicas y patológicas, debido a la falta de correlación entre la carga de placas amiloides y la gravedad del deterioro cognitivo en pacientes con AD (Terry et al., 1991; Hibbard and McKeel, 1997; McLean et al., 1999; Giannakopoulos et al., 2003). Por otra parte, los modelos murinos de AD que sobreexpresan formas mutadas de APP humana (hAPP) exhiben déficits de comportamiento mucho antes de la aparición de la patología amiloide (Hsia et al., 1999; Mucke et al., 2000; Kawarabayashi et al., 2001; Lesne et al., 2006). Esta observación sugirió que el daño sináptico, y no la muerte neuronal inducida por placas amiloides, encajaba mejor con el deterioro cognitivo observado. La versión más reciente de la "hipótesis de la cascada amiloide" propone que la AD no surge de la citotoxicidad inducida por placas, sino más bién de la toxicidad

sináptica mediada por los agregados globulares solubles de Aβ. Estas formas no fibrilares ni monoméricas de Aβ han demostrado ser el verdadero agente tóxico, capaz de provocar disfunción sináptica y pérdida de sinapsis (Lambert et al., 1998; Walsh et al., 2002a; Cleary et al., 2005; Lesne et al., 2006; Haass and Selkoe, 2007; Lacor et al., 2007; Shankar et al., 2007). Para obtener mayor información sobre los mecanismos de acción de los oligómeros de Aβ, muchos protocolos de laboratorio se han diseñado para obtener estas especies para su uso experimental. Uno de estos protocolos permite la formación *in vitro* de una solución heterogénea compuesta principalmente por trímero, tetrámero, pentámero y oligómeros de hasta 24-mer de péptido Aβ (Lambert et al., 1998; Lambert et al., 2001; Chromy et al., 2003; Krafft and Klein, 2010). Los oligómeros obtenidos mediante este protocolo se han llamado ligandos difusibles derivados de Aβ (ADDLs) y se ha propuesto que ejercen su toxicidad mediante la unión directa a un receptor de membrana en las espinas dendríticas de neuronas piramidales excitatorias (Lacor et al., 2007). Por otra parte, se ha encontrado que los ADDLs son responsables de aberraciones en la morfología de espinas dendríticas, de una reducción en la densidad de espinas dendríticas (Lacor et al., 2007); de la formación de especies reactivas de oxígeno (De Felice et al., 2007); de hiperfosforilación de la proteína Tau (De Felice et al., 2008); y de la inhibición de la potenciación a largo plazo (LTP) (Lambert et al., 1998; Walsh et al., 2002b; Wang et al., 2002). Además, los ADDLs provocan muerte celular con selectividad celular (limitada a las neuronas) y especificidad regional (afectando a neuronas del hipocampo pero no del cerebelo, en paralelo a la patología de AD) (Klein, 2002). Estos resultados han sido corroborados con otros tipos de preparaciones de oligómeros sintéticos y, finalmente, también en el cerebro de AD humano.

La "hipótesis de oligómeros Aβ" ha resuelto la paradoja existente en la "hipótesis de la cascada amiloide" al reconocer que la consecuencia inmediatamente relevante para AD tras la elevada producción de péptido Aβ no es una mayor deposición de placas amiloides, sinó el incremento de la formación de oligómeros. De hecho, los niveles cerebrales de especies Aβ solubles parecen correlacionarse mejor con la gravedad del deterioro cognitivo que la densidad de placas (Lue et al., 1999; Naslund et al., 2000). Desde este punto de vista surgió la noción de que los depósitos de amiloide insolubles funcionan como reservorios de oligómeros bioactivos, que se forman continuamente por el desprendimiento y re-asociación de moléculas que se reciclan dentro de la población de fibrillas (Carulla et al., 2005; Haass and Selkoe, 2007). Por otra parte, ya que los oligómeros se forman a bajas concentraciones de Aβ, posiblemente antes de la formación de placas, proporcionan una explicación de las fluctuaciones en el rendimiento de la memoria de pacientes con AD en etapas muy tempranas de la enfermedad, como posibles cambios transitorios en los niveles de oligómeros. Sin embargo, qué tipo de oligómeros de Aβ son los más patógenos y cómo su acumulación en el cerebro causa la disfunción sináptica y

neuronal, son todavía temas de intenso estudio y debate (Benilova et al., 2012; Huang and Mucke, 2012).

Patología de Tau

Además de las placas amiloides, el otro tipo principal de lesión histopatológica de la AD son los ovillos neurofibrilares (NFT), que se forman intracelularmente y se componen principalmente de la proteína Tau agregada con modificaciones postraduccionales anormales, incluyendo el aumento de su fosforilación y acetilación (Iqbal et al., 2010; Cohen et al., 2013). Tau es la principal proteína asociada a los microtúbulos (MAP) en la neurona madura. Las otras dos MAPs neuronales son MAP1 y MAP2. Una función establecida de las MAP es su interacción con tubulina, la promoción de su ensamblaje en microtúbulos y la estabilización de la red de microtúbulos. La actividad de promoción del ensamblaje de microtúbulos por parte de Tau está regulada por su grado de fosforilación, de hecho, la hiperfosforilación de esta proteína deprime su actividad biológica (Iqbal et al., 2010).

En el cerebro con AD, los niveles de Tau hiperfosforilada son de tres a cuatro veces mayores que en el cerebro adulto sano, y en este estado Tau hiperfosforilada se separa de los microtúbulos empezando a polimerizar en filamentos helicoidales emparejados (PHFs), que a su vez se asocian en haz (*bundle)* de pares, resultando finalmente en la formación de NFT (**Fig. 1.3**) (Grundke-Iqbal et al., 1986).

Tau puede ser fosforilada en residuos de tirosina, treonina o serina por varias proteínas quinasa. Entre ellas GSK-3 en su isoforma β (GSK-3β) es la que fosforila la mayor parte de los sitios relacionados con la AD en la molécula de Tau. La fosforilación de Tau por GSK-3β en sitios específicos se puede analizar mediante el uso de anticuerpos como AT8 o PHF-1, que reconocen respectivamente la fosforilación de Tau en la serina 202 o en las serinas 396-404. Aunque Tau se encuentre predominantemente en los axones, donde está implicada en la estabilización de microtúbulos y el tráfico de vesículas, recientemente se han descubierto tambíen funciones dendriticas. Estudios en cultivos celulares y modelos de ratón genéticamente modificados indican que Tau puede facilitar o mejorar la neurotransmisión excitadora mediante la regulación de la distribución de moléculas de señalización relacionadas con la actividad sináptica. Sin embargo, el enriquecimiento de Tau anormalmente modificada o en conformaciones patógenas en las espinas dendríticas interfiere con la neurotransmisión (Hoover et al., 2010). Además, los oligómeros Aβ promueven el enriquecimiento postsináptico de Tau a través de un proceso que involucra a miembros de la familia de quinasas reguladoras de la asociación MAP/microtúbulos (MARK) (Zempel et al, 2010).

La patología Tau se correlaciona con el deterioro cognitivo (Giannakopoulos et al., 2003) y con el estadiajede AD (Arriagada et al., 1992) mejor que la patología amiloide; así, la escala más utilizada para evaluar el estado de la progresión de la enfermedad se basa en la abundancia NFT

y su propagación a través del cerebro (Braak and Braak, 1995). Sin embargo, en pacientes con AD no se han encontrado mutaciones en el gen que codifica para Tau (*proteína Tau asociada a los microtúbulos* - MAPT). En contraste, mutaciones MAPT se han descrito ser causantes de demencia frontotemporal (FTD) (Cairns et al., 2007).

Modelos murinos de la enfermedad de Alzheimer

La identificación de mutaciones causantes de AD condujo al desarrollo de varios modelos de ratones que reproducen las principales características patológicas de este trastorno. La generación de ratones transgénicos con mutaciones en los genes relacionados con AD (tales como APP, APOE, BACE, PS1, PS2), combinados con el uso de diferentes promotores, resultan en la reproducción de una amplia variedad de fenotipos de AD, que van desde las placas amiloides a los ovillos neurofibrilares, neuritas distroficas, gliosis, déficits sinápticos y deterioro cognitivo. Una lista de los modelos transgénicos actualmente disponibles de AD se puede encontrar en la página web del Alzheimer research forum: http://alzforum.org/res/com/tra/ . Las tablas 3, 4 y 5 resumen respectivamente los modelos de APP/BACE/presenilinas, los modelos de Tau y los modelos cruzados.

La proteína de matriz extracelular Reelina y la enfermedad de Alzheimer

Reelina en el desarrollo y en el cerebro adulto

Reelina es una proteína extracelular crucial para la migración neuronal en el desarrollo del cerebro. Además, cada vez hay más evidencias de que Reelina controla sinaptogénesis y la maduración sináptica durante el desarrollo (D'Arcangelo et al., 1995; Rice and Curran, 2001; Soriano and Del Río, 2005; Cooper, 2008). Reelina actúa a través de los receptores de la apolipoproteína E2 (ApoER2) y del receptor de lipoproteína de muy baja densidad (VLDLR), que desencadenan una cascada de señalización compleja que involucra a miembros de la familia Src, DAB1, las quinasas PI3K, ERK1/2 y GSK3, y CrkL, entre otros (**Fig. 1.7**) (Howell et al., 1997; Hiesberger et al., 1999; Howell et al., 1999; Beffert et al., 2002; Arnaud et al., 2003; Ballif et al., 2004; González - Billault et al., 2005; Simo et al., 2007). Es importante señalar que los ratones Reeler, DAB1(-/-) y ApoER2/VLDLR(-/-) son fenotípicamente idénticos, lo que pone de relieve el papel esencial de DAB1 y los receptores en la vía de señalización. Reelina en el cerebro adulto se expresa en subgrupos de interneuronas GABAérgicas de la corteza cerebral y otras regiones (Alcántara, et al., 1998). Aunque el papel de Reelina en el cerebro adulto no se conoce bién, se ha demostrado que esta proteína se expresa en contactos sinápticos y que las neuronas deficientes en ApoER2 y receptores VLDLR tienen alterada la LTP (Beffert et al.,

2005). Por otra parte, recientemente se ha demostrado que participa en la composición, expresión y el tráfico de las subunidades del receptor NMDA (Qiu et al., 2006; Groc et al., 2007), en la elaboración de las dendritas, y en la formación de espinas dendríticas (Matsuki et al., 2008; Niu et al., 2008). Estos estudios sugieren que la Reelina está implicada en la correcta formación y fisiología de las sinapsis corticales.

La mayoría de estudios sobre las funciones de Reelina en el cerebro adulto han empleado análisis de los ratones *Reeler* deficientes de Reelina (o Dab1 o ApoER2/VLDLR ratones (-/-)) y ratones *Reeler* heterocigotos, como un modelo de haploinsuficiencia de Reelina. Estudios en ratones *Reeler* (o Dab1 o ApoER2/VLDLR ratones (-/-)) se ven obstaculizadas por los defectos dramáticos de estos animales en la laminación y organización del cerebro (y anomalías de comportamiento), lo que plantea la cuestión de si los defectos en la función del ratón *Reeler* son secundarios a los defectos de migración.

Para desentrañar la función de la Reelina en el cerebro adulto ha sido de gran utilidad el modelo de ganancia de función: un ratón transgénico condicional que sobreexpresa Reelina, específicamente en el cerebro anterior postnatal y adulto, bajo el control del promotor de la calcio-calmodulina dependiente quinasa II (TgRln) (Pujadas et al, 2010; **Fig. 1.9**). La sobreexpresión de Reelina en adultos aumenta la neurogénesis del hipocampo y altera la migración y colocación de las neuronas generadas en el hipocampo adulto. Además, la sobreexpresión de Reelina en hipocampo provoca un aumento de los contactos sinápticos y la hipertrofia de las espinas dendríticas (**Fig. 1.10**). Asimismo, los ratones TgRln tienen potenciada la LTP (Pujadas et al, 2010). Por lo tanto, los niveles de Reelina en el cerebro adulto regulan la neurogénesis y la migración, así como las propiedades estructurales y funcionales de las sinapsis, lo que a su vez implica que Reelina controla procesos de desarrollo que se mantienen activos en el cerebro adulto.

Interacción de la vía de Reelina y la enfermedad de Alzheimer

La investigación en el campo de Reelina ha producido nuevas evidencias de una relación entre la vía de Reelina y AD. La primera proviene de enlace de ApoER2, uno de los principales transductores de la vía Reelina y al mismo tiempo, un receptor para la isoforma de ε4 ApoE, el principal factor de riesgo genético para la AD esporádica (Tsai et al., 1994). En segundo lugar, la señalización de Reelina suprime la actividad de GSK-3β, la principal quinasa de la proteína Tau (González-Billault et al., 2005; Beffert U et al., 2002) y ratones mutantes que tienen déficits en Reelina, en su transductor Dab1 o en ApoER2 y/o VLDLR presentan un incremento de los niveles de fosforilación de Tau (Hiesberger et al., 1999). En tercer lugar, tanto Dab1 como Reelina interactuan físicamente con APP y regulan su tráfico y procesamiento proteolítico, promoviendo así el corte no amiloidogénico de APP (Hoe et al, 2006;. Hoe et al, 2008;. Hoe et al, 2009). En cuarto lugar, Reelin antagoniza la disminución de la transmisión sináptica

glutamatérgica inducida por Aβ (**Fig. 1.11**) (Durakoglugil et al., 2009). Por último, el gen *RELN* tiene variantes polimórficas asociadas con función cognitiva normal en casos de AD (Kramer et al., Seripa et al., 2008). Todas estas observaciones indican un posible papel protector de la vía Reelin en la patogénesis de la AD. En cambio hay otros aspectos de la relación Reelin-AD que no son tan fácilmente explicables. En primer lugar, Reelina se acumula en agregados extracelulares en cepas salvajes de ratones y primates adultos y colocaliza con Aβ en placas extracelulares en modelos de ratones de AD (Doehner et al, 2010; Knuesel et al, 2009). Además la haploinsuficiencia de Reelina incrementa la patología de Tau y provoca una formación acelerada de placas amiloides en modelos transgénicos de AD (Kocherhans et al., 2010). En segundo lugar, los pacientes con AD muestran un aumento de alrededor del 40% en los niveles de Reelina en la corteza frontal y en el líquido cefalorraquídeo y una alteración del patrón de glicosilación (Botella-López et al., 2006). En cambio, una disminución de Reelina ha sido encontrada en corteza entorrinal de modelos murinos y en pacientes humanos de AD (Chin et al., 2007). En conjunto, estos hallazgos apuntan a una contribución de Reelina, sus receptores y proteínas de señalización a la etiología de AD. El análisis de los mecanismos moleculares con los que Reelina está implicada en AD y de su posible papel neuroprotector o neurodegenerativo son objeto de estudio del presente trabajo.

RESULTADOS

Purificación in vitro de Reelina

Purificación de Reelina de sobrenadantes celulares

Con el objetivo de analizar posibles interacciones *in vitro* entre Reelina y el péptido Aβ, primero necesitamos poner a punto las condiciones para la purificación de Reelina de sobrenadantes de la línea de células 293, transfectadas establemente con Reelina *full-lenght* (clon pCrl, Forster et al., 2002). Para evitar cualquier tipo de interferencia de otras proteínas en la preparación, que puedan afectar a la especificidad de los resultados observados, decidimos purificar los sobrenadantes enriquecidos en Reelina mediante dos procesos de cromatografía: cromatografía de intercambio iónico (ANX) seguida por una cromatografía de exclusión por peso molecular (SEC) en un sistema de cromatografía líquida rápida de proteínas (FPLC).

Los sobrenadantes enriquecidos en Reelina se pasaron así a través de una columna HiTrap ANX IEX cargada positivamente en una fase móvil de NaCl 30 mM/tampón fosfato 10 mM a pH 7.6. La elución se realizó mediante el aumento de la fuerza iónica de la fase móvil en cinco pasos. Esto nos permitió separar un pico de Reelina (**Fig. 4.1a**), corroborado por western blot/dot blot de las fracciones eluidas. A continuación, la muestra de Reelina conseguida por ANX se concentró y se pasó a través de una columna de SEC con el fin de separar por filtración en gel las impurezas todavía restantes, procedentes de la etapa anterior. La muestra fué procesada mediente elución isocrática en 10 mM de tampón fosfato/NaCl 30 mM (pH 7.4). Como podemos ver en el cromatograma, alrededor del 11 ml se eluye un pico que contiene Reelina (**Fig. 4.1b**, el pico de la curva continua roja entre las líneas discontinuas de color gris), corroborado por western blot de las fracciones recogidas. En paralelo a Reelina, como control negativo, sobrenadantes Mock fueron producidos a partir de células 293 transfectadas de forma estable con GFP (Forster et al., 2002) y se sometieron al mismo protocolo de purificación. El perfil de elución del Mock se indica mediante las curvas discontinuas rojas en la figura **4.1a** y **4.1b**. Es importante señalar en el cromatograma de ANX que en correspondencia con el pico Reelin, Mock presenta un pico de cierta intensidad en la fracción eluida (**Fig 4.1a**), lo que significa que la muestra de Reelina procedente de la primera etapa de purificación todavía contiene otras proteínas procedentes del medio de cultivo celular.

Análisis de la pureza de Reelina

Con el fin de probar el grado de pureza de Reelina obtenido, las muestras de Reelina y Mock se analizaron por tinción de Coomassie (o alternativamente de Sypro Ruby). Se observó una disminución en la proporción de bandas no específicas a lo largo del proceso de purificación,

con un incremento concomitante en la proporción de bandas de peso molecular correspondientes a Reelina (**Fig. 4.2**). El nivel de pureza obtenido se estimó ser el 86,3% sobre el total de proteínas contenidas en la preparación.

Para confirmar la presencia de Reelina en las muestras purificadas se eligió un enfoque proteómico bottom up, basado principalmente en una digestión con tripsina de extractos de bandas obtenidas de un gel SDS-PAGE de Reelina, seguida de la separación de los péptidos de digestión por cromatografía de líquidos (LC), acoplada a Espectrometría de Masas en tándem (MS/MS). Esta estrategia permite la secuenciación de los péptidos en un enfoque en el cual el espectro de masas de fragmentación de cada péptido se utiliza para identificar la proteína de la que derivan mediante la búsqueda contra una base de datos de secuencias de proteínas. De esta manera, los péptidos se pueden identificar de forma inequívoca y mapar en la secuencia de la proteína. Puesto que Reelina está altamente glicosilada en su extremo N-terminal, para evitar problemas de detección que reducirían la sensibilidad de la técnica, las muestras de Reelina y de Mock purificadas fueron sometidas primero a desglicosilación con la PNGasa F, una amidasa que escinde las N-glicososilaciones de las asparaginas produciendo un péptido que contiene en cambio un residuo de aspartato. Las muestras, con o sin desglicosilación, fueron teñidas con Sypro Ruby y las bandas de peso molecular correspondiente a Reelina (450, 350 y 180 kDa), fueron extraidas, digeridas con tripsina, separados por LC y analizadas por MS/MS (**Fig. 4.3a y b**).

En los espectros de masa de péptidos de muestras que efectivamente sufrieron desglicosilación se registró una diferencia de 1 Dalton entre la masa esperada (peso molecular teórico del péptido no glicosilado) y la masa obtenida experimentalmente, debido a la desamidación de un residuo de asparagina por acción de la amidasa. Los espectros de masas se analizaron con el programa Proteome Discoverer y el buscador SEQUEST, y se alinearon con la Base de Datos UniprotSwissport. Este análisis reveló correspondencia con la secuencia Reelina en 123 péptidos distintos con confianza mediana-alta (Percolator), lo que confirma la obtención de Reelina en el proceso de purificación (**Fig. 4.3c**).

A pesar de que se sabe que la proteína Reelina está altamente glicosilada (D'Arcangelo et al., 1997), sus sitios exactos de la glicosilación y el tipo de glicanos que participan, aún no se han descrito. Para determinar los residuos de Reelina que están implicados en la N-glicosilación se realizó un análisis *in silico* de la secuencia de Reelina con el Servidor NetNGlyc 1.0 (Blom et al., 2004). Este análisis indicó 25 posibles sitios de N-glicosilación para Reelina a lo largo de su secuencia, con diferentes grados de probabilidad, con puntuaciones de 0 a 1. Puntuaciones menores de 0,5 indican los sitios potenciales de N-glicosilación, mientras que las puntuaciones superiores a 0,5 indican sitios de N-glicosilación predichos (**Fig. 4.3d**).

Con el objetivo de averiguar algunos de los sitios de N-glicosilación predichos por nuestro análisis bioinformático, se analizó la desamidación de Asn en los espectros de masa de péptidos

de muestras desglicosiladas *versus* muestras no desglicosiladas. En particular, se espera que los péptidos no glicosilados se encuentren en un estado no desamidado, tanto antes como después de la reacción de desglicosilación. Los péptidos glicosilados en cambio se espera que no se detecten antes de la reacción de desglicosilación y que se encuentren en un estado desamidado después de la desglicosilación. Según este criterio encontramos específicamente en la muestra deglicosilada 3 péptidos que contienen asparagina desamidada, que no se detectaron en la muestra no deglicosilada (**Fig. 4.3e**). Esto indica un posible 100% de N-glicosilación de estos péptidos que les hizo indetectables en las muestras no desglicosilada. Los tres fragmentos glicosilados detectados se encuentran en el dominio N-terminal y se extienden respectivamente a partir de los aminoácidos 290-300, 303-321 y 1267-1282. Esta búsqueda estableció que tres residuos de Asn de la proteína Reelina indicados como sitios de N-glicosilación potenciales (Asn 291 y 1267) o predichos (Asn 306) (**Fig. 4.3d)** en nuestro análisis bioinformático, en realidad presentan esta modificación.

Análisis de la funcionalidad biológica de Reelina purificada

Para evaluar la funcionalidad biológica de Reelina purificada, cultivos primarios de neuronas de ratón E16 fueron mantenidos durante 3-5 días y tratados con muestras Reelina o Mock puridicados. El tratamiento con Reelina durante 15 minutos produjo un incremento de la fosforilación de su transductor Dab1, detectado por inmunoprecipitación de Dab1 seguida por detección por WB de la fosforilación en tirosinas . El tratamiento con sobrenatantes de Reelina produjo un incremento de 8,6 *veces* en los niveles de Dab1 fosforilada por comparación con células no tratadas, mientras que los niveles totales de Dab1 no cambian (**Fig. 4.4a**, carriles 4 y 3). El tratamiento con Mock no indujo la fosforilación de Dab1, siendo sus niveles comparables a los de la muestra sin tratar (**Fig. 4.4a**, carriles 3 y 2). El proceso de purificación de Reelina y su almacenamiento por congelación con nitrógeno o congelación con nitrógeno seguido de liofilización, no afectó a sus propiedades biológicas (**Fig. 4.4a**, carriles 4, 5, 6 y 7).

Análisis in vitro de la influencia de Reelina sobre las dinámicas de agregación amiloide y la toxicidad de los oligómeros de Aβ

Reelina retrasa la fomación de fibrillas β-amiloides

Para analizar si Reelina afecta a la cinética de la agregación de $A\beta_{42}$ en fibrillas amiloides, monoméros de $A\beta_{42}$ recién purificados (24 μM) se dejaron agregar en presencia o en ausencia de Reelina purificada o volúmenes equivalentes de Mock (**Capítulo 4.1.1**). La agregación se llevó a cabo en condiciones de baja salinidad (NaCl 5 mM). Se prepararon las siguientes mezclas: $A\beta_{42}$; $A\beta_{42}$: Reelina ($A\beta_{42}$/Rln) en relación 6:1 w/w y $A\beta_{42}$: Mock ($A\beta_{42}$/Mock) (volumen equivalente al de Reelina). Además, se prepararon muestras de Reelina (Rln) y Mock sin adición de $A\beta_{42}$. El proceso de agregación se llevó a cabo a 20 ºC y fué monitoreado cada 24 horas usando tioflavina T (ThT) y microscopía electrónica de transmisión (TEM). En ausencia de Reelina (muestras $A\beta_{42}$ y $A\beta_{42}$/Mock) se observó un aumento dependiente del tiempo en la fluorescencia de ThT a partir del día siete (**Fig. 4.5a**, curva gris y negra). La *Lag-phase* de la agregación, considerada como la fase de nucleación anterior al crecimiento de fibrillas, se calculó mediante el ajuste de una curva sigmoidal a los datos experimentales (8,3 días para $A\beta_{42}$ y 7,9 días para $A\beta_{42}$/Mock). $A\beta_{42}$/Rln muestra una desaceleración en la cinética del proceso de agregación, con aproximadamente 2,5 días de retardo en la aparición de fibrillas (**Fig. 4.5a**, curva roja) y con una duración de la *Lag-phase* de 10,9 días. Las imágenes de TEM confirmaron los datos de ThT (**Fig. 4.5b**). Por último demostramos que el retraso inducido por Reelina es específico y dosis-dependiente (**Fig. 4.6**).

Reelina alarga el tiempo de vida de los oligómeros de $A\beta_{42}$

Para obtener una visión de los mecanismos moleculares del retraso inducido por Reelina en la formación de fibrillas, se estudiaron las especies oligoméricas de $A\beta_{42}$ presentes durante las etapas iniciales del proceso de agregación amiloide. Con el objetivo de comprobar si Reelina afecta a la distribución de poblaciones oligoméricas específicas, se analizaron por PICUP, seguido por WB contra Aβ, la distribución de oligómeros de $A\beta_{42}$ de bajo peso molecular (LMW) (de dímeros a heptámeros). Antes de la aparición de fibrillas, no encontramos variaciones en la distribución de las especies oligoméricas LMW entre $A\beta_{42}$/Mock y muestras $A\beta_{42}$/Rln (día 6 en **Fig. 4.7a**, carriles 1 y 2). En cambio, durante el retardo de 2,5 días, los oligómeros LMW desaparecieron de la muestra $A\beta_{42}$/Mock mientras se mantuvieron en la muestra $A\beta_{42}$/Rln (día 9 en **Fig. 4.7a**, carriles 3 y 4). Los oligómeros LMW ya no eran visibles después de la formación de fibrillas tanto en muestras $A\beta_{42}$/Rln como $A\beta_{42}$/Mock y (**Fig. 4.7a**, carriles 5 y 6). Oligómeros solubles de alto peso molecular (HMW), que contienen especies de hasta 40-mer, se estudiaron mediante análisis de dot blot con anticuerpo A11, un anticuerpo

específico de conformación que se une a las formas oligoméricas de Aβ, pero no a los monómeros ni a las fibrillas. Nuestros resultados mostraron una señal específica de A11 prolongada 2 días durante la fase de retraso de la agregación en la muestra $A\beta_{42}$/Rln en comparación con la figura $A\beta_{42}$/Mock (**Fig. 4.7b**). En total, estos resultados indican que Reelina está retrasando *in vitro* la formación de fibrillas de $A\beta_{42}$, ampliando el tiempo de vida de las especies oligoméricas de LMW y HMW.

Reelina interactua con las formas solubles de $A\beta_{42}$, queda secuestrada en las fibrillas amiloides y pierde su funcionalidad biológica

Tras observar que Reelina modula la formación de fibrillas de $A\beta_{42}$, se examinaron las posibles interacciones entre las especies amiloides y Reelina. Para ello, se realizaron ensayos de inmunoprecipitación de muestras $A\beta_{42}$/Rln obtenidos en las etapas pre-fibrilares de la agregación (días 2-4), en las condiciones utilizadas para el experimento en la **Fig. 4.5**: 10 mM tampón fosfato/5 mM NaCl, $A\beta_{42}$ 24 mM, ratio $A\beta_{42}$:Reelin 6:1 w/w. Western blot de muestras inmunoprecipitadas anti-Aβ y anti-Reelina revelaron una interacción específica entre Reelina y las especies solubles de $A\beta_{42}$ (**Fig. 4.8a**).

A continuación se analizó la distribución de Reelina en muestras $A\beta_{42}$/Rln tomadas en la etapa de la agregación fibrilar, cuando se forman fibrillas insolubles $A\beta_{42}$. Western blot de alícuotas de $A\beta_{42}$/Rln tomadas durante la agregación revelaron que, de forma concomitante con el inicio de la formación de fibrillas, las bandas de Reelina desaparecen del peso molecular esperado y aparecen en el fondo del pocillo del gel (día 12, **Fig. 4.8b**). Esto podría ser explicado por un secuestro de Reelina en las fibrillas amiloides, difíciles de quebrar con el tratamiento con SDS. Como una prueba más de la interacción entre Reelina y fibrillas de $A\beta_{42}$, fibrillas de $A\beta_{42}$/Rln agregadas in vitro fueron sometidas a doble marcaje *Immunogold* para Reelina y $A\beta_{42}$, con partículas Nanogold de diámetro de 18 y 12 nm respectivamente. Micrografías electrónicas revelaron la co-localización de Reelina y $A\beta_{42}$ en las fibrillas agregadas *in vitro* (**Fig. 4.8c**). En conjunto, nuestros experimentos muestran una interacción directa entre Reelina y $A\beta_{42}$ en las etapas pre-fibrilares de agregación amiloide. Por otra parte, en la etapa de la agregación de amiloide fibrilar, nuestros datos apoyan la interacción de Reelin $A\beta_{42}$ y fibrillas, que se produce independientemente de interactores adicionales que pueden estar presentes en las placas seniles in vivo.

Para analizar si la presencia de Reelina en las fibrillas de $A\beta_{42}$ podría tener algún efecto sobre sus propiedades estructurales, se llevó a cabo la difracción de rayos X con fibras alineadas. Tanto las fibras de $A\beta_{42}$/Mock como las de $A\beta_{42}$/Rln mostraron las dos reflexiones perpendiculares características correspondientes a la estructura fibrilar beta cruzada (cross-beta) clásica (con láminas β dispuestas perpendiculares al eje de la fibrilla (Petkova et al., 2002) (**Fig. 4.8d**). Además de mantener la alineación, las distancias de reflexión también se conservan en

ambas muestras a 4,73 y 10,5 Å (correspondiente a las distancias de los enlaces por puente de hidrógeno y de las cadenas laterales en las láminas beta) (**Fig. 4.8d**). Por lo tanto Reelina no promueve alteraciones sistemáticas en el patrón fibrilar, sino más bien podría interactuar con Aβ a lo largo de la superficie de la fibrilla.

Paralelamente analizamos la funcionalidad biológica de Reelina a lo largo del proceso de agregación. En concreto, miramos en los niveles de fosforilación del transductor de Reelina Dab1 en cultivos primarios neuronales de embriones de ratón tratados con $A\beta_{42}$/Mock, $A\beta_{42}$/Rln o Reelina purificada antes de la aparición de las fibrillas (fase pre-fibrilar) o en el punto final de la agregación (fase fibrilar). Las muestras no tratadas con Reelina muestran bajos niveles basales de fosforilación de Dab1 (**Fig. 4.9**, carriles 1 y 4). $A\beta_{42}$/Rln es capaz de inducir la fosforilación de Dab1 en la fase prefibrillar, pero no en la fase fibrilar (**fig. 4.9**, carriles 2 y 5). Un control de Reelina sometido a las mismas condiciones experimentales, pero en ausencia de $A\beta_{42}$, conserva su actividad biológica durante todo el experimento, lo que indica que las condiciones experimentales no causan la pérdida de funcionalidad de Reelina (**fig. 4.9**, carriles 3 y 6), sino que ésta se debe específicamente a su secuestro en las fibrillas de $A\beta_{42}$.

Reelina rescata la citotoxicidad inducida por ADDLs

Los oligómeros solubles de $A\beta_{42}$ se consideran las verdaderas formas patógenas de Aβ en AD (Haass and Selkoe, 2007). Para probar cómo afecta Reelina a la citotoxicidad inducida por los oligómeros de Aβ, se trataron durante 24 horas cultivos neuronales primarios de hipocampo con oligómeros Aβ solubles en la forma de ADDLs (**Chapter 1.1.2**; Lambert et al., 2001, Lambert et al., 1998, PNAS), añadiendo sobrenadantes purificados de Reelina o de Mock. El daño celular se evaluó mediante tinción nuclear de yoduro de propidio (PI). La exposición de los cultivos a los ADDLs durante 24 horas provocó un aumento de la tinción nuclear de PI en comparación con el tratamiento con el vehículo (**Fig. 4.10c**). La supervivencia celular después del tratamiento con ADDLs 5 o 10 μM se reduce a 70,4 y 62,6%, respectivamente, en comparación con neuronas tratadas con vehículo (100% de supervivencia) (**Fig. 4.10c**). Reelina, pero no Mock, es capaz de rescatar la supervivencia neuronal hasta 94,4 y 81,5% para tratamiento con ADDLs 5 y 10 μM respectivamente (**Fig. 4.10b**).

Para corroborar la protección de Reelina contra la muerte neuronal inducida por ADDLs también se realizaron ensayos de MTT en las mismas condiciones. Tras el tratamiento de 24 horas con ADDLs 10 μM se encontró una supervivencia celular por debajo de 50%, en comparación con el vehículo (**Fig. 4.10d**). El tratamiento con Reelina rescató la toxicidad inducida por ADDLs, llevando la viavilidad al 68,7%, (**Fig. 4.10d**).

Análisis in vivo de los efectos de la sobreexpresión de Reelina en modelos murinos de la enfermedad de Alzheimer (AD)

Generación y caracterización de modelos murinos de AD que sobreexpresan Reelina

El modelo de ratón transgénico de sobreexpresión condicional de Reelina (TgRln) (**capítulo 1.2.1** y Pujadas et al., 2010) se cruzó con dos modelos diferentes de AD/Taupathology, con el fin de obtener una visión *in vivo* de la participación de Reelina en patología de Alzheimer. El primer modelo de ratón de AD utilizado sobreexpresa una forma mutada del gen APP humano con las mutaciones Swedish e Indiana (cepa J20 de The Jackson Laboratory) (**Capítulo 1.1.4** y Mucke et al., 2000). Los animales transgénicos triples de la cría de ratones TgRln con J20 (TgRln/J20) se identificaron por PCR. Una representación esquemática del modelo transgénico generado se da en la **Fig. 4.11**. La expresión transgénica de hAPP en ratones TgRln/J20 se encontró en neocórtex y en CA1, CA2, CA3 y las capas de células granulares del hipocampo (**Fig. 4.12**). La sobreexpresión de Reelina en ratones TgRln/J20 se detectó en estriado, corteza y hipocampo (principalmente en la capa CA1 y en las capas de células granulares del giro dentado); éstas distribuciones son idénticas a las esperadas y coinciden con la expresión en transgénicos simples J20 y TgRln (**Fig. 4.12**). Con el objetivo de analizar si la sobreexpresión de Reelina en ratones AD podría conducir a cambios en la actividad GSK-3β y en la fosforilación de Tau, decidimos cruzar el TgRln con un segundo modelo de ratón de AD: el modelo de sobreexpresión condicional de GSK-3β (Tet/GSK-3β) (**Capítulo 1.1.4** y Lucas et al, 2001), que recapitula aspectos de la neuropatología de la AD tales como hiperfosforilación de Tau, neurodegeneración giro dentado del hipocampo, astrocitosis reactiva y microgliosis, así como déficits de aprendizaje espacial. Triple animales transgénicos TgRln/GSK-3β se identificaron por PCR. Una representación esquemática del modelo transgénico generado se da en la **Fig. 4.13**. Siendo tanto Reelina cómo GSK-3β bajo el control del promotor CamKIIα, su expresión en ratones TgRln/GSK-3β se lleva a cabo en los mismos tejidos: estriado, corteza frontal y diferentes zonas del hipocampo incluyendo subículo, CA1, CA2 y las capas de células granulares del giro dentado (**Fig. 4.14**). Por la expresión del gen de la β-galactosidasa reportero, la GSK-3β transgénica se puede distinguir de la endógena ya sea por tinción con X-Gal o por inmunohistoquímica contra la β-galactosidasa.

La sobreexpresión de Reelina acentúa la atrofia del giro dentado en ratones TgRln/J20

El análisis de preparaciones histológicas de hipocampo de TgRln/J20 nos reveló un marcado fenotipo de atrofia del giro dentado a los 4 meses de edad. El análisis del volumétrico de la zona del giro dentado en tinciones de Nissl de secciones coronales de tejido adulto, expresada en porcentaje sobre el área total del hipocampo, indica que la sobreexpresión de Reelina por sí sola

es capaz de reducir ligeramente, pero significativamente el área de giro dentado en comparación con los animales control (reducción desde el 29% de los wt al 24,5% de los TgRln, **Fig. 4.15**). Los ratones J20 muestran una reducción significativa y más fuerte en la zona de giro dentado, alcanzando valores alrededor del 17% de la superficie total del hipocampo (**Fig. 4.15**). Finalmente los TgRln/J20 muestran la atrofia más severa, con el volume de giro dentado equivalente a un 8,6% de la superficie total del hipocampo (**Fig. 4.15**). El análisis de las capas del giro dentado afectadas por la atrofia reveló que los animales TgRln no están sufriendo de reducción de volumen en la capa de células granulares (GCL), sino que en la capa molecular (ML) (**Fig. 4.15**). Los Animales J20 muestran una fuerte reducción tanto en GCL como en MCL. Finalmente los TgRln/J20 muestran una reducción mayor en el volumen de ambos GCL y MCL (**Fig. 4.15**).

Para evaluar si la pérdida de volumen del GCL observada en J20 y TgRln/J20 podría ser debida a una disminución en la neurogénesis de las células madre proliferantes en el GCL, realizamos IHC con doblecortina (DCX), un marcador de neuronas recién nacidas que marca las células generadas en el giro dentado adulto durante un período aproximado de 12 días (**Fig 4.16**) (Rao and Shetty, 2004). Los datos muestran que J20 y TgRln/J20 tienen una tendencia, más pronunciada en TgRln/J20, a una reducción de la neurogénesis en comparación con los wt y TgRln. Estos resultados indican que la toxicidad de Aβ es responsable de en los J20 de una reducción en el volumen del giro dentado, que se caracteriza tanto por la pérdida de volumen de GCL, posiblemente a través de deterioro de la neurogénesis, como por la pérdida de volumen del ML. La sobreexpresión de Reelina en el GCL de los TgRln/J20 acentúa este fenotipo, principalmente a través de una mayor pérdida en el volumen de ML.

La sobreexpresión de Reelina disminuye la deposición de placas amiloides en corteza y hipocampo de ratones AD J20

En el modelo TgRln/J20 comprobamos la presencia de Reelina en las placas amiloides (**Fig. 4.17**). Para analizar si los cambios observados en la agregación de $A\beta_{42}$ *in vitro* en presencia de Reelina se correlacionan *in vivo* con variaciones en la carga de placas amiloides en TgRln/J20, se cuantificó el área ocupada por las placas en diferentes zonas del cerebro y en comparación con la de los animales J20. En hipocampo se analizaron los niveles de placas a los 4, 8 y 12 meses de edad. A los 4 meses la deposición de placas es muy baja en ambos genotipos (alrededor de un 0,04% de la superficie total). A los 8 meses, la carga de placas en los TgRln/J20 se incrementa ligeramente en comparación con los J20 con valores de 1,2% y 0,5%, respectivamente (**Fig. 4.18a**). En animales de 12 meses, el porcentaje de área ocupada por las placas es significativamente menor en TgRln/J20 que en J20 con los valores de 9% y 13%, respectivamente (**Fig. 4.18a**). Las áreas corticales, se comportan de manera similar como el hipocampo: en la corteza retrosplenial a la edad de 12 meses, se observó una tendencia menor

de deposición de placas en TgRln/J20 comparados con J20 (**Fig. 4.18c**, paneles superiores). En la corteza entorrinal se observaron las mismas tendencias, alcanzando significación (**Fig. 4.18c**, paneles inferiores).

Reelina previene la pérdida de espinas dendríticas y el deterioro cognitivo en el modelo murino de AD J20

Modelos murino y pacientes humanos afectados por AD muestran una disminución de los contactos sinápticos (Spires-Jones et al., 2007; DeKosky and Scheff, 1990). Ya que Reelina es capaz de reducir *in vitro* algunos de los efectos tóxicos de las especies amiloides, se evaluó si la sobreexpresión de Reelina podría correlacionar *in vivo* con una reducida toxicitad sináptica. Para ello, animales J20 y TgRln/J20, además de controles wt y TgRln, se procesaron para la tinción de Golgi y se contaron espinas dendríticas de neuronas piramidales en de stratum radiatum (SR) y lacunosum moleculare (SLM) de hipocampo (**Fig. 4.19**). En ambas áreas, los J20 muestran un reducido número de espinas dendríticas en comparación con los animales WT y TgRln. En TgRln/J20 animales la sobreexpresión de Reelina rescató significativamente la densidad de espinas dendríticas (ANOVA P <0,05, F = XX).

Como se ha demostrado que la reducción del número de contactos sinápticos en ratones AD se correlaciona con déficits cognitivos (Terry et al., 1991), quisimos analizar si el rescate de la densidad de espinas dendriticas produido por sobreexpresión de Reelina fuese capaz de prevenir también alteraciones del comportamiento. Para ello, ratones de los diferentes genotipos (control; TgRln, J20, y TgRln/J20) fueron sometidos a prueba de *Novel Ojbect Recognition* (NOR) a los 4-5 y 8-10 meses de edad. Los animales wt y TgRln fueron capaces de pasar la tarea hasta los 8-10 meses (índice de discriminación (DI) > 0,3) (**Fig. 4.20**, panel superior). Los J20 fallaron en la tarea en todas las edades analizadas, mostrando una menor preferencia por el objeto nuevo (DI <0.2), como ya se ha documentado (Harris et al., 2010) (**Fig. 4.20**, panel superior y el panel inferior, izquierda). Los TgRln/J20 actuaron como los controles tanto a los 4-5 meses como a los 8-10 meses (**Fig. 4.20**, panel superior), con diferencias significativas con los J20. Estos datos indican que Reelina provoca una reversión significativa de los déficits de memoria de reconocimiento no espacial observados en J20 hasta 8-10 meses. En animales de mayor edad de 11 a 12 meses el grupo de control no difirió de los J20, lo que demuestra una disminución dependiente de la edad en la memoria de reconocimiento no espacial (**Fig. 4.20**, panel inferior izquierda). Sin embargo, en la misma edad, los TgRln mantuvieron parcialmente la capacidad de reconocimiento (DI entre 0,2 y 0,3) significativamente mayor que la del grupo control. También los TgRln/J20 conservaron el mismo nivel de capacidad de reconocimiento que los TgRln a esa edad, a pesar la producción anormal de Aβ (**Fig. 4.20**, panel inferior izquierda). Los grupos fueron reevaluados después de un mes de tratamiento con doxiciclina para detener la sobreexpresión de Reelina. El DI de ambos grupos disminuye hasta llegar a cero, lo que indica

una pérdida completa de la protección dependiente de Reelina de larga duración en un mes de depleción (**Fig. 4.20**, panel inferior, derecha). En conjunto, nuestros datos indican que la sobreexpresión de Reelina recupera el deterioro cognitivo causado por la producción de Aβ en J20, probablemente a través de la interacción de Reelina con formas solubles de Aβ y del rescate de la densidad de las espinas dendríticas. Además la sobreexpresión de Reelina también disminuye el deterioro cognitivo dependiente de la edad fisiológica de los animales de control. El efecto beneficioso de la sobreexpresión de Reelina se pierde en un mes depleción de Reelina, demostrando que dependía específicamente su sobreexpresión.

Por último, quisimos poner a prueba el potencial de Reelina como factor terapéutico en caso de AD manifiestada. Para ello, J20 y TgRln/J20, además de controles wt y TgRln, fueron sometidos a dieta de doxociclina desde el nacimiento hasta la edad de 4 meses, evitando así la sobreexpresión de Reelina transgénica hasta poder apreciar la aparición de la enfermedad (fenotipo a nivel de comportamiento comprobado por NOR). A continuación, la dieta normal sustituyó le de doxociclina, y los ratones fueron re-evaluados por NOR después de 1 y 4 meses de sobreexpresión de Reelina. No vimos ningún rescate en la prueba de NOR en las dos edades testadas (5 meses y 8 meses, **Fig. 4.21**, medio y derecha). Esto significa que, mientras que la sobreexpresión de Reelina continuada desde el nacimiento es capaz de prevenir la aparición de déficits cognitivos en AD, su sobreexpresión condicional en sujetos adultos no es capaz de superar estas deficiencias una vez que la patología se haya desarrollado.

Reelina reduce la fosforilación de Tau en ratones sobreexpresantes de GSK-3β

Para investigar el efecto de la sobreexpresión de Reelina en la actividad de GSK-3β y la fosforilación de Tau, se analizaron por Western blot extractos de hipocampo de ratones TgRln/GSK-3β, así cómo de controles, TgRln y Tet/GSK-3β a diferentes edades. A la edad de cinco meses la sobreexpresión de GSK-3β causó un aumento en los niveles de fosforilación de Tau, detectados con los anticuerpos PHF-1, AT8 y AT180 (**Fig. 4.22**). Estas fosforilaciones se han descrito como relacionadas con la formación de agregados de Tau en estado de ovillo neurofibrilar (Lucas et al., 2001, Bertrand et al., 2010). La sobreexpresión de Reelina en TgRln/GSK-3β reduce la fosforilación de Tau, restaurando los niveles de fosforilación detectados en los animales control (**Fig. 4.22**). La reducción en la fosforilación de Tau GSK-3β-dependiente producida por Reelina no es debida a niveles alterados de la proteína Tau total, ya que los niveles de Tau total detectados con el anticuerpo independiente de la fosforilación Tau5 no varían.

La fosforilación de Tau en los epítopos reconocidos por los anticuerpos PHF-1, AT8 y AT180 se cree que comenze en el axón y conlleve al desprendimiento de Tau de microtúbulos y a su redistribución al compartimiento somato-dendrítico (Bertrand et al., 2010). Para analizar la distribución en hipocampo y la localización intracelular de Tau fosforilada, se realizó

inmunohistoquímica con PHF-1 en rebanadas de hipocampo de ratones TgRln/GSK-3β más sus correspondientes wt, TgRln y Tet/GSK-3β, a la misma edad de los western blots (5 meses). Todos los genotipos muestran tinción apreciable de interneuronas del hipocampo en todas las capas, aunque la sobreexpresión de Reelina, tanto en TgRln como en TgRln/GSK-3β, parece reducir el número de células teñidas (**Fig. 4.23a**, puntas de flecha). Asímismo la tinción de PHF-1 reveló que los animales wt y TgRln muestran una señal axónica predominante en las fibras musgosas, tanto en el segmento proximal (Hilus) como en el distal que proyecta a CA3 (**Fig. 4.23a**, fragmento distal indicado por flechas). También se detectó inmunorreactividad somato-dendrítica en algunas células granulares del giro dentado y esporádicamente en las células musgosas hiliares (**Fig. 4.23b**). Los animales Tet/GSK-3β, como ya se ha descrito, muestran un cambio hacia una mayor inmunoreactividad somato-dendríticas en las células granulares (**Fig. 4.23b**, flecha), indicando el desprendimiento de Tau de microtúbulos y su localización en el compartimento somato-dendrítico, donde se asemblan en estructuras pretangle-like (Lucas et al., 2001). Además detectamos tinción somato-dendrítica de las células musgosas (**Fig. 4.23b**, puntas de flecha) mientras se encontró que la marca axónica en el fragmento distal de las fibras musgosas en CA3 desapareció casi del todo (Fig. **4.23a**). Animales TgRln/GSK-3β, de manera similar a los animales wt y TgRln, vuelven a una señal axónica predominante en las fibras musgosas, tanto en el segmento proximal y en el distal, lo que indica que la disminución en la fosforilación de Tau inducida por la sobreexpresión de Reelina posiblemente impide el desprendimiento de Tau de microtúbulos y su localización somato-dentrítica.

DISCUSIÓN

Papel neuroprotector de Reelina en la AD: interpretación de los resultados in vitro

Nuestro abordaje *in vitro* (**Secciones 3.1 y 3.2**) contribuyó a esclarecer la relación molecular entre Reelina y $A\beta_{42}$ en el proceso de agregación amiloide. En primer lugar, se detectó una influencia directa de la proteína Reelina en la cinética de la agregación de $A\beta_{42}$. En nuestro sistema experimental Reelina retrasó la agregación amiloide de manera específica y dosis dependiente. En segundo lugar, se encontró que el retraso en la agregación fue acompañado por una prolongada duración de la vida de ambos LMW y HMW oligómeros de $A\beta_{42}$. En tercer lugar, Reelina interactúa con especies solubles de $A\beta_{42}$ en la etapa pre-fibrilar de la agregación amiloide. A medida que el proceso de agregación de $A\beta_{42}$ continúa, la Reelina desaparece progresivamente de la fracción soluble , según resultados de Western blot , y queda atrapada en las fibrillas amiloides que forman finalmente, como se visualiza mediante microscopía electrónica. Al mismo tiempo, la Reelina pierde su funcionalidad biológica, siendo incapaz de inducir la fosforilación su transductor Dab1 después del secuestro en las fibrillas $A\beta_{42}$. En cuarto lugar, aunque se encontró que la Reelina forma parte de fibrillas amiloides, ni la estructura fibrilar β-cruzada clásica ni las distancias entre las cadenas laterales se alteran. Este hallazgo implica que Reelina posiblemente interactúa con estructuras en la superficie de las fibrillas de $A\beta_{42}$ de una manera no regular. Por último, tratamiento a corto plazo de los cultivos neuronales con oligómeros tóxicos de $A\beta_{42}$ (ADDLs) en presencia de Reelina demostraron que la Reelina es protectora, reduciendo la citotoxicidad en dos ensayos de supervivencia: tinción PI y MTT.

El conjunto de datos que hemos recogido con nuestro enfoque *in vitro* proporciona una visión nueva e interesante en el campo de Reelina y AD. La perspectiva emergente para Reelina en este contexto es la de un factor neuroprotector que ralentiza la agregación amiloide, y que, a pesar de la prolongación de la duración de la vida de las especies oligoméricas tóxicas, les impide de ejercer su toxicidad, por lo menos en el nivel celular. Experimentos en curso evaluarán el efecto de la Reelina en la toxicitad sinaptica mediada por los oligómeros de $A\beta_{42}$, mirando a la densidad de las espinas dendríticas en cultivos primarios de hipocampo de baja densidad tratados con $A\beta_{42}$ en presencia o en ausencia de Reelina.

La elucidación de los mecanismos moleculares que subyacen a la neuroprotección mediada por Reelina requerirá investigación adicional, aunque se pueden hacer algunas especulaciones sobre la base de estos hallazgos. La interacción de Reelina con los oligómeros $A\beta_{42}$, aunque no afectara a su tamaño o a su distribución, tal cómo se muestra por PICUP en oligómeros de LMW, todavía podría inducir alguna modificación conformacional de las especies oligoméricas

que a su vez puede afectar a sus propiedades biológicas. Por ejemplo, un cambio conformacional inducido por Reelina en los oligómeros $A\beta_{42}$ puede afectar a la interacción de estos últimos con sus receptores de membrana a nivel sináptico, posiblemente mecanismo que explicaría el importante fenómeno de reducción de toxicidad que se observó. Alternativamente, la mera interacción de los oligómeros con Reelina podría detener los oligómeros de la interacción con las sinapsis, por lo tanto tener oligómeros extracelulares para períodos más largos, pero sin ser tóxicos. Además, es posible que la Reelina, aunque no cambie la estructura fibrilar amiloide, en realidad la estabilize, lo que dificultaría el reciclaje de oligómeros. Por último, es concebible que Reelina, al interactuar con las fibrillas amiloides, interactúe simultáneamente con oligómeros de $A\beta_{42}$ que se forman en un proceso de "nucleación secundaria" (descrito en Cohen et al., 2013) en la superficie de las fibrillas amiloides preformadas. La presencia de Reelina en la superficie de las fibrillas amiloides afectaría entonces a las reacciones de nucleación de especies oligoméricas, reduciendo de este modo su toxicidad (**Fig. 5.4**).

Papel neuroprotector de Reelina en AD: interpretación de los resultados in vivo

Nuestro abordaje *in vivo* (**Sección 4.3**) reveló el impacto de la sobreexpresión continuada de Reelina en dos modelos de AD, uno caracterizado por la sobreexpresión de una forma mutada de APP humana (J20) y el otro por la patología Tau causada por la sobreexpresión de la quinasa GSK-3β (Tet/GSK-3β).

El aumento en la expresión de Reelina en el cerebro adulto de ratones J20 proporcionó pruebas *in vivo* de la influencia de Reelina en la acumulación de fibrillas amiloides. En los TgRln/J20, la acumulación de depósitos amiloides no se bloqueó ni se atrasó, sin embargo, en animales viejos se observó una acumulación significativamente reducida de placas amiloides en comparación con los ratones J20. Esta observación es consistente con la evidencia *in vitro* de que Reelina retrasa la formación de depósitos amiloides. Los datos *in vivo* también indican un papel clave para la Reelina en la neuroprotección a nivel sináptico. En consonancia con la mejora inducida por Reelina de las propiedades sinapticas estructurales y funcionales (Pujadas et al., 2010), en TgRln/J20 los niveles de espinas dendríticas fueron idénticos a los de los animales wt, en contraste con los J20, que muestran pérdida de sinapsis como consecuencia de la enfermedad (Spires et al., 2005; Spires-Jones and Knafo, 2012). Así Reelina contrarresta *in vivo* la toxicidad sináptica inducida por Aβ. Consecuentemente, los animales TgRln/J20 mostraron una recuperación de habilidades cognitivas, como se ve por *NOR*, dónde Reelina previene las alteraciones de memoria de los ratones J20 durante toda la vida: antes de la formación de placas (hasta 4-6 meses) y durante la deposición de amiloide (8-12 meses). Esta recuperación se perdió

tras un mes de impedir la sobreexpresión de Reelin. Esta observación implica que la recuperación es dependiente de la generación continua de nueva Reelina e indica que Reelina actúa como un protector "en tiempo real". En conjunto, nuestros datos indican que la Reelina induce una recuperación sináptica *in vivo* subyacente a la recuperación funcional de las habilidades cognitivas en un modelo de AD.

Con el cambio de enfoque sobre la toxicidad de las especies amiloides centrado en los oligómeros, con la formulación de la "hipótesis de los oligómeros Aβ" (**Capítulo 1.1.2**), se podían llegar a considerar las fibrillas amiloides como agregados inertes con ninguna toxicidad *per se* (Haass and Selkoe, 2007)(Haass and Selkoe, 2007). Sin embargo, este punto de vista no es coherente con la observación del daño sináptico a cargo de las espinas dendríticas que se manifiesta en la proximidad de las placas, y de forma dependiente de la distancia entre espinas y placas (Spires-Jones et al., 2007), lo que implica que las placas amiloides siguen ejerciendo toxicidad sináptica. Además, las estructuras amiloides sufren mecanismos de continua disociación y reasociación de Aβ por los que existe un reciclaje de Aβ dentro de la población de fibrillas y los péptidos pueden ser liberados y generar nuevas especies tóxicas (Carulla et al., 2005). Una posible reconciliación de estos hallazgos viene de la descripción de la nucleación secundaria (mencionada arriba y descrita en (Cohen et al., 2013) (**Fig. 5.4**), un proceso en el que tanto el péptido monomérico y las fibrillas están involucrados en la formación de oligómeros tóxicos. Esta hipótesis resTaura la posibilidad de que una reducción en la concentración de fibrillas amiloides sería de protección contra la patología de la AD y, en nuestro caso, explicaría por qué la reducción de la carga de placas amiloides inducida por Reelina *in vivo* se superpone con una disminución de la toxicidad a nivel sináptico.

Por otra parte, la sobreexpresión de Reelina en un modelo de sobreexpresión de GSK-3β (TgRln/GSK-3β) nos permitió evaluar la influencia de la vía de señalización de Reelina en el contexto de la patología de Tau. La sobreexpresión de Reelina en ratones TgRln/GSK-3β reduce significativamente la cantidad de Tau fosforilada en el hipocampo, restaurando de los niveles de fosforilación de animales wt, sin cambiar las tasas totales de producción Tau (**Fig. 4.22**).

Por otra parte, mientras que los ratones Tet/GSK-3β muestran localización somato-dendrítica de fosfo-Tau (Lucas et al., 2001), asociada con estructuras tipo tangle, la sobreexpresión de Reelina revierte este fenotipo, restaurando la localización mayoritariamente axónica de fosfo-Tau (**Fig. 4.23**). En paralelo hemos probado las funciones cognitivas TgRln/GSK-3β en el NOR y en el Morris water maze, dos tareas de memoria en las que están alterados los ratones Tet/GSK-3β (Engel et al., 2006ª; Hernández F. et al., 2002). Los resultados preliminares apuntan en ambas tareas a una reversión mediada por Reelina de los déficits de memoria de reconocimiento asociados con Tau hiperfosforilada en Tet/GSK-3β. Sin embargo será necesario aumentar la población por genotipo para evaluar la importancia estadistica y finalmente evaluar

que los fenotipos mediados por la sobreexpresión de Reelina en Tet/GSK-3β realidad conduczcan a un rescate cognitivo. También queda por abordar si la sobreexpresión de Reelina reverte otros aspectos de la patología de AD en ratones Tet/GSK-3β, como los procesos de microgliosis, astrocitosis y neurodegeración del giro dentado del hipocampo.

En conjunto, las observaciones realizadas en ratones TgRln/GSK-3β fortalecen los resultados encontrados en el modelo J20 de FAD y confirman a Reelina cómo factor clave de protección en el contexto de la patología de la AD. En efecto, puesto que la GSK-3β se ha descrito ser un mediador importante que une Aβ a la fosforilación de Tau (Takashima et al., 1993; Busciglio et al., 1995; Takashima et al., 1996), la Reelina, antagonizando la actividad de GSK-3β, se posicionaría en el cruce de las dos vías principales relacionadas con AD, reduciendo la toxicidad de las dos.

Reelina cómo posible diana terapéutica para el AD

Consideramos la retención de las capacidades cognitivas de los ratones J20 inducida por Reelina de gran interés para un posible papel de la vía de Reelina cómo diana terapéutica para AD. En efecto, Reelina ha demostrado no sólo retrasar el progreso de AD, sinó también ser necesaria para prevenir la aparición de los trastornos cognitivos de la enfermedad, y sólo cuando la sobreexpresión de Reelina se suprime en los TgRln/J20 se detecta la pérdida de la habilidad cognitiva. Nuestros resultados están en línea con la hipótesis (sugerida en Herring et al., 2012) de que la depleción de la señalización de Reelina es uno de los primeros eventos en la aparición de AD, y están de acuerdo con la observación de que la haploinsuficiencia de Reelina en ratones transgénicos AD resulta en una aceleración de la patología de AD (Kocherhans et al., 2010; Knuesel et al., 2010).

La estrategia seguida para poner a prueba el potencial terapéutico de Reelina ha sido permitiendo el desarrollo de la patología Alzheimer en ratones TgRln/J20 suprimiendo la sobreexpresión de Reelina por administración de doxiciclina durante los primeros 4 meses de vida de los animales. Una vez se apreció por NOR las consecuencias del desarrollo de la enfermedad, la administración de doxiciclina se detuvo y los ratones fueron re-evaluados para los *NOR* después de 1 y 4 meses de sobreexpresión continuada de Reelina con el fin de abordar posibles mejoras dependientes de Reelina en las habilidades cognitivas. La sobreexpresión inducida de Reelina en ratones adultos no recuperó los déficits manifestados en la prueba de *NOR* una vez que AD estaba desarrollada. Este hallazgo indica que, a pesar de que la sobreexpresión continuada de Reelina previene la aparición de déficits cognitivos en ratones J20, la inducción condicional de la sobreexpresión de Reelina en casos de AD ya manifestados no es suficiente para revertir los deterioros cognitivos. Sin embargo, no podemos descartar todavía la reversión de otras características de la enfermedad cómo la toxicidad a nivel sináptico. Además, ya que la depleción de Reelina parece ser un fenómeno muy temprano en

AD, otra posibilidad terapéuticamente relevante podría ser la administración de esta proteína inmediatamente antes de la aparición de AD, en un intento para complementar el agotamiento muy temprano de la vía de señalización de Reelina. Este enfoque requeriría un análisis muy cuidadoso para establecer en primer lugar si en J20, cómo ocurre en otros modelos, y especialmente en pacientes, la depleción de Reelina es un fenómeno precoz de AD (Chin et al., 2007). En segundo lugar habría que determinar el periodo temporal preciso y las áreas del cerebro en la que esta depleción ocurre. Con esta información, se puede diseñar un enfoque más complejo y preciso para testar el potencial terapéutico de Reelina. Por último, en un esfuerzo por extrapolar estas observaciones al desarrollo de AD en los pacientes humanos, la cuestión que surge como más relevante es la necesidad de mejorar la detección precoz de AD, indispensable para el éxito de muchos enfoques terapéuticos.

Atrofia y neurogenesis de giro dentado en ratones AD y participación de Reelina

La atrofia del hipocampo es una de las primeras manifestaciones de AD observada en biopsias (Braak y Braak, 1997; Kerchner et al., 2012), y en muchos casos incluso precede al estado de deterioro cognitivo leve (MCI) (Smith et CD al., 2012). En particular se ha descrito atrofia de CA1 con pedida de células piramidales y el adelgazamiento de los estratos de CA-stratum radiatum y stratum lacunosum moleculare (CA1-SRLM) se ha correlacionado con la pérdida de memoria episódica y con los primeros síntomas cognitivos en pacientes con AD (Kerchner et al, 2012). Por el contrario, el tamaño del DG y de la CA3 no parece correlacionarse con ningún aspecto del rendimiento de la memoria (Kerchner et al., 2012). A diferencia de los humanos, modelos de ratones transgénicos con hAPP no se caracterizan por una pérdida neuronal masiva, aunque muestran signos de neurodegeneración, como neurítas distroficas y la pérdida de sinapsis. Una posible explicación de esta observación es que la duración típica de la vida del ratón es demasiado corta para que la toxicidad de Aβ llegue a matar neuronas, o que el fenotipo neurodegenerativo es atribuible más bién a otros aspectos de la patología, como la toxicidad de Tau o la neuroinflamación. Sin embargo, la falta de fenotipo de muerte celular es de hecho una deventaja añadida de los modelos hAPP de AD.

Nuestros datos indican por primera vez una marcada atrofia del giro dentado de ratones J20 a la edad de 4 meses, antes de la aparición de placas. Tanto la capa molecular (ML) como la capa de células granulares (GCL) se ven afectadas por el adelgazamiento a través de un mecanismo que todavía no está claro (**Fig. 4.15**). Tal reducción de volumen del giro dentado puede apuntar a neurodegeneración especialmente considerando que el adelgazamiento de la capa de GCL puede indicar disminución del número de neuronas granulares.

En un primer intento de conocer las razones del fenotipo de atrofia del giro dentado observado, se analizó si fuera causado por un aumento de la frecuencia de la muerte neuronal. Para este fin, se realizó inmunohistoquímica contra caspasa-3-activada para visualizar neuronas apoptóticas. No encontramos incrememento de las tasas de la apoptosis mediante este enfoque, aunque no podemos descartar que otros tipos de muerte neuronal, como la necrosis, estén teniendo lugar. Otra posible causa de la disminución de la GCL podría ser una tasa reducida de neurogénesis.

En varios modelos transgénicos de AD, la neurogénesis adulta se ve comprometida, tanto disminuida como aumentada, y también se han descrito alteraciones en pacientes con AD (Lazarov y Marr, 2010 ; Marlatt y Lucassen , 2010 ; Winner et al, 2011 ; Perry et al, 2012). En nuestro caso, el análisis del número de células marcadas con DCX nos reveló una disminución de los niveles de neurogénesis en animales J20 en comparación con los animales wt y TgRln (**Fig. 4.16**). En ratones J9, otro modelo de sobreexpresión de hAPP bajo el mismo promotor de J20 (promotor PDGF-β), fue encontrado un aumento de la taxa de neurogénesis en el hipocampo y en la zona subventricular, tanto a los 3 y a los 12 meses, tal como se muestra mediante tinción con BrdU (Jin et al., 2004a). También en ratones J20 se detectó un aumento de la neurogénesis en el hipocampo, evaluado también por tinción con BrdU, a la edad de 3 meses (Lopez-Toledano and Shelanski, 2007). Sin embargo, este aumento revirtió con la edad de los animales, ya que no era más detectado en las edades de 5, 9 y 11 meses. Además se encontró que el aumento en la neurogénesis se correlaciona con niveles detectables de Aβ oligomérica, medidos por ELISA y western blot. Un aumento de la tasa de neurogénesis adulta puede ser considerado como un mecanismo de compensación en procesos neurodegenerativos, por lo tanto, tiene sentido mecanístico encontrar este proceso aumentado en modelos de AD, sobre todo, como posible respuesta a la toxicidad de oligómeros de Aβ o de Tau. Por otro lado, la estimulación sostenida de la neurogénesis, para compensar la toxicidad continua de especies tóxicas de Aβ, incluso podría dar lugar a un agotamiento de los nichos de células madre, con el siguiente deterioro en la sustitución de las células en división en etapas posteriores de la vida. Considerando esta posibilidad, una explicación para nuestro hallazgo de neurogenesis reducida en J20 sería que éste hipotético incremento de la neurogénesis ocurra en las primeras etapas de AD, previo a los 4 meses, seguido de un agotamiento de los nichos de células madre que a su vez conlleve un adelgazamiento de la GCL en etapas posteriores. Esta hipótesis explicaría el aumento que se describe en la neurogénesis de ratones J20 en una etapa temprana de la edad adulta (3 meses), seguido por una reversión a las edades de 5, 9 y 11 meses. Por otra parte la incongruencia con el aumento de la neurogénesis en ratones hAPP J9 hasta la edad de 12 meses podría explicarse teniendo en cuenta las diferencias intrínsecas entre los dos modelos. En efecto, los ratones J9 y J20 expresan diferentes niveles del transgén $hAPP_{swe/Ind}$ y diferentes niveles de péptido Aβ (**Capítulo 1.1.4**). Esto podría traducirse en una menor sobreestímulación de la

neurogénesis en los J9, en comparación con los J20, y por lo tanto, podría hacer que los J9 mantengan el aumento de neurogenesis durante tiempos más largos.

En total, estas observaciones podrían reconciliar los datos de aumento de la neurogénesis en J9 y J20 en a la edad de 3 meses con nuestro hallazgo de la reducción de la neurogénesis en J20 a los 4 meses. En realidad, este podría ser el resultado de un posible agotamiento de los nichos de células madre después de una sostenida sobreestimulación de neurogénesis en etapas anteriores de la vida adulta. El análisis de la tasa de neurogénesis en puntos adicionales de tiempo (por ejemplo, 1, 2, 3 y 5 meses), y la correlación con los niveles de péptido Aβ en circulación, debe llevarse a cabo para verificar la hipótesis planteada.

Por otra parte, hemos encontrado alteraciones morfológicas en las células DCX-positivas. Éste hallazgo plantea la cuestión de si las células recién generadas pueden integrarse correctamente en el GCL. Si esto ocurriera, la generación de neuronas no funcionales podría estimular nuevas oleadas de neurogénesis, contribuyendo a la hipótesis del agotamiento de nichos de células madre. En los ratones J20, la distribución de las células que proliferan a lo largo de la zona subgranular (SGZ) no es homogénea y parece corresponderse con el adelgazamiento de la GCL en las zonas con menores tasas de proliferación, apoyando así la hipótesis de que GCL adelgazamiento es atribuible a una disminución en la proporción de sustitución neuronal. En segundo lugar, se observó un posicionamiento erróneo de las células DCX-positivas, con cuerpos a diferentes profundidades de la GCL, a veces incluso localizados en el hilus. En tercer lugar, se observaron árboles dendríticos menos desarrollados y en algunos casos extendiéndose erróneamente hacia el hilus en lugar de orientarse hacia la ML. Por último, también se observaron neuritas con morfología aprenteemente distrófica (**Fig. 4.16**).

También se detectó una participación de Reelin tanto en la atrofia del giro dentado como en las alteraciones de la neurogénesis adulta. Nuestros datos indican que la sobreexpresión de Reelina es responsable de un adelgazamiento significativo de ML en ratones TgRln a la edad de 4 meses, mientras que el GCL no se ve afectada, lo que significa que mientras que el número de células no se reduce, sus árboles dendríticos ocupan menos espacio (**Fig. 4.15**). El análisis de las tasas de neurogénesis reveló un aumento del número de células recién generadas con árboles dendríticos aparentemente más desarrollados en TgRln (Pujadas et al., 2010). Por otra parte, la sobreexpresión de Reelina es también responsable de alteraciones en la migración, con un aumento del número de células DCX-positivas posicionadas erróneamente en dentro de la capa de GCL (Pujadas et al., 2010). Este hallazgo se debe posiblemente a la expresión ectópica de Reelina en las neuronas piramidales de la GCL.

Por último, los efectos combinados de la sobreexpresión de Reelina y hAPP causan una reducción más pronunciada tanto de ML como de GCL (**Fig. 4.15**), de nuevo sin cambios aparentes en la tasa de apoptosis. Además, el análisis de las tasas de neurogénesis reveló, como

en J20, una disminución del número de células recién generadas (**Fig. 4.15**). La observación morfológica muestra una combinación de los fenotipos de J20 y de TgRln. Podemos especular que el adelgazamiento de la GCL observado en animales TgRln/J20 deriva, como se sospecha para el caso de J20, a partir de un agotamiento de los nichos de células madre (objeto de divesos experimentos en curso). En el caso de TgRln/J20 éste fenotipo se vería agravado por el hecho de que la sobreexpresión de Reelina por sí sola es capaz de inducir un aumento significativo en la neurogénesis en el hipocampo (Pujadas et al., 2010). Así, en el contexto patológico inducido por altos niveles circulantes de péptido Aβ, sumado con la imposibilidad de integración de las nuevas neuronas debido al fenotipo J20, los TgRln/J20 se verían facilitados en comparación con los J20 para establecer una estimulación sostenida de la neurogénesis, con un agotamiento más temprano y acelerado de las células madre del nicho que conllevaría a un adelgazamiento más pronunciado de GCL a la edad testada.

Ni para el módelo J20 ni para el módelo TgRln/J20 se ha descrito hasta la fecha una atrofia de la CA1-SRLM, lo que es el fenotipo más evidente en seres humanos. Además, vale la pena señalar que, como se mencionó anteriormente, no se ha encontrado correlación entre el tamaño del DG en y las habilidades cognitivas.

Se ha propuesto que la población excitable de células granulares del DG está formada por un número muy pequeño de células sobre el total, mientras que el 90-95% de la población podría estar efectivamente "retirada" (Alme et al., 2010). Por lo tanto un número muy pequeño de fibras musgosas que conectan células granulares a CA 3 puede sin embargo ser suficiente para mantener la funcionalidad de la red (Rolls, 2013). Esta teoría encaja con nuestros datos, ya que los TgRln/J20 muestran una fuerte atrofia del DG mientras que sus habilidades cognitivas, según la evaluación de las pruebas de comportamiento, no se ven afectadas (aunque esto sí ocurre en J20) y fueron incluso protegidas por la sobreexpresión de Reelina. Por lo tanto, puede tener sentido que el aprendizaje hipocampo-dependiente no se vea afectado por la atrofia encontrada en los ratones TgRln/J20, sugiriendo que las células que se mantienen en el DG son plenamente funcionales.

Perspectivas futuras

El conjunto de datos presentados en este trabajo sugiere que Reelina antagoniza la toxicidad de Aβ a múltiples niveles, de las sinapsis, a las células, hasta las redes neuronales. Aunque aparentemente participa con Aβ en la neurodegeneración del giro dentado del hipocampo, la sobreexpresión de Reelina en ratones J20 (TgRln/J20) es suficiente para llevar a una recuperación funcional completa de las anomalías de comportamiento típicas de AD, conforme con el rescate de la densidad de la espinas dendríticas y la reducción de la muerte neuronal. Un gran esfuerzo queda por hacer en descifrar los mecanismos moleculares que subyacen a la

neuroprotección de Reelina en AD, y para que eso encaje con el fenotipo de atrofia del giro dentado observado.

El análisis de los niveles de Aβ solubles en los animales TgRln/J20 es sin duda una cuestión de gran importancia con el fin de profundizar en el conocimiento de los mecanismos moleculares por los cuales Reelina reduce la extensión de placas amiloides y la toxicidad de las especies de Aβ. Cabe destacar que, en un enfoque *in vitro*, fué descrito que Reelina regula el tráfico y el procesamiento proteolítico de APP, promoviendo la escisión no amiloidogénica de αAPP (Hoe et al, 2006; Hoe et al, 2008; Hoe et al, 2009). Sería de gran relevancia corroborar estos datos en nuestro sistema *in vivo*. Además, la obtención de información sobre los mecanismos de interacción entre Reelina y las especies de Aβ, como los oligómeros, es sin duda una cuestión futura de gran relevancia para abordar.

Otro mecanismo clave para elucidar *in vivo* es el atrapamiento de Reelina en las fibrillas de $A\beta_{42}$, con la siguiente pérdida de señalización de la vía de Reelina. En el cerebro adulto, se ha demostrado que la vía de Reelina favorece el procesamiento del CTD de APP, disminuye la actividad de la GSK-3β y la fosforilación de Tau, potencia la neurotransmisión glutamatérgica, la LTP y la plasticidad sináptica estructural, y regula positivamente la neurogénesis adulta en el hipocampo. Todos estos procesos son necesarios para la correcta fisiología neuronal y las funciones cognitivas en adultos, y se han encontrado alterados en el AD. Debido a la función de Reelina en estos eventos relevantes, un posible mecanismo por corroborar es que la vía de Reelina actúa como una importante vía "homeostática" de regulación de numerosos aspectos de la función normal del cerebro adulto y cuya disfunción, posiblemente debida al secuestro de Reelina en las placas amiloides, puede contribuir a los rasgos cognitivos típicos de la patológia de Alzheimer.

Queda por abordar también si la sobreexpresión de Reelina rescata otros aspectos de la patología de la AD en ratones, tales como procesos de neuroinflamación.

Por último, se necesita dilucidar los mecanismos subyacentes a la reducción Reelina-dependiente de volumen de la ML del giro dentado y la acción combinada de Reelina y Aβ en la atrofia de la GCL en el modelo TgRln/J20. Consideramos que es muy pertinente abordar las posibles consecuencias funcionales de la sobreexpresión de Reelina sobre la neurogénesis adulta en el contexto de AD.

ABBREVIATIONS

AD	Alzheimer's disease
ADDLs	amyloid β-derived diffusible ligands
AICD	intracellular carboxy-terminal domain of APP
AMPA	α-amino-3-hydroxy-5-methyl-4-isoxazole propionic acid
ANX	anion exchange
ApoE	Apolipoprotein E
ApoER2	Apolipoprotein E2 receptor
APP	amyloid beta precursor protein
Aβ	amyloid beta peptide
$Aβ_{40}$	40-aminoacid form of amyloid beta peptide
$Aβ_{42}$	42-aminoacid form of amyloid beta peptide
β-gal	β-galactosidase
CR	Cajal-Retzius cells
DCX	doublecortin
DG	dentate gyrus
DI	discrimination index
DOX	doxocycline
ECM	Extracellular Matrix
ECS	Extracellular space
EOAD	early-onset Alzheimer's disease
FAD	familial Alzheimer's disease
FTD	fronto temporal dementia
GCL	granular cell layer
GSK-3β	glycogen synthase kinase 3 beta
hAPP	human APP
HMW	high molecular weight
KA	kainic acid
LC	liquid chromatography
LMW	low molecular weight
LOAD	late-onset Alzheimer's disease
LRP	low density lipoprotein receptor
LTP	long term potentiation
MAP	microtubule-associated protein
MAPT	microtubule-associated protein Tau
ML	molecular layer
MS/MS	tandem mass spectometry
MZ	marginal zone
NFTs	neurofibrillary tangles
NMDA	N-methyl-$_D$-aspartate
NOR	novel object recognition
pCaMKIIα	calcium-calmodulin dependent kinase II α promoter
PDGF-β	platelet-derived growth factor-β
PHFs	paired helical filaments
PI	propidium iodide
PI3K	phosphatidylinositol-3-kinase
PICUP	Photo-Induced Crosslinking of Unmodified Proteins
PKB	protein kinase B
PS1 – PSEN1	presenilin 1
PS2 – PSEN2	presenilin 2

PSD95	postsynaptic density protein 95
SAD	sporadic Alzheimeir's disease
sAPPβ	soluble extracellular domain of APP
SEC	size exclusion chromatography
SFKs	Src family of tyrosine kinases
SGZ	subgranular zone
slm	stratum lacunosum molecolare
so	stratum oriens
sp	stratum piramidale
sr	stratum radiatum
TEM	transmission electron microscopy
ThT	thioflavin T
tTA	tetracycline-controlled transactivator
VLDLR	very low density lipoprotein receptors

BIBLIOGRAPHY

Aebi M (2013) N-linked protein glycosylation in the ER. Biochimica et biophysica acta 1833:2430-2437.

Akiyama H et al. (2000) Inflammation and Alzheimer's disease. Neurobiology of aging 21:383-421.

Alcantara S, Ruiz M, D'Arcangelo G, Ezan F, de Lecea L, Curran T, Sotelo C, Soriano E (1998) Regional and cellular patterns of reelin mRNA expression in the forebrain of the developing and adult mouse. The Journal of neuroscience : the official journal of the Society for Neuroscience 18:7779-7799.

Alme CB, Buzzetti RA, Marrone DF, Leutgeb JK, Chawla MK, Schaner MJ, Bohanick JD, Khoboko T, Leutgeb S, Moser EI, Moser MB, McNaughton BL, Barnes CA (2010) Hippocampal granule cells opt for early retirement. Hippocampus 20:1109-1123.

Alonso Adel C, Mederlyova A, Novak M, Grundke-Iqbal I, Iqbal K (2004) Promotion of hyperphosphorylation by frontotemporal dementia tau mutations. The Journal of biological chemistry 279:34873-34881.

Alpar A, Ueberham U, Bruckner MK, Seeger G, Arendt T, Gartner U (2006) Different dendrite and dendritic spine alterations in basal and apical arbors in mutant human amyloid precursor protein transgenic mice. Brain research 1099:189-198.

Alzheimer A, Stelzmann RA, Schnitzlein HN, Murtagh FR (1995) An English translation of Alzheimer's 1907 paper, "Uber eine eigenartige Erkankung der Hirnrinde". Clinical anatomy (New York, NY 8:429-431.

Allen B, Ingram E, Takao M, Smith MJ, Jakes R, Virdee K, Yoshida H, Holzer M, Craxton M, Emson PC, Atzori C, Migheli A, Crowther RA, Ghetti B, Spillantini MG, Goedert M (2002) Abundant tau filaments and nonapoptotic neurodegeneration in transgenic mice expressing human P301S tau protein. The Journal of neuroscience : the official journal of the Society for Neuroscience 22:9340-9351.

Arendash GW, Garcia MF, Costa DA, Cracchiolo JR, Wefes IM, Potter H (2004) Environmental enrichment improves cognition in aged Alzheimer's transgenic mice despite stable beta-amyloid deposition. Neuroreport 15:1751-1754.

Arendt T (2012) Cell cycle activation and aneuploid neurons in Alzheimer's disease. Molecular neurobiology 46:125-135.

Arnaud L, Ballif BA, Cooper JA (2003a) Regulation of protein tyrosine kinase signaling by substrate degradation during brain development. Molecular and cellular biology 23:9293-9302.

Arnaud L, Ballif BA, Forster E, Cooper JA (2003b) Fyn tyrosine kinase is a critical regulator of disabled-1 during brain development. Curr Biol 13:9-17.

Arriagada PV, Growdon JH, Hedley-Whyte ET, Hyman BT (1992) Neurofibrillary tangles but not senile plaques parallel duration and severity of Alzheimer's disease. Neurology 42:631-639.

Avila J, Gomez de Barreda E, Engel T, Lucas JJ, Hernandez F (2010) Tau phosphorylation in hippocampus results in toxic gain-of-function. Biochemical Society transactions 38:977-980.

Avila J, Leon-Espinosa G, Garcia E, Garcia-Escudero V, Hernandez F, Defelipe J (2012) Tau Phosphorylation by GSK3 in Different Conditions. International journal of Alzheimer's disease 2012:578373.

Axelman K, Basun H, Winblad B, Lannfelt L (1994) A large Swedish family with Alzheimer's disease with a codon 670/671 amyloid precursor protein mutation. A clinical and genealogical investigation. Archives of neurology 51:1193-1197.

Ballard C, Gauthier S, Corbett A, Brayne C, Aarsland D, Jones E (2011) Alzheimer's disease. Lancet 377:1019-1031.

Ballatore C, Lee VM, Trojanowski JQ (2007) Tau-mediated neurodegeneration in Alzheimer's disease and related disorders. Nature reviews Neuroscience 8:663-672.

Ballif BA, Arnaud L, Arthur WT, Guris D, Imamoto A, Cooper JA (2004) Activation of a Dab1/CrkL/C3G/Rap1 pathway in Reelin-stimulated neurons. Curr Biol 14:606-610.

Beffert U, Morfini G, Bock HH, Reyna H, Brady ST, Herz J (2002) Reelin-mediated signaling locally regulates protein kinase B/Akt and glycogen synthase kinase 3beta. The Journal of biological chemistry 277:49958-49964.

Beffert U, Weeber EJ, Durudas A, Qiu S, Masiulis I, Sweatt JD, Li WP, Adelmann G, Frotscher M, Hammer RE, Herz J (2005) Modulation of synaptic plasticity and memory by Reelin involves differential splicing of the lipoprotein receptor Apoer2. Neuron 47:567-579.

Bekris LM, Yu CE, Bird TD, Tsuang DW (2010) Genetics of Alzheimer disease. Journal of geriatric psychiatry and neurology 23:213-227.

Benilova I, Karran E, De Strooper B (2012) The toxic Abeta oligomer and Alzheimer's disease: an emperor in need of clothes. Nature neuroscience 15:349-357.

Berger Z, Roder H, Hanna A, Carlson A, Rangachari V, Yue M, Wszolek Z, Ashe K, Knight J, Dickson D, Andorfer C, Rosenberry TL, Lewis J, Hutton M, Janus C (2007) Accumulation of pathological tau species and memory loss in a conditional model of tauopathy. The Journal of neuroscience : the official journal of the Society for Neuroscience 27:3650-3662.

Bertram L, Lill CM, Tanzi RE The genetics of Alzheimer disease: back to the future. Neuron 68:270-281.

Bertram L, Lill CM, Tanzi RE (2010) The genetics of Alzheimer disease: back to the future. Neuron 68:270-281.

Bertram L, McQueen MB, Mullin K, Blacker D, Tanzi RE (2007) Systematic meta-analyses of Alzheimer disease genetic association studies: the AlzGene database. Nature genetics 39:17-23.

Bertrand J, Plouffe V, Senechal P, Leclerc N (2010) The pattern of human tau phosphorylation is the result of priming and feedback events in primary hippocampal neurons. Neuroscience 168:323-334.

Bettens K, Sleegers K, Van Broeckhoven C (2010) Current status on Alzheimer disease molecular genetics: from past, to present, to future. Human molecular genetics 19:R4-R11.

Bitan G, Teplow DB (2004) Rapid photochemical cross-linking--a new tool for studies of metastable, amyloidogenic protein assemblies. Acc Chem Res 37:357-364.

Blennow K, de Leon MJ, Zetterberg H (2006) Alzheimer's disease. Lancet 368:387-403.

Blom N, Sicheritz-Ponten T, Gupta R, Gammeltoft S, Brunak S (2004) Prediction of post-translational glycosylation and phosphorylation of proteins from the amino acid sequence. Proteomics 4:1633-1649.

Bock HH, Herz J (2003) Reelin activates SRC family tyrosine kinases in neurons. Current biology : CB 13:18-26.

Bock HH, Jossin Y, May P, Bergner O, Herz J (2004) Apolipoprotein E receptors are required for reelin-induced proteasomal degradation of the neuronal adaptor protein Disabled-1. The Journal of biological chemistry 279:33471-33479.

Bonneh-Barkay D, Wiley CA (2009) Brain extracellular matrix in neurodegeneration. Brain pathology 19:573-585.

Borchelt DR, Ratovitski T, van Lare J, Lee MK, Gonzales V, Jenkins NA, Copeland NG, Price DL, Sisodia SS (1997) Accelerated amyloid deposition in the brains of transgenic mice coexpressing mutant presenilin 1 and amyloid precursor proteins. Neuron 19:939-945.

Botella-Lopez A, Cuchillo-Ibanez I, Cotrufo T, Mok SS, Li QX, Barquero MS, Dierssen M, Soriano E, Saez-Valero J (2010) Beta-amyloid controls altered Reelin expression and processing in Alzheimer's disease. Neurobiology of disease 37:682-691.

Botella-Lopez A, Burgaya F, Gavin R, Garcia-Ayllon MS, Gomez-Tortosa E, Pena-Casanova J, Urena JM, Del Rio JA, Blesa R, Soriano E, Saez-Valero J (2006) Reelin expression and glycosylation patterns are altered in Alzheimer's disease. Proceedings of the National Academy of Sciences of the United States of America 103:5573-5578.

Braak H, Braak E (1991) Neuropathological stageing of Alzheimer-related changes. Acta neuropathologica 82:239-259.

Braak H, Braak E (1995) Staging of Alzheimer's disease-related neurofibrillary changes. Neurobiology of aging 16:271-278; discussion 278-284.

Braak H, Braak E (1997) Frequency of stages of Alzheimer-related lesions in different age categories. Neurobiology of aging 18:351-357.

Buckner RL, Snyder AZ, Shannon BJ, LaRossa G, Sachs R, Fotenos AF, Sheline YI, Klunk WE, Mathis CA, Morris JC, Mintun MA (2005) Molecular, structural, and functional characterization of Alzheimer's disease: evidence for a relationship between default activity, amyloid, and memory. The Journal of neuroscience : the official journal of the Society for Neuroscience 25:7709-7717.

Busciglio J, Lorenzo A, Yeh J, Yankner BA (1995) beta-amyloid fibrils induce tau phosphorylation and loss of microtubule binding. Neuron 14:879-888.

Cai H, Wang Y, McCarthy D, Wen H, Borchelt DR, Price DL, Wong PC (2001) BACE1 is the major beta-secretase for generation of Abeta peptides by neurons. Nature neuroscience 4:233-234.

Cairns NJ et al. (2007) Neuropathologic diagnostic and nosologic criteria for frontotemporal lobar degeneration: consensus of the Consortium for Frontotemporal Lobar Degeneration. Acta neuropathologica 114:5-22.

Cao X, Sudhof TC (2001) A transcriptionally [correction of transcriptively] active complex of APP with Fe65 and histone acetyltransferase Tip60. Science 293:115-120.

Carulla N, Caddy GL, Hall DR, Zurdo J, Gairi M, Feliz M, Giralt E, Robinson CV, Dobson CM (2005) Molecular recycling within amyloid fibrils. Nature 436:554-558.

Castellano JM, Kim J, Stewart FR, Jiang H, DeMattos RB, Patterson BW, Fagan AM, Morris JC, Mawuenyega KG, Cruchaga C, Goate AM, Bales KR, Paul SM, Bateman RJ, Holtzman DM (2011) Human apoE isoforms differentially regulate brain amyloid-beta peptide clearance. Science translational medicine 3:89ra57.

Caviness VS, Jr. (1976) Patterns of cell and fiber distribution in the neocortex of the reeler mutant mouse. The Journal of comparative neurology 170:435-447.

Celio MR, Spreafico R, De Biasi S, Vitellaro-Zuccarello L (1998) Perineuronal nets: past and present. Trends in neurosciences 21:510-515.

Cirrito JR, Yamada KA, Finn MB, Sloviter RS, Bales KR, May PC, Schoepp DD, Paul SM, Mennerick S, Holtzman DM (2005) Synaptic activity regulates interstitial fluid amyloid-beta levels in vivo. Neuron 48:913-922.

Cleary JP, Walsh DM, Hofmeister JJ, Shankar GM, Kuskowski MA, Selkoe DJ, Ashe KH (2005) Natural oligomers of the amyloid-beta protein specifically disrupt cognitive function. Nature neuroscience 8:79-84.

Cohen SI, Linse S, Luheshi LM, Hellstrand E, White DA, Rajah L, Otzen DE, Vendruscolo M, Dobson CM, Knowles TP (2013) Proliferation of amyloid-beta42 aggregates occurs through a secondary nucleation mechanism. Proceedings of the National Academy of Sciences of the United States of America 110:9758-9763.

Cohen TJ, Guo JL, Hurtado DE, Kwong LK, Mills IP, Trojanowski JQ, Lee VM (2011) The acetylation of tau inhibits its function and promotes pathological tau aggregation. Nature communications 2:252.

Cole SL, Vassar R (2008) The role of amyloid precursor protein processing by BACE1, the beta-secretase, in Alzheimer disease pathophysiology. The Journal of biological chemistry 283:29621-29625.

Cooper JA (2008) A mechanism for inside-out lamination in the neocortex. Trends in neurosciences 31:113-119.

Corder EH, Saunders AM, Strittmatter WJ, Schmechel DE, Gaskell PC, Small GW, Roses AD, Haines JL, Pericak-Vance MA (1993) Gene dose of apolipoprotein E type 4 allele and the risk of Alzheimer's disease in late onset families. Science 261:921-923.

Chen G, Chen KS, Knox J, Inglis J, Bernard A, Martin SJ, Justice A, McConlogue L, Games D, Freedman SB, Morris RG (2000) A learning deficit related to age and beta-amyloid plaques in a mouse model of Alzheimer's disease. Nature 408:975-979.

Chen KS, Masliah E, Grajeda H, Guido T, Huang J, Khan K, Motter R, Soriano F, Games D (1998) Neurodegenerative Alzheimer-like pathology in PDAPP 717V->F transgenic mice. Progress in brain research 117:327-334.

Chen Y, Beffert U, Ertunc M, Tang TS, Kavalali ET, Bezprozvanny I, Herz J (2005) Reelin modulates NMDA receptor activity in cortical neurons. J Neurosci 25:8209-8216.

Chin J, Massaro CM, Palop JJ, Thwin MT, Yu GQ, Bien-Ly N, Bender A, Mucke L (2007) Reelin depletion in the entorhinal cortex of human amyloid precursor protein transgenic mice and humans with Alzheimer's disease. The Journal of neuroscience : the official journal of the Society for Neuroscience 27:2727-2733.

Chin J, Palop JJ, Puolivali J, Massaro C, Bien-Ly N, Gerstein H, Scearce-Levie K, Masliah E, Mucke L (2005) Fyn kinase induces synaptic and cognitive impairments in a transgenic mouse model of Alzheimer's disease. The Journal of neuroscience : the official journal of the Society for Neuroscience 25:9694-9703.

Chromy BA, Nowak RJ, Lambert MP, Viola KL, Chang L, Velasco PT, Jones BW, Fernandez SJ, Lacor PN, Horowitz P, Finch CE, Krafft GA, Klein WL (2003) Self-assembly of Abeta(1-42) into globular neurotoxins. Biochemistry 42:12749-12760.

D'Arcangelo G, Curran T (1998) Reeler: new tales on an old mutant mouse. BioEssays : news and reviews in molecular, cellular and developmental biology 20:235-244.

D'Arcangelo G, Miao GG, Chen SC, Soares HD, Morgan JI, Curran T (1995) A protein related to extracellular matrix proteins deleted in the mouse mutant reeler. Nature 374:719-723.

D'Arcangelo G, Nakajima K, Miyata T, Ogawa M, Mikoshiba K, Curran T (1997) Reelin is a secreted glycoprotein recognized by the CR-50 monoclonal antibody. The Journal of neuroscience : the official journal of the Society for Neuroscience 17:23-31.

D'Arcangelo G, Homayouni R, Keshvara L, Rice DS, Sheldon M, Curran T (1999) Reelin is a ligand for lipoprotein receptors. Neuron 24:471-479.

Dansie LE, Ethell IM (2011) Casting a net on dendritic spines: the extracellular matrix and its receptors. Developmental neurobiology 71:956-981.

Davies DC, Horwood N, Isaacs SL, Mann DM (1992) The effect of age and Alzheimer's disease on pyramidal neuron density in the individual fields of the hippocampal formation. Acta neuropathologica 83:510-517.

Dayanandan R, Van Slegtenhorst M, Mack TG, Ko L, Yen SH, Leroy K, Brion JP, Anderton BH, Hutton M, Lovestone S (1999) Mutations in tau reduce its microtubule binding properties in intact cells and affect its phosphorylation. FEBS letters 446:228-232.

De Felice FG, Velasco PT, Lambert MP, Viola K, Fernandez SJ, Ferreira ST, Klein WL (2007) Abeta oligomers induce neuronal oxidative stress through an N-methyl-D-aspartate receptor-dependent mechanism that is blocked by the Alzheimer drug memantine. The Journal of biological chemistry 282:11590-11601.

De Felice FG, Wu D, Lambert MP, Fernandez SJ, Velasco PT, Lacor PN, Bigio EH, Jerecic J, Acton PJ, Shughrue PJ, Chen-Dodson E, Kinney GG, Klein WL (2008) Alzheimer's disease-type neuronal tau hyperphosphorylation induced by A beta oligomers. Neurobiology of aging 29:1334-1347.

DeKosky ST, Scheff SW (1990) Synapse loss in frontal cortex biopsies in Alzheimer's disease: correlation with cognitive severity. Annals of neurology 27:457-464.

Del Rio JA, Heimrich B, Borrell V, Forster E, Drakew A, Alcantara S, Nakajima K, Miyata T, Ogawa M, Mikoshiba K, Derer P, Frotscher M, Soriano E (1997) A role for Cajal-Retzius cells and reelin in the development of hippocampal connections. Nature 385:70-74.

Delacourte A, Buee L (1997) Normal and pathological Tau proteins as factors for microtubule assembly. International review of cytology 171:167-224.

Derer P, Derer M, Goffinet A (2001) Axonal secretion of Reelin by Cajal-Retzius cells: evidence from comparison of normal and Reln(Orl) mutant mice. The Journal of comparative neurology 440:136-143.

Deshpande A, Mina E, Glabe C, Busciglio J (2006) Different conformations of amyloid beta induce neurotoxicity by distinct mechanisms in human cortical neurons. The Journal of neuroscience : the official journal of the Society for Neuroscience 26:6011-6018.

Deshpande A, Kawai H, Metherate R, Glabe CG, Busciglio J (2009) A role for synaptic zinc in activity-dependent Abeta oligomer formation and accumulation at excitatory synapses. The Journal of neuroscience : the official journal of the Society for Neuroscience 29:4004-4015.

Desikan RS, McEvoy LK, Thompson WK, Holland D, Roddey JC, Blennow K, Aisen PS, Brewer JB, Hyman BT, Dale AM, Alzheimer's Disease Neuroimaging I (2011) Amyloid-beta associated volume loss occurs only in the presence of phospho-tau. Annals of neurology 70:657-661.

DeSilva U, D'Arcangelo G, Braden VV, Chen J, Miao GG, Curran T, Green ED (1997) The human reelin gene: isolation, sequencing, and mapping on chromosome 7. Genome research 7:157-164.

Dityatev A, Schachner M, Sonderegger P (2010) The dual role of the extracellular matrix in synaptic plasticity and homeostasis. Nature reviews Neuroscience 11:735-746.

Dodart JC, Meziane H, Mathis C, Bales KR, Paul SM, Ungerer A (1999) Behavioral disturbances in transgenic mice overexpressing the V717F beta-amyloid precursor protein. Behavioral neuroscience 113:982-990.

Doehner J, Madhusudan A, Konietzko U, Fritschy JM, Knuesel I Co-localization of Reelin and proteolytic AbetaPP fragments in hippocampal plaques in aged wild-type mice. J Alzheimers Dis 19:1339-1357.

Doehner J, Madhusudan A, Konietzko U, Fritschy JM, Knuesel I (2010) Co-localization of Reelin and proteolytic AbetaPP fragments in hippocampal plaques in aged wild-type mice. J Alzheimers Dis 19:1339-1357.

Domnitz SB, Robbins EM, Hoang AW, Garcia-Alloza M, Hyman BT, Rebeck GW, Greenberg SM, Bacskai BJ, Frosch MP (2005) Progression of cerebral amyloid angiopathy in transgenic mouse models of Alzheimer disease. Journal of neuropathology and experimental neurology 64:588-594.

Dong H, Martin MV, Chambers S, Csernansky JG (2007) Spatial relationship between synapse loss and beta-amyloid deposition in Tg2576 mice. The Journal of comparative neurology 500:311-321.

Dubey M, Chaudhury P, Kabiru H, Shea TB (2008) Tau inhibits anterograde axonal transport and perturbs stability in growing axonal neurites in part by displacing kinesin cargo: neurofilaments attenuate tau-mediated neurite instability. Cell motility and the cytoskeleton 65:89-99.

Durakoglugil MS, Chen Y, White CL, Kavalali ET, Herz J (2009) Reelin signaling antagonizes beta-amyloid at the synapse. Proceedings of the National Academy of Sciences of the United States of America 106:15938-15943.

Engel T, Hernandez F, Avila J, Lucas JJ (2006a) Full reversal of Alzheimer's disease-like phenotype in a mouse model with conditional overexpression of glycogen synthase kinase-3. The Journal of neuroscience : the official journal of the Society for Neuroscience 26:5083-5090.

Engel T, Lucas JJ, Gomez-Ramos P, Moran MA, Avila J, Hernandez F (2006b) Cooexpression of FTDP-17 tau and GSK-3beta in transgenic mice induce tau polymerization and neurodegeneration. Neurobiology of aging 27:1258-1268.

Falconer DS (1951) Two new mutants, 'trembler' and 'reeler', with neurological actions in the house mouse (Mus musculus L.). Journal of Genetics 50 192-205.

Fancy DA, Kodadek T (1999) Chemistry for the analysis of protein-protein interactions: rapid and efficient cross-linking triggered by long wavelength light. Proceedings of the National Academy of Sciences of the United States of America 96:6020-6024.

Farrer LA, Cupples LA, Haines JL, Hyman B, Kukull WA, Mayeux R, Myers RH, Pericak-Vance MA, Risch N, van Duijn CM (1997) Effects of age, sex, and ethnicity on the association between apolipoprotein E genotype and Alzheimer disease. A meta-analysis. APOE and Alzheimer Disease Meta Analysis Consortium. JAMA : the journal of the American Medical Association 278:1349-1356.

Fatemi SH (2002) The role of Reelin in pathology of autism. Molecular psychiatry 7:919-920.

Fatemi SH (2005) Reelin glycoprotein in autism and schizophrenia. International review of neurobiology 71:179-187.

Fatemi SH, Kroll JL, Stary JM (2001) Altered levels of Reelin and its isoforms in schizophrenia and mood disorders. Neuroreport 12:3209-3215.

Fatemi SH, Snow AV, Stary JM, Araghi-Niknam M, Reutiman TJ, Lee S, Brooks AI, Pearce DA (2005) Reelin signaling is impaired in autism. Biological psychiatry 57:777-787.

Ferrari A, Hoerndli F, Baechi T, Nitsch RM, Gotz J (2003) beta-Amyloid induces paired helical filament-like tau filaments in tissue culture. The Journal of biological chemistry 278:40162-40168.

Forster E, Tielsch A, Saum B, Weiss KH, Johanssen C, Graus-Porta D, Muller U, Frotscher M (2002) Reelin, Disabled 1, and beta 1 integrins are required for the formation of the radial glial scaffold in the hippocampus. Proceedings of the National Academy of Sciences of the United States of America 99:13178-13183.

Frackowiak J, Mazur-Kolecka B, Kaczmarski W, Dickson D (2001) Deposition of Alzheimer's vascular amyloid-beta is associated with decreased expression of brain L-3-hydroxyacyl-coenzyme A dehydrogenase (ERAB). Brain research 907:44-53.

Frame S, Cohen P (2001) GSK3 takes centre stage more than 20 years after its discovery. The Biochemical journal 359:1-16.

Frotscher M (2010) Role for Reelin in stabilizing cortical architecture. Trends in neurosciences 33:407-414.

Fryer JD, Taylor JW, DeMattos RB, Bales KR, Paul SM, Parsadanian M, Holtzman DM (2003) Apolipoprotein E markedly facilitates age-dependent cerebral amyloid angiopathy and spontaneous hemorrhage in amyloid precursor protein transgenic mice. The Journal of neuroscience : the official journal of the Society for Neuroscience 23:7889-7896.

Games D, Adams D, Alessandrini R, Barbour R, Berthelette P, Blackwell C, Carr T, Clemens J, Donaldson T, Gillespie F, et al. (1995) Alzheimer-type neuropathology in transgenic mice overexpressing V717F beta-amyloid precursor protein. Nature 373:523-527.

Gao Y, Pimplikar SW (2001) The gamma -secretase-cleaved C-terminal fragment of amyloid precursor protein mediates signaling to the nucleus. Proceedings of the National Academy of Sciences of the United States of America 98:14979-14984.

Garcia-Marin V, Blazquez-Llorca L, Rodriguez JR, Boluda S, Muntane G, Ferrer I, Defelipe J (2009) Diminished perisomatic GABAergic terminals on cortical neurons adjacent to amyloid plaques. Frontiers in neuroanatomy 3:28.

Garcia ML, Cleveland DW (2001) Going new places using an old MAP: tau, microtubules and human neurodegenerative disease. Current opinion in cell biology 13:41-48.

Gasteiger E, Hoogland C, Gattiker A, Duvaud S, Wilkins MR, Appel RD, A. B (2005) Protein Identification and Analysis Tools on the ExPASy Server. In: The Proteomics Protocols Handbook (Walker JM, ed), pp 571-607: Humana Press.

Gatz M, Reynolds CA, Fratiglioni L, Johansson B, Mortimer JA, Berg S, Fiske A, Pedersen NL (2006) Role of genes and environments for explaining Alzheimer disease. Archives of general psychiatry 63:168-174.

Ghosal K, Vogt DL, Liang M, Shen Y, Lamb BT, Pimplikar SW (2009) Alzheimer's disease-like pathological features in transgenic mice expressing the APP intracellular domain. Proceedings of the National Academy of Sciences of the United States of America 106:18367-18372.

Ghosh P, Kumar A, Datta B, Rangachari V (2010) Dynamics of protofibril elongation and association involved in Abeta42 peptide aggregation in Alzheimer's disease. BMC bioinformatics 11 Suppl 6:S24.

Giannakopoulos P, Herrmann FR, Bussiere T, Bouras C, Kovari E, Perl DP, Morrison JH, Gold G, Hof PR (2003) Tangle and neuron numbers, but not amyloid load, predict cognitive status in Alzheimer's disease. Neurology 60:1495-1500.

Glenner GG, Wong CW (1984) Alzheimer's disease: initial report of the purification and characterization of a novel cerebrovascular amyloid protein. Biochemical and biophysical research communications 120:885-890.

Goate A, Chartier-Harlin MC, Mullan M, Brown J, Crawford F, Fidani L, Giuffra L, Haynes A, Irving N, James L, et al. (1991) Segregation of a missense mutation in the amyloid precursor protein gene with familial Alzheimer's disease. Nature 349:704-706.

Goedert M, Jakes R (2005) Mutations causing neurodegenerative tauopathies. Biochimica et biophysica acta 1739:240-250.

Goedert M, Spillantini MG (2006) A century of Alzheimer's disease. Science 314:777-781.

Goes FS, Willour VL, Zandi PP, Belmonte PL, Mackinnon DF, Mondimore FM, Schweizer B, Depaulo JR, Jr., Gershon ES, McMahon FJ, Potash JB (2009) Sex-specific association of the reelin gene with bipolar disorder. Am J Med Genet B Neuropsychiatr Genet.

Gonzalez-Billault C, Del Rio JA, Urena JM, Jimenez-Mateos EM, Barallobre MJ, Pascual M, Pujadas L, Simo S, Torre AL, Gavin R, Wandosell F, Soriano E, Avila J (2005) A role of MAP1B in Reelin-dependent neuronal migration. Cereb Cortex 15:1134-1145.

Gotz J, Ittner LM (2008) Animal models of Alzheimer's disease and frontotemporal dementia. Nature reviews Neuroscience 9:532-544.

Gotz J, Chen F, Barmettler R, Nitsch RM (2001a) Tau filament formation in transgenic mice expressing P301L tau. The Journal of biological chemistry 276:529-534.

Gotz J, Tolnay M, Barmettler R, Chen F, Probst A, Nitsch RM (2001b) Oligodendroglial tau filament formation in transgenic mice expressing G272V tau. The European journal of neuroscience 13:2131-2140.

Gotz J, Streffer JR, David D, Schild A, Hoerndli F, Pennanen L, Kurosinski P, Chen F (2004) Transgenic animal models of Alzheimer's disease and related disorders: histopathology, behavior and therapy. Molecular psychiatry 9:664-683.

Greenberg SG, Davies P, Schein JD, Binder LI (1992) Hydrofluoric acid-treated tau PHF proteins display the same biochemical properties as normal tau. The Journal of biological chemistry 267:564-569.

Griffin WS (2006) Inflammation and neurodegenerative diseases. The American journal of clinical nutrition 83:470S-474S.

Griffin WS, Sheng JG, Royston MC, Gentleman SM, McKenzie JE, Graham DI, Roberts GW, Mrak RE (1998) Glial-neuronal interactions in Alzheimer's disease: the potential role of a 'cytokine cycle' in disease progression. Brain pathology 8:65-72.

Groc L, Choquet D, Stephenson FA, Verrier D, Manzoni OJ, Chavis P (2007) NMDA receptor surface trafficking and synaptic subunit composition are developmentally regulated by the extracellular matrix protein Reelin. The Journal of neuroscience : the official journal of the Society for Neuroscience 27:10165-10175.

Grundke-Iqbal I, Iqbal K, Tung YC, Quinlan M, Wisniewski HM, Binder LI (1986) Abnormal phosphorylation of the microtubule-associated protein tau (tau) in Alzheimer cytoskeletal pathology. Proceedings of the National Academy of Sciences of the United States of America 83:4913-4917.

Grutzendler J, Helmin K, Tsai J, Gan WB (2007) Various dendritic abnormalities are associated with fibrillar amyloid deposits in Alzheimer's disease. Annals of the New York Academy of Sciences 1097:30-39.

Gyure KA, Durham R, Stewart WF, Smialek JE, Troncoso JC (2001) Intraneuronal abeta-amyloid precedes development of amyloid plaques in Down syndrome. Archives of pathology & laboratory medicine 125:489-492.

Haass C, Selkoe DJ (2007) Soluble protein oligomers in neurodegeneration: lessons from the Alzheimer's amyloid beta-peptide. Nature reviews Molecular cell biology 8:101-112.

Haass C, Lemere CA, Capell A, Citron M, Seubert P, Schenk D, Lannfelt L, Selkoe DJ (1995) The Swedish mutation causes early-onset Alzheimer's disease by beta-secretase cleavage within the secretory pathway. Nature medicine 1:1291-1296.

Halagappa VK, Guo Z, Pearson M, Matsuoka Y, Cutler RG, Laferla FM, Mattson MP (2007) Intermittent fasting and caloric restriction ameliorate age-related behavioral deficits in the triple-transgenic mouse model of Alzheimer's disease. Neurobiology of disease 26:212-220.

Hanger DP, Anderton BH, Noble W (2009) Tau phosphorylation: the therapeutic challenge for neurodegenerative disease. Trends in molecular medicine 15:112-119.

Hardy J (1997) Amyloid, the presenilins and Alzheimer's disease. Trends in neurosciences 20:154-159.

Hardy J, Selkoe DJ (2002) The amyloid hypothesis of Alzheimer's disease: progress and problems on the road to therapeutics. Science 297:353-356.

Hardy JA, Higgins GA (1992) Alzheimer's disease: the amyloid cascade hypothesis. Science 256:184-185.

Harold D et al. (2009) Genome-wide association study identifies variants at CLU and PICALM associated with Alzheimer's disease. Nature genetics 41:1088-1093.

Harris JA, Devidze N, Halabisky B, Lo I, Thwin MT, Yu GQ, Bredesen DE, Masliah E, Mucke L (2010) Many neuronal and behavioral impairments in transgenic mouse models of Alzheimer's disease are independent of caspase cleavage of the amyloid precursor protein. The Journal of neuroscience : the official journal of the Society for Neuroscience 30:372-381.

Hashimoto T, Serrano-Pozo A, Hori Y, Adams KW, Takeda S, Banerji AO, Mitani A, Joyner D, Thyssen DH, Bacskai BJ, Frosch MP, Spires-Jones TL, Finn MB, Holtzman DM, Hyman BT (2012) Apolipoprotein E, especially apolipoprotein E4, increases the oligomerization of amyloid beta peptide. The Journal of neuroscience : the official journal of the Society for Neuroscience 32:15181-15192.

Helenius A, Aebi M (2004) Roles of N-linked glycans in the endoplasmic reticulum. Annual review of biochemistry 73:1019-1049.

Heneka MT, O'Banion MK (2007) Inflammatory processes in Alzheimer's disease. Journal of neuroimmunology 184:69-91.

Hernandez F, Lucas JJ, Avila J GSK3 and tau: two convergence points in Alzheimer's disease. J Alzheimers Dis 33 Suppl 1:S141-144.

Hernandez F, Borrell J, Guaza C, Avila J, Lucas JJ (2002) Spatial learning deficit in transgenic mice that conditionally over-express GSK-3beta in the brain but do not form tau filaments. Journal of neurochemistry 83:1529-1533.

Herreman A, Hartmann D, Annaert W, Saftig P, Craessaerts K, Serneels L, Umans L, Schrijvers V, Checler F, Vanderstichele H, Baekelandt V, Dressel R, Cupers P, Huylebroeck D, Zwijsen A, Van Leuven F, De Strooper B (1999) Presenilin 2 deficiency causes a mild pulmonary phenotype and no changes in amyloid precursor protein processing but enhances the embryonic lethal phenotype of presenilin 1 deficiency. Proceedings of the National Academy of Sciences of the United States of America 96:11872-11877.

Herring A, Donath A, Steiner KM, Widera MP, Hamzehian S, Kanakis D, Kolble K, ElAli A, Hermann DM, Paulus W, Keyvani K (2012) Reelin depletion is an early phenomenon of Alzheimer's pathology. J Alzheimers Dis 30:963-979.

Herrup K (2010) Reimagining Alzheimer's disease--an age-based hypothesis. The Journal of neuroscience : the official journal of the Society for Neuroscience 30:16755-16762.

Herz J, Chen Y (2006) Reelin, lipoprotein receptors and synaptic plasticity. Nature reviews Neuroscience 7:850-859.

Hibbard LS, McKeel DW, Jr. (1997) Automated identification and quantitative morphometry of the senile plaques of Alzheimer's disease. Analytical and quantitative cytology and histology / the International Academy of Cytology [and] American Society of Cytology 19:123-138.

Hiesberger T, Trommsdorff M, Howell BW, Goffinet A, Mumby MC, Cooper JA, Herz J (1999) Direct binding of Reelin to VLDL receptor and ApoE receptor 2 induces tyrosine phosphorylation of disabled-1 and modulates tau phosphorylation. Neuron 24:481-489.

Hisanaga A, Morishita S, Suzuki K, Sasaki K, Koie M, Kohno T, Hattori M (2012) A disintegrin and metalloproteinase with thrombospondin motifs 4 (ADAMTS-4) cleaves Reelin in an isoform-dependent manner. FEBS letters 586:3349-3353.

Hoe HS, Tran TS, Matsuoka Y, Howell BW, Rebeck GW (2006) DAB1 and Reelin effects on amyloid precursor protein and ApoE receptor 2 trafficking and processing. The Journal of biological chemistry 281:35176-35185.

Hoe HS, Minami SS, Makarova A, Lee J, Hyman BT, Matsuoka Y, Rebeck GW (2008) Fyn modulation of Dab1 effects on amyloid precursor protein and ApoE receptor 2 processing. The Journal of biological chemistry 283:6288-6299.

Hoe HS, Lee KJ, Carney RS, Lee J, Markova A, Lee JY, Howell BW, Hyman BT, Pak DT, Bu G, Rebeck GW (2009) Interaction of reelin with amyloid precursor protein promotes neurite outgrowth. The Journal of neuroscience : the official journal of the Society for Neuroscience 29:7459-7473.

Hof PR, Bouras C, Perl DP, Sparks DL, Mehta N, Morrison JH (1995) Age-related distribution of neuropathologic changes in the cerebral cortex of patients with Down's syndrome. Quantitative regional analysis and comparison with Alzheimer's disease. Archives of neurology 52:379-391.

Hollingworth P et al. (2011) Common variants at ABCA7, MS4A6A/MS4A4E, EPHA1, CD33 and CD2AP are associated with Alzheimer's disease. Nature genetics 43:429-435.

Hong M, Zhukareva V, Vogelsberg-Ragaglia V, Wszolek Z, Reed L, Miller BI, Geschwind DH, Bird TD, McKeel D, Goate A, Morris JC, Wilhelmsen KC, Schellenberg GD, Trojanowski JQ, Lee VM (1998) Mutation-specific functional

impairments in distinct tau isoforms of hereditary FTDP-17. Science 282:1914-1917.

Hoover BR, Reed MN, Su J, Penrod RD, Kotilinek LA, Grant MK, Pitstick R, Carlson GA, Lanier LM, Yuan LL, Ashe KH, Liao D (2010) Tau mislocalization to dendritic spines mediates synaptic dysfunction independently of neurodegeneration. Neuron 68:1067-1081.

Hounsell EF, Davies MJ, Renouf DV (1996) O-linked protein glycosylation structure and function. Glycoconjugate journal 13:19-26.

Howell BW, Herrick TM, Cooper JA (1999) Reelin-induced tyrosine [corrected] phosphorylation of disabled 1 during neuronal positioning. Genes & development 13:643-648.

Howell BW, Hawkes R, Soriano P, Cooper JA (1997) Neuronal position in the developing brain is regulated by mouse disabled-1. Nature 389:733-737.

Hsia AY, Masliah E, McConlogue L, Yu GQ, Tatsuno G, Hu K, Kholodenko D, Malenka RC, Nicoll RA, Mucke L (1999) Plaque-independent disruption of neural circuits in Alzheimer's disease mouse models. Proceedings of the National Academy of Sciences of the United States of America 96:3228-3233.

Hsiao K, Chapman P, Nilsen S, Eckman C, Harigaya Y, Younkin S, Yang F, Cole G (1996) Correlative memory deficits, Abeta elevation, and amyloid plaques in transgenic mice. Science 274:99-102.

Hsieh H, Boehm J, Sato C, Iwatsubo T, Tomita T, Sisodia S, Malinow R (2006) AMPAR removal underlies Abeta-induced synaptic depression and dendritic spine loss. Neuron 52:831-843.

Huang Y, Mucke L (2012) Alzheimer mechanisms and therapeutic strategies. Cell 148:1204-1222.

Hutton M et al. (1998) Association of missense and 5'-splice-site mutations in tau with the inherited dementia FTDP-17. Nature 393:702-705.

Iqbal K, Liu F, Gong CX, Grundke-Iqbal I (2010) Tau in Alzheimer disease and related tauopathies. Current Alzheimer research 7:656-664.

Irizarry MC, Soriano F, McNamara M, Page KJ, Schenk D, Games D, Hyman BT (1997) Abeta deposition is associated with neuropil changes, but not with overt neuronal loss in the human amyloid precursor protein V717F (PDAPP) transgenic mouse. The Journal of neuroscience : the official journal of the Society for Neuroscience 17:7053-7059.

Ittner LM, Gotz J (2011) Amyloid-beta and tau--a toxic pas de deux in Alzheimer's disease. Nature reviews Neuroscience 12:65-72.

Ittner LM, Ke YD, Delerue F, Bi M, Gladbach A, van Eersel J, Wolfing H, Chieng BC, Christie MJ, Napier IA, Eckert A, Staufenbiel M, Hardeman E, Gotz J (2010) Dendritic function of tau mediates amyloid-beta toxicity in Alzheimer's disease mouse models. Cell 142:387-397.

Jin K, Galvan V, Xie L, Mao XO, Gorostiza OF, Bredesen DE, Greenberg DA (2004a) Enhanced neurogenesis in Alzheimer's disease transgenic (PDGF-APPSw,Ind) mice. Proceedings of the National Academy of Sciences of the United States of America 101:13363-13367.

Jin K, Peel AL, Mao XO, Xie L, Cottrell BA, Henshall DC, Greenberg DA (2004b) Increased hippocampal neurogenesis in Alzheimer's disease. Proceedings of the National Academy of Sciences of the United States of America 101:343-347.

Jones MW, Errington ML, French PJ, Fine A, Bliss TV, Garel S, Charnay P, Bozon B, Laroche S, Davis S (2001) A requirement for the immediate early gene Zif268

in the expression of late LTP and long-term memories. Nature neuroscience 4:289-296.

Jossin Y, Gui L, Goffinet AM (2007) Processing of Reelin by embryonic neurons is important for function in tissue but not in dissociated cultured neurons. The Journal of neuroscience : the official journal of the Society for Neuroscience 27:4243-4252.

Jossin Y, Ogawa M, Metin C, Tissir F, Goffinet AM (2003) Inhibition of SRC family kinases and non-classical protein kinases C induce a reeler-like malformation of cortical plate development. The Journal of neuroscience : the official journal of the Society for Neuroscience 23:9953-9959.

Ju W, Morishita W, Tsui J, Gaietta G, Deerinck TJ, Adams SR, Garner CC, Tsien RY, Ellisman MH, Malenka RC (2004) Activity-dependent regulation of dendritic synthesis and trafficking of AMPA receptors. Nature neuroscience 7:244-253.

Kaczmarek L (2013) Mmp-9 inhibitors in the brain: can old bullets shoot new targets? Current pharmaceutical design 19:1085-1089.

Kamenetz F, Tomita T, Hsieh H, Seabrook G, Borchelt D, Iwatsubo T, Sisodia S, Malinow R (2003) APP processing and synaptic function. Neuron 37:925-937.

Kang JE, Lim MM, Bateman RJ, Lee JJ, Smyth LP, Cirrito JR, Fujiki N, Nishino S, Holtzman DM (2009) Amyloid-beta dynamics are regulated by orexin and the sleep-wake cycle. Science 326:1005-1007.

Kawarabayashi T, Younkin LH, Saido TC, Shoji M, Ashe KH, Younkin SG (2001) Age-dependent changes in brain, CSF, and plasma amyloid (beta) protein in the Tg2576 transgenic mouse model of Alzheimer's disease. The Journal of neuroscience : the official journal of the Society for Neuroscience 21:372-381.

Kayed R, Head E, Thompson JL, McIntire TM, Milton SC, Cotman CW, Glabe CG (2003) Common structure of soluble amyloid oligomers implies common mechanism of pathogenesis. Science 300:486-489.

Kerchner GA, Deutsch GK, Zeineh M, Dougherty RF, Saranathan M, Rutt BK (2012) Hippocampal CA1 apical neuropil atrophy and memory performance in Alzheimer's disease. NeuroImage 63:194-202.

Klein WL (2002) Abeta toxicity in Alzheimer's disease: globular oligomers (ADDLs) as new vaccine and drug targets. Neurochemistry international 41:345-352.

Knuesel I (2010) Reelin-mediated signaling in neuropsychiatric and neurodegenerative diseases. Progress in neurobiology 91:257-274.

Knuesel I, Nyffeler M, Mormede C, Muhia M, Meyer U, Pietropaolo S, Yee BK, Pryce CR, LaFerla FM, Marighetto A, Feldon J (2009) Age-related accumulation of Reelin in amyloid-like deposits. Neurobiology of aging 30:697-716.

Kocherhans S, Madhusudan A, Doehner J, Breu KS, Nitsch RM, Fritschy JM, Knuesel I (2010) Reduced Reelin expression accelerates amyloid-beta plaque formation and tau pathology in transgenic Alzheimer's disease mice. The Journal of neuroscience : the official journal of the Society for Neuroscience 30:9228-9240.

Kopeikina KJ, Hyman BT, Spires-Jones TL (2012) Soluble forms of tau are toxic in Alzheimer's disease. Translational neuroscience 3:223-233.

Krafft GA, Klein WL (2010) ADDLs and the signaling web that leads to Alzheimer's disease. Neuropharmacology 59:230-242.

Kramer PL, Xu H, Woltjer RL, Westaway SK, Clark D, Erten-Lyons D, Kaye JA, Welsh-Bohmer KA, Troncoso JC, Markesbery WR, Petersen RC, Turner RS, Kukull WA, Bennett DA, Galasko D, Morris JC, Ott J Alzheimer disease

pathology in cognitively healthy elderly: A genome-wide study. Neurobiology of aging.

Krstic D, Knuesel I (2013) Deciphering the mechanism underlying late-onset Alzheimer disease. Nature reviews Neurology 9:25-34.

Krstic D, Rodriguez M, Knuesel I (2012a) Regulated proteolytic processing of Reelin through interplay of tissue plasminogen activator (tPA), ADAMTS-4, ADAMTS-5, and their modulators. PloS one 7:e47793.

Krstic D, Madhusudan A, Doehner J, Vogel P, Notter T, Imhof C, Manalastas A, Hilfiker M, Pfister S, Schwerdel C, Riether C, Meyer U, Knuesel I (2012b) Systemic immune challenges trigger and drive Alzheimer-like neuropathology in mice. Journal of neuroinflammation 9:151.

Kubo K, Mikoshiba K, Nakajima K (2002) Secreted Reelin molecules form homodimers. Neuroscience research 43:381-388.

Kuo G, Arnaud L, Kronstad-O'Brien P, Cooper JA (2005) Absence of Fyn and Src causes a reeler-like phenotype. The Journal of neuroscience : the official journal of the Society for Neuroscience 25:8578-8586.

Lacor PN, Grayson DR, Auta J, Sugaya I, Costa E, Guidotti A (2000) Reelin secretion from glutamatergic neurons in culture is independent from neurotransmitter regulation. Proceedings of the National Academy of Sciences of the United States of America 97:3556-3561.

Lacor PN, Buniel MC, Furlow PW, Clemente AS, Velasco PT, Wood M, Viola KL, Klein WL (2007) Abeta oligomer-induced aberrations in synapse composition, shape, and density provide a molecular basis for loss of connectivity in Alzheimer's disease. The Journal of neuroscience : the official journal of the Society for Neuroscience 27:796-807.

Lambert de Rouvroit C, de Bergeyck V, Cortvrindt C, Bar I, Eeckhout Y, Goffinet AM (1999) Reelin, the extracellular matrix protein deficient in reeler mutant mice, is processed by a metalloproteinase. Experimental neurology 156:214-217.

Lambert JC et al. (2009) Genome-wide association study identifies variants at CLU and CR1 associated with Alzheimer's disease. Nature genetics 41:1094-1099.

Lambert MP, Viola KL, Chromy BA, Chang L, Morgan TE, Yu J, Venton DL, Krafft GA, Finch CE, Klein WL (2001) Vaccination with soluble Abeta oligomers generates toxicity-neutralizing antibodies. Journal of neurochemistry 79:595-605.

Lambert MP, Barlow AK, Chromy BA, Edwards C, Freed R, Liosatos M, Morgan TE, Rozovsky I, Trommer B, Viola KL, Wals P, Zhang C, Finch CE, Krafft GA, Klein WL (1998) Diffusible, nonfibrillar ligands derived from Abeta1-42 are potent central nervous system neurotoxins. Proceedings of the National Academy of Sciences of the United States of America 95:6448-6453.

Lazarov O, Marr RA (2010) Neurogenesis and Alzheimer's disease: at the crossroads. Experimental neurology 223:267-281.

Lee EB, Zhang B, Liu K, Greenbaum EA, Doms RW, Trojanowski JQ, Lee VM (2005) BACE overexpression alters the subcellular processing of APP and inhibits Abeta deposition in vivo. The Journal of cell biology 168:291-302.

Leon-Espinosa G, DeFelipe J, Munoz A (2012) Effects of amyloid-beta plaque proximity on the axon initial segment of pyramidal cells. J Alzheimers Dis 29:841-852.

Lesne S, Koh MT, Kotilinek L, Kayed R, Glabe CG, Yang A, Gallagher M, Ashe KH (2006) A specific amyloid-beta protein assembly in the brain impairs memory. Nature 440:352-357.

Lewis J, Dickson DW, Lin WL, Chisholm L, Corral A, Jones G, Yen SH, Sahara N, Skipper L, Yager D, Eckman C, Hardy J, Hutton M, McGowan E (2001) Enhanced neurofibrillary degeneration in transgenic mice expressing mutant tau and APP. Science 293:1487-1491.

Lewis J, McGowan E, Rockwood J, Melrose H, Nacharaju P, Van Slegtenhorst M, Gwinn-Hardy K, Paul Murphy M, Baker M, Yu X, Duff K, Hardy J, Corral A, Lin WL, Yen SH, Dickson DW, Davies P, Hutton M (2000) Neurofibrillary tangles, amyotrophy and progressive motor disturbance in mice expressing mutant (P301L) tau protein. Nature genetics 25:402-405.

Lim F, Hernandez F, Lucas JJ, Gomez-Ramos P, Moran MA, Avila J (2001) FTDP-17 mutations in tau transgenic mice provoke lysosomal abnormalities and Tau filaments in forebrain. Molecular and cellular neurosciences 18:702-714.

Liscic RM, Storandt M, Cairns NJ, Morris JC (2007) Clinical and psychometric distinction of frontotemporal and Alzheimer dementias. Archives of neurology 64:535-540.

Lopez-Toledano MA, Shelanski ML (2007) Increased neurogenesis in young transgenic mice overexpressing human APP(Sw, Ind). J Alzheimers Dis 12:229-240.

Lucas J, Hernández F, Gómez-Ramos P, Morán M, Hen R, Avila J (2001) Decreased nuclear beta-catenin, tau hyperphosphorylation and neurodegeneration in GSK-3beta conditional transgenic mice. EMBO J 20:27-39.

Lue LF, Kuo YM, Roher AE, Brachova L, Shen Y, Sue L, Beach T, Kurth JH, Rydel RE, Rogers J (1999) Soluble amyloid beta peptide concentration as a predictor of synaptic change in Alzheimer's disease. The American journal of pathology 155:853-862.

Ma H, Lesne S, Kotilinek L, Steidl-Nichols JV, Sherman M, Younkin L, Younkin S, Forster C, Sergeant N, Delacourte A, Vassar R, Citron M, Kofuji P, Boland LM, Ashe KH (2007) Involvement of beta-site APP cleaving enzyme 1 (BACE1) in amyloid precursor protein-mediated enhancement of memory and activity-dependent synaptic plasticity. Proceedings of the National Academy of Sciences of the United States of America 104:8167-8172.

Ma QL, Lim GP, Harris-White ME, Yang F, Ambegaokar SS, Ubeda OJ, Glabe CG, Teter B, Frautschy SA, Cole GM (2006) Antibodies against beta-amyloid reduce Abeta oligomers, glycogen synthase kinase-3beta activation and tau phosphorylation in vivo and in vitro. Journal of neuroscience research 83:374-384.

Maeda S, Sahara N, Saito Y, Murayama M, Yoshiike Y, Kim H, Miyasaka T, Murayama S, Ikai A, Takashima A (2007) Granular tau oligomers as intermediates of tau filaments. Biochemistry 46:3856-3861.

Mandelkow EM, Stamer K, Vogel R, Thies E, Mandelkow E (2003) Clogging of axons by tau, inhibition of axonal traffic and starvation of synapses. Neurobiology of aging 24:1079-1085.

Mariani J, Crepel F, Mikoshiba K, Changeux JP, Sotelo C (1977) Anatomical, physiological and biochemical studies of the cerebellum from Reeler mutant mouse. Philosophical transactions of the Royal Society of London Series B, Biological sciences 281:1-28.

Marlatt MW, Lucassen PJ (2010) Neurogenesis and Alzheimer's disease: Biology and pathophysiology in mice and men. Current Alzheimer research 7:113-125.

Masliah E, Sisk A, Mallory M, Games D (2001) Neurofibrillary pathology in transgenic mice overexpressing V717F beta-amyloid precursor protein. Journal of neuropathology and experimental neurology 60:357-368.

Matsuki T, Pramatarova A, Howell BW (2008) Reduction of Crk and CrkL expression blocks reelin-induced dendritogenesis. Journal of cell science 121:1869-1875.

Mayford M, Bach ME, Huang YY, Wang L, Hawkins RD, Kandel ER (1996) Control of memory formation through regulated expression of a CaMKII transgene. Science 274:1678-1683.

McGeer PL, Schulzer M, McGeer EG (1996) Arthritis and anti-inflammatory agents as possible protective factors for Alzheimer's disease: a review of 17 epidemiologic studies. Neurology 47:425-432.

McKhann G, Drachman D, Folstein M, Katzman R, Price D, Stadlan EM (1984) Clinical diagnosis of Alzheimer's disease: report of the NINCDS-ADRDA Work Group under the auspices of Department of Health and Human Services Task Force on Alzheimer's Disease. Neurology 34:939-944.

McKhann GM, Albert MS, Grossman M, Miller B, Dickson D, Trojanowski JQ, Work Group on Frontotemporal D, Pick's D (2001) Clinical and pathological diagnosis of frontotemporal dementia: report of the Work Group on Frontotemporal Dementia and Pick's Disease. Archives of neurology 58:1803-1809.

McLean CA, Cherny RA, Fraser FW, Fuller SJ, Smith MJ, Beyreuther K, Bush AI, Masters CL (1999) Soluble pool of Abeta amyloid as a determinant of severity of neurodegeneration in Alzheimer's disease. Annals of neurology 46:860-866.

Miyata T, Nakajima K, Mikoshiba K, Ogawa M (1997) Regulation of Purkinje cell alignment by reelin as revealed with CR-50 antibody. The Journal of neuroscience : the official journal of the Society for Neuroscience 17:3599-3609.

Moolman DL, Vitolo OV, Vonsattel JP, Shelanski ML (2004) Dendrite and dendritic spine alterations in Alzheimer models. Journal of neurocytology 33:377-387.

Moore SJ, Deshpande K, Stinnett GS, Seasholtz AF, Murphy GG (2013) Conversion of short-term to long-term memory in the novel object recognition paradigm. Neurobiology of learning and memory 105:174-185.

Morimura T, Hattori M, Ogawa M, Mikoshiba K (2005) Disabled1 regulates the intracellular trafficking of reelin receptors. The Journal of biological chemistry 280:16901-16908.

Mucke L, Masliah E, Yu GQ, Mallory M, Rockenstein EM, Tatsuno G, Hu K, Kholodenko D, Johnson-Wood K, McConlogue L (2000) High-level neuronal expression of abeta 1-42 in wild-type human amyloid protein precursor transgenic mice: synaptotoxicity without plaque formation. The Journal of neuroscience : the official journal of the Society for Neuroscience 20:4050-4058.

Mullan M (1992) Familial Alzheimer's disease: second gene locus located. BMJ (Clinical research ed 305:1108-1109.

Nacharaju P, Lewis J, Easson C, Yen S, Hackett J, Hutton M, Yen SH (1999) Accelerated filament formation from tau protein with specific FTDP-17 missense mutations. FEBS letters 447:195-199.

Naj AC et al. (2011) Common variants at MS4A4/MS4A6E, CD2AP, CD33 and EPHA1 are associated with late-onset Alzheimer's disease. Nature genetics 43:436-441.

Nakajima K, Mikoshiba K, Miyata T, Kudo C, Ogawa M (1997) Disruption of hippocampal development in vivo by CR-50 mAb against reelin. Proceedings of the National Academy of Sciences of the United States of America 94:8196-8201.

Naslund J, Haroutunian V, Mohs R, Davis KL, Davies P, Greengard P, Buxbaum JD (2000) Correlation between elevated levels of amyloid beta-peptide in the brain and cognitive decline. JAMA : the journal of the American Medical Association 283:1571-1577.

Nielsen L, Khurana R, Coats A, Frokjaer S, Brange J, Vyas S, Uversky VN, Fink AL (2001) Effect of environmental factors on the kinetics of insulin fibril formation: elucidation of the molecular mechanism. Biochemistry 40:6036-6046.

Nikolaev A, McLaughlin T, O'Leary DD, Tessier-Lavigne M (2009) APP binds DR6 to trigger axon pruning and neuron death via distinct caspases. Nature 457:981-989.

Nilsberth C, Westlind-Danielsson A, Eckman CB, Condron MM, Axelman K, Forsell C, Stenh C, Luthman J, Teplow DB, Younkin SG, Naslund J, Lannfelt L (2001) The 'Arctic' APP mutation (E693G) causes Alzheimer's disease by enhanced Abeta protofibril formation. Nature neuroscience 4:887-893.

Niu S, Yabut O, D'Arcangelo G (2008) The Reelin signaling pathway promotes dendritic spine development in hippocampal neurons. The Journal of neuroscience : the official journal of the Society for Neuroscience 28:10339-10348.

Nussbaum RL, Ellis CE (2003) Alzheimer's disease and Parkinson's disease. The New England journal of medicine 348:1356-1364.

O'Brien RJ, Wong PC (2011) Amyloid precursor protein processing and Alzheimer's disease. Annual review of neuroscience 34:185-204.

Oddo S, Caccamo A, Kitazawa M, Tseng BP, LaFerla FM (2003a) Amyloid deposition precedes tangle formation in a triple transgenic model of Alzheimer's disease. Neurobiology of aging 24:1063-1070.

Oddo S, Caccamo A, Tran L, Lambert MP, Glabe CG, Klein WL, LaFerla FM (2006) Temporal profile of amyloid-beta (Abeta) oligomerization in an in vivo model of Alzheimer disease. A link between Abeta and tau pathology. The Journal of biological chemistry 281:1599-1604.

Oddo S, Caccamo A, Shepherd JD, Murphy MP, Golde TE, Kayed R, Metherate R, Mattson MP, Akbari Y, LaFerla FM (2003b) Triple-transgenic model of Alzheimer's disease with plaques and tangles: intracellular Abeta and synaptic dysfunction. Neuron 39:409-421.

Ogawa M, Miyata T, Nakajima K, Yagyu K, Seike M, Ikenaka K, Yamamoto H, Mikoshiba K (1995) The reeler gene-associated antigen on Cajal-Retzius neurons is a crucial molecule for laminar organization of cortical neurons. Neuron 14:899-912.

Ohkubo N, Lee YD, Morishima A, Terashima T, Kikkawa S, Tohyama M, Sakanaka M, Tanaka J, Maeda N, Vitek MP, Mitsuda N (2003) Apolipoprotein E and Reelin ligands modulate tau phosphorylation through an apolipoprotein E receptor/disabled-1/glycogen synthase kinase-3beta cascade. FASEB journal : official publication of the Federation of American Societies for Experimental Biology 17:295-297.

Orsucci D, Mancuso M, Ienco EC, Simoncini C, Siciliano G, Bonuccelli U (2013) Vascular factors and mitochondrial dysfunction: a central role in the pathogenesis of Alzheimer's disease. Current neurovascular research 10:76-80.

Oyama F, Sawamura N, Kobayashi K, Morishima-Kawashima M, Kuramochi T, Ito M, Tomita T, Maruyama K, Saido TC, Iwatsubo T, Capell A, Walter J, Grunberg J, Ueyama Y, Haass C, Ihara Y (1998) Mutant presenilin 2 transgenic mouse:

effect on an age-dependent increase of amyloid beta-protein 42 in the brain. Journal of neurochemistry 71:313-322.

Palop JJ, Mucke L (2010) Synaptic depression and aberrant excitatory network activity in Alzheimer's disease: two faces of the same coin? Neuromolecular medicine 12:48-55.

Palop JJ, Chin J, Bien-Ly N, Massaro C, Yeung BZ, Yu GQ, Mucke L (2005) Vulnerability of dentate granule cells to disruption of arc expression in human amyloid precursor protein transgenic mice. The Journal of neuroscience : the official journal of the Society for Neuroscience 25:9686-9693.

Palop JJ, Jones B, Kekonius L, Chin J, Yu GQ, Raber J, Masliah E, Mucke L (2003) Neuronal depletion of calcium-dependent proteins in the dentate gyrus is tightly linked to Alzheimer's disease-related cognitive deficits. Proceedings of the National Academy of Sciences of the United States of America 100:9572-9577.

Palop JJ, Chin J, Roberson ED, Wang J, Thwin MT, Bien-Ly N, Yoo J, Ho KO, Yu GQ, Kreitzer A, Finkbeiner S, Noebels JL, Mucke L (2007) Aberrant excitatory neuronal activity and compensatory remodeling of inhibitory hippocampal circuits in mouse models of Alzheimer's disease. Neuron 55:697-711.

Peineau S, Taghibiglou C, Bradley C, Wong TP, Liu L, Lu J, Lo E, Wu D, Saule E, Bouschet T, Matthews P, Isaac JT, Bortolotto ZA, Wang YT, Collingridge GL (2007) LTP inhibits LTD in the hippocampus via regulation of GSK3beta. Neuron 53:703-717.

Perez M, Ribe E, Rubio A, Lim F, Moran MA, Ramos PG, Ferrer I, Isla MT, Avila J (2005) Characterization of a double (amyloid precursor protein-tau) transgenic: tau phosphorylation and aggregation. Neuroscience 130:339-347.

Perry EK, Johnson M, Ekonomou A, Perry RH, Ballard C, Attems J (2012) Neurogenic abnormalities in Alzheimer's disease differ between stages of neurogenesis and are partly related to cholinergic pathology. Neurobiology of disease 47:155-162.

Petkova AT, Ishii Y, Balbach JJ, Antzutkin ON, Leapman RD, Delaglio F, Tycko R (2002) A structural model for Alzheimer's beta -amyloid fibrils based on experimental constraints from solid state NMR. Proceedings of the National Academy of Sciences of the United States of America 99:16742-16747.

Poorkaj P, Bird TD, Wijsman E, Nemens E, Garruto RM, Anderson L, Andreadis A, Wiederholt WC, Raskind M, Schellenberg GD (1998) Tau is a candidate gene for chromosome 17 frontotemporal dementia. Annals of neurology 43:815-825.

Powell SK, Kleinman HK (1997) Neuronal laminins and their cellular receptors. The international journal of biochemistry & cell biology 29:401-414.

Pujadas L, Gruart A, Bosch C, Delgado L, Teixeira CM, Rossi D, de Lecea L, Martinez A, Delgado-Garcia JM, Soriano E Reelin regulates postnatal neurogenesis and enhances spine hypertrophy and long-term potentiation. J Neurosci 30:4636-4649.

Pujadas L, Gruart A, Bosch C, Delgado L, Teixeira CM, Rossi D, de Lecea L, Martinez A, Delgado-Garcia JM, Soriano E (2010) Reelin regulates postnatal neurogenesis and enhances spine hypertrophy and long-term potentiation. The Journal of neuroscience : the official journal of the Society for Neuroscience 30:4636-4649.

Qiu S, Zhao LF, Korwek KM, Weeber EJ (2006) Differential reelin-induced enhancement of NMDA and AMPA receptor activity in the adult hippocampus. The Journal of neuroscience : the official journal of the Society for Neuroscience 26:12943-12955.

Rahimi F, Maiti P, Bitan G (2009) Photo-induced cross-linking of unmodified proteins (PICUP) applied to amyloidogenic peptides. Journal of visualized experiments : JoVE.

Rama N, Goldschneider D, Corset V, Lambert J, Pays L, Mehlen P (2012) Amyloid precursor protein regulates netrin-1-mediated commissural axon outgrowth. The Journal of biological chemistry 287:30014-30023.

Rao MS, Shetty AK (2004) Efficacy of doublecortin as a marker to analyse the absolute number and dendritic growth of newly generated neurons in the adult dentate gyrus. The European journal of neuroscience 19:234-246.

Rapoport M, Dawson HN, Binder LI, Vitek MP, Ferreira A (2002) Tau is essential to beta -amyloid-induced neurotoxicity. Proceedings of the National Academy of Sciences of the United States of America 99:6364-6369.

Rauk A (2008) Why is the amyloid beta peptide of Alzheimer's disease neurotoxic? Dalton transactions:1273-1282.

Ribe EM, Perez M, Puig B, Gich I, Lim F, Cuadrado M, Sesma T, Catena S, Sanchez B, Nieto M, Gomez-Ramos P, Moran MA, Cabodevilla F, Samaranch L, Ortiz L, Perez A, Ferrer I, Avila J, Gomez-Isla T (2005) Accelerated amyloid deposition, neurofibrillary degeneration and neuronal loss in double mutant APP/tau transgenic mice. Neurobiology of disease 20:814-822.

Rice DS, Curran T (2001) Role of the reelin signaling pathway in central nervous system development. Annual review of neuroscience 24:1005-1039.

Roberson ED, Scearce-Levie K, Palop JJ, Yan F, Cheng IH, Wu T, Gerstein H, Yu GQ, Mucke L (2007) Reducing endogenous tau ameliorates amyloid beta-induced deficits in an Alzheimer's disease mouse model. Science 316:750-754.

Roberson ED, Halabisky B, Yoo JW, Yao J, Chin J, Yan F, Wu T, Hamto P, Devidze N, Yu GQ, Palop JJ, Noebels JL, Mucke L (2011) Amyloid-beta/Fyn-induced synaptic, network, and cognitive impairments depend on tau levels in multiple mouse models of Alzheimer's disease. The Journal of neuroscience : the official journal of the Society for Neuroscience 31:700-711.

Rogers JT, Rusiana I, Trotter J, Zhao L, Donaldson E, Pak DT, Babus LW, Peters M, Banko JL, Chavis P, Rebeck GW, Hoe HS, Weeber EJ (2011) Reelin supplementation enhances cognitive ability, synaptic plasticity, and dendritic spine density. Learning & memory 18:558-564.

Rolls ET (2013) A quantitative theory of the functions of the hippocampal CA3 network in memory. Frontiers in cellular neuroscience 7:98.

Ronnback A, Zhu S, Dillner K, Aoki M, Lilius L, Naslund J, Winblad B, Graff C (2011) Progressive neuropathology and cognitive decline in a single Arctic APP transgenic mouse model. Neurobiology of aging 32:280-292.

Rovelet-Lecrux A, Hannequin D, Raux G, Le Meur N, Laquerriere A, Vital A, Dumanchin C, Feuillette S, Brice A, Vercelletto M, Dubas F, Frebourg T, Campion D (2006) APP locus duplication causes autosomal dominant early-onset Alzheimer disease with cerebral amyloid angiopathy. Nature genetics 38:24-26.

Rovio S, Kareholt I, Helkala EL, Viitanen M, Winblad B, Tuomilehto J, Soininen H, Nissinen A, Kivipelto M (2005) Leisure-time physical activity at midlife and the risk of dementia and Alzheimer's disease. Lancet neurology 4:705-711.

Royaux I, Lambert de Rouvroit C, D'Arcangelo G, Demirov D, Goffinet AM (1997) Genomic organization of the mouse reelin gene. Genomics 46:240-250.

Rutten BP, Van der Kolk NM, Schafer S, van Zandvoort MA, Bayer TA, Steinbusch HW, Schmitz C (2005) Age-related loss of synaptophysin immunoreactive

presynaptic boutons within the hippocampus of APP751SL, PS1M146L, and APP751SL/PS1M146L transgenic mice. The American journal of pathology 167:161-173.

Sahara N, Maeda S, Takashima A (2008) Tau oligomerization: a role for tau aggregation intermediates linked to neurodegeneration. Current Alzheimer research 5:591-598.

Salter MW, Kalia LV (2004) Src kinases: a hub for NMDA receptor regulation. Nature reviews Neuroscience 5:317-328.

Sanchez L, Madurga S, Pukala T, Vilaseca M, Lopez-Iglesias C, Robinson CV, Giralt E, Carulla N (2011) Abeta40 and Abeta42 amyloid fibrils exhibit distinct molecular recycling properties. Journal of the American Chemical Society 133:6505-6508.

Saunders AM, Schmader K, Breitner JC, Benson MD, Brown WT, Goldfarb L, Goldgaber D, Manwaring MG, Szymanski MH, McCown N, et al. (1993) Apolipoprotein E epsilon 4 allele distributions in late-onset Alzheimer's disease and in other amyloid-forming diseases. Lancet 342:710-711.

Schmechel DE, Saunders AM, Strittmatter WJ, Crain BJ, Hulette CM, Joo SH, Pericak-Vance MA, Goldgaber D, Roses AD (1993) Increased amyloid beta-peptide deposition in cerebral cortex as a consequence of apolipoprotein E genotype in late-onset Alzheimer disease. Proceedings of the National Academy of Sciences of the United States of America 90:9649-9653.

Schwab C, Hosokawa M, McGeer PL (2004) Transgenic mice overexpressing amyloid beta protein are an incomplete model of Alzheimer disease. Experimental neurology 188:52-64.

Selkoe DJ (2011) Alzheimer's disease. Cold Spring Harbor perspectives in biology 3.

Seripa D, Matera MG, Franceschi M, Daniele A, Bizzarro A, Rinaldi M, Panza F, Fazio VM, Gravina C, D'Onofrio G, Solfrizzi V, Masullo C, Pilotto A (2008) The RELN locus in Alzheimer's disease. J Alzheimers Dis 14:335-344.

Serrano-Pozo A, Frosch MP, Masliah E, Hyman BT (2011) Neuropathological alterations in Alzheimer disease. Cold Spring Harbor perspectives in medicine 1:a006189.

Shankar GM, Bloodgood BL, Townsend M, Walsh DM, Selkoe DJ, Sabatini BL (2007) Natural oligomers of the Alzheimer amyloid-beta protein induce reversible synapse loss by modulating an NMDA-type glutamate receptor-dependent signaling pathway. The Journal of neuroscience : the official journal of the Society for Neuroscience 27:2866-2875.

Shen J, Bronson RT, Chen DF, Xia W, Selkoe DJ, Tonegawa S (1997) Skeletal and CNS defects in Presenilin-1-deficient mice. Cell 89:629-639.

Sheng M, Sabatini BL, Sudhof TC (2012) Synapses and Alzheimer's disease. Cold Spring Harbor perspectives in biology 4.

Simo S, Pujadas L, Segura MF, La Torre A, Del Rio JA, Urena JM, Comella JX, Soriano E (2007) Reelin induces the detachment of postnatal subventricular zone cells and the expression of the Egr-1 through Erk1/2 activation. Cerebral cortex 17:294-303.

Sinagra M, Verrier D, Frankova D, Korwek KM, Blahos J, Weeber EJ, Manzoni OJ, Chavis P (2005) Reelin, very-low-density lipoprotein receptor, and apolipoprotein E receptor 2 control somatic NMDA receptor composition during hippocampal maturation in vitro. The Journal of neuroscience : the official journal of the Society for Neuroscience 25:6127-6136.

Smalheiser NR, Costa E, Guidotti A, Impagnatiello F, Auta J, Lacor P, Kriho V, Pappas GD (2000) Expression of reelin in adult mammalian blood, liver, pituitary pars intermedia, and adrenal chromaffin cells. Proceedings of the National Academy of Sciences of the United States of America 97:1281-1286.

Smith CD, Andersen AH, Gold BT, Alzheimer's Disease Neuroimaging I (2012) Structural brain alterations before mild cognitive impairment in ADNI: validation of volume loss in a predefined antero-temporal region. J Alzheimers Dis 31 Suppl 3:S49-58.

Soriano E, Del Rio JA (2005) The cells of cajal-retzius: still a mystery one century after. Neuron 46:389-394.

Spillantini MG, Murrell JR, Goedert M, Farlow MR, Klug A, Ghetti B (1998) Mutation in the tau gene in familial multiple system tauopathy with presenile dementia. Proceedings of the National Academy of Sciences of the United States of America 95:7737-7741.

Spires-Jones T, Knafo S (2012) Spines, plasticity, and cognition in Alzheimer's model mice. Neural plasticity 2012:319836.

Spires-Jones TL, Meyer-Luehmann M, Osetek JD, Jones PB, Stern EA, Bacskai BJ, Hyman BT (2007) Impaired spine stability underlies plaque-related spine loss in an Alzheimer's disease mouse model. The American journal of pathology 171:1304-1311.

Spires TL, Meyer-Luehmann M, Stern EA, McLean PJ, Skoch J, Nguyen PT, Bacskai BJ, Hyman BT (2005) Dendritic spine abnormalities in amyloid precursor protein transgenic mice demonstrated by gene transfer and intravital multiphoton microscopy. The Journal of neuroscience : the official journal of the Society for Neuroscience 25:7278-7287.

Stamer K, Vogel R, Thies E, Mandelkow E, Mandelkow EM (2002) Tau blocks traffic of organelles, neurofilaments, and APP vesicles in neurons and enhances oxidative stress. The Journal of cell biology 156:1051-1063.

Steiner H (2008) The catalytic core of gamma-secretase: presenilin revisited. Current Alzheimer research 5:147-157.

Stewart WF, Kawas C, Corrada M, Metter EJ (1997) Risk of Alzheimer's disease and duration of NSAID use. Neurology 48:626-632.

Strasser V, Fasching D, Hauser C, Mayer H, Bock HH, Hiesberger T, Herz J, Weeber EJ, Sweatt JD, Pramatarova A, Howell B, Schneider WJ, Nimpf J (2004) Receptor clustering is involved in Reelin signaling. Molecular and cellular biology 24:1378-1386.

Strittmatter WJ, Saunders AM, Schmechel D, Pericak-Vance M, Enghild J, Salvesen GS, Roses AD (1993a) Apolipoprotein E: high-avidity binding to beta-amyloid and increased frequency of type 4 allele in late-onset familial Alzheimer disease. Proceedings of the National Academy of Sciences of the United States of America 90:1977-1981.

Strittmatter WJ, Weisgraber KH, Huang DY, Dong LM, Salvesen GS, Pericak-Vance M, Schmechel D, Saunders AM, Goldgaber D, Roses AD (1993b) Binding of human apolipoprotein E to synthetic amyloid beta peptide: isoform-specific effects and implications for late-onset Alzheimer disease. Proceedings of the National Academy of Sciences of the United States of America 90:8098-8102.

Sturchler-Pierrat C, Abramowski D, Duke M, Wiederhold KH, Mistl C, Rothacher S, Ledermann B, Burki K, Frey P, Paganetti PA, Waridel C, Calhoun ME, Jucker M, Probst A, Staufenbiel M, Sommer B (1997) Two amyloid precursor protein transgenic mouse models with Alzheimer disease-like pathology. Proceedings of

the National Academy of Sciences of the United States of America 94:13287-13292.

Takashima A, Noguchi K, Sato K, Hoshino T, Imahori K (1993) Tau protein kinase I is essential for amyloid beta-protein-induced neurotoxicity. Proceedings of the National Academy of Sciences of the United States of America 90:7789-7793.

Takashima A, Noguchi K, Michel G, Mercken M, Hoshi M, Ishiguro K, Imahori K (1996) Exposure of rat hippocampal neurons to amyloid beta peptide (25-35) induces the inactivation of phosphatidyl inositol-3 kinase and the activation of tau protein kinase I/glycogen synthase kinase-3 beta. Neuroscience letters 203:33-36.

Tanemura K, Murayama M, Akagi T, Hashikawa T, Tominaga T, Ichikawa M, Yamaguchi H, Takashima A (2002) Neurodegeneration with tau accumulation in a transgenic mouse expressing V337M human tau. The Journal of neuroscience : the official journal of the Society for Neuroscience 22:133-141.

Tanemura K, Akagi T, Murayama M, Kikuchi N, Murayama O, Hashikawa T, Yoshiike Y, Park JM, Matsuda K, Nakao S, Sun X, Sato S, Yamaguchi H, Takashima A (2001) Formation of filamentous tau aggregations in transgenic mice expressing V337M human tau. Neurobiology of disease 8:1036-1045.

Tanzi RE (2012) The genetics of Alzheimer disease. Cold Spring Harbor perspectives in medicine 2.

Tanzi RE, Bertram L (2005) Twenty years of the Alzheimer's disease amyloid hypothesis: a genetic perspective. Cell 120:545-555.

Tarentino AL, Plummer TH, Jr. (1994) Enzymatic deglycosylation of asparagine-linked glycans: purification, properties, and specificity of oligosaccharide-cleaving enzymes from Flavobacterium meningosepticum. Methods in enzymology 230:44-57.

Tatebayashi Y, Miyasaka T, Chui DH, Akagi T, Mishima K, Iwasaki K, Fujiwara M, Tanemura K, Murayama M, Ishiguro K, Planel E, Sato S, Hashikawa T, Takashima A (2002) Tau filament formation and associative memory deficit in aged mice expressing mutant (R406W) human tau. Proceedings of the National Academy of Sciences of the United States of America 99:13896-13901.

Teixeira CM, Kron MM, Masachs N, Zhang H, Lagace DC, Martinez A, Reillo I, Duan X, Bosch C, Pujadas L, Brunso L, Song H, Eisch AJ, Borrell V, Howell BW, Parent JM, Soriano E (2012) Cell-autonomous inactivation of the reelin pathway impairs adult neurogenesis in the hippocampus. The Journal of neuroscience : the official journal of the Society for Neuroscience 32:12051-12065.

Terry RD, Masliah E, Salmon DP, Butters N, DeTeresa R, Hill R, Hansen LA, Katzman R (1991) Physical basis of cognitive alterations in Alzheimer's disease: synapse loss is the major correlate of cognitive impairment. Annals of neurology 30:572-580.

Thal DR, Rub U, Orantes M, Braak H (2002) Phases of A beta-deposition in the human brain and its relevance for the development of AD. Neurology 58:1791-1800.

Tissir F, Goffinet AM (2003) Reelin and brain development. Nature reviews Neuroscience 4:496-505.

Tomidokoro Y, Harigaya Y, Matsubara E, Ikeda M, Kawarabayashi T, Shirao T, Ishiguro K, Okamoto K, Younkin SG, Shoji M (2001a) Brain Abeta amyloidosis in APPsw mice induces accumulation of presenilin-1 and tau. The Journal of pathology 194:500-506.

Tomidokoro Y, Ishiguro K, Harigaya Y, Matsubara E, Ikeda M, Park JM, Yasutake K, Kawarabayashi T, Okamoto K, Shoji M (2001b) Abeta amyloidosis induces the

initial stage of tau accumulation in APP(Sw) mice. Neuroscience letters 299:169-172.

Tomiyama T, Nagata T, Shimada H, Teraoka R, Fukushima A, Kanemitsu H, Takuma H, Kuwano R, Imagawa M, Ataka S, Wada Y, Yoshioka E, Nishizaki T, Watanabe Y, Mori H (2008) A new amyloid beta variant favoring oligomerization in Alzheimer's-type dementia. Annals of neurology 63:377-387.

Tsai J, Grutzendler J, Duff K, Gan WB (2004) Fibrillar amyloid deposition leads to local synaptic abnormalities and breakage of neuronal branches. Nature neuroscience 7:1181-1183.

Tsai MS, Tangalos EG, Petersen RC, Smith GE, Schaid DJ, Kokmen E, Ivnik RJ, Thibodeau SN (1994) Apolipoprotein E: risk factor for Alzheimer disease. American journal of human genetics 54:643-649.

Utsunomiya-Tate N, Kubo K, Tate S, Kainosho M, Katayama E, Nakajima K, Mikoshiba K (2000) Reelin molecules assemble together to form a large protein complex, which is inhibited by the function-blocking CR-50 antibody. Proceedings of the National Academy of Sciences of the United States of America 97:9729-9734.

Ventruti A, Kazdoba TM, Niu S, D'Arcangelo G (2011) Reelin deficiency causes specific defects in the molecular composition of the synapses in the adult brain. Neuroscience 189:32-42.

Vlad SC, Miller DR, Kowall NW, Felson DT (2008) Protective effects of NSAIDs on the development of Alzheimer disease. Neurology 70:1672-1677.

von Bergen M, Barghorn S, Li L, Marx A, Biernat J, Mandelkow EM, Mandelkow E (2001) Mutations of tau protein in frontotemporal dementia promote aggregation of paired helical filaments by enhancing local beta-structure. The Journal of biological chemistry 276:48165-48174.

Walsh DM, Klyubin I, Fadeeva JV, Rowan MJ, Selkoe DJ (2002a) Amyloid-beta oligomers: their production, toxicity and therapeutic inhibition. Biochemical Society transactions 30:552-557.

Walsh DM, Klyubin I, Fadeeva JV, Cullen WK, Anwyl R, Wolfe MS, Rowan MJ, Selkoe DJ (2002b) Naturally secreted oligomers of amyloid beta protein potently inhibit hippocampal long-term potentiation in vivo. Nature 416:535-539.

Wang HW, Pasternak JF, Kuo H, Ristic H, Lambert MP, Chromy B, Viola KL, Klein WL, Stine WB, Krafft GA, Trommer BL (2002) Soluble oligomers of beta amyloid (1-42) inhibit long-term potentiation but not long-term depression in rat dentate gyrus. Brain research 924:133-140.

Wang Q, Yu S, Simonyi A, Sun GY, Sun AY (2005) Kainic acid-mediated excitotoxicity as a model for neurodegeneration. Molecular neurobiology 31:3-16.

Ward SM, Himmelstein DS, Lancia JK, Binder LI (2012) Tau oligomers and tau toxicity in neurodegenerative disease. Biochemical Society transactions 40:667-671.

Weeber EJ, Beffert U, Jones C, Christian JM, Forster E, Sweatt JD, Herz J (2002) Reelin and ApoE receptors cooperate to enhance hippocampal synaptic plasticity and learning. The Journal of biological chemistry 277:39944-39952.

Wei W, Nguyen LN, Kessels HW, Hagiwara H, Sisodia S, Malinow R (2010) Amyloid beta from axons and dendrites reduces local spine number and plasticity. Nature neuroscience 13:190-196.

Westerman MA, Cooper-Blacketer D, Mariash A, Kotilinek L, Kawarabayashi T, Younkin LH, Carlson GA, Younkin SG, Ashe KH (2002) The relationship between Abeta and memory in the Tg2576 mouse model of Alzheimer's disease. The Journal of neuroscience : the official journal of the Society for Neuroscience 22:1858-1867.

Willem M, Dewachter I, Smyth N, Van Dooren T, Borghgraef P, Haass C, Van Leuven F (2004) beta-site amyloid precursor protein cleaving enzyme 1 increases amyloid deposition in brain parenchyma but reduces cerebrovascular amyloid angiopathy in aging BACE x APP[V717I] double-transgenic mice. The American journal of pathology 165:1621-1631.

Winner B, Kohl Z, Gage FH (2011) Neurodegenerative disease and adult neurogenesis. The European journal of neuroscience 33:1139-1151.

Wlodarczyk J, Mukhina I, Kaczmarek L, Dityatev A (2011) Extracellular matrix molecules, their receptors, and secreted proteases in synaptic plasticity. Developmental neurobiology 71:1040-1053.

Yang Y, Geldmacher DS, Herrup K (2001) DNA replication precedes neuronal cell death in Alzheimer's disease. The Journal of neuroscience : the official journal of the Society for Neuroscience 21:2661-2668.

Yang Y, Wang XB, Frerking M, Zhou Q (2008) Spine expansion and stabilization associated with long-term potentiation. J Neurosci 28:5740-5751.

Young-Pearse TL, Bai J, Chang R, Zheng JB, LoTurco JJ, Selkoe DJ (2007) A critical function for beta-amyloid precursor protein in neuronal migration revealed by in utero RNA interference. The Journal of neuroscience : the official journal of the Society for Neuroscience 27:14459-14469.

Yuste R, Bonhoeffer T (2001) Morphological changes in dendritic spines associated with long-term synaptic plasticity. Annual review of neuroscience 24:1071-1089.

Zempel H, Thies E, Mandelkow E, Mandelkow EM (2010) Abeta oligomers cause localized Ca(2+) elevation, missorting of endogenous Tau into dendrites, Tau phosphorylation, and destruction of microtubules and spines. The Journal of neuroscience : the official journal of the Society for Neuroscience 30:11938-11950.

Zhao S, Chai X, Frotscher M (2007) Balance between neurogenesis and gliogenesis in the adult hippocampus: role for reelin. Developmental neuroscience 29:84-90.